Université de Montréal

# Study of Histone H3 Lysine 56 Deacetylation in *Saccharomyces cerevisiae*

par
Neda Delgoshaie

Programmes de biologie moléculaire
Faculté de médecine

Thèse présentée à la Faculté de médecine
en vue de l'obtention du grade de *Philosophiæ Doctor* (Ph.D.)
en biologie moléculaire
option biologie des systèmes

Avril 2013

# Résumé

Chez la levure *Saccharomyces cerevisiae*, l'acétylation de l'histone H3 sur la lysine 56 (H3K56ac) est présente sur les histones néo-synthétisées déposées derrière les fourches de réplication et est essentielle pour préserver la viabilité cellulaire en réponse au dommage à l'ADN. La désacétylation d'H3K56 sur l'ensemble du génome catalysée par Hst3 et Hst4 et a lieu en phase G2 ou M. H3K56ac est une lame à double tranchant. L'absence d'H3K56ac rend les cellules sensibles aux dommages à l'ADN. En revanche, un excès d'acétylation d'H3K56 dans un mutant *hst3*Δ *hst4*Δ a des conséquences encore plus sévères tels que la thermo-sensibilité, l'hypersensibilité aux agents génotoxiques, l'instabilité génomique ainsi qu'une courte durée de vie réplicative. Les désacétylases Hst3 et Hst4 sont étroitement régulées au cours du cycle cellulaire afin de permettre à l'H3K56ac d'exercer son rôle en réponse aux dommages à l'ADN tout en évitant les conséquences néfastes de l'hyperacétylation d'H3K56. Dans cette thèse, nous avons identifié la machinerie moléculaire responsable de la dégradation de Hst3. De plus, nous avons exploré les raisons pour lesquelles l'absence de désacétylation donne lieu aux phénotypes du mutant *hst3*Δ *hst4*Δ.

Au chapitre 2, nous démontrons que la dégradation d'Hst3 peut être complétée avant l'anaphase. Ceci suggère que la désacétylation de H3K56 a lieu durant une courte fenêtre du cycle cellulaire se situant entre la complétion de la phase S et la métaphase. De plus, nous avons identifié deux sites de phosphorylation d'Hst3 par la kinase cycline-dépendante 1 (Cdk1) et démontré que ces évènements de phosphorylation conduisent à la dégradation d'Hst3 *in vivo*. Nous avons aussi démontré que l'ubiquityltransférase Cdc34 et l'ubiquitine ligase $SCF^{Cdc4}$ sont requises pour la dégradation d'Hst3. Finalement, nous avons montré que la phosphorylation d'Hst3 par la kinase mitotique Clb2-Cdk1 peut directement entraîner l'ubiquitylation d'Hst3 par $SCF^{Cdc4}$ *in vitro*.

Au chapitre 3, nous avons étudié les mécanismes moléculaires sous-jacents à la sensibilité extrême du mutant *hst3*Δ *hst4*Δ aux agents qui endommagent l'ADN. Nous avons établi

qu'en raison de la présence anormale d'H3K56ac devant les fourches de réplication, le mutant *hst3*Δ *hst4*Δ exhibe une forte perte de viabilité lorsqu'exposé au méthyl méthanesulfonate (MMS) durant un seul passage à travers la phase S. Nous avons aussi découvert que, malgré le fait que le point de contrôle de réponse aux dommages à l'ADN est activé normalement dans le mutant *hst3*Δ *hst4*Δ, ce mutant est incapable de compléter la réplication de l'ADN et d'inactiver le point de contrôle pour une longue période de temps après exposition transitoire au MMS. L'ensemble de nos résultats suggère que les lésions à l'ADN induites par le MMS dans le mutant *hst3*Δ *hst4*Δ causent une forte perte de viabilité parce que ce mutant est incapable de compléter la réplication de l'ADN après une exposition transitoire au MMS.

Dans la deuxième section du chapitre 3, nous avons employé une approche génétique afin d'identifier de nouveaux mécanismes de suppression de deux phénotypes prononcés du mutant *hst3*Δ *hst4*Δ. Nous avons découvert que la délétion de plusieurs gènes impliqués dans la formation de frontières entre l'hétérochromatine et de l'euchromatine atténue les phénotypes du mutant *hst3*Δ *hst4*Δ sans réduire l'hyperacétylation d'H3K56. Nos résultats indiquent aussi que l'abondante acétylation de l'histone H4 sur la lysine 16 (H4K16ac) est néfaste au mutant *hst3*Δ *hst4*Δ. Ce résultat suggère un lien génétique intriguant entre l'acétylation d'H3K56 et celle d'H4K16. L'existence de ce lien était jusqu'à présent inconnu. Nous avons identifié un groupe de suppresseurs spontanés où H3K56ac est indétectable, mais la majorité de nos suppresseurs ne montrent aucune réduction flagrante d'H3K56ac ou d'H4 K16ac par rapport aux niveaux observés dans le mutant *hst3*Δ *hst4*Δ. Une étude plus approfondie de ce groupe de suppresseurs est susceptible de mener à la découverte de nouveaux mécanismes génétiques ou épigénétiques permettant d'éviter les conséquences catastrophiques de l'hyperacétylation d'H3K56 chez le mutant *hst3*Δ *hst4*Δ.

En résumé, cette thèse identifie la machinerie moléculaire responsable de la dégradation d'Hst3 (une désacétylase d'H3K56) durant une fenêtre de temps situées entre la fin de la phase S et la métaphase. Nos résultats permettent aussi d'expliquer pourquoi la dégradation d'Hst3 précède le début de la phase S durant laquelle l'acétylation d'H3K56 s'accumule derrière les fourches de réplication afin d'exercer son rôle de mécanisme de défense contre

le dommage à l'ADN. De plus, nous avons identifié plusieurs suppresseurs qui permettent de contourner le rôle important d'Hst3 et Hst4 en réponse au dommage à l'ADN. Plusieurs suppresseurs révèlent un lien génétique inattendu entre deux formes abondantes d'acétylation des histones chez *Saccharomyces cerevisiae*, soit H3K56ac et H4K16ac.

**Mots-clés:** chromatine, acétylation de l'histone H3, acétylation de l'histone H4, H3K56ac, H4K16ac, Hst3, Hst4, $SCF^{Cdc4}$, Clb2-Cdk1, dommage à l'ADN, agent génotoxique, réplication de l'ADN, cycle cellulaire, acétylation, désacétylation

# Abstract

In *Saccharomyces cerevisiae*, histone H3 lysine 56 acetylation (H3K56ac) is found in new histones deposited behind DNA replication forks and is needed for DNA damage survival. Genome-wide removal of H3K56ac by the deacetylases Hst3 and Hst4 occurs during G2 and/or M phase. H3K56ac is a double-edged sword. Lack of H3K56ac results in DNA damage sensitivity. In contrast, overabundance of H3K56ac in *hst3*Δ *hst4*Δ mutants gives rise to even more severe and wide-ranging phenotypes, namely thermosensitivity, genotoxic agent hypersensitivity, genome instability and short replicative lifespan. The deacetylases Hst3 and Hst4 are tightly controlled during the cell cycle such that H3K56ac can contribute to the DNA damage response during each passage through S phase, while avoiding abnormal conditions where H3K56 remains hyperacetylated. In this thesis, we identified the molecular machinery that promotes Hst3 degradation. Moreover, we explored why failure to deacetylate H3K56 gives rise to the phenotypes of *hst3*Δ *hst4*Δ cells.

In chapter 2, we showed that degradation of Hst3 can be completed prior to anaphase. This suggests that removal of H3K56ac occurs during a short time window between completion of S phase and metaphase. In addition, we found that Hst3 is phosphorylated at two cyclin-dependent kinase 1 (Cdk1) sites and demonstrated that these phosphorylation events promote degradation of Hst3 *in vivo*. Moreover, we demonstrated that the ubiquitin-conjugating enzyme Cdc34 and the $SCF^{Cdc4}$ ubiquitin ligase are required for degradation of Hst3. Lastly, we showed that phosphorylation of Hst3 by the mitotic kinase Clb2-Cdk1 can directly drive its ubiquitylation by $SCF^{Cdc4}$ *in vitro*.

In chapter 3, we investigated the molecular mechanisms that underlie the severe sensitivity of *hst3*Δ *hst4*Δ cells to DNA damaging agents. We established that the aberrant presence of H3K56ac in front of DNA replication forks causes *hst3*Δ *hst4*Δ cells to lose viability after a single passage through S phase in the presence of methyl methanesulfonate (MMS). We also found that, although *hst3*Δ *hst4*Δ cells show normal activation of the DNA damage checkpoint, these mutants fail to complete DNA replication and inactivate the checkpoint

long after MMS removal. Collectively, our results suggest that MMS-induced DNA lesions cause a severe loss of viability in *hst3*Δ *hst4*Δ cells because the mutant cells fail to complete DNA replication after MMS removal.

In the second part of chapter 3, we employed a genetic approach to identify novel mechanisms for suppression of two pronounced phenotypes of *hst3*Δ *hst4*Δ mutants. We found that deletion of several genes involved in creating boundaries between heterochromatic and euchromatic regions alleviates the phenotypes of *hst3*Δ *hst4*Δ mutants without reducing H3K56 hyperacetylation. Our results also indicate that the highly abundant histone H4 lysine 16 acetylation (H4K16ac) is deleterious to *hst3*Δ *hst4*Δ mutants, suggesting an intriguing and hitherto undiscovered genetic link between H3K56ac and H4K16ac. We identified a group of spontaneous suppressors that exhibited undetectable levels of H3K56ac, but the majority did not show obvious decreases in H3K56ac or H4K16ac compared to the levels observed in *hst3*Δ *hst4*Δ cells. Further characterization of these suppressors might unravel additional genetic or epigenetic mechanisms that circumvent the catastrophic consequences of H3K56 hyperacetylation in *hst3*Δ *hst4*Δ cells.

In summary, this thesis describes the molecular machinery that triggers destruction of the main H3K56 deacetylase Hst3 during a period of time delineated by the end of S phase and metaphase. Our findings also explain why degradation of Hst3 always precedes the onset of S phase when H3K56ac needs to accumulate behind DNA replication forks in order to act as defense mechanism against DNA damage. In addition, we uncover several novel suppressors that bypass the role of Hst3 and Hst4 in DNA damage resistance. Several suppressors reveal an unexpected genetic link between two abundant forms of histone acetylation, namely H3K56ac and H4K16ac.

**Keywords**: chromatin, histone H3 acetylation, histone H4 acetylation, H3K56ac, H4K16ac, Hst3, Hst4, $SCF^{Cdc4}$, Clb2-Cdk1, DNA damage, genotoxic agent, DNA replication, cell cycle, acetylation, deacetylation

# Table of contents

# List of tables

# List of figures

# List of abbreviations

| | |
|---|---|
| Acetyl-CoA | acetyl coenzyme A |
| ADP | adenosine diphosphate |
| APC | anaphase promoting complex |
| ATP | adenosine 5´-triphosphate |
| CAF-1 | Chromatin Assembly Factor 1 |
| CC | coiled-coil |
| Cdk | cyclin-dependent kinase |
| CNS | COP9 signalosome |
| CP | core particle |
| CPD | Cdc4 phosphodegron |
| CPT | Camptothecin |
| C-terminus | carboxyl terminus |
| DDR | DNA damage response |
| DNA | deoxyribonucleic acid |
| dNTP | deoxyribonucleoside triphosphate |
| DSB | double-strand break |
| DTT | dithiothreitol |
| DUB | deubiquitinating enzyme |
| FACS | fluorescence-activated cell sorting |
| GNAT | Gcn5 N-acetyltransferase |
| H2AP | histone H2A serine 129 phosphorylation |
| H3K56ac | Histone H3 lysine 56 acetylation |
| H4K16ac | histone H4 lysine 16 acetylation |
| HAT | histone acetyltransferase |
| HCl | hydrogen chloride |
| HDAC | Histone deacetylase |
| HECT | homologous to the E6-AP carboxyl terminus |
| HEPES | N-(2-hydroxyethyl) piperazine-N´-(2-ethanosulfonic acid) |
| His | histidine |
| HML | homothallic mating type loci L |
| HMR | homothallic mating type loci R |
| HR | homologous recombination |
| HST | homolog of sir two |
| HU | hydroxyurea |
| IPTG | isopropyl-β-D-thiogalactopyranoside |
| Leu | leucine |
| LOH | loss of heterozygosity |

| | |
|---|---|
| LRR | Leucine-rich repeat |
| m/z | mass-to-charge |
| MgCl2 | magnesium chloride |
| MMS | methyl methanesulfonate |
| MRX | Mre11-Rad50-Xrs2 |
| NaCl | sodium chloride |
| NAD+ | nicotinamide adenine dinucleotide |
| NHEJ | non-homologous end joining |
| N-terminus | amino terminus |
| PCNA | Proliferating Cell Nuclear Antigen |
| PCR | polymerase chain reaction |
| PFGE | pulsed field gel electrophoresis |
| PH | Pleckstrin homology |
| PHD | plant homeodomain |
| PIKK | phosphoinositide 3-kinase related kinase |
| PTM | post-translational modification |
| PVDF | polyvinylidene difluoride |
| rDNA | ribosomal DNA |
| RFB | replication fork block |
| RFC | replication factor C |
| RING | really interesting new gene |
| RNA | ribonucleic acid |
| RNR | ribonucleotide reductase |
| RP | regulatory particle |
| RPA | replication protein A |
| RSC | remodel the structure of chromatin |
| SAHA | suberoylanilide hydroxamic acid |
| SAS-I | something about silencing-I |
| SC | synthetic complete |
| SCF | Skp1-Cullin-F-box |
| SCR | sister chromatid recombination |
| SDS | sodium dodecyl sulfate |
| SDS-PAGE | sodium dodecyl sulfate polyacrylamide gel |
| ssDNA | single-strand DNA |
| SWI/SNF | SWItch/Sucrose NonFermentable |
| TAP | tandem affinity purification |
| Top1 | topoisomerase I |
| Tr | thermoresistant |
| Trp | triptophane |
| Ts | thermosensitivity |
| TSA | trichostatin A |

| | |
|---|---|
| URA | uracil |
| WT | wild-type |
| YPD | yeast peptone dextrose |
| 5-FOA | 5-Fluoroorotic acid |
| γ-H2AX | H2AX serine 139 phosphorylation |

# Acknowledgements

First, I would like to express my special gratitude to my research director and mentor, Dr. Alain Verreault, for granting me the opportunity to pursue my Ph.D. studies under his supervision. I am very grateful for all that I have learnt from him during my doctoral studies in his research group as well as during the graduate courses taught by him. I am especially thankful to him for teaching me the essence of critical thinking and scientific integrity, for all the insightful discussions that improved my scientific outlook, and for his unconditional support and understanding throughout these years. I will be always grateful for my Ph.D. experience because of him.

Moreover, I would like to thank the members of my Ph.D. committee, Dr. Richard Bertrand, Dr. Dindial Ramotar and Dr. Jason Tanny, for their helpful advice on my research project.

I am also thankful to all previous and present members of the Verreault lab for their help and support, for our scientific discussions and for creating an enjoyable work environment. I am especially thankful to my former colleague, Dr. Hugo Wurtele, for providing me with technical help and scientific advice on my research project, and for our fruitful collaboration on the research project presented in chapter 3 of this dissertation.

Finally, my most special thanks go to my parents, my partner and my siblings whose love and continual support, even from far away, encouraged me to carry on with my endeavor during the long years of the Ph.D. studies. I am utterly grateful for having them in my life.

I would also like to acknowledge the Cole Foundation and the Molecular Biology Program of the Université de Montréal for their scholarships.

# 1. Introduction

## 1.1. Chromatin structure and function

In eukaryotic cells, several meters of genomic DNA is confined in a nuclear space of micrometers in diameter. To achieve this compaction, DNA undergoes multiple levels of higher-order organization starting at formation of a nucleoprotein structure with histones known as chromatin. Chromatin formation is a barrier to cellular processes that require access to the DNA substrate including transcription, DNA replication and repair. To accommodate these processes, a plethora of enzymatic activities modulate chromatin structure, many of which mediate covalent modification of core histones (Khorasanizadeh 2004). In this section we describe the structure of chromatin and introduce post-translational modifications of histones with a focus on histone acetylation and its enzymatic regulation.

### 1.1.1. The nucleosome core particle

The fundamental repeating unit of chromatin is the disk-shaped nucleosome core particle. Each nucleosome is composed of a protein octamer containing two molecules each of histones H2A, H2B, H3 and H4 around which 147 base pairs of left-handed superhelical DNA is wrapped in 1.7 turns (Figure 1.1) (Luger *et al.* 1997). Histones are small highly conserved proteins which are enriched for basic residues. Core histones are organized into a central "histone fold" domain composed of three α-helices (α1-α3) connected by two loops, L1 and L2. Histone fold domains are involved in histone-histone and histone-DNA contacts that stabilize the nucleosome structure: histone pairs interact through these globular domains to construct H2A-H2B and H3-H4 heterodimers. Histone H3 has a central role in stabilization of the nucleosome core particle, because it makes additional contacts outside of its heterodimer with histone H2A and also with the DNA helix at its entry and exit points around the nucleosome. Histones also form flexible N- and/or C-terminal extensions known as histone tail domains that protrude from the nucleosome core particle. These disordered regions associate with other nucleosomes or non-histone proteins and are involved in higher order organization of the chromatin fiber (Khorasanizadeh 2004).

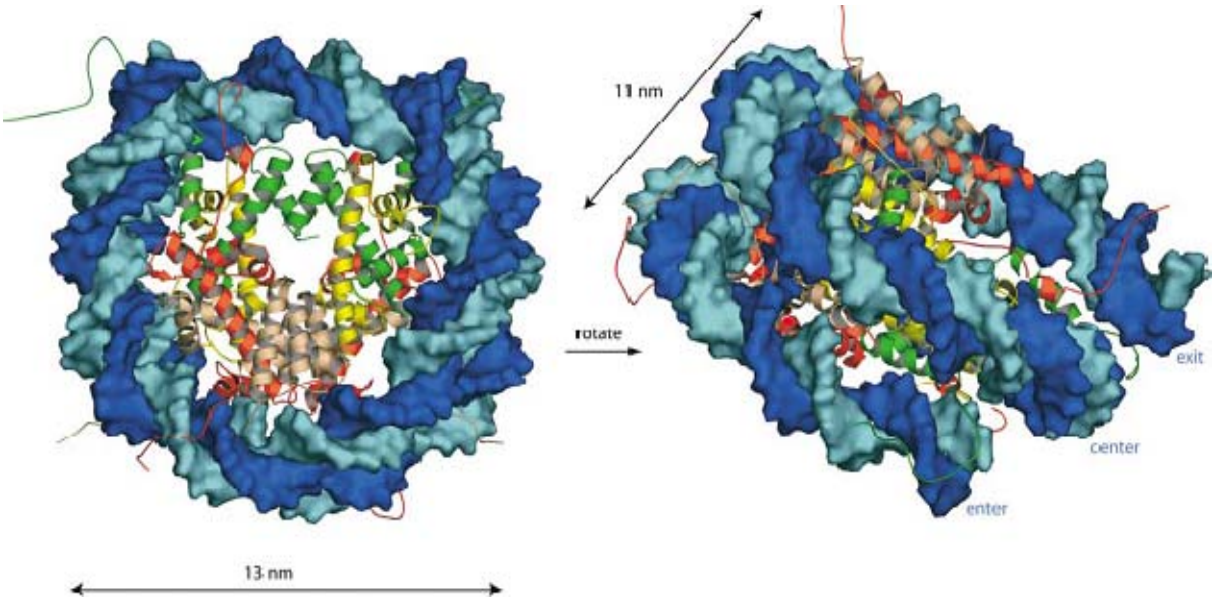


**Figure 1.1 The structure of the nucleosome core particle.** The DNA duplex, shown in dark and light blue, makes 1.7 turns around an octamer of core histones to form the disk-shaped nucleosome. Histones H3, H4, H2A and H2B are shown is green, yellow, red and pink, respectively (Khorasanizadeh 2004).

### 1.1.2. Post-translational modifications of histones

Core histones are subject to a diverse array of dynamically regulated post-translational modifications (PTMs) including acetylation, methylation, phosphorylation, ubiquitination, sumoylation and poly (ADP) ribosylation (Khorasanizadeh 2004). Although the majority of PTMs are clustered on the accessible histone tails, technical advances in mass spectrometry have allowed identification of covalent modifications within histone fold domains. For instance in *Saccharomyces cerevisiae*, histone H3 is acetylated at K56 (Masumoto *et al.* 2005) and methylated at K79 (van Leeuwen *et al.* 2002), and histone H4 is acetylated at K91 (Ye *et al.* 2005) within their globular domains.

Histone PTMs have been implicated in regulation of all cellular processes involving DNA transactions. Acetylation and phosphorylation reduce the positive charge of histones that might directly affect histone-histone or histone-DNA interactions. However, the majority of histone PTMs exert their biological effect by recruiting chromatin "readers" that interact

with modified histones through specialized protein domains (Bannister *et al.* 2011, Yun *et al.* 2011). Moreover, numerous lines of evidence suggest an active interplay between different histone marks in regulation of chromatin function (Jenuwein *et al.* 2001). Hence, it has been proposed that modulation of chromatin structure and function is achieved through the sequential action or a combination of histone PTMs constituting a "histone code" (Strahl *et al.* 2000).

#### 1.1.2.1. Histone acetylation

One of the most-studied modifications of core histones is the acetylation of lysine residues. Histone acetylation affects diverse nuclear processes such as transcription, DNA replication and repair, nucleosome assembly, and establishment of boundaries between heterochromatin and euchromatin. This reversible modification is added by histone acetyltransferases (HATs) and removed by histone deacetylases (HDACs) (Kurdistani *et al.* 2003). Although HATs and HDACs were originally discovered based on their ability to modify histones, many of these enzymes were later found to have non-histone substrates *in vivo*. For instance, the tumor suppressor p53 is acetylated by the HAT p300/CBP and deacetylated by two HDACs, namely HDAC1 and SIRT1 (Glozak *et al.* 2005).

Histone acetylation neutralizes the positive charge of the lysine side chain that allows its interaction with a specialized protein motif named the bromodomain. The bromodomain is a conserved 100 amino-acid module that contains a hydrophobic pocket to bind acetyl-lysines and is found in numerous chromatin-interacting proteins (Dhalluin *et al.* 1999). In addition to bromodomains, other protein domains can also interact with acetyl-lysines. For instance, in *S.cerevisiae* the PH-like domain of the histone chaperone Rtt106 was shown to interact with K56 acetylated histone H3, and thus represents a novel class of acetyl-lysine binding domains (Li *et al.* 2008). Moreover, a tandem zinc-binding protein module named the PHD finger can bind to acetylated histone H3 and H4 molecules in human cells (Zeng *et al.* 2008).

#### 1.1.2.1.1. Histone acetyltransferases

Histone acetyltransferases (HATs) mediate conjugation of an acetyl group from acetyl coenzyme A (acetyl-CoA) to the ε-amine of the lysine side chain of histones (Marmorstein 2001a). HATs often reside in multisubunit protein complexes containing specialized histone interacting domains that direct their enzymatic activity to appropriate chromatin regions. Based on catalytic domains, HATs are grouped into two major families: The Gcn5 N-acetyltransferase (GNAT) family which was founded by Gcn5 and also includes PCAF, Elp3, Hat1, Hpa2 and Nut1, and the MYST family whose name is derived from its founding members Morf, Ybf2 (Sas3), Sas2 and Tip60. However, several HATs such as p300/CBP, Taf1 and the fungal Rtt109 lack consensus HAT domains and do not belong to either of the aforementioned families (Lee *et al.* 2007).

HATs were originally classified in two distinct groups based on their cellular localization and substrate specificity: nuclear A-type HATs that acetylate nucleosomal histones, and cytoplasmic B-type HATs that acetylate newly synthesized histones prior to their deposition into chromatin (Brownell *et al.* 1996). In *S. cerevisiae*, acetylation of redundant sites in the N-terminal tails of newly synthesized histones H3 and H4 is essential for the replication-coupled nucleosome assembly and cell viability. Hence, identification of enzymes that acetylate these sites has been of particular interest. The first identified B-type HAT was Hat1 that mediates the evolutionarily-conserved pattern of new histone H4 acetylation at lysines 5 and 12. Newly synthesized histone H3 is also acetylated at multiple sites prior to its deposition, but unlike histone H4, its acetylation pattern varies across specifies (Verreault 2000).

Rtt109 is a fungal-specific HAT that mediates acetylation of newly synthesized histone H3. Rtt109 enzymatic activity is highly stimulated by the histone chaperones Vps75 and Asf1. Vps75 is tightly associated with Rtt109 and promotes its stability *in vivo*, but Asf1 has a weak and transient interaction with Rtt109. Moreover, the substrate specificity of these two enzymatic complexes is different *in vivo*: Rtt109-Asf1 can only associate with H3-H4 heterodimers and exclusively acetylates H3 at lysine 56. In contrast, Rtt109-Vps75 binds

both H3-H4 dimers and $(H3\text{-}H4)_2$ heterotetramers and catalyzes acetylation of histone H3 at lysines 9 and 27, which are also acetylated by Gcn5 (D'Arcy *et al.* 2011).

#### 1.1.2.1.2. Histone deacetylases

Histone deacetylases (HDACs) remove the acetyl moiety from the lysine side chain to restore its positive charge. Based on sequence homology, eukaryotic HDACs are divided into three families: Class I HDACs are nuclear enzymes with sequence homology to yeast Rpd3. This family of HDACs also includes yeast Hos3 and human HDAC1, HDAC2 and HDAC3. The catalytic activity of these enzymes is inhibited by trichostatin A (TSA) and its derivative compounds such as suberoylanilide hydroxamic acid (SAHA) and trapoxin. Enzymes with sequence homology to yeast Hda1 constitute the Class II family of HDACs that also includes yeast Hos1 and Hos2 and human HDACs 4-8. These HDACs share the catalytic domain of Class I enzymes and are also inhibited by TSA and its related compounds. Nevertheless, members of this family contain additional N-terminal domains that are absent from Class I proteins. Moreover, Class II HDACs are cytoplasmic proteins that are transiently transported to the nucleus to deacetylate histones. Class III HDACs, also known as sirtuins, are nicotinamide adenine dinucleotide ($NAD^+$)-dependent enzymes that are homologous to yeast Sir2. Sirtuins catalyze transfer of the acetyl group from the acetylated protein to the ADP-ribose moiety of $NAD^+$ producing O-acetyl-ADP-ribose and nicotinamide (NAM) in the process. Therefore, the catalytic activity of these enzymes is inhibited by excess amounts of the reaction product NAM. This family of enzymes consists of five members in yeast (Sir2 and Hst1-4), and seven members in humans (SIRT1-7). Moreover, unlike the two other classes, different members of this family show nuclear or cytoplasmic localization (Marmorstein 2001b).

## 1.2. Replication-coupled nucleosome assembly

During S phase nucleosomes are transiently disrupted by progression of the DNA replication machinery, but nascent sister chromatids are rapidly reassembled into chromatin

behind the replication fork. Duplication of genetic material during DNA synthesis demands new histone supply for efficient packaging of nascent DNA duplexes. Therefore, maintenance of chromatin structure following DNA replication is achieved by two independent processes: first, parental histones are transferred behind replication forks in a process referred to as parental histone segregation, and the gaps in nucleosome arrays are then filled by incorporation of newly synthesized histones during replication-coupled (*de novo*) nucleosome assembly (Verreault 2000).

Under physiological conditions, positively charged histones form insoluble aggregates with negatively charged DNA *in vitro*. To inhibit non-specific binding of histones to DNA, a variety of histone chaperones contribute to chromatin assembly *in vivo* by shielding the positive charge of histones and escorting them to sites of nucleosome assembly at the replication fork. During *de novo* nucleosome assembly, Chromatin Assembly Factor 1 (CAF-1) first mediates deposition of two H3-H4 dimers onto nascent DNA. CAF-1 is recruited to the replication fork through its interaction with the DNA polymerase processivity clamp PCNA. The histone chaperone Asf1 binds to H3-H4 dimers and probably functions as the histone donor for CAF-1. Two H2A-H2B dimers then associate with the $(H3\text{-}H4)_2$ heterotetramer to complete nucleosome formation. The histone chaperone NAP1 might be implicated in this process, but the assembly factors that directly deposit H2A-H2B dimers onto chromatin remain unidentified (Annunziato 2012). In *S. cerevisiae*, the histone chaperone Rtt106 also interacts with the large subunit of CAF-1 and binds to $(H3\text{-}H4)_2$ heterotetramers *in vivo*. Therefore, it has been proposed that H3-H4 dimers might be assembled into tetramers on Rtt106 before their deposition onto chromatin by CAF-1 (Fazly *et al.* 2012, Huang *et al.* 2005).

As noted earlier, acetylation sites in the N-terminal domains of H3 and H4 function redundantly to promote *de novo* nucleosome assembly and cell viability in *S. cerevisiae*. The most common pre-deposition pattern is the diacetylation of histone H4 at lysines 5 and 12 which is conserved from yeast to humans. However, the N-terminal domain of histone H4 is also acetylated at lysine 8 in budding yeast (Verreault 2000). New histone H3 is acetylated at lysines 9, 14, 23 and 27 in the N-terminal tail (Verreault 2000) and at lysine

56 in its histone fold domain (Masumoto*, et al.* 2005). H3K56ac promotes nucleosome assembly by CAF-1 and Rtt106 (Li*, et al.* 2008). Moreover, association of histone H3 with CAF-1 and Rtt106 is reduced in *GCN5* deleted cells suggesting that Gcn5-mediated acetylation of new histone H3 at lysines 9 and 27 is also important for *de novo* nucleosome assembly (Burgess *et al.* 2010).

## 1.3. DNA damage during S phase

During S phase, progression of DNA replication forks is frequently challenged by DNA lesions from endogenous and exogenous sources. In order to maintain genomic integrity in the face of constant DNA damage, eukaryotic cells have evolved an elaborate surveillance mechanism known as the S phase checkpoint that coordinates DNA replication with DNA repair and chromosome segregation (Nyberg *et al.* 2002). In this section, we briefly describe the mechanism of action for several types of genotoxic agents that interfere with completion of DNA replication and introduce components of the S phase checkpoint.

### 1.3.1. Inhibitors of topoisomerase I

Topoisomerase I (Top1) relaxes supercoiled DNA in front of DNA replication forks or transcription complexes by catalyzing a two-step reaction. First, Top1 induces a transient single-strand break in DNA allowing rotation of the supercoiled double helix around the nick to relax DNA. At this step, an active site tyrosine of Top1 is covalently linked to the phosphate group at the 3´ end of the DNA nick in an enzyme-DNA intermediate known as the Top1 cleavage complex. The second step, or the religation reaction, occurs when the free 5´-hydroxyl end of nicked DNA attacks the tyrosyl-DNA phosphodiester link to regenerate intact DNA and release Top1.

A variety of DNA lesions and genotoxic agents including camptothecin (CPT) trap Top1 cleavage complexes by displacing the 5´-hydroxyl DNA end and inhibiting the Top1 religation reaction. Stabilized Top1 cleavage complexes can give rise to DNA damage

through multiple mechanisms. For instance, during S phase DNA polymerases involved in leading strand synthesis can collide into Top1 cleavage complexes trapped by CPT giving rise to cytotoxic DNA double-strand breaks (DSBs) (Pommier *et al.* 2003).

### 1.3.2. DNA methylating agents

DNA methylating agents react with DNA at different sites to generate N- and O-methylated bases or methylphosphotriesters in the DNA backbone. Nevertheless, most of these agents including methyl methanesulfonate (MMS) methylate DNA to generate $N^7$-methylguanine (7-meG) and $N^3$-methyladenine (3-meA) (Sedgwick 2004). MMS treatment activates the DNA damage checkpoint only during the S phase of the cell cycle, suggesting that methylated DNA becomes genotoxic during DNA replication (Tercero *et al.* 2003). Moreover, it has been shown that the presence of 3-meA in the template DNA blocks replication *in vitro* (Larson *et al.* 1985).

### 1.3.3. Ribonucleotide reductase inhibitors

The building blocks of DNA are deoxyribonucleoside triphosphates (dNTPs). Ribonucleotide reductase (RNR) is the enzyme that controls the rate-limiting step in the production of dNTPs by reducing ribonucleotides to deoxyribonucleotides. Unlike higher eukaryotes, *S. cerevisiae* cells lack deoxyribonucleoside kinase activity and therefore completely rely on RNR for dNTP synthesis during S phase. Therefore, RNR inhibitors such as hydroxyurea (HU) slow down progression of DNA replication forks by limiting the dNTP pools that are available to replicative polymerases (Reichard 1988). As described below, although treatment with HU does not cause DNA damage, it activates the S phase checkpoint response.

### 1.3.4. S phase checkpoint

In response to limiting pools of dNTPs during S phase or replication forks blocked by DNA lesions, eukaryotic cells initiate a complex signaling cascade called the S phase checkpoint that promotes cell viability through multiple mechanisms. The checkpoint response slows down DNA replication by preventing the firing of new replication origins and protects stalled replication forks until DNA synthesis can resume. Moreover, the S phase checkpoint recruits the DNA repair machinery to sights of DNA damage.

The key components of the S phase checkpoint and their global mode of action are evolutionarily conserved. In this signaling pathway, presence of stalled replication forks is relayed by several "sensors" to ATM (yeast Tel1) and ATR (yeast Mec1) that belong to the phosphoinositide 3-kinase related family of protein kinases (PIKKs). ATR activity requires its association with a protein named ATRIP (yeast Ddc2) *in vivo*. ATM and ATR activate the serine/threonine kinases CHK1 and CHK2 (yeast Rad53) that in turn phosphorylate numerous downstream effectors. In spite of significant overlap, replication forks stalled at DNA lesions engage a different branch of the S phase checkpoint as opposed to replication forks that have slowed down in the absence of DNA damage (Nyberg*, et al.* 2002). These signaling cascades are known as the DNA damage checkpoint and the DNA replication checkpoint, respectively.

#### 1.3.4.1. DNA damage checkpoint

In eukaryotes, different types of DNA lesions are probably converted to single-strand DNA (ssDNA) or double-strand breaks (DSBs) before triggering the checkpoint response. In *S. cerevisiae*, DSBs are initially recognized by the MRX complex composed of Mre11, Rad50 and Xrs2. The MRX complex holds the DSB ends together, initiates resection of the DSB 5′ ends, and recruits Tel1 to sites of DNA damage. Resection of the DSB 5′ ends is initiated by Sae2, and assisted by Mre11, and extended by Exo1 and/or Dna2 to produce 3′ single-stranded overhangs (ssDNA). The replication protein A (RPA) then covers ssDNA

and recruits a number of downstream checkpoint proteins: the clamp loader Rad24-RFC complex, composed of Rad24 and Rfc2-5 subunits, binds RPA and loads the 9-1-1 clamp composed of Ddc1, Mec3 and Rad17 onto DNA. Moreover, RPA-coated ssDNA recruits Ddc2 and its binding partner Mec1 to sites of DNA damage. Upon activation, Mec1 phosphorylates the adaptor protein Rad9 and the checkpoint kinase Rad53 that, in turn, phosphorylates other downstream effectors. The DNA damage checkpoint also triggers changes in the chromatin structure that subsequently contribute to checkpoint signaling. For instance, both Tel1 and Mec1 phosphorylate histone H2A at serine 129 (H2AP), which serves as a molecular marker of DSBs in several eukaryotes. H2AP functions in concert with histone H3 lysine 79 methylation (H3K79me) to increase the affinity of Rad9 for chromatin where it gets directly phosphorylated by Tel1 (Figure 1.2) (Lisby *et al.* 2009).

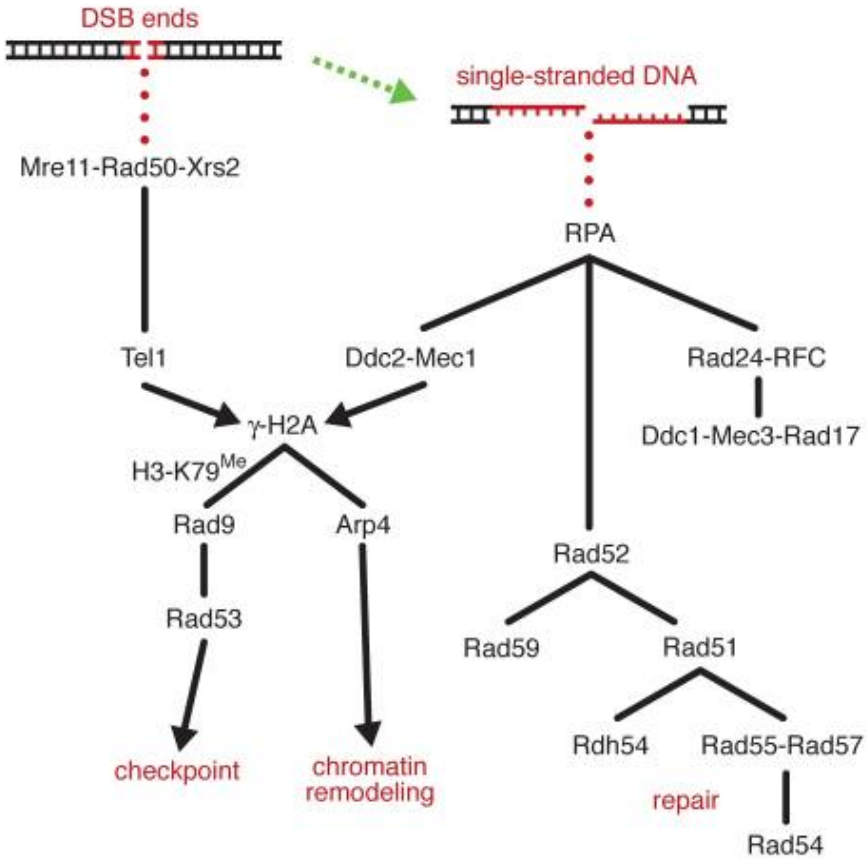


**Figure 1.2 The DNA damage checkpoint and its downstream effectors in *S. cerevisiae*.** Solid black lines show absolute requirements. Red dotted lines represent specific interactions, and arrows indicate modifying functions (Lisby, *et al.* 2009).

#### 1.3.4.2. DNA replication checkpoint

In response to defects in DNA replication, for instance in the presence of HU, stalled forks activate the DNA replication checkpoint that maintains the integrity of the replication machinery until DNA synthesis can resume. However, microarray evidence has revealed that DNA replication continues at slow rates in the presence of HU and all the programmed origins of replication eventually fire in the same order as in the absence of replicative stress (Alvino *et al.* 2007). Therefore, the checkpoint response to HU differs from the canonical S phase checkpoint in that it does not inhibit the firing of late origins of replication.

At the stalled replication fork, the MCM helicase may continue to unwind the DNA duplex in front of the blocked DNA polymerase, thereby generating sufficient ssDNA to initiate the checkpoint response. RPA-coated ssDNA recruits Mec1-Ddc2 that phosphorylates the checkpoint mediator Mrc1 and activates Rad53. Mrc1, Tof1 and Csm3 constitute the replication-pausing checkpoint complex. This complex associates with the MCM helicase and other components of the replisome and contributes to the integrity of the stalled replication forks (Branzei *et al.* 2006). Moreover, when DNA replication slows down (*e.g.* in the presence of HU) or when the replicative polymerases are blocked at DNA lesions, Mec1 and Rad53 activate a downstream kinase named Dun1 that stimulates the activity of the ribonucleotide reductase (RNR) through multiple mechanisms to expand dNTP pools. Dun1 stimulates expression of *RNR* genes by inhibiting the transcriptional repressor Crt1. Moreover, Dun1 promotes RNR activity by phosphorylating the RNR inhibitors Sml1 and Dif1 and triggering their subsequent degradation by the proteasome (Labib *et al.* 2011).

## 1.4. The ubiquitin-proteasome system

Ubiquitin is a highly conserved 76-residue protein that controls diverse cellular functions through its conjugation to target proteins. Formation of specific types of ubiquitin chains on proteins directs them to a multisubunit protease called the proteasome for degradation. The ubiquitin-proteasome pathway mediates hydrolysis of the majority of short-lived proteins in

eukaryotes. Therefore, this proteolytic system controls every aspect of cellular function including cell cycle progression, transcription and signal transduction (Hershko *et al.* 1998). In this section, we describe the enzymatic cascade for ubiquitin-protein conjugation and introduce the proteasome.

### 1.4.1. The ubiquitin transfer enzymatic cascade

Ubiquitin-protein conjugation results in formation of an isopeptide bond between the C-terminal glycine residue (G76) of ubiquitin and the ε-amine of a lysine residue on substrate proteins. Ubiquitin transfer requires the sequential activity of three enzymes: first, the ubiquitin activating enzyme (E1) forms a high energy thioester bond between its cysteine residue and the carboxyl group of ubiquitin G76 in an ATP-dependent manner. Activated ubiquitin is then transferred to the ubiquitin conjugating enzyme (E2) by forming a thioester linkage with an active site cysteine of the E2. Lastly, the ubiquitin ligase (E3) promotes formation of the isopeptide bond between ubiquitin and the target protein (Figure 1.3) (Pickart 2001). The ubiquitin transfer cascade has a hierarchical organization. For instance, yeast has a single E1 enzyme (Uba1), eleven E2 enzymes and a large repertoire of putative E3 enzymes (60-100). (Finley *et al.* 2012)

Ubiquitin can be conjugated through its G76 to the lysine side chain of another ubiquitin molecule. Successive rounds of ubiquitin transfer to previously conjugated moieties results in formation of polyubiquitin chains on the target protein (Figure 1.3). Ubiquitin harbors seven lysine residues, namely K6, K11, K27, K29, K33, K48 and K63, all of which form polymers *in vivo* (Peng *et al.* 2003). In *S. cerevisiae*, the most abundant polyubiquitin chain that functions as the canonical signal for the proteasome is K48-linked (Xu *et al.* 2009). Consistent with its key role in protein degradation, mutation of lysine 48 of ubiquitin into an arginine (*K48R*) is lethal in yeast (Finley *et al.* 1994). Nevertheless, a quantitative mass spectrometry study revealed that noncanonical ubiquitin chains are also abundant *in vivo* and that all, but K63-linked chains, can trigger protein degradation (Xu*, et al.* 2009). Moreover, even K63-linked ubiquitin chains have been shown to trigger destruction of

specific substrates (Saeki *et al.* 2009). In support of these observations, K48 of ubiquitin cannot sustain cell viability in the absence of all other lysine residues, suggesting that K48 and the other six lysines of ubiquitin have non-redundant signaling functions (Xu*, et al.* 2009). Different E2-E3 complexes preferentially catalyze formation of specific types of ubiquitin chains. For instance, the yeast E2 enzyme Cdc34 that associates with the Skp1-Cullin-F-box (SCF) complex mainly generates K48-linked ubiquitin chains (Petroski *et al.* 2005), and the human E2 enzyme UbcH10 that collaborates with the anaphase promoting complex (APC) synthesizes K11-linked ubiquitin chains (Jin *et al.* 2008).

Substrate selectivity of the ubiquitin-proteasome pathway is conferred by specific interactions between target proteins and their cognate E3 ubiquitin ligases. Target proteins often expose short primary sequence motifs known as degrons that are recognized and bound by specialized binding domains in E3 enzymes (Pickart 2001).

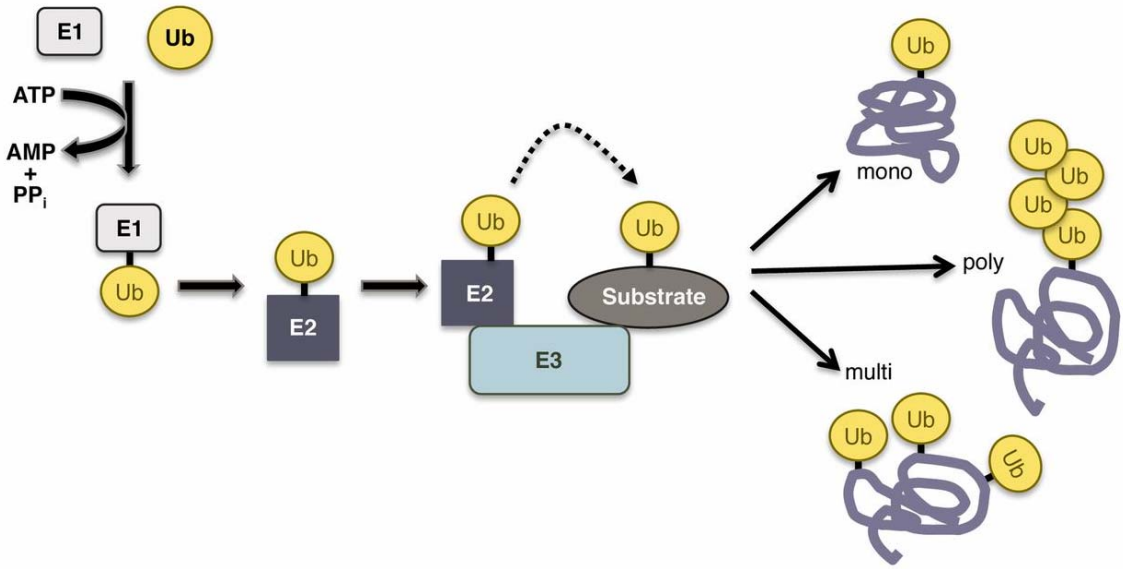


**1.3 The ubiquitin conjugation cascade.** A) Ubiquitin is first activated by the ubiquitin activating enzyme (E1) in an ATP-dependent reaction. Activated ubiquitin is then transferred to the ubiquitin-conjugating enzyme (E2) and is subsequently attached to the substrate protein in a reaction catalyzed, or assisted, by the ubiquitin ligase (E3). Repeated rounds of ubiquitin transfer to the same lysine reside of the substrate generates a polyubiquitylated protein (Finley*, et al.* 2012).

#### 1.4.1.1. E3 ubiquitin ligases

E3 enzymes are divided into two families based on presence of either of two characteristic domains that define their mechanism of action. Ubiquitin ligases of the HECT domain family contain a highly conserved active-site cysteine in the C-terminal lobe of their ~350-residue HECT domain that forms a thioester bond with ubiquitin prior to its transfer to the substrate protein. The N-terminal lobe of the HECT domain is responsible for recruiting the charged E2-Ub enzyme. In contrast, the RING domain family of E3 enzymes cannot directly bind to ubiquitin and are catalytically inert. These ubiquitin ligases use their zinc-binding globular RING domain to recruit a charged E2-Ub enzyme and facilitate direct ubiquitin transfer from E2 to their bound protein target (Figure 1.4). Substrate recognition in this family of enzymes is either achieved by substrate binding domains within the same protein (single subunit RING E3) or by association of specialized substrate receptors to form multi-subunit E3 enzymes. In fact, most E3 enzymes of the RING domain family are modular proteins in which substrate recognition and ubiquitin conjugation have been delegated to separate subunits (Pickart 2001). *S. cerevisiae* has only five known HECT E3 ligases and the vast majority of its ubiquitin ligases belong to the RING domain family (Finley*, et al.* 2012).

The consensus structural RING domain contains eight conserved cysteine and histidine residues that bind two zinc ions and are classified in two groups: the RING-HC domain that encompasses seven cysteines and one histidine, and the RING-H2 domain that contains six cysteines and two histidines in a special configuration. However, some E3 ligases of this family have structural variants of the RING domain. For instance, APC and SCF are multisubunit E3 ligases that contain the RING domain variants Apc11 and Rbx1, respectively. In these non-canonical RING domains, three zinc ions, instead of two, are coordinated by three clusters of conserved residues (Willems *et al.* 2004).

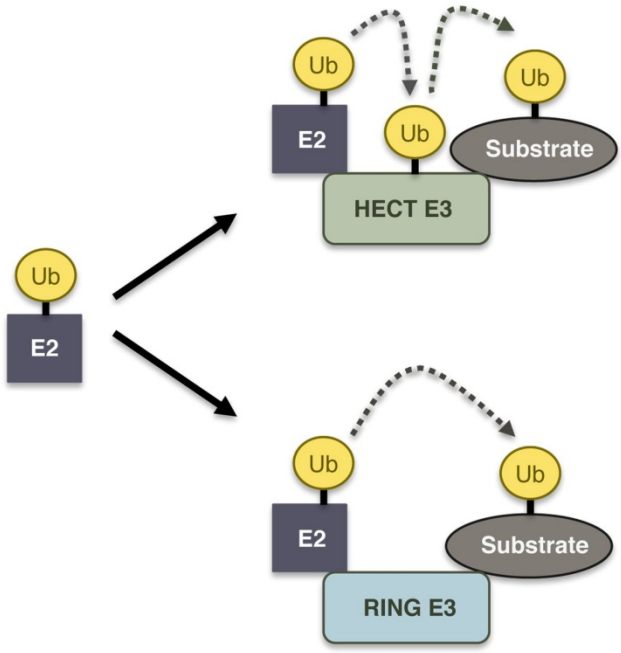


**Figure 1.4 HECT and RING domain E3 ligases.** HECT E3s form a thioester intermediate with ubiquitin before transferring it to the substrate, whereas RING E3s promote direct ubiquitin transfer from activated E2 to the substrate protein (Finley*, et al.* 2012).

#### 1.4.1.1.1. The Skp1-Cullin-F-box (SCF) complex

Skp1-Cullin-F-box (SCF) complexes are conserved E3 ubiquitin ligases that trigger degradation of numerous substrates during the cell cycle. SCF is composed of an unvarying core of three subunits: the linker protein Skp1, the scaffold cullin subunit (human CUL1, yeast Cdc53) and the RING-H2 variant Rbx1 (also known as Hrt1or Roc1). The SCF core complex is assembled around the cullin subunit with Skp1 and Rbx1 binding to the N-terminal and C-terminal regions of Cdc53, respectively. SCF substrates are recognized by a repertoire of adaptor subunits known as F-box proteins. These adaptor subunits bind Skp1 through a 40-residue F-box motif and recruit their specific substrates through various protein interaction domains including WD-40 repeats and leucine-rich repeats (LRR). Rbx1 then recruits an activated E2-Ub that directly conjugates ubiquitin to the SCF-bound target proteins. To date, Cdc34 is the only identified E2 enzyme that collaborates with the SCF complexes in *S. cerevisiae* (Willems*, et al.* 2004).

#### 1.4.1.1.1.1. Regulation of SCF assembly and function

SCF activity is regulated at multiple levels by post-translational modification of the cullin subunit, association of regulatory proteins, F-box protein dimerization and turnover, and substrate modifications.

The cullin subunit of SCF is modified by the ubiquitin-like protein NEDD8 (Rub1 in yeast) that is conjugated to a conserved lysine residue in its C-terminal domain. NEDD8 conjugation, also known as neddylation, is mediated by the heterodimeric E1-like enzyme composed of ULA1 and UBA3, the E2 enzyme UBC12, and the E3 ligase DCN1. This conserved enzymatic cascade is essential for viability in all studied organisms except *S. cerevisiae*. Neddylation promotes SCF activity by inducing a major conformational change in the C-terminal region of cullin such that RBX1 and its bound E2-Ub are positioned close to the F-box protein and its bound substrate for efficient ubiquitin transfer. Moreover, neddylation contributes to the SCF core assembly by preventing the inhibitor protein CAND1 from binding to cullin. CAND1 sequesters the cullin-RBX1 subcomplex by wrapping around unmodified cullin and occluding its N-terminal SKP1 binding site. However, neddylation is dynamically regulated and NEDD8 is removed from cullin by the CNS5 subunit of the COP9 signalosome (CNS) (Merlet *et al.* 2009). In budding yeast, The CNS5 ortholog Rri1 contributes to removal of Rub1 from Cdc53 (Cope *et al.* 2002). Moreover, the yeast deubiquitinating enzyme (DUB) Yuh1 functions primarily in Rub1 removal (Linghu *et al.* 2002).

SCF activity is also regulated by dimerization of its adaptor subunits. Various F-box proteins including human FBW7 and its yeast ortholog Cdc4 form homodimers through a conserved 40-residue D domain located upstream of the F-box motif (Merlet*, et al.* 2009). Cdc4 dimerization is essential for SCF activity *in vivo* because *CDC4* mutants that cannot dimerize fail to complement cells that are deleted for *CDC4*. Moreover, although dimerization is dispensable for Cdc4 to bind its substrates, dimerization greatly stimulates ubiquitylation of the archetypical Cdc4 substrate Sic1 *in vivo* and *in vitro*. Structural analysis of dimeric $SCF^{Cdc4}$ revealed that dimerization provides different distances between

the catalytic site of Cdc34 and the substrate binding site of each Cdc4 molecule in the homodimer, and this configuration has been proposed to facilitate ubiquitin chain formation and elongation (Figure 1.5) (Tang *et al.* 2007).

Moreover, SCF function is modulated by a self-regulatory mechanism that controls the stability of its adaptor subunits. In yeast, the F-box proteins Cdc4, Grr1 and Met30 show intrinsic instability *in vivo*. In spite of the steady levels of Cdc4 and Grr1 during the cell cycle, these proteins are constantly turned over by the ubiquitin-proteasome pathway. Degradation of Cdc4 and Grr1 occurs in an SCF-dependent manner and requires their intact F-box motifs, suggesting that SCF triggers ubiquitylation and subsequent degradation of its bound F-box proteins. It has been speculated that autoubiquitination allows rapid rearrangement of the SCF composition in response to changes in physiological conditions (Galan *et al.* 1999, Zhou *et al.* 1998).

Lastly, substrate recognition by SCF is often controlled by phosphorylation of target proteins. In most cases, SCF substrates must be phosphorylated by cyclin-dependent kinases (Cdks) or other kinases in order to associate with their cognate F-box proteins. This mode of substrate recognition couples SCF-dependent proteolysis to intracellular signaling pathways that control cell cycle progression and other important cellular functions (Tang *et al.* 2005). In addition to phosphorylation, hydroxylation and glycosylation of protein substrates have also been reported for metazoan SCF and SCF-like complexes (Willems*, et al.* 2004).

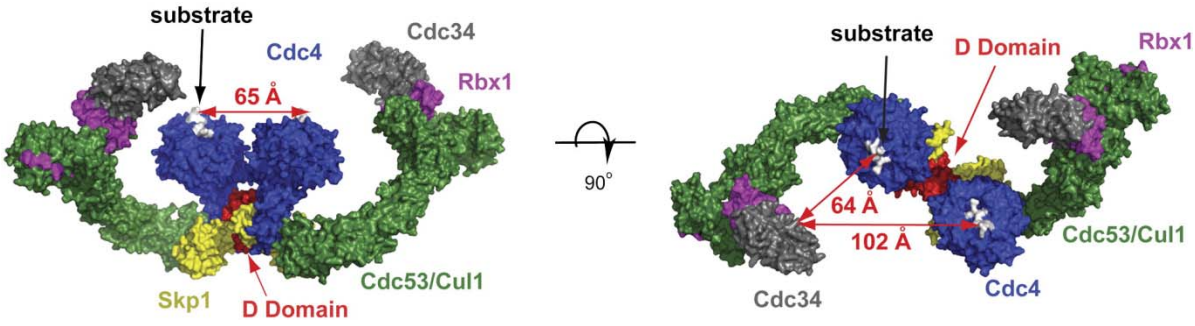


**Figure 1.5 Space-filling representation of the SCF$^{Cdc4}$ homodimer.** The SCF subunits Skp1, Cdc53 and Rbx1 are shown in yellow, green and purple, respectively. The F-box protein Cdc4 is shown in blue and its substrate binding site is in white. The SCF-associated E2 enzyme Cdc34 is shown in grey. The calculated distances between the substrate binding site of each Cdc4 molecule and the Cdc34 catalytic site is also depicted (Tang*, et al.* 2007).

#### 1.4.1.1.1.2. The role of SCF$^{Cdc4}$ in cell cycle regulation

In *S. cerevisiae*, SCF$^{Cdc4}$ is directly involved in control of cell cycle progression. SCF$^{Cdc4}$ triggers the G1/S transition by directing the Cdk1 inhibitor Sic1 to proteasomal degradation, thereby allowing accumulation of cyclin-Cdk1 complexes that drive initiation of DNA synthesis (Willems*, et al.* 2004). Importantly, degradation of Sic1 is sufficient for entry into S phase because a *sic1* null mutation suppresses the G1 arrest phenotype of *CDC4* deleted cells (Goh *et al.* 1999). Furthermore, several lines of evidence suggest that Cdc4 activity contributes to entry and progression through mitosis. First, in addition to a cell cycle arrest in G1, deletion of *CDC4* or inactivation of its conditional alleles gives rise to a population of cells that arrest the cell cycle in G2 or M phase. These *CDC4* mutants take significantly longer to complete mitosis compared to wild-type cells. Moreover, *CDC4* mutants show genetic interactions with mutations in the APC complex and its key mitotic target, securin, that control entry into anaphase. The *cdc4-10* mutation suppresses the thermosensitivity of the APC mutant *cdc20-1*. Moreover, the mitotic arrest phenotype of *cdc4-12* mutants is suppressed by deletion of the yeast ortholog of securin, *PDS1* (Goh*, et al.* 1999). Together, these results suggest that SCF$^{Cdc4}$ might work in parallel with APC to control the metaphase to anaphase transition. Although genetic evidence suggests an

important role for $SCF^{Cdc4}$ during mitosis, mitotic substrates of Cdc4 remain mostly unidentified.

#### 1.4.1.1.1.3. The Cdc4 phosphodegron

To date, all known Cdc4 substrates contain phosphodegron motifs that are mostly generated by Cdk1 (Lyons *et al.* 2013, Tang*, et al.* 2005). Based on the high-affinity phosphodegron of cyclin E, short peptides were generated and characterized for their binding to Cdc4 *in vitro*, yielding I/L-I/L/P-pT-P-$(K/R)_4$ as the consensus Cdc4 phosphodegron (CPD). Surprisingly, in this sequence presence of basic residues, shown in ( ), at the C-terminus of the phosphothreonine was found to be disfavored for Cdc4 binding. Hence, phosphorylation of a consensus Cdk1 site, residing in the S/T-P-X-K/R sequence, generates a weak Cdc4 binding site. Consistent with this prediction, the Cdc4 substrate Sic1 contains nine Cdk1 sites, phosphorylation of at least six of which is required for its degradation. On the other hand, substitution of the weak phosphodegrons of Sic1 with a single high-affinity CPD derived from cyclin E results in premature degradation of Sic1 and causes genomic instability *in vivo*. Therefore, it has been proposed that phosphorylation of Sic1 at multiple Cdk1 sites constitutes a sensitive degradation switch that prevents premature destruction of Sic1 upon small changes in Cdk1 activity during G1 (Nash *et al.* 2001).

In spite of the predicted consensus sequence for Cdc4 binding, study of physiological Cdc4 substrates suggests that CPDs are highly diverse. For instance, in addition to phosphothreonines, phosphoserines are also abundant in natural CPDs (Lyons*, et al.* 2013, Tang*, et al.* 2005). Moreover, the contribution of the residues flanking the phosphorylation site to Cdc4 binding remains uncertain. For example, mutation of the hydrophobic residues preceding the phosphorylation sites in a degron of the Tec1 protein does not affect Tec1 stability *in vivo* (Bao *et al.* 2010). Furthermore, a recent study uncovered that phosphodegrons of several Cdc4 substrates contain two phosphorylation sites that are spaced 2-3 residues apart. This study also demonstrated that the three-residue spacing

between the two phosphorylation sites of the Eco1 degron, S94 and S98, is important for its efficient binding to Cdc4 *in vitro* and Eco1 degradation *in vivo* (Lyons*, et al.* 2013).

### 1.4.2. Protein degradation by the proteasome

As mentioned earlier, formation of specific types of ubiquitin chains on proteins targets them to proteasomal degradation. The proteasome is an ATP-dependent protease that mediates the destruction of polyubiquitylated proteins in eukaryotes. This proteolytic complex consists of two main compartments: the 20S core particle (CP) that contains 28 subunits and the 19S regulatory particle (RP) that is comprised of 19 subunits in *S. cerevisiae*. The CP is organized into a barrel-like structure with its 28 subunits forming four stacks of heptameric rings; the outer α-rings and the inner β-rings. The proteolytic active sites of the enzyme are located in the β1, β2 and β5 subunits and are protected inside the lumen of the CP (Figure 1.6). The α-rings restrict substrate access to the internal chamber of the CP to prevent non-specific proteolysis: in the free form of the CP, the N-terminal regions of all α-subunits occupy the center of the α-ring and block access to the substrate translocation channel of the CP that leads to its catalytic lumen. The α-ring also serves as a docking site for the RP and other CP regulatory proteins. The RP is organized into the nine-subunit lid and the ten-subunit base compartments. The proteasome lid contains the ATP-dependent deubiquitinating enzyme (DUB) Rpn11 that releases ubiquitin chains from RP-bound substrates. The RP base contains the ubiquitin receptors Rpn10 and Rpn13, and a hexameric ATPase ring composed of Rpt1-6. The proteasome holoenzyme forms upon binding of the RP to the end of the CP cylinder (Figure 1.7), and is stabilized by alignment of the Rpt ring of the RP with the α-ring of the CP. This interaction dislocates the N-terminal extensions that occupy the center of the α-ring and opens the substrate translocation channel of the CP (Finley 2009, Finley*, et al.* 2012).

Previous studies have reported physical interaction of the proteasome lid with the components of E3 ligases including SCF and the APC (Verma *et al.* 2000, Xie *et al.* 2000). Therefore, it is possible that E3 enzymes escort their substrates to the degradation

machinery (Willems*, et al.* 2004). Once delivered to the proteasome, the ubiquitin chain of the substrate is recognized and bound by the ubiquitin receptors of the RP. The RP base subunits Rpn10 and Rpn13 and the RP-associated proteins Rad23, Dsk2 and Ddi1 function as ubiquitin receptors. The ubiquitin chain is then removed from the target protein by Rpn11 and the proteasome-associated DUBs Uch37 and Ubp6. The ATP hydrolysis required for Rpn11 activity is probably provided by the Rpt ATPase ring, therefore limiting Rpn11-mediated deubiquitination to proteins that have committed to proteasomal degradation. The Rpt ATPase ring then unfolds bound proteins and passes them into the substrate translocation channel of the CP. Unfolded proteins eventually reach the catalytic lumen of the CP where they are degraded into short peptides by a repertoire of site-specific proteases (Finley 2009, Finley*, et al.* 2012).

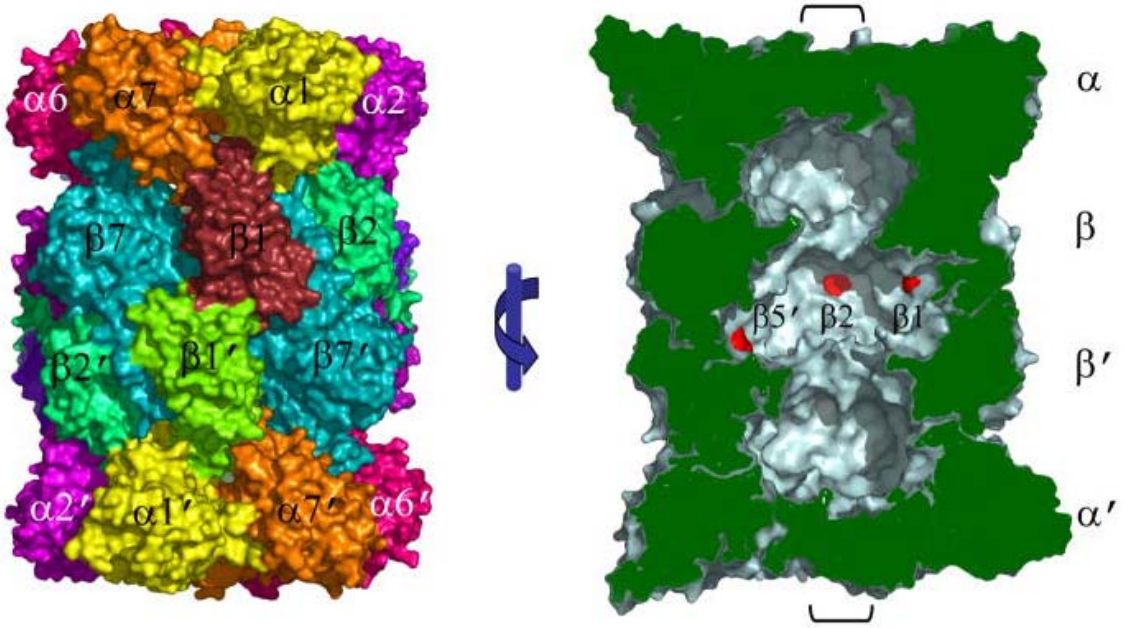


**Figure 1.6 The proteasome core particle (CP)** Left: Surface representation of the free CP along its twofold symmetry axis showing the four stacks of heptameric rings. Each pair of subunits is shown in the same color except for β1 and β1′. Right: medial section of the closed-channel state of the CP demonstrating sequestration of its proteolytic active sites (in red). The approximate position of the entry port of the CP channel in its open state is shown with brackets (Finley 2009).

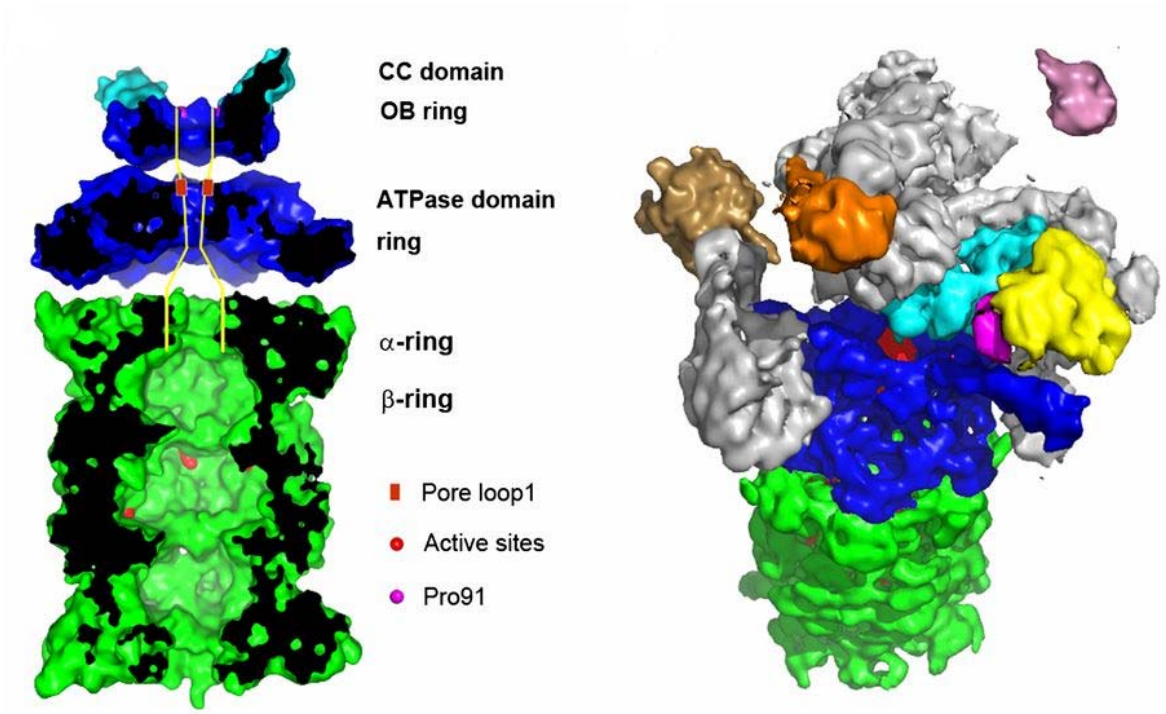


**Figure 1.7 The yeast proteasome holoenzyme.** Left: medial view of the Rpt ring of the RP base in association with the CP. The Rpt ring was modeled based on crystallographic studies of the orthologous PAN ATPase of Archaea. Slice surfaces are shown in black. The ATPase domain and the OB ring of the Rpt ring are shown in blue and its coiled-coil (CC) domain is shown in turquoise. The CP is shown in green and its proteolytic active sites are in red. The yellow lines indicate the presumptive location of the substrate translocation channel. Some structural features of the Rpt ring were not explained in the text for simplicity. Right: Tilted view of the RP. The Rpt ring and the CP are colored as in the left panel. The DUB Rpn11 is shown in turquoise and the presumptive substrate entry port is shown in red directly beneath it. The ubiquitin receptors Rpn13 and Rpn10 are shown in orange and yellow, respectively. Other RP subunits are in gray. Free ubiquitin is shown, in pink, at upper right for comparison (Finley*, et al.* 2012).

## 1.5. Histone H3 lysine 56 acetylation (H3K56ac)

Histone H3 lysine 56 acetylation (H3K56ac) has been detected in several fungal species including *S. cerevisiae* (Masumoto*, et al.* 2005), *Schizosaccharomyces pombe* (Recht *et al.* 2006) and *Candida albicans* (Lopes da Rosa *et al.* 2010, Wurtele *et al.* 2010) and in higher eukaryotes such as Drosophila (Xu *et al.* 2005). The abundance of H3K56ac in human cells has been a matter of controversy. Numerous studies have reported H3K56ac as an abundant histone modification in human cells that contributes to important cellular functions such as the DNA damage response (Das *et al.* 2009, Miller *et al.* 2010, Tjeertes *et al.* 2009, Vempati *et al.* 2010, Yuan *et al.* 2009). Moreover, H3K56ac has been proposed as a diagnostic biomarker for several types of human cancer (Das*, et al.* 2009). However, a quantitative mass spectrometry study established that the stoichiometry of H3K56ac is roughly 0.04% in transformed human cells and does not increase after treatment with several classes of HDAC inhibitors. This work also demonstrated that several commercial antibodies against H3K56ac strongly cross-react with other acetylated lysines in the N-terminal region of histone H3 which have a similar sequence context to K56. This finding suggests that the abundant signal detected by these antibodies probably represents acetylation of histone H3 at sites other than K56 in human cells (Drogaris *et al.* 2012).

Lysine 56 is the last residue of the α-N helix of histone H3 located between the N-terminal tail and the histone fold domain. Based on the crystal structure of the nucleosome core particle, the amino group of H3K56 makes weak electrostatic interactions with the DNA superhelix at its entry and exit points around the histone octamer (Figure 1.8) (Luger*, et al.* 1997). Therefore, it has been speculated that H3K56ac might weaken these histone-DNA contacts by neutralizing the positive charge of lysine (Masumoto*, et al.* 2005, Neumann *et al.* 2009, Xu*, et al.* 2005).

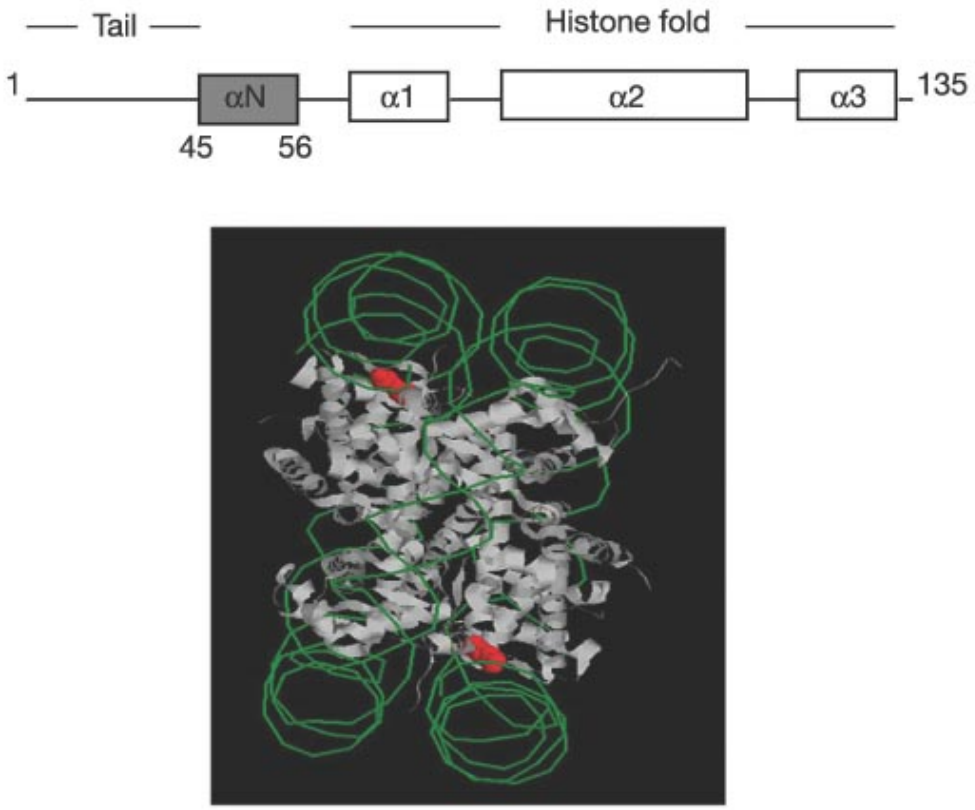


**Figure 1.8 Position of histone H3 lysine 56 in the nucleosome core particle.** Top: lysine 56 is the last residue of the α-N helix of histone H3 located upstream of its histone fold domain. Bottom: the ε-amine group of H3K56, shown in red, makes electrostatic contacts with DNA, shown in green, at the entry and exit points of the nucleosome (Masumoto*, et al.* 2005).

### 1.5.1. Regulation of H3K56ac during the cell cycle and in response to DNA damage

In *S. cerevisiae*, H3K56ac levels peak concomitant to new histone synthesis during S phase (Masumoto*, et al.* 2005). Moreover, this histone mark accumulates prior to the first meiotic division (Recht*, et al.* 2006). Mass spectrometry analysis demonstrated that in the absence of deacetylase activity the stoichiometry of H3K56ac increases to about 50% as cells go from G1 to G2, suggesting that all new H3 molecules that account for 50% of total histones by the end of S phase bear this modification (Celic *et al.* 2006). H3K56ac is mediated by Rtt109 in concert with the histone chaperone Asf1 (Driscoll *et al.* 2007, Han *et al.* 2007a,

Han *et al.* 2007b, Tsubota *et al.* 2007). In the absence of DNA lesions, H3K56ac is removed from the genome during G2 or M phase. However, in response to DNA damage during S phase H3K56ac is sustained by the DNA damage checkpoint. For instance, persistence of H3K56ac in the presence of CPT requires the checkpoint proteins Mec1 and Rad9 (Masumoto*, et al.* 2005).

#### 1.5.1.1. Cell cycle regulated H3K56 deacetylation by Hst3 and Hst4

Deacetylation of H3K56 during G2 or M phase is performed by two HDACs, namely Hst3 and Hst4 (Maas *et al.* 2006, Thaminy *et al.* 2007). Hst3 and Hst4 belong to the sirtuin family of $NAD^+$-dependent deacetylases (Class III), and they were named after the founding member of this family, Sir2 (Homolog of SIR Two) (Brachmann *et al.* 1995). Although the structures of Hst3 and Hst4 remain unresolved, mutational studies have established that the predicted $NAD^+$ binding residues of Hst3, namely, N152, D154 and H184 are required for H3K56 deacetylation *in vivo* (Celic*, et al.* 2006). Moreover, full-length recombinant Hst3 and Hst4 require $NAD^+$ to remove H3K56ac from oligonucleosomes *in vitro*. In addition, as expected for class III HDACs, Hst3 and Hst4 are inhibited by nicotinamide but not TSA (Hachinohe *et al.* 2011). Thus far, H3K56ac is the only known substrate of these sirtuins *in vivo*, because lack of Hst3 and Hst4 does not increase acetylation at other sites in the N-terminal region of histones H3 or H4 (Celic*, et al.* 2006).

Hst3 makes the major contribution to H3K56ac removal by the end of the cell cycle: when arrested in mitosis, *HST3* single mutants (*hst3*Δ cells) show increased levels of H3K56ac, while deletion of *HST4* has no detectable effect on H3K56ac levels measured by immunoblotting. Nevertheless, Hst3 and Hst4 are functionally redundant because in the absence of either sirtuin, H3K56ac is still completely removed from the genome by G1. In contrast, cells deleted for both *HST3* and *HST4* (*hst3*Δ *hst4*Δ cells) show almost 100% H3K56ac throughout the cell cycle confirming these sirtuins as the only H3K56 deacetylases *in vivo* (Celic*, et al.* 2006).

The H3K56ac cycle is maintained by regulation of Hst3 and Hst4 levels during the cell cycle. *HST3* belongs to the same cluster of genes as the mitotic cyclin *CLB2* and is expressed during G2 (Koranda *et al.* 2000, Zhu *et al.* 2000), later than the incorporation of new K56-acetylated H3 molecules into nascent chromatin. Hst3 has a short half-life and is degraded by the ubiquitin-proteasome pathway (Thaminy*, et al.* 2007) by the end of the cell cycle (Maas*, et al.* 2006). However, the molecular machinery that controls the proteasomal destruction of Hst3 at the end of the cell cycle was not identified. Hst4 levels peak later than Hst3 during mitosis, but this sirtuin is still degraded before S phase when H3K56ac levels accumulate behind DNA replication forks (Maas*, et al.* 2006). Hst4 degradation is also controlled by the ubiquitin-proteasome system: Hst4 is phosphorylated by Cdk1 and polyubiquitylated by $SCF^{Cdc4}$ *in vitro*, and its degradation *in vivo* requires Cdc4 activity (Tang*, et al.* 2005).

#### 1.5.1.2. Regulation of Hst3 in response to DNA damage

The main H3K56 deacetylase, Hst3, is downregulated in response to DNA damage during S phase, thus allowing H3K56ac to persist in the genome and contribute to the DNA damage response. Degradation of Hst3 following MMS treatment requires the checkpoint kinases Mec1 and Rad53, but not Dun1 (Maas*, et al.* 2006, Thaminy*, et al.* 2007).

In response to genotoxic stress during S phase, Mec1 might control downregulation of Hst3 by two distinct mechanisms. First, since expression of the *HST3* gene is not detectable in cells released into S phase in the presence of MMS, a previous study proposed that Mec1 promotes transcriptional repression of *HST3* (Maas*, et al.* 2006). However, lack of *HST3* expression in MMS might be a passive consequence of delayed cell cycle progression and reflect the fact that cells did not reach G2 when they normally express *HST3*. In a second pathway, Mec1 triggers phosphorylation of Hst3 and directs it to ubiquitin-mediated degradation by the proteasome, although direct phosphorylation of Hst3 by Mec1 has not been established. Consistent with this, in asynchronously growing wild-type cells the half-life of Hst3 is significantly reduced in the presence of MMS, while Hst3 levels are not affected in *mec1*Δ cells after MMS treatment (Thaminy*, et al.* 2007).

## 1.5.2. Cellular functions of H3K56ac

In *S. cerevisiae*, H3K56ac has been implicated in a number of important cellular functions including replication-coupled nucleosome assembly, replication-independent histone deposition, regulation of gene expression and the DNA damage response. In this section, we describe the evidence that supports a role for this histone modification in the above-mentioned processes.

### 1.5.2.1. The role of H3K56ac in replication-coupled nucleosome assembly

As mentioned earlier, the histone chaperone Rtt106 might assist CAF-1 in deposition of new histones H3 and H4 during replication-coupled nucleosome assembly (Fazly*, et al.* 2012, Huang*, et al.* 2005). H3 molecules that are bound to CAF-1 and Rtt106 during S phase are K56-acetylated (Li*, et al.* 2008, Masumoto*, et al.* 2005). Moreover, H3K56ac enhances the affinity of CAF-1 and Rtt106 for histone H3 *in vitro* and *in vivo*, and promotes nucleosome assembly by these histone chaperones *in vitro*. In addition, the association of CAF-1 with chromatin is partially compromised in the absence of H3K56ac in *rtt109*Δ cells. Altogether, these results indicate that the acetylation of new histone H3 at K56 promotes H3-H4 deposition by CAF-1 and Rtt106 onto nascent chromatin during S phase. Moreover, H3K56ac might direct CAF-1 to the sites of chromatin assembly at the replication fork. Lastly, mutations that abolish H3K56ac show synthetic lethality with mutation of lysine residues in the N-terminal tails of H3 or H4 in the presence of genotoxic agents that cause DNA damage during S phase (Li*, et al.* 2008). This finding might suggest that H3K56ac works in parallel with the redundant acetylation sites in the N-terminal domains of histones H3 and H4 to promote replication-coupled chromatin assembly.

### 1.5.2.2. The role of H3K56ac in replication-independent histone deposition

Acetylation of histone H3 at K56 is not limited to S phase; new H3 molecules that are synthesized during G1 are also K56-acetylated (Masumoto*, et al.* 2005, Rufiange *et al.*

2007). Moreover, although the bulk of new histones are incorporated into chromatin during DNA replication, histone deposition also occurs outside of S phase (Kaplan *et al.* 2008, Rufiange*, et al.* 2007, Verzijlbergen *et al.* 2010). A genome-wide study demonstrated that the replication-independent incorporation of histone H3 largely correlates with transcription and is mainly targeted to promoter regions. However, basal H3 deposition at gene promoters is detectable even in the absence of transcription. This work demonstrated that H3K56ac is enriched at the promoter regions of actively transcribed genes and its abundance correlates with global levels of the transcription-dependent histone H3 deposition (Rufiange*, et al.* 2007). Furthermore, study of histone turnover rates at single nucleosome resolution demonstrated that during G1, Rtt109 and Asf1 promote new histone deposition mostly at dynamically exchanged nucleosomes. Since H3K56 is the only known substrate of Rtt109-Asf1 *in vivo*, this observation suggests that H3K56ac is important for rapid histone turnover at dynamic chromatin regions (Kaplan*, et al.* 2008). Collectively, these results support a role for H3K56ac in replication-independent histone deposition at genomic regions where nucleosomes are rapidly exchanged.

#### 1.5.2.3. The role of H3K56ac in regulation of gene expression

A group of studies have implicated H3K56ac in regulation of gene expression. Cells in which H3 lysine 56 has been mutated into a non-acetylateable arginine (*H3K56R* mutants) have decreased expression of genes encoding histones H2A and H2B. It has been proposed that reduced transcription in *H3K56R* mutants results from diminished recruitment of the SWI/SNF chromatin remodeling complex to the promoter and the coding region of histone genes in the absence of H3K56ac (Xu*, et al.* 2005). Consistently, another group demonstrated that *rtt109*Δ cells have reduced expression of the histone gene *HTA1* encoding histone H2A (Fillingham *et al.* 2009). Moreover, it has been suggested that Asf1 and H3K56ac promote transcription of the model gene *PHO5* by driving chromatin disassembly at its promoter region (Williams *et al.* 2008). In support of these experiments, global levels of H3K56ac correlate with RNA polymerase II occupancy at the promoter region and along the open reading frame of transcribed genes (Rufiange*, et al.* 2007). These results suggest that the incorporation of K56-acetylated histone H3 at transcribed loci might

further enhance gene expression by facilitating recruitment or progression of the transcription machinery at active genomic regions.

#### 1.5.2.4. The contribution of H3K56ac to the DNA damage response

Cells lacking H3K56ac (*i.e. rtt109*Δ, *asf1*Δ or *H3K56R* mutants) are severely sensitive to genotoxic agents that cause DNA damage during S phase, such as MMS or CPT (Driscoll*, et al.* 2007, Han*, et al.* 2007a, Hyland *et al.* 2005, Masumoto*, et al.* 2005, Ozdemir *et al.* 2005, Recht*, et al.* 2006, Schneider *et al.* 2006). These phenotypes indicate that H3K56ac has a critical importance for cell survival following genotoxic stress during DNA synthesis. After transient exposure to MMS during S phase, *rtt109*Δ cells fail to complete DNA replication of large genomic regions and show continual activation of the DNA damage checkpoint. Moreover, these cells show high abundance of persistent nuclear Rad52 foci suggesting the presence of unresolved recombination intermediates. Therefore, the pronounced genotoxic agent sensitivity in the absence of H3K56ac might stem from defects in completion of DNA replication or repair of certain types of DNA lesions (Wurtele *et al.* 2012). However, the precise contribution of H3K56ac to the DNA damage response remains elusive.

A previous study proposed that H3K56ac allows recovery from the DNA damage checkpoint by driving chromatin assembly after completion of DNA repair. This work demonstrated that in the absence of H3K56ac (*asf1*Δ or *rtt109*Δ cells), cells fail to reassemble chromatin and inactivate the DNA damage checkpoint after successful repair of a site-specific HO endonuclease-induced DSB (Chen *et al.* 2008). Nevertheless, it was subsequently demonstrated that a single site-specific DSB is not lethal to *H3K56R* mutant cells (Wurtele*, et al.* 2012). Hence, this system does not recapitulate the severe sensitivity of cells lacking H3K56ac to genome-wide DNA damage caused by genotoxic agents. Moreover, two lines of evidence suggest that the genotoxic agent sensitivity of cells lacking H3K56ac does not result from defects in S phase checkpoint inactivation. First, although deletion of the checkpoint adaptor *RAD9* attenuates activation of Rad53 in response to MMS, *RAD9* deletion severely exacerbates the sensitivity of *rtt109*Δ cells to genotoxic

stress (Thaminy, *et al.* 2007). Moreover, pharmacological inhibition of the S phase checkpoint kinases Mec1 and Tel1 by caffeine does not improve the viability of *rtt109*Δ cells after transient exposure to MMS (Wurtele, *et al.* 2012).

## 1.6. The role of Hst3 and Hst4 in the maintenance of genomic stability

Since Hst3 and Hst4 are functionally redundant, deletion of either sirtuin does not result in severe phenotypes. In contrast, cells lacking both H3K56 deacetylases (*hst3*Δ *hst4*Δ mutants) show pronounced phenotypes such as elevated rates of spontaneous DNA damage, thermosensitivity at 37°C, hypersensitivity to genotoxic agents that damage DNA during S phase, mitotic chromosome missegregation, telomeric silencing defects and reduced sister chromatid cohesion (Brachmann, *et al.* 1995, Celic, *et al.* 2006, Maas, *et al.* 2006, Thaminy, *et al.* 2007, Yang *et al.* 2008). Moreover, *hst3*Δ *hst4*Δ cells have a significantly reduced replicative life span, and their progeny show increased loss of heterozygosity (LOH) which is indicative of genomic instability. It was demonstrated that the LOH phenotype of *hst3*Δ *hst4*Δ daughter cells is mainly caused by an increased incidence of chromosomal truncations, which are highly deleterious to genetic integrity (Hachinohe, *et al.* 2011). The broad range of deleterious phenotypes manifested in the absence of Hst3 and Hst4 suggest that these sirtuins have an essential role in the regulation of DNA metabolism and the maintenance of genomic stability. The severe phenotypes of *hst3*Δ *hst4*Δ cells stem, at least in part, from the failure of the deacetylase mutants to remove H3K56ac from the genome, because the *H3K56R* mutation completely suppresses the temperature sensitivity of *hst3*Δ *hst4*Δ cells and partially alleviates other phenotypes such as the high frequency of mitotic chromosome loss, and sensitivity to genotoxic agents (Celic, *et al.* 2006). Nonetheless, the link between hyperacetylation of H3K56 and genomic instability is poorly understood.

The genomic instability of *hst3*Δ *hst4*Δ cells is also reflected by the fact that these mutants rapidly accumulate spontaneous suppressors of thermosensitivity (Ts) when grown at 37°C (Brachmann, *et al.* 1995). A previous study reported that the vast majority of the Ts

suppressors of H3K56 deacetylase mutants do not show reduced levels of H3K56ac compared to *hst3*Δ *hst4*Δ cells (Miller *et al.* 2006). This finding indicates that unknown genetic and/or epigenetic mechanisms can allow *hst3*Δ *hst4*Δ cells to avoid the catastrophic consequences of H3K56 hyperacetylation.

### 1.6.1. The DNA damage response in *hst3*Δ *hst4*Δ cells

In addition to sensitivity to genotoxic agents, cells lacking Hst3 and Hst4 exhibit spontaneous activation of the DNA damage checkpoint. For instance, *hst3*Δ *hst4*Δ cells show spontaneous accumulation of nuclear foci for the checkpoint protein Ddc2 (Thaminy*, et al.* 2007). Moreover, the H3K56 deacetylase mutants show high levels of Rad53 phosphorylation and strong induction of the DNA damage response genes *HUG1* and *RNR3* in the absence of exogenous genotoxic stress (Celic *et al.* 2008, Thaminy*, et al.* 2007). These phenotypes indicate that *hst3*Δ *hst4*Δ cells suffer from increased levels of spontaneous DNA damage and show chronic activation of the S phase checkpoint.

A previous genetic screen unraveled that *hst3*Δ cells have elevated levels of spontaneous Rad52 foci, which might reflect defects in homologous recombination (HR) (Alvaro *et al.* 2007). During HR in diploid cells, the choice of the identical sister chromatid over the homolog chromosome as repair template is critical for the maintenance of genomic integrity. A recent study demonstrated that repair of DSBs with the sister chromatid, also known as sister chromatid recombination (SCR), is significantly compromised in *hst3*Δ *hst4*Δ cells (Munoz-Galvan *et al.* 2013). This finding unravels yet another mechanism underlying the genomic instability of *hst3*Δ *hst4*Δ cells and suggests that the elevated rates of spontaneous DNA damage in H3K56 deacetylase mutants might partly result from defective repair of specific types of DNA lesions.

### 1.6.2. Genetic interactions of *hst3*Δ *hst4*Δ cells

As noted earlier, in spite of the important role of Hst3 and Hst4 in the maintenance of genomic stability, the mechanisms underlying the severe phenotypes of *hst3*Δ *hst4*Δ mutants remain unknown. Several studies employed a genetic approach to elucidate the cellular pathways that are affected in the absence of Hst3 and Hst4. These studies uncovered genetic interactions between *hst3*Δ *hst4*Δ cells and mutations of genes involved in DNA replication or the DNA damage response.

*hst3*Δ *hst4*Δ cells show genetic interactions with several components of the DNA replication machinery. For instance, overexpression of *RFC1*, the large subunit of the replicative clamp loader, partially suppresses the themosensitivity and genotoxic agent sensitivity of *hst3*Δ *hst4*Δ cells without decreasing the high levels of H3K56ac. On the other hand, H3K56 deacetylase mutants are extremely sensitive to small perturbations in the DNA replication machinery. Introducing the truncated *pol2-11* allele of the DNA polymerase ε causes lethality in *hst3*Δ *hst4*Δ cells. Moreover, epitope tagging of PCNA (Pol30) or the replication protein Cdc45 is lethal in the *hst3*Δ *hst4*Δ background (Celic*, et al.* 2008).

Genetic interactions have also been reported between *hst3*Δ *hst4*Δ cells and mutations in the components of the DNA damage response. Deletion of the checkpoint kinase *MEC1* is lethal in the *hst3*Δ *hst4*Δ background, while deletion of its downstream kinases *CHK1* and *RAD53* are tolerated in these mutants. Moreover, as mentioned earlier Mec1 requires Rad9, the Rad24-RFC clamp loader, and the 9-1-1 clamp (composed of Ddc1-Mec3-Rad17) to relay the DNA damage signal to its effectors. Intriguingly, *RAD9* deletion exacerbates the genotoxic agent sensitivity of *hst3*Δ *hst4*Δ cells (Brachmann*, et al.* 1995, Thaminy*, et al.* 2007), but deletion of *RAD24* or components of the 9-1-1 clamp suppresses the thermosensitivity of these mutants (Celic*, et al.* 2008). Collectively, these interactions suggest that *hst3*Δ *hst4*Δ cells depend on specific components of the S phase checkpoint to survive endogenous and exogenous DNA damage. In addition, *hst3*Δ *hst4*Δ cells show

synthetic lethality with deletion of several components of the DSB repair machinery: deletion of *RAD52*, any of the three subunits of the MRX complex (*MRE11*, *RAD50* or *XRS2*), *SRS2* or *SLX4* is lethal to *hst3*Δ *hst4*Δ cells (Celic*, et al.* 2008). Surprisingly, Rad51, which is also involved in repair of DSBs, is dispensable for viability of cells lacking Hst3 and Hst4. These genetic interactions suggest that *hst3*Δ *hst4*Δ cells depend on certain components of the DNA repair machinery to survive DNA damage.

## 1.7. Problematic and research objectives

As previously mentioned, there is still much to understand about how H3K56 deacetylation is regulated during an unperturbed cell cycle and in response to DNA damage. Moreover, it is not clear how high levels of H3K56ac give rise to the numerous severe phenotypes of *hst3*Δ *hst4*Δ cells. In this thesis, we took advantage of diverse biochemical and genetic approaches to further our understanding of the regulation of H3K56 deacetylation in *S. cerevisiae.*

In the second chapter of this thesis, we first set out to determine the stage of the cell cycle when the main H3K56 deacetylase, Hst3, is degraded. We prioritized this objective in order to understand how the deacetylase-free window is established during each passage through S phase to allow accumulation of H3K56ac behind DNA replication forks. Moreover, since the molecular machinery that promotes proteasomal degradation of Hst3 was previously unidentified, we sought to map the enzymatic cascade that carries out poly-ubiquitylation of Hst3 and directs it to the proteasome by the end of the cell cycle.

In chapter 3, we investigated the mechanisms that underlie the severe phenotypes of H3K56 deacetylase mutants (*hst3*Δ *hst4*Δ cells). In the first section of this study, we used a biochemical approach to gain better insight into the hypersensitivity of *hst3*Δ *hst4*Δ cells to genotoxic stress during S phase. In the second part of this study, we used a genetic approach to identify mechanisms that can bypass the role of Hst3 and Hst4 in the DNA damage response.

# 2. The histone deacetylase Hst3 is regulated by Cdk1 and SCF$^{Cdc4}$ in *Saccharomyces cerevisiae*

Neda Delgoshaie, Xiaojing Tang, Evgeny D. Kanshin,
Pierre Thibault, Mike Tyers and Alain Verreault

(In preparation for submission to the *Journal of Biological Chemistry*)

Dr. Xiaojing Tang from Dr. Mike Tyers' lab performed the *in vitro* kinase assay and the SCF ubiquitination assay on Figure 2.6B
Dr. Evgeny Kanshin from Dr. Pierre Thibault's lab performed the SILAC experiment and mass spectrometry analysis for Figure 2.2C and mass spectrometry analysis for Figure 2.6A
Neda Delgoshaie performed all other experiments and prepared the manuscript

## 2.1. Abstract

In *Saccharomyces cerevisiae*, histone H3 lysine 56 acetylation (H3K56ac) is a modification of new H3 molecules deposited throughout the genome during S phase. H3K56ac is removed primarily by the sirtuin Hst3 after completion of DNA replication. Previous studies have indicated that regulated degradation of Hst3 plays an important role in the genome-wide waves of H3K56 acetylation and deacetylation that occur during each cell cycle. In this manuscript we identify several components of the machinery that regulates Hst3 degradation during the cell cycle. Our *in vivo* and *in vitro* data indicate that Hst3 degradation is mediated by an SCF (Skp1-Cullin-F-box) ubiquitin ligase that contains the F-box protein Cdc4. We also report that Hst3 is phosphorylated at two Cdk1 sites, threonines 380 and 384, *in vivo*. Moreover, we show that phosphorylation of Hst3 at T380 and T384 is important for its degradation, suggesting that these Cdk1 sites comprise an Hst3 "phosphodegron" recognized by $SCF^{Cdc4}$. Unexpectedly, we find that Hst3 is degraded sometime between G2 and anaphase, a period of the cell cycle when Hst3 is needed for genome-wide deacetylation of H3K56. Our results suggest that H3K56 deacetylation and the subsequent degradation of Hst3 by $SCF^{Cdc4}$ are tightly coordinated.

## 2.2. Introduction

During each passage through S phase, eukaryotic cells synthesize new histones that are needed to fill in the gaps in the nucleosome arrays created during DNA duplication. Newly synthesized histones H3 and H4 are acetylated at multiple lysine residues in their N-terminal domains, and acetylation of these sites has been implicated in the replication-coupled nucleosome assembly and the DNA damage response (Verreault 2000). In *Saccharomyces cerevisiae*, histone H3 is also acetylated at lysine 56 within its globular "histone fold" domain (Masumoto*, et al.* 2005, Ozdemir*, et al.* 2005, Xu*, et al.* 2005). Histone H3 lysine 56 acetylation (H3K56ac) occurs in all new H3 molecules that are deposited onto nascent chromatin behind DNA replication forks during S phase (Masumoto*, et al.* 2005). This modification is mediated by the histone acetyltransferase

Rtt109 in concert with the histone chaperone Asf1 (Driscoll, *et al.* 2007, Han, *et al.* 2007a, Han, *et al.* 2007b, Tsubota, *et al.* 2007). H3K56ac promotes cell viability in the face of DNA damage, because cells that lack this modification (*i.e. RTT109* or *ASF1*-deleted cells or *H3K56R* mutants in which lysine 56 has been mutated into a non-acetylateable arginine) show severe sensitivity to genotoxic agents that cause DNA damage during S phase (Driscoll, *et al.* 2007, Han, *et al.* 2007a, Hyland, *et al.* 2005, Masumoto, *et al.* 2005, Ozdemir, *et al.* 2005, Recht, *et al.* 2006, Schneider, *et al.* 2006, Tsubota, *et al.* 2007, Wurtele, *et al.* 2012). In the absence of DNA lesions that interfere with completion of DNA replication, H3K56ac is removed from the genome during G2 or M phase (Masumoto, *et al.* 2005) by two cell cycle-regulated histone deacetylases known as Hst3 and Hst4 (Celic, *et al.* 2006, Maas, *et al.* 2006, Thaminy, *et al.* 2007). However, in response to DNA damage during S phase, H3K56ac is maintained in the genome by the DNA damage response, where it persists at sites of DNA damage (Maas, *et al.* 2006, Masumoto, *et al.* 2005).

Hst3 and Hst4 belong to the sirtuin family of nicotinamide adenine dinucleotide ($NAD^+$)-dependent deacetylases (Brachmann, *et al.* 1995). *HST3* is expressed from the end of S phase until mitosis as part of a gene cluster including the mitotic cyclin *CLB2* (Koranda, *et al.* 2000, Zhu, *et al.* 2000). Hst3 is a short-lived protein, and it gets degraded near the end of the cell cycle by the proteasome (Thaminy, *et al.* 2007). However, the molecular machinery that controls the destruction of Hst3 has not been identified. Hst4 levels peak later than Hst3 in G2 or M phase, but Hst4 degradation is also completed before S phase when H3K56ac accumulates in the genome (Maas, *et al.* 2006). Hst3 and Hst4 show some functional redundancy because H3K56ac removal is only completely abolished in the absence of both sirtuins (*hst3*Δ *hst4*Δ cells) (Celic, *et al.* 2006, Maas, *et al.* 2006). In fact, mass spectrometry analysis has established that the stoichiometry of H3K56ac increases to about 98% in *hst3*Δ *hst4*Δ cells arrested in G2/M (Celic, *et al.* 2006). Nevertheless, *HST3* single mutants (*hst3*Δ) show a much greater increase in H3K56ac levels compared to *HST4* deleted cells (*hst4*Δ) suggesting that Hst3 is the main H3K56 deacetylase (Celic, *et al.* 2006, Maas, *et al.* 2006).

Skp1-Cullin-F-box (SCF) is a conserved E3 ubiquitin ligase that controls the degradation of numerous substrates by the proteasome. In *S. cerevisiae*, the SCF core is composed of the linker protein Skp1, the scaffold protein Cdc53 and the RING protein Rbx1 (also known as Hrt1 or Roc1). The SCF substrates are recruited by a variety of adaptor F-box subunits, each recognizing a specific set of target proteins. SCF also associates with the E2 ubiquitin conjugating enzyme Cdc34 that directly builds lysine 48-linked ubiquitin chains onto substrates that are bound to F-box proteins. In most cases, phosphorylation of SCF substrates by cyclin-dependent kinase 1 (Cdk1) or other kinases is necessary for their recognition by cognate F-box proteins (Willems*, et al.* 2004). For instance, all known substrates of the F-box protein Cdc4 are phosphorylated, often by Cdk1, as a prerequisite for their SCF-mediated destruction (Lyons*, et al.* 2013, Tang*, et al.* 2005). $SCF^{Cdc4}$ is directly involved in the regulation of cell cycle progression. Cdc4 controls the G1/S transition of the cell cycle by directing the Cdk1 inhibitor Sic1 to the proteasome, thereby allowing accumulation of Cdk1 activity required for the initiation of DNA synthesis (Verma *et al.* 1997). Moreover, genetic evidence suggests an important function for Cdc4 in entry and progression through mitosis (Goh*, et al.* 1999), although mitotic substrates of Cdc4 remain mostly unknown.

In this manuscript, we investigated the mechanisms that control Hst3 degradation during the cell cycle in *S. cerevisiae*. We found that Hst3 degradation can be completed prior to anaphase. Moreover, we identified phosphorylation of Hst3 at two Cdk1 sites, threonines 380 and 384, and demonstrated that these phosphorylation events limit the abundance of Hst3 *in vivo*. Our results indicate that Hst3 levels are directly controlled by Cdk1 and $SCF^{Cdc4}$, therefore establishing Hst3 as an immediate target of the molecular machinery that regulates progression through the cell cycle.

## 2.3. Material and methods

### 2.3.1. Yeast strains

All strains used in this study are listed in Table 2.1. Yeast strains were generated by standard methods and grown under standard conditions unless otherwise stated.

**Table 2.1 Yeast strains**

| | |
|---|---|
| NDY1 | *MAT*a *leu2-3,112 ura3-1 trp1-1 his3-11,15 ade2-1 can1-100 HST3-TAP::HIS3MX6* |
| NDY7 | *MAT*a *leu2-3,112 ura3-1 TRP1 his3-11,15 ade2-1 can1-100* [*PSI+*] *rad5-535 cdc23-1 HST3-TAP::HIS3MX6* |
| NDY224 | *MAT*a *ade2-1 can1-100 his3-11,15 leu2-3, 112 trp1-1 ura3-1* [*PSI+*] *rad5-535 PDS1-HA::URA3 HST3-TAP::HIS3MX6* |
| HWYG12 | FY *MAT*a *his3Δ200 leu2Δ1 lys2Δ202 trp1Δ63 ura3-52 hst3Δ::KANMX hst4Δ::TRP1* |
| NDY241 | FY *MAT*a *his3Δ200 leu2Δ1 lys2Δ202 trp1Δ63 ura3-52 hst3Δ::KANMX hst4Δ::TRP1* [p*CEN-URA3-HST3*] [p*CEN-LEU2-HST3-TAP*] |
| NDY244 | FY *MAT*a *his3Δ200 leu2Δ1 lys2Δ202 trp1Δ63 ura3-52 hst3Δ::KANMX hst4Δ::TRP1* [*pCEN-URA3-HST3*] [p*CEN-LEU2-HST3 T380A-TAP*] |
| NDY247 | FY *MAT*a *his3Δ200 leu2Δ1 lys2Δ202 trp1Δ63 ura3-52 hst3Δ::KANMX hst4Δ::TRP1* [p*CEN-URA3-HST3*] [*pCEN-LEU2-HST3 T384A-TAP*] |
| NDY250 | FY *MAT*a *his3Δ200 leu2Δ1 lys2Δ202 trp1Δ63 ura3-52 hst3Δ::KanMX hst4Δ::TRP1* [p*CEN-URA3-HST3*] [p*CEN-LEU2-HST3 2A-TAP*] |
| NDY343 | *MAT*a *leu2-3,112 ura3-1 trp1-1 his3-11,15 ade2-1 can1-100 cdc34-2 HST3-TAP::HIS3MX6* |
| NDY344 | *MAT*a *leu2-3,112 ura3-1 trp1-1 his3-11,15 ade2-1 can1-100 cdc53-1 HST3-TAP::HIS3MX6* |
| NDY196 | *MAT*a *ade2-1 can1-100 his3-11,15 leu2-3,112 trp1-1 ura3-1* [*PSI+*] *rad5-535 cdc4-1 HST3-TAP::HIS3MX6* |
| NDY310 | *MAT*a *cdc4-10 leu2-3,112 his3-11 trp1-1 ura3 HST3-TAP::HIS3MX6* |
| NDY318 | *MAT*a *cdc4Δ::URA3 leu2-1,112 his3-11 trp1-1* [p*CEN-cdc4-12-TRP1-LEU2*] *HST3-TAP::HIS3MX6* |

### 2.3.2. Construction of p*CEN-Hst3-TAP* plasmids

The original plasmid used to generate all p*CEN-HST3-TAP* constructs was the p*CEN-URA3-HST3* plasmid that was previously described (Celic*, et al.* 2006). We employed homologous recombination in yeast to replace the *URA3* marker on the original plasmid with *LEU2* and generate the p*CEN-LEU2-HST3* plasmid. We used the same method to TAP-tag the C-terminal domain of Hst3 in p*CEN-LEU2-HST3*. The resulting construct was p*CEN-LEU2-HST3-TAP* that is referred to as p*CEN-HST3-TAP* throughout the manuscript. Either or both Cdk1 sites of Hst3, T380 and T384, were mutated into alanine in p*CEN-HST3-TAP* by site-directed mutagenesis using the PfuTurbo DNA polymerase (Agilent) to generate p*CEN-HST3 T380A-TAP*, p*CEN-HST3 T384A-TAP* and p*CEN-HST3 2A-TAP*, respectively. These plasmids were individually transformed into the *hst3*Δ *hst4*Δ [p*CEN-URA3-HST3*] strain (HWYG12) to generate the yeast strains NDY241, NDY244, NDY247 and NDY250 (Table 2.1). Because *hst3*Δ *hst4*Δ mutants rapidly accumulate spontaneous suppressors (Brachmann*, et al.* 1995), the aforementioned strains were covered by the p*CEN-URA3-HST3* plasmid encoding wild-type Hst3, in case that the Cdk1 site mutants of *HST3* behaved as null mutations. Prior to each experiment, strains were streaked on plates containing 5-Fluoroorotic Acid (5-FOA) to remove the p*CEN-URA3-HST3* plasmid.

### 2.3.3. Time course experiments and cell synchronization techniques

For time course experiments, cultures were grown to early exponential phase at 30°C (or at 23°C for thermosensitive mutants) overnight. Cells were arrested in G1 with 5 μg/ml of α-factor for 2-3 h. To release cells from the G1 arrest, cell pellets were washed with water and resuspended in fresh medium containing 100 μg/ml pronase. For nocodazole arrest, cells were released from G1 into fresh medium containing 15 μg/ml of nocodazole added from a 15 mg/ml stock in dimethyl sulfoxide. To inactivate all thermosensitive mutants, cultures were switched to the restrictive temperature of 37°C. During the time course, aliquots were taken for immunoblots and determination of DNA content by flow

cytometry. Immunoblot samples were immediately flash frozen on dry ice. Flow cytometry samples were fixed in 70% ethanol and processed as described below.

### 2.3.4. Measurement of DNA content by flow cytometry

Cellular DNA content was measured by fluorescence-activated cell sorting (FACS) using Sytox Green (Invitrogen) as nucleic acid stain (Haase *et al.* 2002). About $2x10^6$ cells were fixed in 70% ethanol for a minimum of 30 min at 4°C. Cells were pelleted, resuspended in 500 µl of 50 mM Tris-HCl, pH 7.5 containing 400 µg/ml of ribonuclease A (Sigma) and incubated at 37°C overnight. Cell pellets were resuspended in 200 µl of 50 mM Tris-HCl, pH 7.5 buffer containing 400 µg/ml proteinase K (Sigma) and incubated for 30 min at 50°C. Cells were then resuspended in 500 µl of 50 mM Tris-HCl, pH 7.5. Samples were prepared by adding 100 µl of processed cell suspension to 900 µl of 50 mM Tris-HCl, pH 7.5 containing 1 µM Sytox Green (Invitrogen). FACS analysis was performed on BD Biosciences LSR II or FACSCanto II cytometers using the FACS Diva software. Histograms were generated using the FCS Express Version 3 software.

### 2.3.5. Immunoblots

Whole-cell yeast extracts were prepared from flash-frozen samples using a previously described alkaline method (Kushnirov 2000). For Hst3 immunoblots, whole-cell extracts were separated through SDS 12%–polyacrylamide gels by electrophoresis. Proteins were transferred to PVDF membranes using standard Towbin buffer (25 mM Tris, 192 mM glycine) containing 5% methanol and 0.02% SDS on a Bio-Rad SD semi-dry transfer apparatus. Transfer settings were 1 $mA/cm^2$ of transfer area at 20 V for 2 h. The anti-TAP antibody was purchased from Open Biosystems. The anti-HA monoclonal antibody was 12CA5.

### 2.3.6. Mass spectrometry identification of Hst3 phosphorylation sites

Hst3 phosphorylation sites were identified during the course of a phosphoproteome study performed with wild-type cells (Kanshin *et al.* 2012). The Hst3 phosphorylation sites were identified from whole-cell lysates without prior purification of the Hst3 protein. The *in vivo* phosphorylation data were obtained from a SILAC experiment that used [$^{13}C_6$, $^{15}N_4$] heavy arginine, rather than the [$^{12}C_6$, $^{14}N_4$] natural form of arginine. Because of this, the mass of the doubly charged precursor peptide obtained from Hst3 in whole-cell lysates grown in SILAC medium is 5 Da higher than the theoretical mass of the natural peptide (Figure 2.2C). The phosphorylated peptide of Hst3 identified after an *in vitro* kinase reaction was derived from the recombinant protein containing only naturally occurring amino acids (Figure 2.6A).

### 2.3.7. Expression and purification of recombinant Hst3

Recombinant wild-type Hst3 was expressed from the previously described p*ET28b-FLAG-HIS10-HST3* plasmid (PHM187) (Hachinohe*, et al.* 2011). The Hst3 expression construct was transformed into ArcticExpress (Agilent) *E. coli* cells. Expression of Hst3 was induced by addition of 1 mM isopropyl-β-D-thiogalactopyranoside (IPTG) to cells grown in LB medium at 11.5°C. Cells were collected after 48 h of induction and flash-frozen on dry ice. His-tagged Hst3 was purified from ArcticExpress cell lysates using the Ni-NTA spin kit according to the manufacturer's instructions (Qiagen).

### 2.3.8. *In vitro* kinase and $SCF^{Cdc4}$ ubiquitylation assays on recombinant Hst3

Hst3 was phosphorylated by Clb2-Cdk1 or cyclin A-CDK2 after incubation for 1 h at 30°C in 50 mM HEPES, pH 7.2, 2 mM ATP, 10 mM $MgCl_2$ and 1 mM DTT. Ubiquitylation reactions contained 0.4 µM E1 (Uba1), 2 µM Cdc34, 0.1 µM $SCF^{Cdc4}$, 40 µM ubiquitin (K0), 2 mM ATP, 10 mM $MgCl_2$, 50 mM NaCl, 0.1 mM DTT and 50 mM HEPES, pH 7.2.

Reactions were incubated for 1 h at 30°C. Clb2-Cdk1 was kindly provided by Dr. Adam Rudner (University of Ottawa).

## 2.4. Results

### 2.4.1. The H3K56 deacetylase Hst3 can be degraded prior to anaphase

In this manuscript, we investigated the molecular mechanisms that control the proteasomal degradation of the main H3K56 deacetylase, Hst3, during the cell cycle in *S. cerevisiae*. Although it has not been formally established, previous studies suggest that the degradation of Hst3 occurs by the end of the cell cycle (Maas*, et al.* 2006, Thaminy*, et al.* 2007). In order to identify the molecular machinery that controls Hst3 levels, we first set out to determine when Hst3 was degraded during the cell cycle. Wild-type cells expressing TAP-tagged Hst3 were synchronized in G1 and released in the presence of the microtubule-depolymerizing agent nocodazole. Through activation of the spindle checkpoint, nocodazole prevents cells from entering anaphase. Immunoblots revealed that Hst3 was degraded in cells arrested in metaphase in the presence of nocodazole (Figure 2.1A). The anaphase promoting complex (APC) is an E3 ubiquitin ligase that controls entry into anaphase by triggering the degradation of securin (yeast Pds1) and unleashing separase (yeast Esp1)-mediated cleavage of proteins involved in sister chromatid cohesion (Ciosk *et al.* 1998, Cohen-Fix *et al.* 1996). To confirm that Hst3 degradation occurs prior to anaphase, we employed the APC thermosensitive *cdc23-1* mutant expressing TAP-tagged Hst3. *cdc23-1* cells were released from G1 at the permissive temperature of 23°C and were later switched to the restrictive temperature of 37°C to inactivate APC and block cells in metaphase. Consistent with our previous result, Hst3 was degraded in *cdc23-1* cells at the restrictive temperature (Figure 2.1B). Lastly, we also monitored the timing of Hst3 degradation relative to the APC substrate Pds1. We released cells co-expressing TAP-tagged Hst3 and HA-tagged Pds1 from G1 in the presence of nocodazole and found that Hst3 was degraded while Pds1 levels remained mostly stable (Figure 2.1C). Taken

together, these results demonstrate that Hst3 degradation can occur prior to entry into anaphase and does not require APC activity.

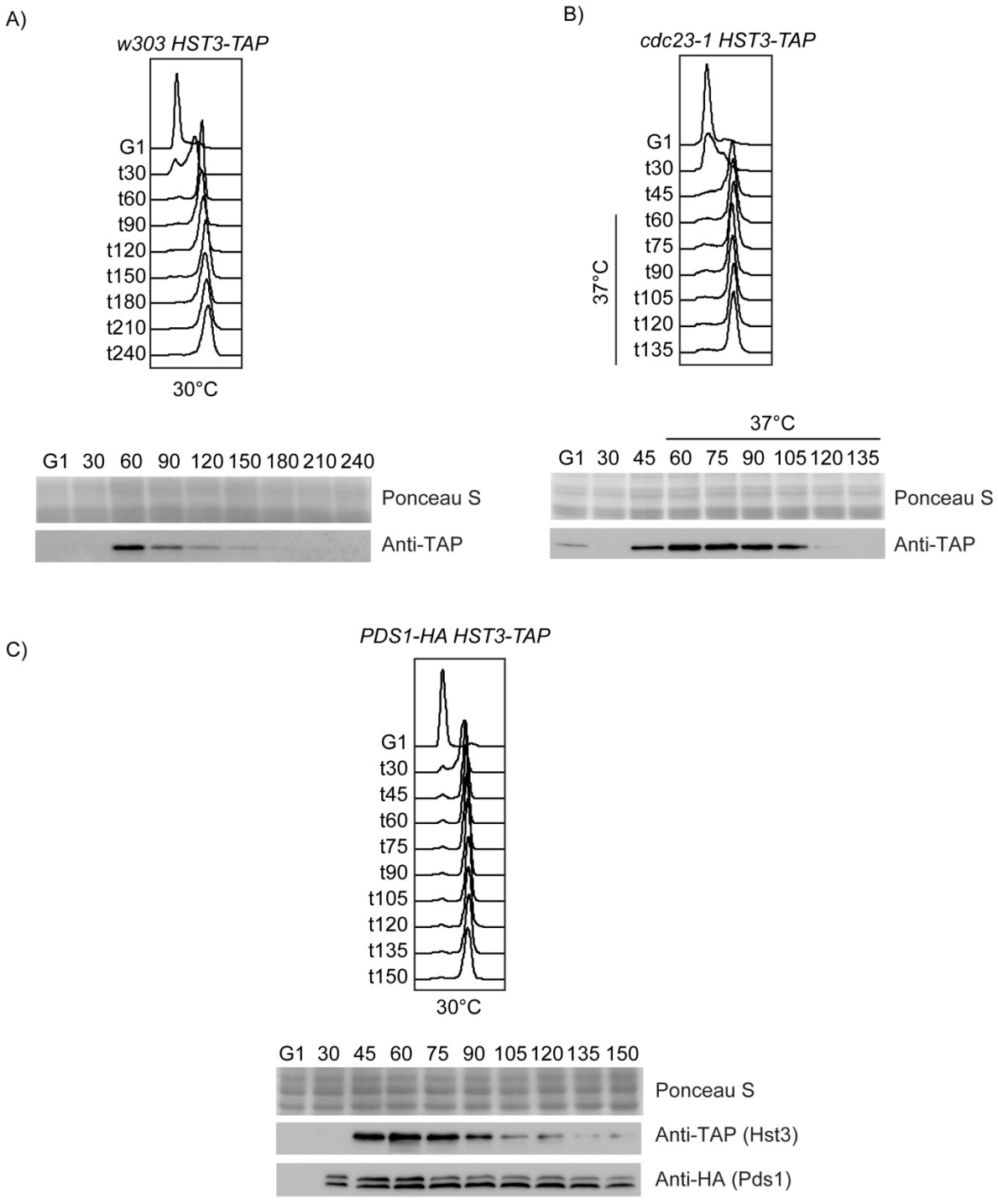


**Figure 1**

**Figure 2.1 The degradation of Hst3 can be completed before anaphase.** A) Hst3 is down-regulated in cells arrested in nocodazole. Wild-type cells expressing TAP-tagged Hst3 were released from G1 in the presence of nocodazole at 30°C, and aliquots were

collected as a function of time. Cell cycle progression was monitored by FACS. Hst3 levels were assessed by immunoblotting with anti-TAP antibody. Ponceau S staining is shown as a loading control. B) Hst3 can be degraded prior to anaphase in the absence of APC activity. *cdc23-1 HST3-TAP* cells were released from G1 at 23°C and switched to the restrictive temperature of 37°C after 45 min to inactivate APC. Samples were analyzed as in panel A. C) Hst3 degradation occurs when the APC substrate Pds1 is stable. *PDS1-HA HST3-TAP* cells were released from G1 into nocodazole at 30°C. Samples were processed as in panel A.

### 2.4.2. Hst3 is phosphorylated at two Cdk1 sites, threonines 380 and 384, *in vivo*

To gain insight into mechanisms that control the degradation of Hst3 before anaphase, we searched for the presence of putative regulatory motifs in the Hst3 sequence. Cdk1 is an integral component of the cell cycle control machinery that phosphorylates a myriad of proteins during the cell cycle. The consensus sequence for phosphorylation by Cdk1 is S/T*-P-X-R/K, in which the phosphorylation site (marked with *) is followed by a basic residue at the +3 position, but many Cdk1 substrates are also phosphorylated at minimal S/T-P motifs (Holt *et al.* 2009, Ubersax *et al.* 2003). We found that the C-terminal domain of Hst3 contains a consensus Cdk1 site at T384 closely preceded by a minimal Cdk1 site at T380. These threonine residues are located outside the predicted catalytic core of Hst3 (Figure 2.2A). Sequence alignments of Hst3 orthologs from several fungal species revealed that these two Cdk1 sites of Hst3 and their spacing are conserved in the pathogenic fungi *Candida albicans* and *Candida tropicalis* (Figure 2.2B), suggesting that phosphorylation of Hst3 at these sites might have an important regulatory function. In support of this, mass spectrometry analysis of whole cell lysates prepared from asynchronous *S. cerevisiae* cultures revealed that Hst3 is phosphorylated at both T380 and T384 *in vivo* (Figure 2.2C).

A)

```
   > Hst3 (YOR025W)
  1  MTSVSPSPPA SRSGSMCSDL PSSLQTEKLA HIIGLDADDE VLRRVTKQLS
 51  RSRRIACLTG AGISCNAGIP DFRSSDGLYD LVKKDCSQYW SIKSGREMFD
101  ISLFRDDFKI SIFAKFMERL YSNVQLAKPT KTHKFIAHLK DRNKLLRCYT
151  QNIDGLEESI GLTLSNRKLP LTSFSSHWKN LDVVQLHGDL KTLSCTKCFQ
201  TFPWSRYWSR CLRRGELPLC PDCEALINKR LNEGKRTLGS NVGILRPNIV
251  LYGENHPSCE IITQGLNLDI IKGNPDFLII MGTSLKVDGV KQLVKKLSKK
301  IHDRGGLIIL VNKTPIGESS WHGIIDYQIH SDCDNWVTFL ESQIPDFFKT
351  QDQIKKLRQL KREASDLRKQ MKAQKDSIGT PPTTPLRTAQ GIDIQGNNEL
401  NTKIKSLNTV KRKILSPENS SEEDEEENLD TRKRAKIRPT FGDNQAS*
```

B)

| Hst3 ortholog | Sequence extract |
|---|---|
| *S. cerevisiae* Hst3 (YOR025W) | 380 TPPTTPLR 387 |
| *C. albicans* Hst3 (SC5314) | 409 TPPTTPHK 416 |
| *C. tropicalis* C05386 | 440 SPPTTPNK 447 |

C) Hst3 376-387: DSIGpTPPTpTPLR

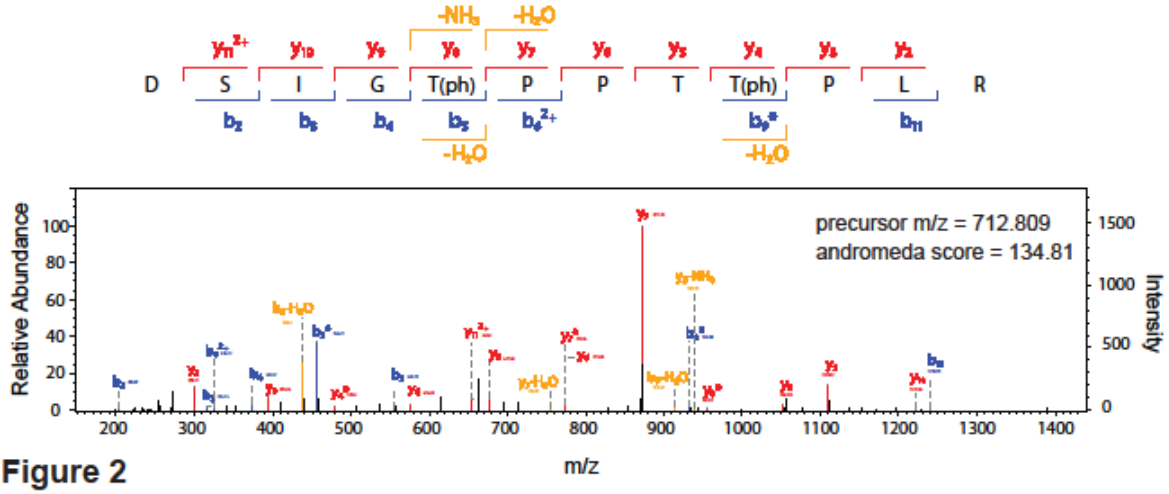


Figure 2

**Figure 2.2 Hst3 is phosphorylated at the Cdk1 sites T380 and T384 *in vivo*.** A) Hst3 contains two putative Cdk1 sites at T380 and T384, highlighted in red. These Cdk1 sites are located outside of the predicted catalytic core of Hst3, residues 53-340, shown in bold characters. B) The two Cdk1 sites of Hst3 and their spacing are conserved in the pathogenic fungi *C. albicans* and *C. tropicalis*. C) Hst3 is phosphorylated at T380 and T384 *in vivo*. The figure shows a fragmentation spectrum containing a near complete *y*-ion series and a partial *b*-ion series. The positions of the two phospho-threonines are consistent with the observed masses of several *y*- and *b*-ions. The measured *m/z* ratio of the $[M+2H]^{2+}$ precursor peptide is indicated. The phosphorylated Hst3 peptide was identified from a phosphoproteome of cells labeled with [$^{13}$C6, $^{15}$N4] arginine. The experimentally determined mass of the intact peptide is within ppm of the theoretical mass for the doubly phosphorylated peptide containing a C-terminal [$^{13}$C6, $^{15}$N4] arginine.

### 2.4.3. Phosphorylation of Hst3 at T380 and T384 promotes its degradation

In order to uncover the physiological function of Hst3 phosphorylation at T380 and T384, we mutated either or both Cdk1 sites of Hst3 into non-phosphorylatable alanine. These constructs were named Hst3 T380A, Hst3 T384A and Hst3 2A, respectively. Wild-type or Cdk1 site mutants of Hst3 were expressed from the natural *HST3* promoter on a centromeric plasmid in cells lacking endogenous copies of *HST3* and *HST4* (*hst3*Δ *hst4*Δ cells). When cells were released from G1 in the presence of nocodazole, all three Cdk1 site mutants of Hst3 showed a significant increase in abundance, and unlike wild-type Hst3, these mutants were not degraded in the presence of nocodazole. Moreover, mutation of either Cdk1 site stabilized Hst3 to the same extent as mutation of both Cdk1 sites (Figure 2.3). Collectively, these results suggest that phosphorylation of Hst3 at T380 and T384 constitutes a "phosphodegron" that triggers its subsequent degradation.

### 2.4.4. Hst3 degradation requires components of the SCF ubiquitin ligase

Our results indicated that phosphorylation of Hst3 at its Cdk1 sites is a prerequisite for its degradation. This requirement is characteristic of SCF substrates (Tang, *et al.* 2005). Hence, we tested whether the destruction of Hst3 was dependent on SCF activity by assessing Hst3 levels in the temperature-sensitive *cdc53-1* mutant. *cdc53-1* cells were released from G1 in the presence of nocodazole at permissive temperature and were switched to the restrictive temperature of 37°C after 120 min. Late inactivation of *cdc53-1* was to ensure that SCF performed its essential roles during the G1/S and G2/M transitions so that cells reached the metaphase block in nocodazole. Hst3 was not degraded in *cdc53-1* cells at restrictive temperature even after 4 h in the presence of nocodazole (Figure 2.4A). This is much longer than the time required for the degradation of Hst3 in wild-type cells (Figure 2.1A).

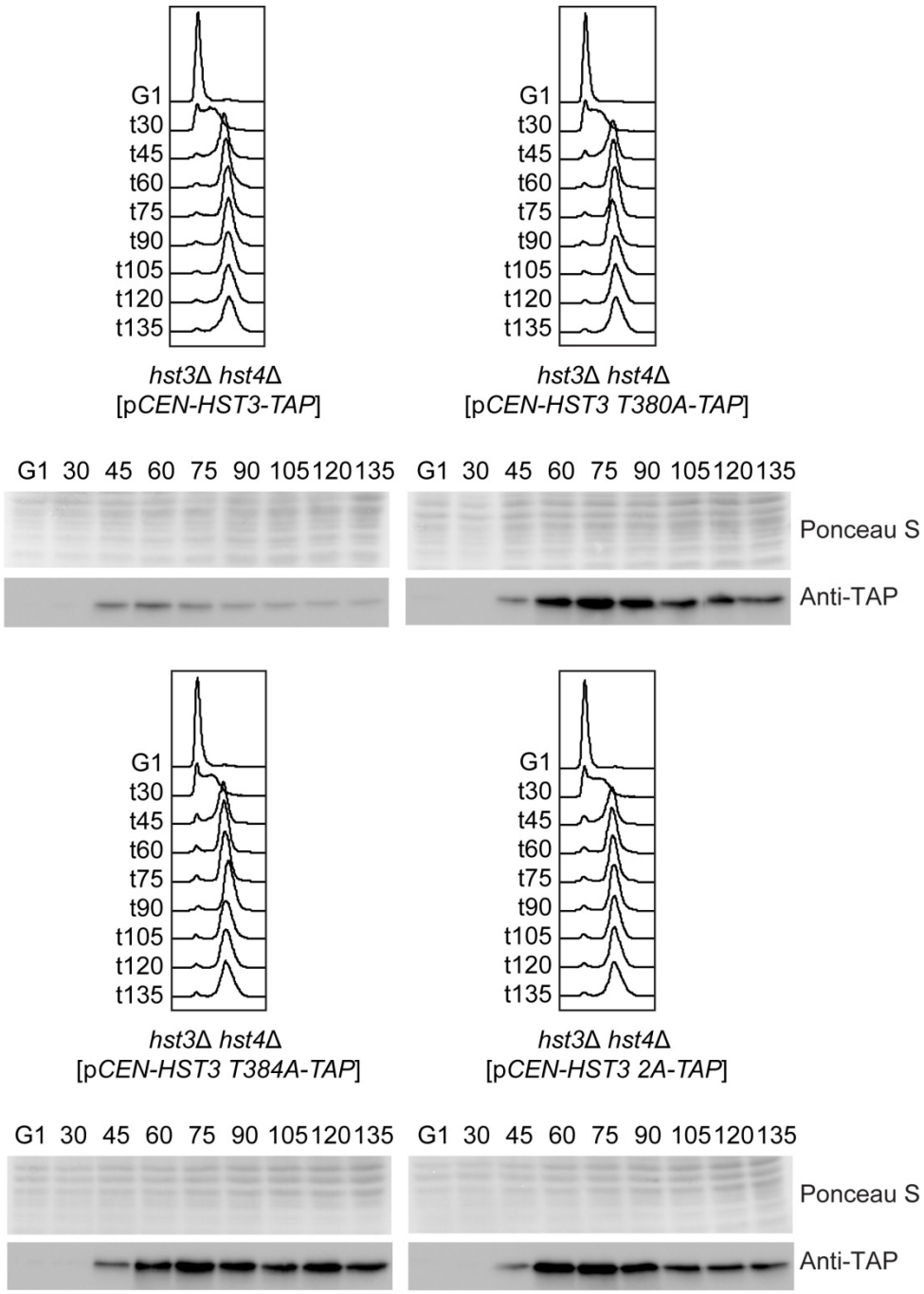


**Figure 3**

**Figure 2.3 Phosphorylation of Hst3 at T380 and T384 promotes its destruction.** Cells expressing TAP-tagged wild-type Hst3, as control, or the Cdk1 site mutants of Hst3 were synchronized in G1 and released in the presence of nocodazole at 30°C. Samples were processed by FACS, and immunoblotting with anti-TAP antibody. Ponceau S is shown as a loading control.

Next, we employed the thermosensitive *cdc34-2* mutant to verify whether the SCF-associated E2 enzyme Cdc34 was required for the degradation of Hst3. *cdc34-2* cells were released from G1 into medium containing nocodazole and were switched to the restrictive temperature of 37°C after 90 min. Consistent with our previous result, *cdc34-2* cells also failed to degrade Hst3 at restrictive temperature after 4 h in the presence of nocodazole (Figure 2.4B). These results demonstrate that SCF activity is required for Hst3 degradation prior to anaphase.

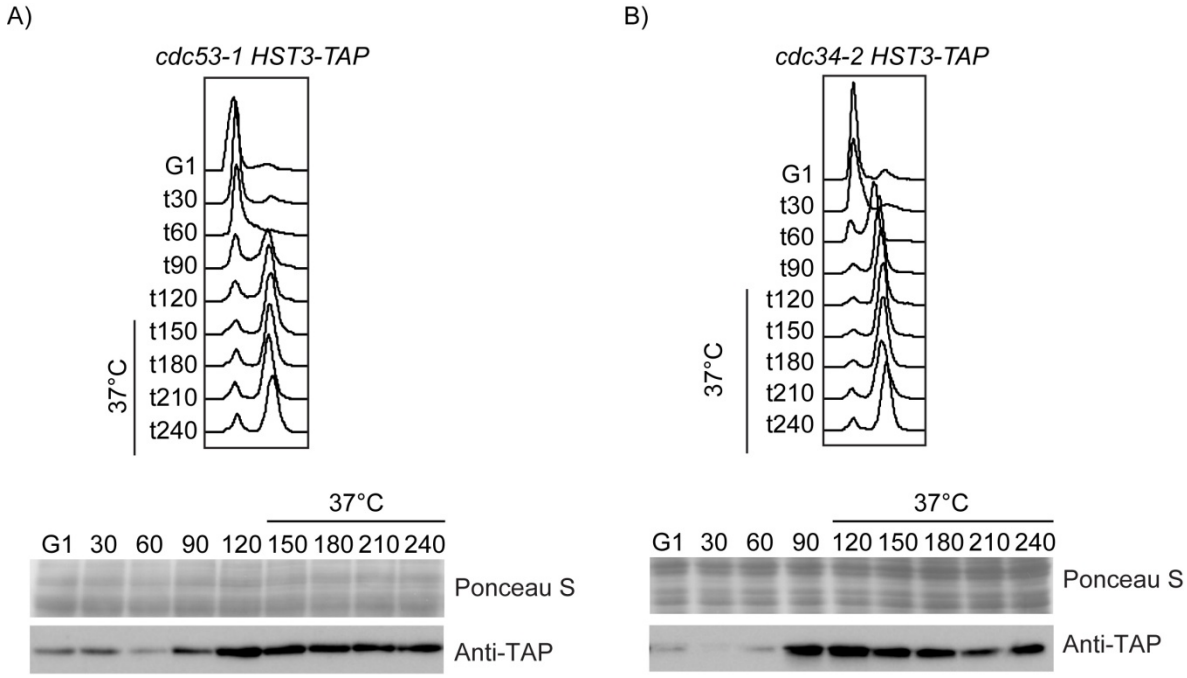


**Figure 4**

**Figure 2.4 SCF and Cdc34 are required for Hst3 degradation *in vivo*.** A) Inactivation of the SCF subunit Cdc53 stabilizes Hst3 in G2/M. *cdc53-1 HST3-TAP* cells were released from G1 in nocodazole at 23°C and were switched to 37°C after 120 min to inactivate SCF. B) Hst3 cannot be degraded in the absence of the E2 enzyme Cdc34. *cdc34-2 HST3-TAP* cells were released from G1 at 23°C in the presence of nocodazole and were switched to 37°C after 90 min to inactivate Cdc34. In both experiments, samples were analyzed by FACS, and immunoblotting with anti-TAP antibody. Ponceau S staining is shown as a loading control.

### 2.4.5. The SCF-dependent degradation of Hst3 requires Cdc4

Hst3 degradation is controlled by an SCF-dependent mechanism (Figure 2.4). Moreover, phosphorylation of Hst3 at the two Cdk1 sites, T380 and T384, promotes its subsequent degradation (Figure 2.3). Numerous substrates of the F-box protein Cdc4 contain diphosphorylated degrons in which the two phosphorylation sites are 2-3 residues apart (Lyons*, et al.* 2013). Therefore, we tested whether Cdc4 was required for the degradation of Hst3 in cells arrested in mitosis. We monitored Hst3 levels in cells released from G1 into nocodazole in three independent thermosensitive mutants of *CDC4*, namely *cdc4-1*, *cdc4-10* and *cdc4-12*. Similar to other SCF mutants, *CDC4* mutants were initially released at the permissive temperature of 23°C and later switched to the restrictive temperature of 37°C to allow cell cycle progression until metaphase. We found that all three *CDC4* mutants failed to degrade Hst3 at restrictive temperature after 150-240 min in the presence of nocodazole (Figure 2.5). Taken together, our findings suggest that Cdc34 in association with $SCF^{Cdc4}$ promotes the degradation of Hst3 before entry into anaphase.

### 2.4.6. Hst3 is a substrate for Clb2-Cdk1 and $SCF^{Cdc4}$ *in vitro*

Our results suggest that phosphorylation of Hst3 at the Cdk1 sites T380 and T384 promotes its degradation by an SCF-dependent pathway. In order to establish Hst3 as a *bona fide* Cdk1 substrate, we investigated whether the main mitotic kinase Clb2-Cdk1 phosphorylated Hst3 *in vitro*. We performed a kinase assay on recombinant wild-type Hst3 using Clb2-Cdk1 purified from *S. cerevisiae*. Mass spectrometry analysis revealed that the consensus Cdk1 site of Hst3, T384, was phosphorylated by Clb2-Cdk1 *in vitro* (Figure 2.6A). Next, we tested whether phosphorylation of Hst3 by Clb2-Cdk1 primed it for ubiquitylation by $SCF^{Cdc4}$ *in vitro*. As a control for kinase activity, recombinant Hst3 was also phosphorylated by active cyclin A-CDK2 in the same experiment. Hst3 phosphorylated by Clb2-Cdk1, or cyclin A-CDK2, was incubated with a ubiquitylation reaction mixture containing the yeast E1, E2 and E3 enzymes Uba1, Cdc34, and $SCF^{Cdc4}$, respectively. The ubiquitylation reaction on Hst3 phosphorylated by Clb2-Cdk1 produced

poly-ubiquitylated Hst3 species, demonstrating that phosphorylated Hst3 is a substrate for $SCF^{Cdc4}$ *in vitro* (Figure 6B). Hence, our results strongly suggest that Hst3 is directly targeted by Cdk1 and $SCF^{Cdc4}$ during the cell cycle in *S. cerevisiae*.

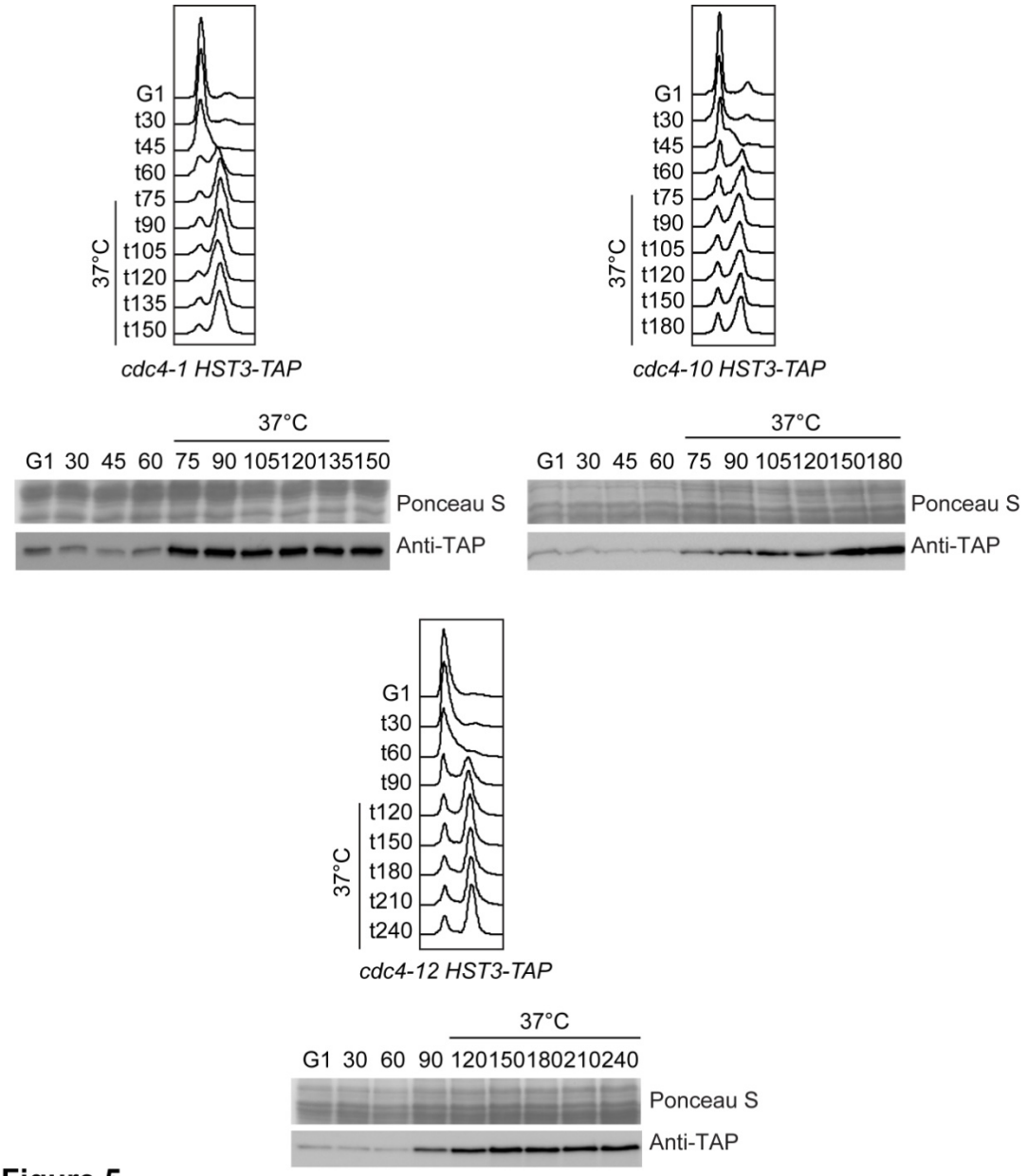


**Figure 5**

**Figure 2.5 Hst3 degradation requires the F-box protein Cdc4.** *cdc4-1*, *cdc4-10* and *cdc4-12* mutants expressing TAP-tagged Hst3 were released from G1 in nocodazole at 23°C and were switched to 37°C at the indicated times. Cell cycle progression was monitored by FACS. Whole cell lysates were probed by immunoblotting with anti-TAP antibody to monitor Hst3 levels. Ponceau S staining is shown as a loading control.

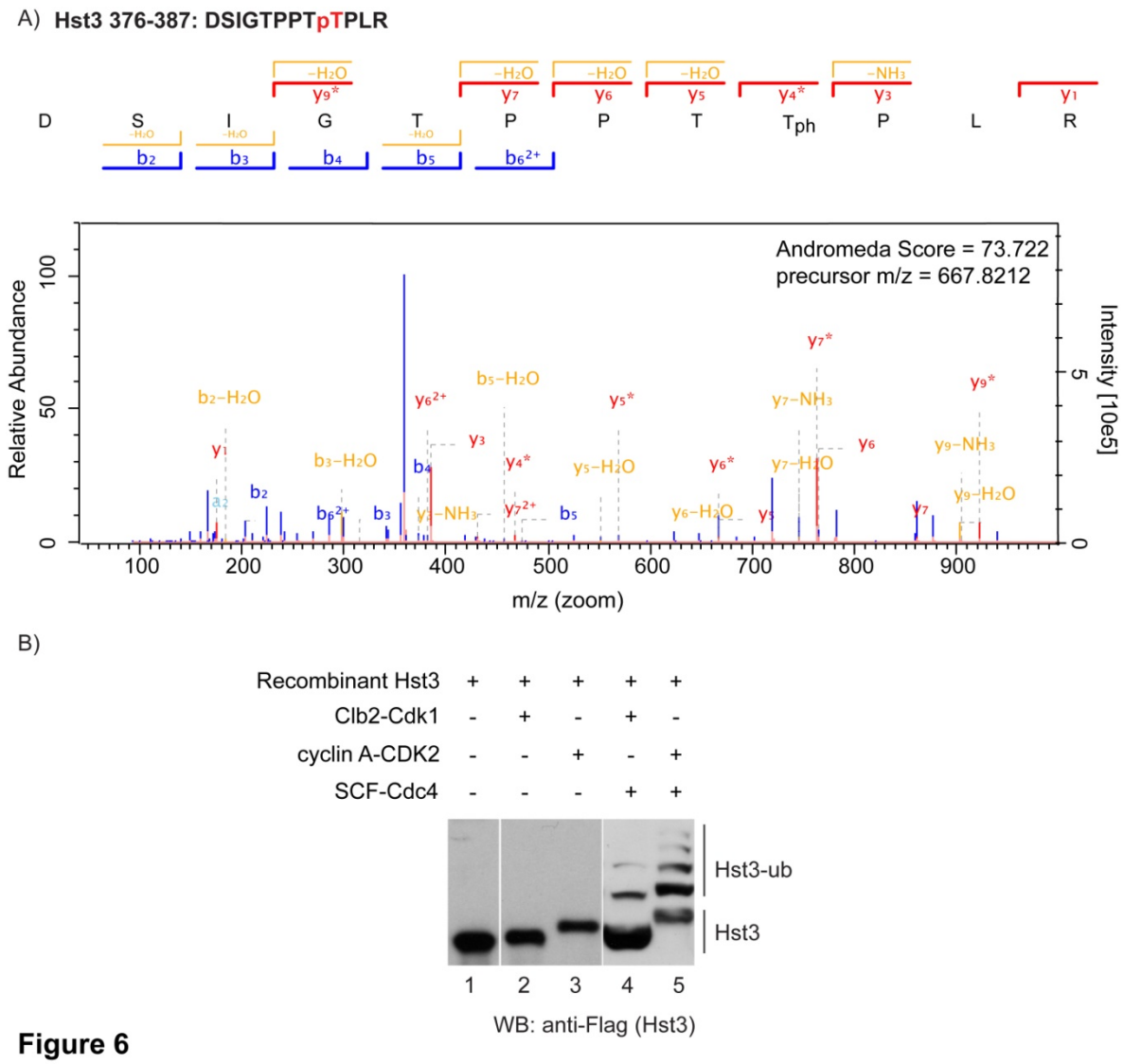


**Figure 6**

**Figure 2.6 Hst3 is targeted by the mitotic kinase Clb2-Cdk1 and SCF$^{Cdc4}$ *in vitro*.** A) Phosphorylation of Hst3 T384 by Clb2-Cdk1. The figure shows a fragmentation spectrum containing partial *y*-ion and *b*-ion series. The position of the phospho-threonine is consistent with the observed masses of several *y*-ions. The experimentally determined *m/z* ratio of the $[M+2H]^{2+}$ precursor peptide is indicated. The corresponding mass is within ppm of the theoretical mass for the singly phosphorylated peptide. B) Recombinant Hst3-Flag (lane 1) was phosphorylated by Clb2-Cdk1 (lane 2), or cyclinA-CDK2 as control (lane3), and subsequently ubiquitinated by Cdc34-SCF$^{Cdc4}$ (Lanes 4 and 5). Reactions were resolved by SDS-PAGE followed by anti-FLAG immunoblotting.

## 2.5. Discussion

In *S. cerevisiae*, H3K56ac makes an important contribution to the DNA damage response during S phase (Driscoll*, et al.* 2007, Han*, et al.* 2007a, Hyland*, et al.* 2005, Masumoto*, et al.* 2005, Ozdemir*, et al.* 2005, Recht*, et al.* 2006, Schneider*, et al.* 2006, Tsubota*, et al.* 2007, Wurtele*, et al.* 2012). Therefore, the H3K56 deacetylases Hst3 and Hst4 must be degraded prior to initiation of DNA synthesis to allow accumulation of H3K56ac behind DNA replication forks. Indeed, a previous study demonstrated that both Hst3 and Hst4 are degraded before S phase (Maas*, et al.* 2006). However, it was not clear how the degradation of H3K56 deacetylases is temporally coordinated with waves of H3K56ac during the cell cycle. Moreover, although Hst3 was known to be degraded by the ubiquitin-proteasome system near the end of the cell cycle (Thaminy*, et al.* 2007), the mechanism that controls its destruction remained completely unknown.

Our results demonstrate that Hst3 degradation can be completed before entry into anaphase (Figure 2.1). Interestingly, we found that Hst3 is degraded in wild-type cells in the presence of nocodazole (Figure 2.1A), which is in contrast to results from a previous work (Maas*, et al.* 2006). We speculate that this discrepancy may result from different experimental designs: in our experiments Hst3 levels were assessed over multiple time points in cells released from G1 into nocodazole. However, the other group assessed Hst3 levels after a 3 h treatment of asynchronously growing cells with nocodazole. Hence, the majority of cells may not have been arrested in metaphase long enough for Hst3 to be degraded. Since Hst3 is the main H3K56 deacetylase, our results imply that H3K56ac removal is mostly completed in a small window of time from the expression of Hst3 in G2 until its degradation prior to anaphase. Therefore, a surveillance mechanism might signal the completion of genome-wide H3K56 deacetylation before Hst3 is targeted to the proteasome. Alternatively, since Hst4 levels peak later than Hst3 during the cell cycle (Maas*, et al.* 2006), Hst4 might complete removal of remaining H3K56ac from the genome after the degradation of Hst3. However, cells lacking *HST4* (*hst4*Δ cells) have no obvious phenotype suggesting that, at least in the absence of Hst4, Hst3 can complete genome-wide removal of H3K56ac before its degradation.

In this work, we also uncovered the molecular machinery that controls Hst3 degradation during the cell cycle. Mass spectrometry analysis revealed that Hst3 is phosphorylated at the two Cdk1 sites T380 and T384 *in vivo* (Figure 2.2C). Mutation of either or both Cdk1 sites into alanine stabilized Hst3 in nocodazole-treated cells, suggesting that phosphorylation of Hst3 at these Cdk1 sites constitutes a phosphodegron that promotes its destruction (Figure 2.3). A recent study reported that several known Cdc4 phosphodegrons (CPDs) encompass two phosphorylation sites, mostly generated by Cdk1, which are separated by two or three residues. Moreover, this work established that the spacing between the two phosphorylation sites is essential for the degradation of the $SCF^{Cdc4}$ substrate Eco1 *in vivo* (Lyons*, et al.* 2013). According to these criteria, phosphorylation of Hst3 at T380 and T384 completely matches the features of a CPD. In support of this, our results demonstrated that the SCF-associated E2 enzyme Cdc34 and $SCF^{Cdc4}$ are required for the degradation of Hst3 *in vivo* (Figures 2.4 and 2.5).

Lastly, we established that Hst3 is a direct target of Cdk1 and $SCF^{Cdc4}$ *in vitro*. Mass spectrometry analysis uncovered that the mitotic kinase Clb2-Cdk1 phosphorylates Hst3 at its consensus Cdk1 site T384 *in vitro* (Figure 2.6A). We speculate that the minimal Cdk1 site of Hst3, T380, is not an optimal Clb2-Cdk1 substrate, because we could not detect its phosphorylation *in vitro*. However, we cannot exclude the possibility that phosphorylation of Hst3 at T380 is mediated by a Cdk1 complex other than Clb2-Cdk1 or a different kinase *in vivo*. Nevertheless, our results indicate that phosphorylation of Hst3 by Clb2-Cdk1 is sufficient to drive its polyubiquitylation by $SCF^{Cdc4}$ *in vitro* (Figure 2.6B).

The temporal relationship between completion of H3K56 deacetylation and the time at which Hst3 becomes unstable is poorly defined. Nonetheless, our findings suggest that phosphorylation and subsequent degradation of Hst3 occur around the stage of the cell cycle when this sirtuin is needed for removal of H3K56ac from the genome. The structure of the identified phosphodegron of Hst3 may provide an explanation for how Hst3 is protected from immediate degradation by the proteasome. Sequence characterization of peptides with high-affinity binding to Cdc4 *in vitro* has revealed that the presence of basic residues at the C-terminus of the Cdk1 phosphorylation site is disfavoured for Cdc4

binding. This suggests that phosphorylation of an optimal Cdk1 site within S/T-P-X-R/K sequence constitutes a weak Cdc4 degron (Nash*, et al.* 2001). Therefore, Hst3 phosphorylated at T384, within the sequence TPPTTPLR, should be a weak Cdc4 substrate. This prediction is consistent with the observation that the presence of T384 alone cannot trigger the degradation of Hst3 T380A *in vivo* (Figure 2.3). On the other hand, T380 of Hst3 was not found to be phosphorylated by Clb2-Cdk1 *in vitro*, suggesting that Cdk1 might not readily phosphorylate this site *in vivo*. Consistent with this, phosphorylation of Hst3 T380 alone cannot drive the degradation of Hst3 T384A *in vivo* (Figure 2.3). Hence, the presence of a minimal Cdk1 site (T380) and a weak Cdc4 binding site (T384) in the Hst3 phosphodegron may hinder generation of its destruction signal and create a window of opportunity for Hst3 to complete genome-wide H3K56 deacetylation before it is directed to the proteasome.

In summary, this manuscript demonstrates a direct role for Cdk1 and $SCF^{Cdc4}$ in Hst3 turnover during the cell cycle. $SCF^{Cdc4}$, together with the Cdk1 complexes that are active during G1, controls the G1/S transition of the cell cycle by directing the proteasomal degradation of Sic1 (Verma*, et al.* 1997). Hence, our results on the regulation of Hst3 by $SCF^{Cdc4}$ explain how the degradation of the main H3K56 deacetylase, Hst3, always precedes entry into S phase when H3K56ac levels peak behind DNA replication forks.

## 2.6. References


Brachmann, C. B., Sherman, J. M., Devine, S. E., Cameron, E. E., Pillus, L. and Boeke, J. D. (1995). The SIR2 gene family, conserved from bacteria to humans, functions in silencing, cell cycle progression, and chromosome stability. Genes Dev 9, 2888-902.

Celic, I., Masumoto, H., Griffith, W. P., Meluh, P., Cotter, R. J., Boeke, J. D. and Verreault, A. (2006). The sirtuins hst3 and Hst4p preserve genome integrity by controlling histone h3 lysine 56 deacetylation. Curr Biol 16, 1280-9.

Ciosk, R., Zachariae, W., Michaelis, C., Shevchenko, A., Mann, M. and Nasmyth, K. (1998). An ESP1/PDS1 complex regulates loss of sister chromatid cohesion at the metaphase to anaphase transition in yeast. Cell 93, 1067-76.

Cohen-Fix, O., Peters, J. M., Kirschner, M. W. and Koshland, D. (1996). Anaphase initiation in Saccharomyces cerevisiae is controlled by the APC-dependent degradation of the anaphase inhibitor Pds1p. Genes Dev 10, 3081-93.

Driscoll, R., Hudson, A. and Jackson, S. P. (2007). Yeast Rtt109 promotes genome stability by acetylating histone H3 on lysine 56. Science 315, 649-52.

Goh, P. Y. and Surana, U. (1999). Cdc4, a protein required for the onset of S phase, serves an essential function during G(2)/M transition in Saccharomyces cerevisiae. Mol Cell Biol 19, 5512-22.

Haase, S. B. and Reed, S. I. (2002). Improved flow cytometric analysis of the budding yeast cell cycle. Cell Cycle 1, 132-6.

Hachinohe, M., Hanaoka, F. and Masumoto, H. (2011). Hst3 and Hst4 histone deacetylases regulate replicative lifespan by preventing genome instability in Saccharomyces cerevisiae. Genes Cells 16, 467-77.

Han, J., Zhou, H., Horazdovsky, B., Zhang, K., Xu, R. M. and Zhang, Z. (2007a). Rtt109 acetylates histone H3 lysine 56 and functions in DNA replication. Science 315, 653-5.

Han, J., Zhou, H., Li, Z., Xu, R. M. and Zhang, Z. (2007b). Acetylation of lysine 56 of histone H3 catalyzed by RTT109 and regulated by ASF1 is required for replisome integrity. J Biol Chem 282, 28587-96.

Holt, L. J., Tuch, B. B., Villen, J., Johnson, A. D., Gygi, S. P. and Morgan, D. O. (2009). Global analysis of Cdk1 substrate phosphorylation sites provides insights into evolution. Science 325, 1682-6.

Hyland, E. M., Cosgrove, M. S., Molina, H., Wang, D., Pandey, A., Cottee, R. J. and Boeke, J. D. (2005). Insights into the role of histone H3 and histone H4 core modifiable residues in Saccharomyces cerevisiae. Mol Cell Biol 25, 10060-70.

Kanshin, E., Michnick, S. and Thibault, P. (2012). Sample preparation and analytical strategies for large-scale phosphoproteomics experiments. Semin Cell Dev Biol 23, 843-53.

Koranda, M., Schleiffer, A., Endler, L. and Ammerer, G. (2000). Forkhead-like transcription factors recruit Ndd1 to the chromatin of G2/M-specific promoters. Nature 406, 94-8.

Kushnirov, V. V. (2000). Rapid and reliable protein extraction from yeast. Yeast 16, 857-60.

Li, Q., Zhou, H., Wurtele, H., Davies, B., Horazdovsky, B., Verreault, A. and Zhang, Z. (2008). Acetylation of histone H3 lysine 56 regulates replication-coupled nucleosome assembly. Cell 134, 244-55.

Lyons, N. A., Fonslow, B. R., Diedrich, J. K., Yates, J. R., 3rd and Morgan, D. O. (2013). Sequential primed kinases create a damage-responsive phosphodegron on Eco1. Nat Struct Mol Biol 20, 194-201.

Maas, N. L., Miller, K. M., DeFazio, L. G. and Toczyski, D. P. (2006). Cell cycle and checkpoint regulation of histone H3 K56 acetylation by Hst3 and Hst4. Mol Cell 23, 109-19.

Masumoto, H., Hawke, D., Kobayashi, R. and Verreault, A. (2005). A role for cell-cycle-regulated histone H3 lysine 56 acetylation in the DNA damage response. Nature 436, 294-8.

Nash, P., Tang, X., Orlicky, S., Chen, Q., Gertler, F. B., Mendenhall, M. D., Sicheri, F., Pawson, T. and Tyers, M. (2001). Multisite phosphorylation of a CDK inhibitor sets a threshold for the onset of DNA replication. Nature 414, 514-21.

Ozdemir, A., Spicuglia, S., Lasonder, E., Vermeulen, M., Campsteijn, C., Stunnenberg, H. G. and Logie, C. (2005). Characterization of lysine 56 of histone H3 as an acetylation site in Saccharomyces cerevisiae. J Biol Chem 280, 25949-52.

Recht, J., Tsubota, T., Tanny, J. C., Diaz, R. L., Berger, J. M., Zhang, X., Garcia, B. A., Shabanowitz, J., Burlingame, A. L., Hunt, D. F., Kaufman, P. D. and Allis, C. D. (2006). Histone chaperone Asf1 is required for histone H3 lysine 56 acetylation, a modification associated with S phase in mitosis and meiosis. Proc Natl Acad Sci U S A 103, 6988-93.

Schneider, J., Bajwa, P., Johnson, F. C., Bhaumik, S. R. and Shilatifard, A. (2006). Rtt109 is required for proper H3K56 acetylation: a chromatin mark associated with the elongating RNA polymerase II. J Biol Chem 281, 37270-4.

Tang, X., Orlicky, S., Liu, Q., Willems, A., Sicheri, F. and Tyers, M. (2005). Genome-wide surveys for phosphorylation-dependent substrates of SCF ubiquitin ligases. Methods Enzymol 399, 433-58.

Thaminy, S., Newcomb, B., Kim, J., Gatbonton, T., Foss, E., Simon, J. and Bedalov, A. (2007). Hst3 is regulated by Mec1-dependent proteolysis and controls the S phase checkpoint and sister chromatid cohesion by deacetylating histone H3 at lysine 56. J Biol Chem 282, 37805-14.

Tsubota, T., Berndsen, C. E., Erkmann, J. A., Smith, C. L., Yang, L., Freitas, M. A., Denu, J. M. and Kaufman, P. D. (2007). Histone H3-K56 acetylation is catalyzed by histone chaperone-dependent complexes. Mol Cell 25, 703-12.

Ubersax, J. A., Woodbury, E. L., Quang, P. N., Paraz, M., Blethrow, J. D., Shah, K., Shokat, K. M. and Morgan, D. O. (2003). Targets of the cyclin-dependent kinase Cdk1. Nature 425, 859-64.

Verma, R., Annan, R. S., Huddleston, M. J., Carr, S. A., Reynard, G. and Deshaies, R. J. (1997). Phosphorylation of Sic1p by G1 Cdk required for its degradation and entry into S phase. Science 278, 455-60.

Verreault, A. (2000). De novo nucleosome assembly: new pieces in an old puzzle. Genes Dev 14, 1430-8.

Willems, A. R., Schwab, M. and Tyers, M. (2004). A hitchhiker's guide to the cullin ubiquitin ligases: SCF and its kin. Biochim Biophys Acta 1695, 133-70.

Wurtele, H., Kaiser, G. S., Bacal, J., St-Hilaire, E., Lee, E. H., Tsao, S., Dorn, J., Maddox, P., Lisby, M., Pasero, P. and Verreault, A. (2012). Histone H3 lysine 56 acetylation and the response to DNA replication fork damage. Mol Cell Biol 32, 154-72.

Zhu, G., Spellman, P. T., Volpe, T., Brown, P. O., Botstein, D., Davis, T. N. and Futcher, B. (2000). Two yeast forkhead genes regulate the cell cycle and pseudohyphal growth. Nature 406, 90-4.

# 3. Genetic modifiers of phenotypes caused by histone H3 lysine 56 hyperacetylation

Neda Delgoshaie*, Hugo Wurtele*, Ivana Celic, Junbiao Dai,
Jef D. Boeke and Alain Verreault
* These authors contributed equally to this work
(In preparation for submission to *Genetics*)

Dr. Junbiao Dai and Dr. Ivana Celic from Dr. Jef D. Boeke's lab performed the screen on the histone gene mutants collection (Tables 3.2, 3.3 and 3.4)
Dr. Hugo Wurtele performed experiments on Figures 3.1, 3.2, 3.3, 3.4C and 3.5
Neda Delgoshaie generated data for Figures 3.4A and B, and Figure 3.6 and repeated experiments on Figures 3.1 and 3.2

This manuscript was prepared by Dr. Hugo Wurtele and Neda Delgoshaie

## 3.1. Abstract

In *Saccharomyces cerevisiae*, histone H3 lysine 56 acetylation (H3K56ac) is a modification present in newly synthesized histones deposited throughout the genome during DNA replication. The sirtuins Hst3 and Hst4 are required for genome-wide deacetylation of H3K56 after completion of S phase. In cells lacking Hst3 and Hst4, nearly all the H3 molecules are K56-acetylated throughout the cell cycle. Failure to deacetylate H3K56 results in severe phenotypes: thermosensitivity, persistent spontaneous DNA damage, severe genomic instability, and acute sensitivity to genotoxic agents that damage DNA during replication. In this manuscript, we demonstrate that *hst3*Δ *hst4*Δ cells cannot complete genome duplication when transiently exposed to genotoxic agents during S phase. This phenotype arises from abnormal presence of H3K56ac in front of DNA replication forks in *hst3*Δ *hst4*Δ mutants. We also provide evidence that the thermosensitive phenotype of *hst3*Δ *hst4*Δ mutants is genetically linked to their genotoxic agent sensitivity. In addition, we demonstrate that mutations that impair histone H4 lysine 16 acetylation (H4K16ac) or loss-of-function mutations in the Rsc2 form of the RSC complex and Yta7 attenuate the severe phenotypes of *hst3*Δ *hst4*Δ cells. Our results suggest that, in wild-type cells, DNA replication forks have evolved to proceed through nucleosomes that contain H4K16ac but lack H3K56ac, whereas the phenotypes of *hst3*Δ *hst4*Δ mutants result from the presence of nucleosomes that contain both modifications. Our results therefore shed light on patterns of histone acetylation that are important for completion of DNA replication even when DNA templates are damaged by genotoxic agents.

## 3.2. Introduction

Chromatin structure influences several DNA metabolic processes such as transcription, DNA replication and DNA repair (Campos *et al.* 2009, Wurtele *et al.* 2006). The basic building block of chromatin is the nucleosome core particle, which is composed of 147 base pairs of DNA wrapped around the surface of an octameric protein core that consists of two molecules each of core histones H2A, H2B, H3 and H4. During DNA replication, pre-existing (old) histones are segregated onto sister chromatids, while new histones are deposited onto newly synthesized DNA in order to restore a normal nucleosome density onto nascent sister chromatids (Ransom *et al.* 2010, Su *et al.* 2012). In human cells, newly synthesized histone H3 and H4 molecules are acetylated on multiple residues within their N-terminal tails (Benson *et al.* 2006, Jasencakova *et al.* 2010, Ruiz-Carrillo *et al.* 1975) and they are deacetylated following their incorporation into chromatin (Jackson *et al.* 1976, Taddei *et al.* 1999). N-terminal tail acetylation of new H3 and H4 molecules also occurs in *Saccharomyces cerevisiae* (Burgess*, et al.* 2010, Parthun *et al.* 1996). In addition, histone H3 lysine 56 acetylation (H3K56ac) is present in virtually all newly synthesized H3 molecules deposited throughout the genome during S phase (Celic*, et al.* 2006) but is absent from pre-existing (old) histones (Masumoto*, et al.* 2005). H3K56ac is catalyzed by the Rtt109 acetyltransferase that functions in concert with the histone-binding protein Asf1 (Driscoll*, et al.* 2007, Han*, et al.* 2007a, Han*, et al.* 2007b, Tsubota*, et al.* 2007). The sirtuins Hst3 and Hst4 contribute to H3K56 deacetylation and are absent during S phase (Maas*, et al.* 2006, Thaminy*, et al.* 2007). Hence, H3K56ac peaks after completion of genome duplication (Kaplan*, et al.* 2008, Maas*, et al.* 2006, Masumoto*, et al.* 2005). In the absence of DNA damage, H3K56ac is then removed throughout the genome when Hst3 and Hst4 are expressed during the G2/M phase of the cell cycle (Maas*, et al.* 2006).

This remarkable feature of the yeast chromosome cycle is important for response to DNA damage. Both acetylation and, to an even greater extent, deacetylation of H3K56 help cells survive spontaneous or genotoxic agent-induced lesions that arise during replication (Alvaro*, et al.* 2007, Celic*, et al.* 2006, Hyland*, et al.* 2005, Maas*, et al.* 2006, Masumoto*, et al.* 2005, Munoz-Galvan*, et al.* 2013, Ozdemir*, et al.* 2005, Recht*, et al.* 2006, Reid *et al.*

2011). The molecular mechanisms by which either lack of or excess H3K56ac render cells sensitive to DNA damage are poorly understood. H3K56ac promotes efficient chromatin assembly during DNA replication at least in part by enhancing the affinity of histone chaperones for newly synthesized H3 molecules (Li, *et al.* 2008, Su, *et al.* 2012). However, the fact that H3K56ac persists in response to DNA damage points to a role of H3K56ac in the DNA damage response (DDR) after new H3 molecules have been incorporated into chromatin (Masumoto, *et al.* 2005). Indeed, some DNA lesions that occur during S phase remain unrepaired for long periods of time after the majority of chromosomal DNA has been replicated (Wurtele, *et al.* 2012).

The name Hst was coined because Hst3 and Hst4 are homologous to Sir2 (Brachmann, *et al.* 1995), the founding member of the sirtuin family of nicotinamide adenine dinucleotide ($NAD^+$)-dependent deacetylases (Imai *et al.* 2000, Landry *et al.* 2000, Smith *et al.* 2000, Tanny *et al.* 2001). In several fungi, including human fungal pathogens, there is a single ortholog of Hst3/Hst4 (Haldar *et al.* 2008, Wurtele, *et al.* 2010). In contrast, Hst3 and Hst4 are partially redundant in *S. cerevisiae* (Brachmann, *et al.* 1995, Celic, *et al.* 2006). Deletion of *HST3* causes mild phenotypes such as an elevated incidence of spontaneous DNA damage and a shorter replicative lifespan (Alvaro, *et al.* 2007, Dang *et al.* 2009). In striking contrast, cell lacking both Hst3 and Hst4 (*hst3*Δ *hst4*Δ mutants) display severe phenotypes such as an extreme sensitivity to numerous genotoxic agents (Celic, *et al.* 2006, Celic, *et al.* 2008, Thaminy, *et al.* 2007). The *hst3*Δ *hst4*Δ double mutant cells also exhibit other strong phenotypes that might be related to their inability to respond appropriately to spontaneous DNA damage. These phenotypes include reduced viability even at the permissive temperature of 25°C (Brachmann, *et al.* 1995, Celic, *et al.* 2006), a high frequency of chromosome loss (Brachmann, *et al.* 1995, Celic, *et al.* 2006) and an extremely short replicative lifespan associated with dramatic genomic instability (Hachinohe, *et al.* 2011). Remarkably, many of the phenotypes of *hst3*Δ *hst4*Δ cells are strongly attenuated by mutating H3K56 into a non-acetylateable arginine residue (Celic, *et al.* 2006, Maas, *et al.* 2006). In contrast to *hst3*Δ or *hst4*Δ single mutants, essentially all the H3 molecules are K56-acetylated throughout the genome and during the entire cell cycle in *hst3*Δ *hst4*Δ cells (Celic, *et al.* 2006). These results strongly suggest that H3K56

hyperacetylation and/or the constitutive presence of H3K56ac throughout the cell cycle contribute to the severe phenotypes of *hst3*Δ *hst4*Δ mutants. However, the underlying basis of the severe phenotypes that result from excess H3K56 acetylation is poorly understood.

## 3.3. Material and methods

### 3.3.1. Strains, plasmids and growth conditions

Plasmids pJP11 [p*CEN LYS2 HHT1-HHF1*] and [p*CEN-URA3-HST3*] (pRS416-based) were previously described (Celic*, et al.* 2006, Park *et al.* 2002). The series of pEMH-based plasmids encoding *HHT2-HHF2* gene mutations [p*CEN TRP1 HHT2-HHF2*] were also previously described (Hyland*, et al.* 2005).

All strains used in this work are described in Table 3.1. They were generated by standard methods and grown under standard conditions unless otherwise stated. Strain ICY1345 was used to determine the phenotypes caused by introducing histone H3/H4 gene mutations in cells carrying deletions of the *HST3* and *HST4* genes (Tables 3.2, 3.3 and 3.4). For this purpose, pEMH7-based plasmids that carried various H3 or H4 mutations were transformed into ICY1345 and $Trp^+$ transformants were selected. The following step consisted in selecting against $Lys^+$ cells containing the pJP11 plasmid encoding H3 and H4 on α-aminoadipic acid plates (Ito-Harashima *et al.* 2004). To test whether specific H3 or H4 gene mutations were able to suppress the phenotypes of *hst3*Δ *hst4*Δ cells, the aforementioned strains were plated on SC medium lacking tryptophan but containing 5-fluoroorotic acid (5-FOA) at different temperatures or in the presence of genotoxic agents. The purpose of 5-FOA was to remove the [p*CEN-URA3-HST3*] plasmid. Selection against the *HST3* plasmid to uncover *hst3*Δ *hst4*Δ phenotypes was always performed as the last step prior to phenotypic analysis because the propagation of *hst3*Δ *hst4*Δ mutant cells leads to the emergence of suppressors and genome rearrangements (Brachmann*, et al.* 1995, Hachinohe*, et al.* 2011).

The same strategy was used to isolate spontaneous suppressors of *hst3*Δ *hst4*Δ mutants. Strain ICY703 (see Table 3.1) was used as a starting point to identify spontaneous suppressors of the Ts- phenotype. ICY703 contains chromosomal deletions of the *HST3* and *HST4* genes that are covered by a [p*CEN-URA3-HST3*] plasmid. Cells that grew at 37°C and were resistant to 5-FOA were streaked onto a second set of 5-FOA plates to isolate single colonies that were temperature- and 5-FOA-resistant. Those colonies were tested by PCR to ensure that the *HST3* gene was absent from the thermoresistant strains. The PCR primers chosen for this test amplify a 670 bp 3'-end fragment of *HST3*. The forward primer was Hst3-C (5'- GTCACATTTCTTGAATCCCAAATAC) and the reverse primer was Hst3-D (5'- TTTGTAGACTGTTAAAGAGCCATCC).

**Table 3.1 Yeast strains**

| | |
|---|---|
| HWY19 | BY4743 *MAT*a *ura3*Δ*0 leu2*Δ*0 his3*Δ*1* |
| FY | *MAT*a *his3*Δ*200 leu2*Δ*1 lys2-202 trp1*Δ*63 ura3-52* |
| ICY703 | FY *hst3*Δ*::HIS3 hst4*Δ*::TRP1* [p*CEN URA3 HST3*] |
| ICY918 | FY *hst3*Δ*::HIS3 hst4*Δ*::TRP1* [p*CEN URA3 HST3*] *sas2*Δ*::kanMX* |
| ICY1081 | FY *hst3*Δ*::HIS3 hst4*Δ*::TRP1* [p*CEN URA3 HST3*] *rsc2*Δ*::kanMX* |
| HWY A51 | FY *hst3*Δ*::HIS3 hst4*Δ*::KanMX hht1-hhf1::natMX hht2-hhf2::hygMX* [p*CEN TRP1 HHT2-hhf2 K16R*] [p*CEN URA3 HST3*] |
| HWY C38 | FY *hst3*Δ*::HIS3 hst4*Δ*::TRP1* [p*CEN URA3 HST3*] *yta7*Δ*::LEU2* |
| HWY C24 | FY *hst3*Δ*::HIS3 hst4*Δ*::TRP1* [p*CEN URA3 HST3*] *sir2*Δ*::LEU2* |
| HWY C28 | FY *hst3*Δ*::HIS3 hst4*Δ*::TRP1* [p*CEN URA3 HST3*] *sir2*Δ*::LEU2 sas2*Δ*::KanMX* |
| HWY C30 | FY *hst3*Δ*::HIS3 hst4*Δ*::TRP1* [p*CEN URA3 HST3*] *sir2*Δ*::LEU2 rsc2*Δ*::KanMX* |
| HWY C31 | FY *hst3*Δ*::HIS3 hst4*Δ*::KanMX hht1-hhf1::natMX hht2-hhf2::hygMX sir2*Δ*::LEU2* [p*CEN TRP1 HHT2-hhf2 K16R*] [p*CEN URA3 HST3*] |
| HWY E63 | FY *hst3*Δ*::HIS3 hst4*Δ*::TRP1* [p*CEN URA3 HST3*] *cdc45::CDC45-HA::LEU2* |
| HWY E65 | FY *hst3*Δ*::HIS3 hst4*Δ*::TRP1* [p*CEN URA3 HST3*] *sas2*Δ*::kanMX cdc45::CDC45-HA::LEU2* |
| HWY F7 | FY *hst3*Δ*::HIS3 hst4*Δ*::KanMX hht1-hhf1::natMX hht2-hhf2::hygMX* [p*CEN TRP1 HHT2-hhf2 K16R*] [p*CEN URA3 HST3*] *cdc45::CDC45-HA::LEU2* |
| HWYE71 | FY *hst3*Δ*::HIS3 hst4*Δ*::TRP1* [p*CEN-URA3-HST3*] *rtt109:: PGAL1-3HA-RTT109:: KanMX6* |
| Tr1 | FY *hst3*Δ*::HIS3 hst4*Δ*::TRP1 tr1* |
| Tr2 | FY *hst3*Δ*::HIS3 hst4*Δ*::TRP1 tr2* |
| Tr3 | FY *hst3*Δ*::HIS3 hst4*Δ*::TRP1 tr3* |

| | |
|---|---|
| Tr4 | FY *hst3Δ::HIS3 hst4Δ::TRP1 tr4* |
| Tr5 | FY *hst3Δ::HIS3 hst4Δ::TRP1 tr5* |
| Tr6 | FY *hst3Δ::HIS3 hst4Δ::TRP1 tr6* |
| Tr7 | FY *hst3Δ::HIS3 hst4Δ::TRP1 tr7* |
| Tr8 | FY *hst3Δ::HIS3 hst4Δ::TRP1 tr8* |
| Tr9 | FY *hst3Δ::HIS3 hst4Δ::TRP1 tr9* |
| Tr10 | FY *hst3Δ::HIS3 hst4Δ::TRP1 tr10* |
| Tr11 | FY *hst3Δ::HIS3 hst4Δ::TRP1 tr11* |
| Tr12 | FY *hst3Δ::HIS3 hst4Δ::TRP1 tr12* |
| Tr13 | FY *hst3Δ::HIS3 hst4Δ::TRP1 tr13* |
| Tr16 | FY *hst3Δ::HIS3 hst4Δ::TRP1 tr16* |
| Tr18 | FY *hst3Δ::HIS3 hst4Δ::TRP1 tr18* |
| Tr19 | FY *hst3Δ::HIS3 hst4Δ::TRP1 tr19* |
| Tr20 | FY *hst3Δ::HIS3 hst4Δ::TRP1 tr20* |
| Tr21 | FY *hst3Δ::HIS3 hst4Δ::TRP1 tr21* |
| DWY1 | FY *hst3Δ::HIS3 hst4Δ::TRP1 rtt109::RTT109-Flag::His3MX6* |
| DWY2 | FY *hst3Δ::HIS3 hst4Δ::TRP1 rtt109::RTT109-Flag::His3MX6 tr4* |
| DWY3 | FY *hst3Δ::HIS3 hst4Δ::TRP1 rtt109::RTT109-Flag::His3MX6 tr6* |
| DWY4 | FY *hst3Δ::HIS3 hst4Δ::TRP1 rtt109::RTT109-Flag::His3MX6 tr9* |
| DWY5 | FY *hst3Δ::HIS3 hst4Δ::TRP1 rtt109::RTT109-Flag::His3MX6 tr11* |
| DWY6 | FY *hst3Δ::HIS3 hst4Δ::TRP1 rtt109::RTT109-Flag::His3MX6 tr18* |
| ICY1345 | FY *hst3Δ::HIS3 hst4Δ::kanMX4 hht1-hhf1Δ:: natMX4 hht2-hhf2Δ:: hygMX4* [p*CEN URA3 HST3*] [p*CEN LYS2 HHT1-HHF1*] |

---

### 3.3.2. Cell synchronization, transient treatment with genotoxic agents and cell viability assays

Cells were grown overnight in YPD medium at 25°C and arrested in G1 at 30°C using 5 μg/ml α-factor for 1.5 h, followed by the addition of a second dose of α-factor at 5 μg/ml for 1.25 h. Cells were then released into the cell cycle by washing them once with water and resuspending them in fresh YPD medium containing 50 μg/ml pronase and MMS. In some experiments, asynchronous populations of cells were directly treated with MMS. After transient MMS treatment, cells were washed with 2.5% sodium thiosulfate (a chemical that inactivates MMS) and released into fresh YPD medium. Aliquots of cells were collected as a function of time and flash frozen on dry ice before being processed for immunoblotting or pulsed field gel electrophoresis. Appropriate dilutions of cells were

plated on YPD to measure viability by colony formation assays. Cells were fixed with 70% ethanol prior to FACS flow cytometry analysis of DNA content.

### 3.3.3. Measurement of DNA content by flow cytometry

DNA content was determined by flow cytometry using Sytox Green (Invitrogen) as nucleic acid stain (Haase*, et al.* 2002). Briefly, about $10^6$ cells were resuspended in 70% ethanol and incubated at 4°C from 1 h to overnight. Cells were pelleted, resuspended in 500 µl of 50 mM Tris-HCl pH 7.5 containing 400 µg/ml of ribonuclease A (Sigma), sonicated briefly and incubated for 3 h at 42°C. Cells were then pelleted, resuspended in 200 µl of 50 mM Tris-HCl pH 7.5 buffer containing 400 µg/ml proteinase K (Sigma) and incubated for 30 min at 50°C. Cells were then resuspended in 500 µl of 50 mM Tris-HCl pH 8.0 containing 1 µM Sytox Green (Invitrogen). Flow cytometry was performed on a Becton-Dickinson LSR II instrument using the FACS Diva software. Histograms were generated using the Modfit LT 3.2 or the FCS Express Version 3 software.

### 3.3.4. Immunoblots

Whole-cell lysates were prepared for SDS–polyacrylamide gel electrophoresis using an alkaline method (Kushnirov 2000). SDS-PAGE and protein transfers were performed using standard molecular biology protocols. Our antibodies against H3K56ac (AV105) and H2A phosphorylated at S128 (AV137) and their specificity were previously described (Masumoto*, et al.* 2005). We used the 12CA5 monoclonal antibody to detect the HA epitope and an antibody against H4K16ac was purchased from Upstate (now EMD Millipore). Under our conditions, this antibody was specific for H4K16ac because it did not detect histones from cells bearing an *H4K16R* mutation.

### 3.3.5. Pulsed field gel electrophoresis

$10^7$ cells were embedded in agarose plugs and treated for pulsed field gel electrophoresis as described previously (Maringele *et al.* 2006). Electrophoresis was performed using a Bio-Rad CHEF DRII instrument (Bio-Rad Laboratories).

### 3.3.6. Rad53 autophosphorylation assays

Protein samples were resolved by SDS-PAGE and then transferred to PVDF membranes using standard Towbin buffer (25 mM Tris and 192 mM glycine) without methanol or SDS at 0.8 mA/cm$^2$ of transfer area for 2 h on a Bio-Rad SD semi-dry transfer apparatus. Membranes were then processed as previously described to allow renaturation of Rad53 prior to autophosphorylation assays (Pellicioli *et al.* 1999).

### 3.3.7. Drug susceptibility assays

Colony formation assays were performed as described previously (Tang *et al.* 2008). Colony formation was monitored after 3 to 5 days of incubation at the indicated temperature. Genotoxic agents were purchased from Sigma.

## 3.4. Results

### 3.4.1. Transient exposure to MMS causes persistent DNA damage and loss of viability of *hst3*Δ *hst4*Δ cells

Based on genetic evidence, *S. cerevisiae* cells lacking the *HST3* and *HST4* genes are extremely sensitive to chronic (*i.e.* long term) exposure to genotoxic agents that damage DNA during replication (Celic*, et al.* 2006, Celic*, et al.* 2008, Thaminy*, et al.* 2007). However, it was not clear how rapidly *hst3*Δ *hst4*Δ cells lost viability following exposure

to genotoxic agents. Moreover, physical evidence of genotoxic-induced chromosome damage in *hst3*Δ *hst4*Δ cells has not been reported. We therefore tested if DNA damage caused by transient exposure to genotoxic agents during a single round of S phase led to a loss of viability of *hst3*Δ *hst4*Δ cells. Cells were synchronized in G1 and released in S phase in medium containing MMS. To assess their viability, cells were plated on rich medium (YPD lacking MMS) either before or after transient exposure to MMS for 1.5 h. Transient exposure to low concentrations of MMS during S phase led to an important loss of viability of *hst3*Δ *hst4*Δ cells (Figure 3.1A).

Phosphorylation of yeast histone H2A on serine 128 (H2AP), which is functionally related to H2AX serine 139 phosphorylation in vertebrates (so-called γ-H2AX), is a well-established marker of DNA double-strand breaks. In *S. cerevisiae*, H2AP is catalyzed by the DDR kinases Mec1 and Tel1 (Downs *et al.* 2000). After transient exposure to MMS, we found that both wild-type (WT) and *hst3*Δ *hst4*Δ cells showed a significant increase in H2AP (Figure 3.1B, 30 min time points). In WT cells, the H2AP signal decreased as a function of time after removal of MMS, suggesting that DNA damage was progressively repaired and Mec1/Tel1 were inactivated in these cells (Figure 3.1B). In contrast, H2AP levels remained high in *hst3*Δ *hst4*Δ cells for at least 4.5 h after removal of MMS (Figure 3.1B). The persistence of high levels of H2AP in *hst3*Δ *hst4*Δ cells transiently exposed to MMS during S phase could result from either persistent activity of DDR kinases or failure to dephosphorylate H2AP following DNA repair. Mec1 and Rad53 are central DDR kinases and their activity is required to prevent irreversible damage when replication forks encounter MMS-induced DNA lesions (Segurado *et al.* 2008, Tercero *et al.* 2001). In response to DNA damage Rad53 is phosphorylated and activated by Mec1, and Rad53 also autophosphorylates on many amino acid residues (Pellicioli*, et al.* 1999, Sweeney *et al.* 2005). As measured by autophosphorylation assays (Pellicioli*, et al.* 1999), the kinase activity of Rad53 was transiently detected for a period of 45-90 min after MMS removal in WT cells exposed to MMS during early S phase (Figure 3.1C). In contrast, Rad53 remained active for at least 3 h following MMS removal from *hst3*Δ *hst4*Δ cells (Figure 3.1C).

The persistence of two markers of DNA damage (H2AP and active Rad53) in *hst3*Δ *hst4*Δ cells transiently exposed to MMS suggested that the mutant cells sustain long-lasting DNA damage when replication forks encounter MMS-induced DNA lesions. The primary lesion caused by MMS is 3-methyladenine, which blocks the progression of replicative DNA polymerases (Budzowska *et al.* 2009). We monitored completion of chromosome replication in *hst3*Δ *hst4*Δ cells transiently exposed to MMS by flow cytometry to measure DNA content and pulsed field gel electrophoresis (PFGE) as an indicator of chromosome integrity. Incompletely replicated chromosomes cannot migrate through pulsed field gels and this results in decreased intensity of intact chromosome bands stained with ethidium bromide (Maringele*, et al.* 2006). As a function of time after MMS removal, WT cells completed chromosome duplication as judged by the emergence of chromosome bands in pulsed field gels and the fact that most cells doubled their DNA contents as demonstrated by FACS (Figure 3.1D). In striking contrast to WT cells, none of the chromosomes of *hst3*Δ *hst4*Δ mutant cells entered pulsed field gels and DNA content did not significantly increase for at least 3 h following MMS removal from the culture (Figure 3.1D). These results indicate that MMS-induced DNA lesions in *hst3*Δ *hst4*Δ mutants lead to long delays in the completion of chromosome duplication and that this is true for all chromosomes. Caffeine is an inhibitor of Mec1 and Tel1, the two upstream kinases of the *S. cerevisiae* DDR pathway (Saiardi *et al.* 2005). Intriguingly, we found that simultaneous treatment of *hst3*Δ *hst4*Δ cells with both MMS and caffeine reproducibly increased viability compared with the addition of MMS alone (Figure 3.2A). Moreover, FACS analysis demonstrated that caffeine treatment allowed *hst3*Δ *hst4*Δ cells to complete DNA replication more efficiently in the presence of MMS (Figure 3.2B).

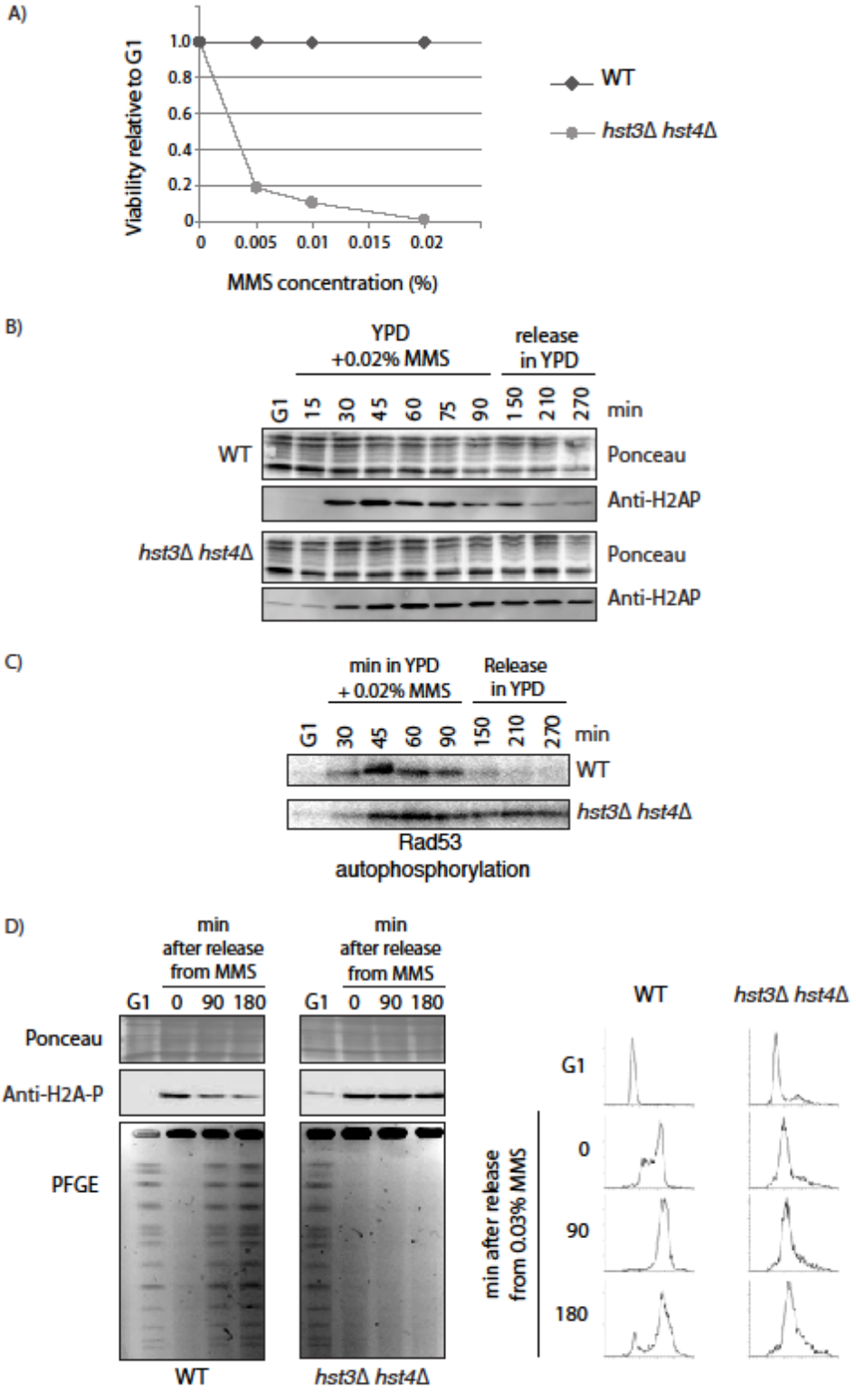
A)
Viability relative to G1
1.0
0.8
0.6
0.4
0.2
0
0
0.005
0.01
0.015
0.02
MMS concentration (%)
WT
hst3Δ hst4Δ
B)
YPD
+0.02% MMS
release
in YPD
G1
15
30
45
60
75
90
150
210
270
min
WT
Ponceau
Anti-H2AP
hst3Δ hst4Δ
Ponceau
Anti-H2AP
C)
min in YPD
+ 0.02% MMS
Release
in YPD
G1
30
45
60
90
150
210
270
min
WT
hst3Δ hst4Δ
Rad53
autophosphorylation
D)
min
after release
from MMS
G1
0
90
180
min
after release
from MMS
G1
0
90
180
Ponceau
Anti-H2A-P
PFGE
WT
hst3Δ hst4Δ
WT
hst3Δ hst4Δ
G1
0
90
180
min after release
from 0.03% MMS

**Figure 1**

**Figure 3.1 Transient exposure of *hst3*Δ *hst4*Δ cells to MMS causes persistent DNA damage and loss of viability.** A) *hst3*Δ *hst4*Δ cells are sensitive to transient exposure to MMS. Cells were released from G1 in the presence of increasing concentrations of MMS for 1.5 h before being plated on YPD. Viability was defined as the ratio of colonies after MMS treatment to those formed by G1 cells before exposure to MMS. B*) hst3*Δ *hst4*Δ cells display markers of persistent DNA damage following transient exposure to MMS. Cells were released from G1 in the presence of 0.02% MMS for 1.5 h before being resuspended in fresh YPD lacking MMS. Whole-cell lysates were analyzed by immunoblotting to detect H2A S128 phosphorylation (H2AP). Ponceau S staining is shown as a loading control. C) The experiment was conducted as in panel B, except that autophosphorylation activity of Rad53 was detected with [γ-32P] ATP and autoradiography. D) *hst3*Δ *hst4*Δ cells cannot complete chromosome duplication after transient exposure to MMS. Experimental protocol was same as in panel B except that 0.03% MMS was used. Samples were taken at the indicated times to detect H2AP by immunoblotting, completion of chromosome duplication by PFGE and DNA content by FACS.

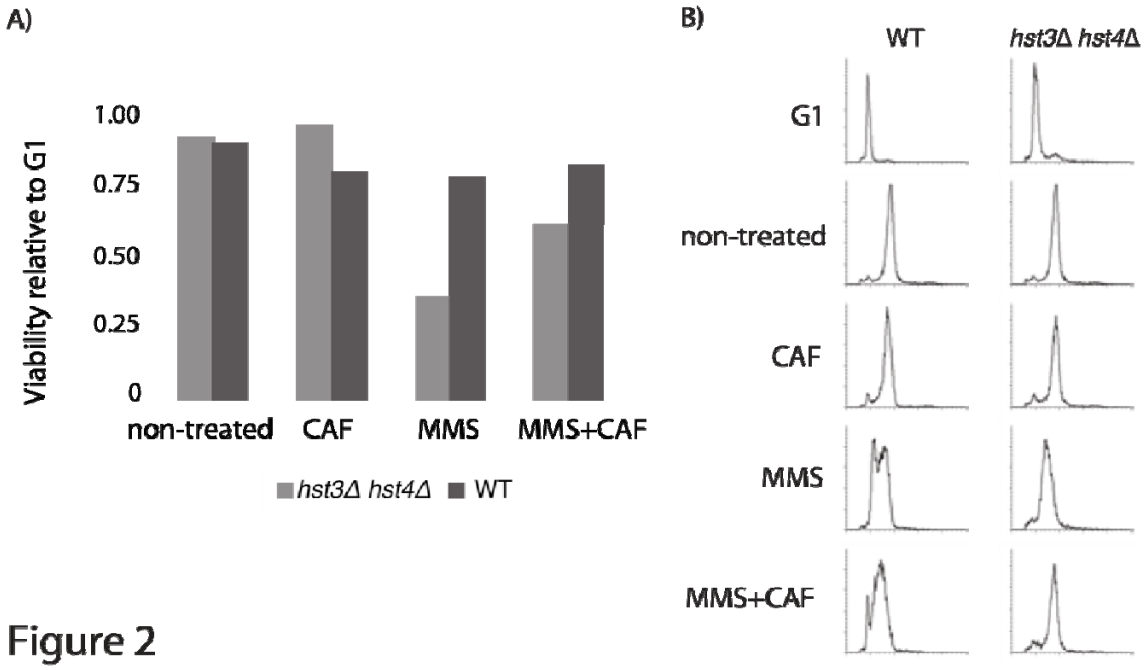


Figure 2

**Figure 3.2 Caffeine improves the viability of *hst3*Δ *hst4*Δ cells exposed to MMS.** A) Cells were arrested in G1 and released into the cell cycle in the presence of the indicated chemicals for 1.5 h at 25°C. The MMS concentration was 0.02% for *hst3*Δ *hst4*Δ cells and 0.04% for WT cells. The caffeine (CAF) concentration was 0.1%. Viability was assessed as in figure 1A. B) The effect of MMS and CAF on progression of DNA replication was monitored by FACS.

### 3.4.2. H3K56ac in front of replication forks causes genotoxic agent sensitivity

Previous studies demonstrated that mutation of H3K56 into an arginine (*H3K56R*) reduces the genotoxic agent sensitivity of *hst3*Δ *hst4*Δ cells (Celic*, et al.* 2006). This suggests that the phenotypes of *hst3*Δ *hst4*Δ cells are caused by hyperacetylation of H3K56 and/or its presence at a stage of the cell cycle when H3K56ac is normally absent in WT cells. H3K56ac is transient in WT cells and largely restricted to new H3 molecules that are deposited onto nascent sister chromatids during replication (Masumoto*, et al.* 2005). In contrast, H3K56ac is present at high stoichiometry (about 98% of H3 molecules are K56-acetylated) throughout the cell cycle in *hst3*Δ *hst4*Δ cells (Celic*, et al.* 2006). This creates an abnormal situation where the mutant cells progress through S phase with H3K56ac both in front and behind DNA replication forks. We sought to determine whether the anomalous presence of H3K56ac in front of replication forks might contribute to the acute sensitivity of *hst3*Δ *hst4*Δ mutants transiently exposed to genotoxic agents during S phase (Figure 3.1A). For this purpose, we generated an *hst3*Δ *hst4*Δ strain in which the *RTT109* gene was under the control of a galactose-inducible promoter (*hst3*Δ *hst4*Δ *PGAL1-3HA-RTT109*). When these cells are grown in galactose, the H3K56 acetyltransferase Rtt109 is strongly expressed and causes genome-wide H3K56ac because this strain cannot deacetylate H3K56. In contrast, glucose-mediated repression of *RTT109* leads to an absence of H3K56ac, which suppresses the extreme genotoxic agent sensitivity of *hst3*Δ *hst4*Δ cells (Celic*, et al.* 2006). Hence, as expected, our strain was more sensitive to MMS when grown in galactose than in glucose (Figure 3.3A). In order to validate that our system works as expected, we first grew our *hst3*Δ *hst4*Δ *PGAL1-3HA-RTT109* strain overnight in galactose, which leads to genome-wide H3K56ac. Cells were then arrested in G1 with α-factor either in the presence of glucose or galactose (Figure 3.3B). Rtt109 was clearly present when cells were arrested in G1 in galactose, but was undetectable in glucose (Figure 3.3B, G1 samples, 3HA-Rtt109 immunoblots). Cells were then released from G1 into the cell cycle in medium containing either galactose (*RTT109* ON) or glucose (*RTT109* OFF) in the absence of genotoxic agent. Consequently, after passage through S phase in glucose, H3K56ac decreased roughly 2-fold because new H3 molecules cannot be K56-

acetylated when Rtt109 is absent (Figure 3.3B, glucose, compare the G1 and 180 min time points). In contrast, H3 molecules were K56-acetylated at similar levels in G1 cells and cells released through S phase in medium containing galactose (Figure 3.3B, galactose, compare the G1 and 180 min time points). This was expected because 3HA-Rtt109 is expressed in galactose, and because of the absence of Hst3 and Hst4 nearly all the H3 molecules are constitutively K56-acetylated in our *hst3*Δ *hst4*Δ *PGAL1-3HA-RTT109* strain. These control experiments demonstrate that our system enables passage through S phase in the presence of old K56-acetylated H3 molecules and new H3 molecules that are either K56-acetylated or not (Figure 3.3E). We then proceeded to test whether these two conditions led to differential genotoxic agent sensitivity.

To address this question, cells released from G1 in glucose or galactose were transiently exposed to either HU or MMS and viability was subsequently assessed (Figure 3.3C). We observed the same loss of viability regardless of whether Rtt109 was expressed or not (Figure 3.3C and 3.3D). In our system, the vast majority of H3 molecules in front of replication forks are K56-acetylated when cells are released from G1 in either glucose or galactose (Figure 3.3E). In contrast, assuming that nearly all H3 molecules are K56-acetylated in G1 cells, deposition of new H3 molecules that cannot be K56-acetylated when *RTT109* is repressed in glucose would result in a stoichiometry of H3K56ac behind each replication fork of roughly 50%. This is the expected H3K56ac stoichiometry behind forks in WT cells (Celic*, et al.* 2006). We conclude that restoring the normal stoichiometry of H3K56ac behind replication forks does not rescue the severe MMS or HU sensitivity of the *hst3*Δ *hst4*Δ strain. Therefore, the genotoxic agent sensitivity of *hst3*Δ *hst4*Δ mutants (expressing *RTT109* from its normal promoter) is not due to excessive H3K56ac stoichiometry behind replication forks. These results imply that the acute genotoxic agent sensitivity of *hst3*Δ *hst4*Δ cells is mainly caused by the presence of H3K56ac in old histones in front of DNA replication forks.

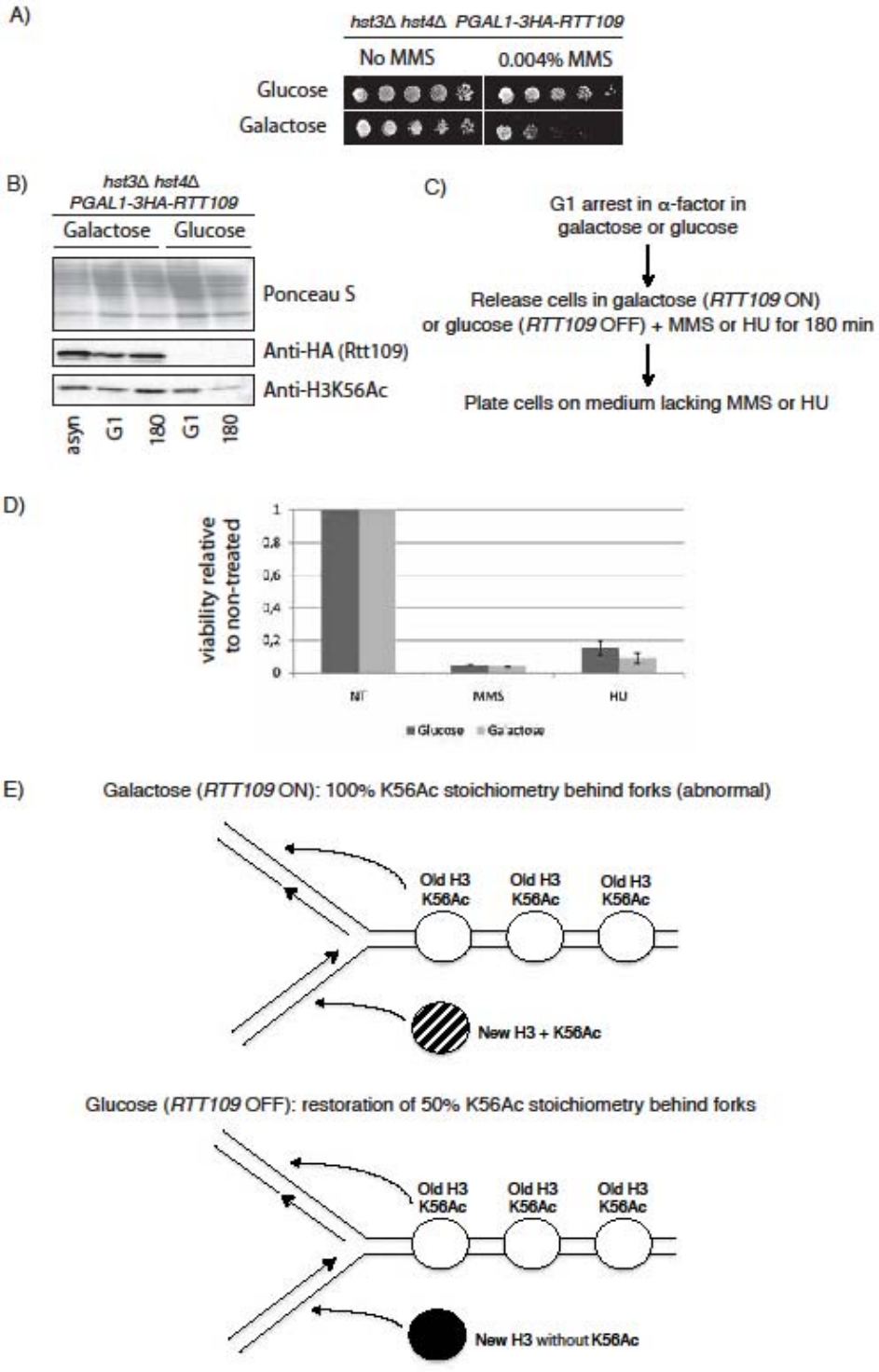
A)
hst3Δ hst4Δ PGAL1-3HA-RTT109
No MMS
0.004% MMS
Glucose
Galactose
B)
hst3Δ hst4Δ
PGAL1-3HA-RTT109
Galactose
Glucose
Ponceau S
Anti-HA (Rtt109)
Anti-H3K56Ac
asyn
G1
180
G1
180
C)
G1 arrest in α-factor in
galactose or glucose
Release cells in galactose (RTT109 ON)
or glucose (RTT109 OFF) + MMS or HU for 180 min
Plate cells on medium lacking MMS or HU
D)
viability relative
to non-treated
1
0,8
0,6
0,4
0,2
0
NT
MMS
HU
Glucose
Galactose
E)
Galactose (RTT109 ON): 100% K56Ac stoichiometry behind forks (abnormal)
Old H3
K56Ac
Old H3
K56Ac
Old H3
K56Ac
New H3 + K56Ac
Glucose (RTT109 OFF): restoration of 50% K56Ac stoichiometry behind forks
Old H3
K56Ac
Old H3
K56Ac
Old H3
K56Ac
New H3 without K56Ac

**Figure 3**

**Figure 3.3 The presence of H3K56ac in front of replication forks contributes to the genotoxic agent sensitivity of *hst3*Δ *hst4*Δ cells.** A) Control experiment showing that glucose-mediated repression of *3HA-RTT109* suppresses the MMS sensitivity of *hst3*Δ *hst4*Δ cells. Five-fold serial dilutions were plated on rich medium containing either glucose or galactose. The plates were incubated at 25°C. B) Control experiment showing that glucose-mediated repression of *3HA-RTT109* leads to a decrease in H3K56ac as cells go from G1 through S phase. Immunoblots showing the levels of 3HA-Rtt109 and H3K56ac in cells arrested in G1 or cells released into the cell cycle for 180 min in the presence of either galactose or glucose (without MMS or HU). C) Protocol for the experiment shown in panel D. D) The *PGAL1-3HA-RTT109 hst3*Δ *hst4*Δ strain was released from G1 in either galactose or glucose (to prevent H3K56ac in new histones) and transiently exposed to 200 mM HU or 0.01% MMS for 180 min. Viability was subsequently assessed as described in Figure 3.1A. E) Stoichiometry of H3K56ac in old and new H3 molecules when the *PGAL1-3HA-RTT109 hst3Δ hst4Δ* strain is released from G1 into S phase in either galactose or glucose. For clarity, old H3 molecules are only shown to segregate onto the "lagging strand chromatid", but it is known that they can be transferred onto either of the two nascent chromatids.

### 3.4.3. Mutations that cripple H4 lysine 16 acetylation suppress *hst3*Δ *hst4*Δ phenotypes

The *H3K56R* mutation that abolishes H3K56ac suppresses many of the phenotypes of *hst3*Δ *hst4*Δ cells (Celic*, et al.* 2006). We sought to determine whether other histone gene mutations suppress the temperature (Ts-) and/or genotoxic agent sensitivity of *hst3*Δ *hst4*Δ cells. For this purpose, we screened a collection of histone H3 or H4 mutants (Hyland*, et al.* 2005). This collection includes mutations of amino acid residues that carry either known or speculated modifications. Most H3 or H4 mutations, including mutations of basic residues located near K56 in H3 sequence, did not suppress *hst3*Δ *hst4*Δ phenotypes (Tables 3.3 and 3.4). As expected (Celic*, et al.* 2006), our screen revealed that histone H3K56 mutations suppressed the Ts-, HU and MMS sensitivity of *hst3*Δ *hst4*Δ mutants (Table 3.2). The phenotypes of *hst3*Δ *hst4*Δ mutants are caused, at least in part, by hyperacetylation of H3K56 (Celic*, et al.* 2006). *H3K56A*, *H3K56R* and *H3K56Q* mutations all suppressed the phenotypes of *hst3*Δ *hst4*Δ mutants (Table 3.2). Our results indicate that a glutamine is, at best, a poor mimic of H3K56ac. Otherwise, the *H3K56Q* mutation could not suppress the phenotypes of *hst3*Δ *hst4*Δ mutants because it would mimic a constitutively acetylated lysine 56.

Interestingly, histone H4 lysine 16 mutations suppressed the temperature, MMS and HU sensitivities of *hst3*Δ *hst4*Δ cells (Table 3.2 and Figure 3.4A). In *S. cerevisiae*, the SAS-I acetyltransferase complex, composed of Sas2, Sas4 and Sas5, is responsible for a major portion of histone H4 lysine 16 acetylation (H4K16ac) (Kimura *et al.* 2002, Suka *et al.* 2002, Sutton *et al.* 2003). Therefore, we asked whether eliminating the contribution of Sas2 to H4K16ac suppressed the phenotypes of *hst3*Δ *hst4*Δ cells (Figure 3.4A). We found that deletion of *SAS2*, which encodes the catalytic subunit of the SAS-I complex (Sutton*, et al.* 2003), also resulted in partial suppression of the Ts- and genotoxic agent sensitivity phenotypes of *hst3*Δ *hst4*Δ mutants (Figure 3.4A). The degree of suppression imparted by the *sas2*Δ mutation was not as pronounced as the suppression conferred by an *H4K16R* mutation (Figure 3.4A). This result may reflect the fact that H4K16ac is completely abolished in *H4K16R* mutants, but a significant amount of H4K16ac persists in *sas2*Δ cells (Figure 3.4B). Regardless, our results imply that both H3K56ac and H4K16ac are detrimental to *hst3*Δ *hst4*Δ mutants

The SAS-I complex and H4K16ac are involved in preventing heterochromatin from invading euchromatic regions (Jambunathan *et al.* 2005, Kimura*, et al.* 2002, Raisner *et al.* 2008, Suka*, et al.* 2002). Hence, we tested whether the suppression of *hst3*Δ *hst4*Δ phenotypes that results from decreased H4K16ac was observed in other mutants where the function of chromatin boundaries is impaired. Rsc2 is a subunit of one of the two forms of the RSC ATP-dependent chromatin remodeling complex (Cairns *et al.* 1999). RSC plays a number of cellular functions (Cairns*, et al.* 1999, Chambers *et al.* 2012, Floer *et al.* 2010), but it is also important to restrict the spread of silencing factors from heterochromatin into euchromatin (Jambunathan*, et al.* 2005). Likewise, Yta7 also contributes to chromatin boundary function (Jambunathan*, et al.* 2005, Raisner*, et al.* 2008, Tackett *et al.* 2005). We found that deletions of either *RSC2* or *YTA7* suppress the phenotypes of *hst3*Δ *hst4*Δ cells (Figure 3.4A). H4K16ac levels were comparable in WT cells and mutants lacking either Rsc2 or Yta7 (Figure 3.4B). This suggests that the *rsc2*Δ and *yta7*Δ mutations do not suppress the phenotypes of *hst3*Δ *hst4*Δ cells by causing a large decrease in H4K16ac. However, we cannot exclude the possibility that a loss of H4K16ac may occur at specific loci in *rsc2*Δ or *yta7*Δ cells.

Interestingly, none of our four suppressor mutations (*H4K16R*, *sas2*Δ, *rsc2*Δ or *yta7*Δ) showed reduced levels of spontaneous H2AP compared with the level observed in *hst3*Δ *hst4*Δ *H4-WT* cells (Figure 3.4B, left panel). Similarly, two of the suppressor mutations (*rsc2*Δ or *yta7*Δ) exhibited spontaneous levels of Rad53 autophosphorylation (a surrogate marker of the overall kinase activity of Rad53) that were similar to that of *hst3*Δ *hst4*Δ cells (Figure 3.4B, right panel). These results suggest that the severe phenotypes of *hst3*Δ *hst4*Δ mutants can be suppressed without any obvious decrease in the extent of spontaneous DNA damage detectable as H2AP or by measuring the kinase activity of Rad53. One notable exception is the *H4K16R* mutation that gives rise to the lowest levels of Rad53 autophosphorylation in an *in situ* kinase assay (Figure 3.4B, right panel). *H4K16R* is also the mutation that suppresses *hst3*Δ *hst4*Δ phenotypes to the greatest extent (Figure 3.4A).

One potential mechanism by which a decrease in H4K16ac could suppress the phenotypes of *hst3*Δ *hst4*Δ cells is the derepression of the silent mating type loci *HMR***a** and *HML*α. Sas2, Rsc2 and Yta7 are involved in the maintenance of chromatin boundaries at *HMR***a** (Jambunathan*, et al.* 2005, Raisner*, et al.* 2008, Tackett*, et al.* 2005). Heterochromatin spreading in *sas2*Δ, *rsc2*Δ or *yta7*Δ mutants likely requires that limiting pools of Sir complexes spread beyond their normal domains of action (Hoppe *et al.* 2002, Smith *et al.* 1998). Because of this, these mutants may have leaky expression of mating type genes located at the silent loci. This would generate pseudo-diploid cells (haploid cells that express genes from both mating types), which are more resistant than haploid *MAT***a** or *MAT*α cells to genotoxic agents such as MMS (Barbour *et al.* 2006, Livi *et al.* 1980). To test this hypothesis, we transformed *hst3*Δ *hst4*Δ *MAT***a** cells with plasmids that express either the *MAT***a** or *MAT*α mating cassettes (Figure 3.4C). These plasmids suppress the MMS sensitivity of several DNA repair mutants of the opposite mating type (Barbour*, et al.* 2006). However, our results clearly show that ectopic expression of *MAT*α mating type genes does not rescue the Ts- phenotype of *hst3*Δ *hst4*Δ *MAT***a** cells (Figure 3.4C). These results indicate that mutations that allow heterochromatin spreading beyond the silent

mating type loci (*sas2*Δ, *rsc2*Δ or *yta7*Δ) do not suppress the phenotypes of *hst3*Δ *hst4*Δ mutants by causing pseudo-diploidy.

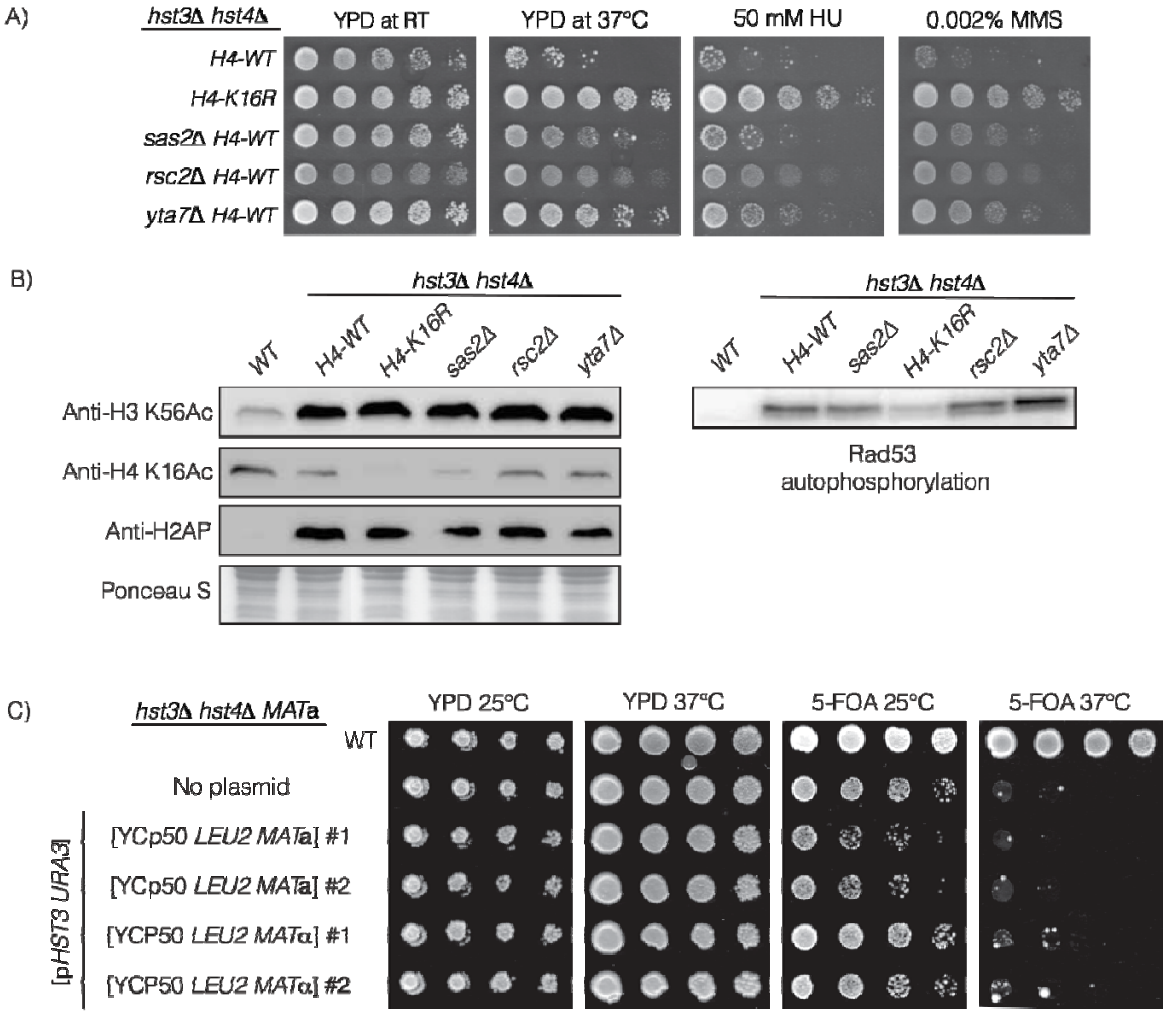


Figure 4

**Figure 3.4 Genetic links between H4K16ac, modulators of chromatin boundaries and the phenotypes of *hst3*Δ *hst4*Δ mutants.** A) Five-fold serial dilutions were spotted on YPD plates containing the indicated concentration of genotoxic agents and were incubated at 25°C or at 37°C. B) Whole-cell lysates of exponentially growing cells were probed by immunoblotting with H3K56ac or H2A pSer128 (H2AP) antibodies or used for *in situ* Rad53 autophosphorylation assays. The strain carrying the *H4K16R* mutation serves as specificity control for the H4K16ac antibody used in this experiment. C) Five-fold serial dilutions were spotted on YPD or 5-FOA plates and incubated at 25°C or 37°C.

**Table 3.2 Suppression of *hst3*Δ *hst4*Δ phenotypes by histone gene mutations**

| Histone mutant | Sensitivity at 37°C | MMS sensitivity | HU sensitivity |
|---|---|---|---|
| *hst3*Δ *hst4*Δ *H3 -WT* | Ts- | S | S |
| *H3 K56A* | Tr | R | S |
| *H3 K56R* | Tr | R | R |
| *H3 K56Q* | Tr | R | R |
| *H4 K16A* | Tr | R | S |
| *H4 K16R* | Tr | R | S |
| *H4 K16Q* | Tr | R | S |

Ts-: Thermosensitive (fails to grow at 37°C)
Tr: Thermoresistant (grows at 37°C)
S: Growth compromised on plates containing either 0.01% MMS or 100 mM HU
R: Histone gene mutations that rescue, at least partially, the MMS or HU sensitivity of *hst3*Δ *hst4*Δ cells.

We previously reported that epitope tagging of replication enzymes essential for cell viability did not result in obvious phenotypes in WT cells. In striking contrast, epitope tagging of same enzymes led to a loss of viability in *hst3*Δ *hst4*Δ cells (Celic*, et al.* 2008). We interpreted these results to mean that *hst3*Δ *hst4*Δ cells are exquisitely sensitive to subtle perturbations of DNA replication that have essentially no effect on the fitness of WT cells. Remarkably, we found that *sas2*Δ or *H4K16R* mutations allowed *hst3*Δ *hst4*Δ cells to survive HA epitope tagging of the essential replication protein Cdc45. However, Cdc45-HA causes lethality in *hst3*Δ *hst4*Δ cells (Figure 3.5A). The *sas2*Δ or *H4K16R* mutations also improved survival of *hst3*Δ *hst4*Δ cells transiently exposed to MMS during a single round of S phase (Figure 3.5B). Consistent with this, PFGE demonstrated that *hst3*Δ *hst4*Δ *H4K16R* cells were able to complete chromosome duplication more effectively than *hst3*Δ *hst4*Δ mutants after transient exposure to MMS during S phase (Figure 3.5C). Taken together, these results demonstrate that the absence of H4K16ac enhances the ability of *hst3*Δ *hst4*Δ cells to survive either subtle perturbations of the replisome (Cdc45-HA) or

DNA lesions caused by genotoxic agents that interfere with DNA replication fork progression (MMS).

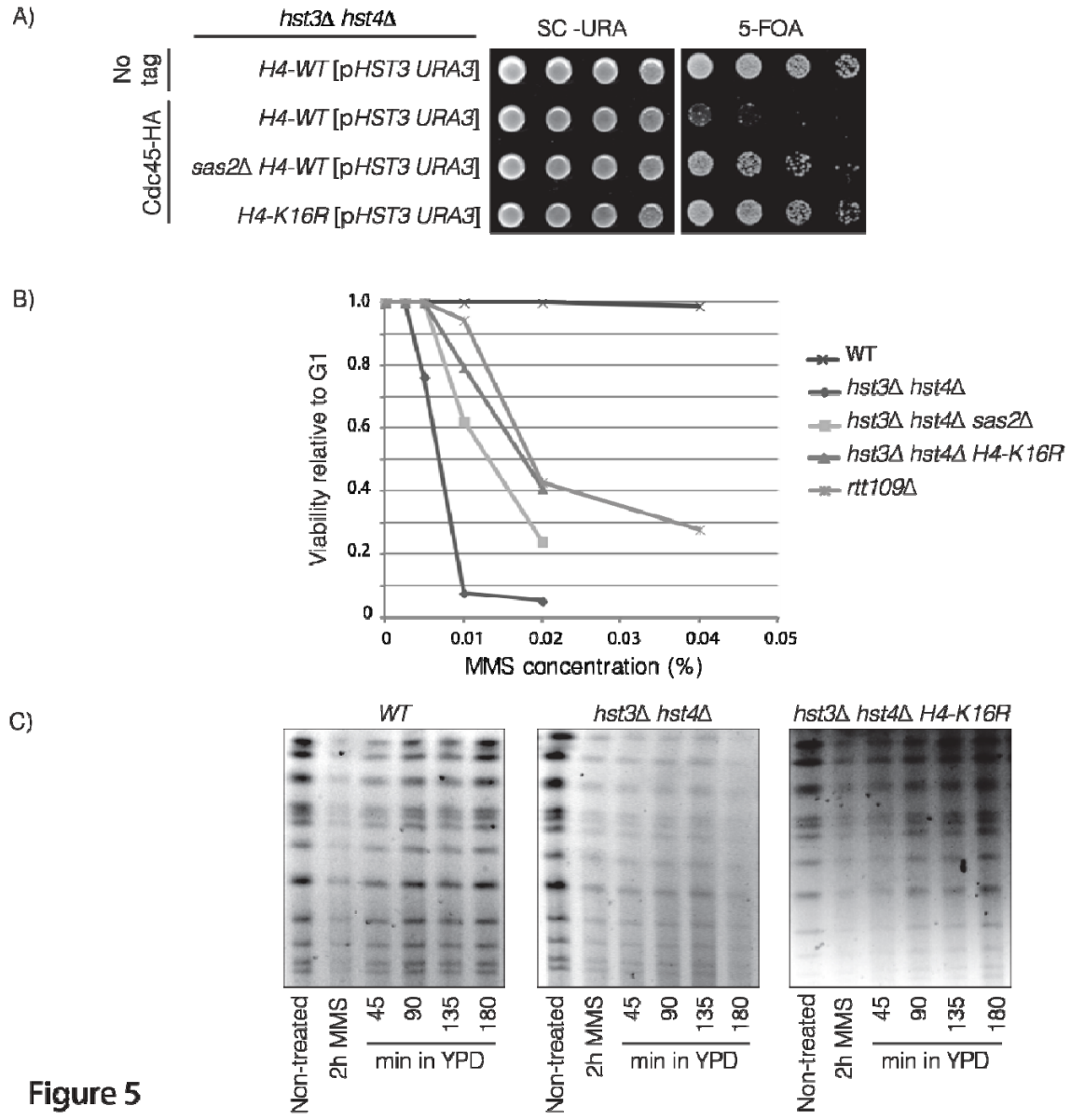


Figure 5

**Figure 3.5 Decreasing H4K16ac suppresses the sensitivity of *hst3*Δ *hst4*Δ mutants to conditions that perturb DNA replication.** A) Five-fold serial dilutions were spotted on SC-URA or 5-FOA plates and incubated at 25°C. B) Cells were arrested in G1 with α-factor and released into the cell cycle in the presence of MMS for 1.5 h. Cells were plated on YPD at G1 arrest or at the end of treatment with MMS. Viability was assessed as in Figure 3.1A. C) Exponentially growing cells were incubated in YPD containing 0.015%

MMS for 2 h at 30°C. After removal of MMS, cells were incubated in YPD for an additional 3 h. Samples were taken at indicated times and processed by PFGE.

### 3.4.4. Links between the thermosensitivity and genotoxic agent sensitivity of *hst3*Δ *hst4*Δ cells

*hst3*Δ *hst4*Δ cells are extremely sensitive to genotoxic agents (Celic*, et al.* 2006, Celic*, et al.* 2008) and cannot grow at the restrictive temperature of 37°C (Brachmann*, et al.* 1995, Celic*, et al.* 2006, Celic*, et al.* 2008). However, the source of the temperature-sensitive (Ts-) phenotype of these mutants is poorly understood. In order to gain insight into the molecular mechanisms that underlie the temperature and genotoxic agent sensitivity of *hst3*Δ *hst4*Δ cells, we isolated spontaneous suppressors of their Ts- phenotype. For this purpose, *hst3*Δ *hst4*Δ cells that carry a *URA3 CEN* plasmid encoding wild-type *HST3* were grown at 37°C on plates containing 5-fluoroorotic acid (5-FOA). This forces surviving cells to lose the *URA3* plasmid encoding *HST3*, thus resulting in *hst3*Δ *hst4*Δ mutant cells that cannot form colonies at 37°C unless they acquire a genetic or epigenetic change that suppresses their Ts- phenotype. Single colonies that were resistant to 5-FOA and grew at 37°C were isolated (Material and Methods). We found that most thermoresistant (Tr) isolates were, to varying degrees, more resistant to genotoxic agents than the starting *hst3*Δ *hst4*Δ mutant strain (Figure 3.6A). Among 18 spontaneous suppressors tested, we found that only one, Tr12, remained sensitive to 50 mM HU and 0.005% MMS. These results demonstrate that the Ts- phenotype and genotoxic agent sensitivity of *hst3*Δ *hst4*Δ cells are generally linked. As mentioned earlier, mutations that prevent H3K56ac partially suppress the phenotypes of *hst3*Δ *hst4*Δ cells (Celic*, et al.* 2006, Celic*, et al.* 2008). Nevertheless, a previous study had reported that spontaneous suppressors of *hst3*Δ *hst4*Δ mutants rarely showed a reduction in H3K56ac levels (2 out of 34 clones or 6%) (Miller*, et al.* 2006). In our study, we found 5 out of 18 suppressors of the Ts- phenotype (28%) where H3K56ac was below our detection threshold (Figure 3.6B: Tr4, Tr6, Tr9, Tr11 and Tr18). H3K56 acetylation requires both Rtt109 and Asf1 (Driscoll*, et al.* 2007, Han*, et al.* 2007a, Han*, et al.* 2007b, Tsubota*, et al.* 2007). In order to understand why H3K56ac was undetectable in this group of suppressors, we epitope-tagged either Rtt109 or Asf1 in these

Tr strains. Strains where H3K56ac was undetectable showed no decrease in the abundance of Asf1 (Figure 3.6C). In contrast, the Rtt109-Flag protein was undetectable in our five suppressors (Figure 3.6F). We confirmed that the *RTT109* gene was appropriately epitope-tagged in these strains (Figure 3.6D and 3.6E). We also identified several Tr strains (72% of all Tr isolates) that were more resistant to genotoxic agents than *hst3*Δ *hst4*Δ mutants but did not show any obvious decrease in H3K56ac (*e.g.* Tr5 and Tr8 in Figure 3.6A and 3.6B). We naturally wondered whether this class of suppressors contained reduced levels of histone H4K16ac. However, our suppressors did not generally show any striking decrease in H4K16ac compared with Ts- *hst3*Δ *hst4*Δ cells (Figure 3.6B). In summary, we have identified two groups of spontaneous suppressors of *hst3*Δ *hst4*Δ mutant phenotypes. The first group includes strains with undetectable levels of Rtt109 and H3K56ac, but normal expression of Asf1. The second group includes strains with apparently normal levels of H3K56ac and H4K16ac. However, the two groups of strains exhibited partial suppression of the Ts- phenotype, HU and MMS sensitivity (Figure 6A).

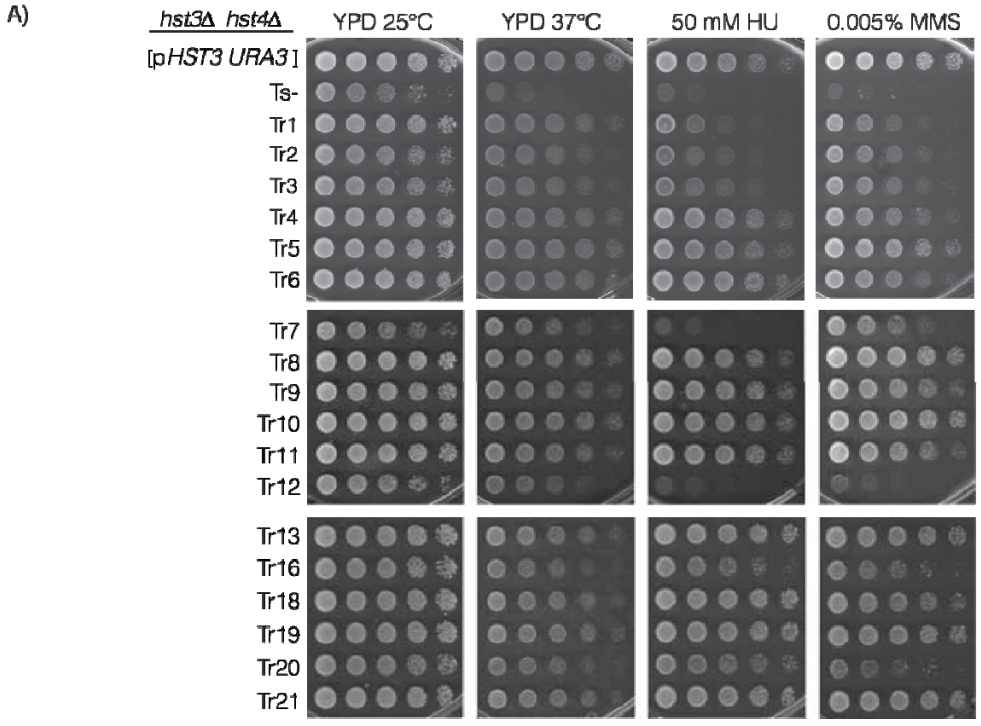

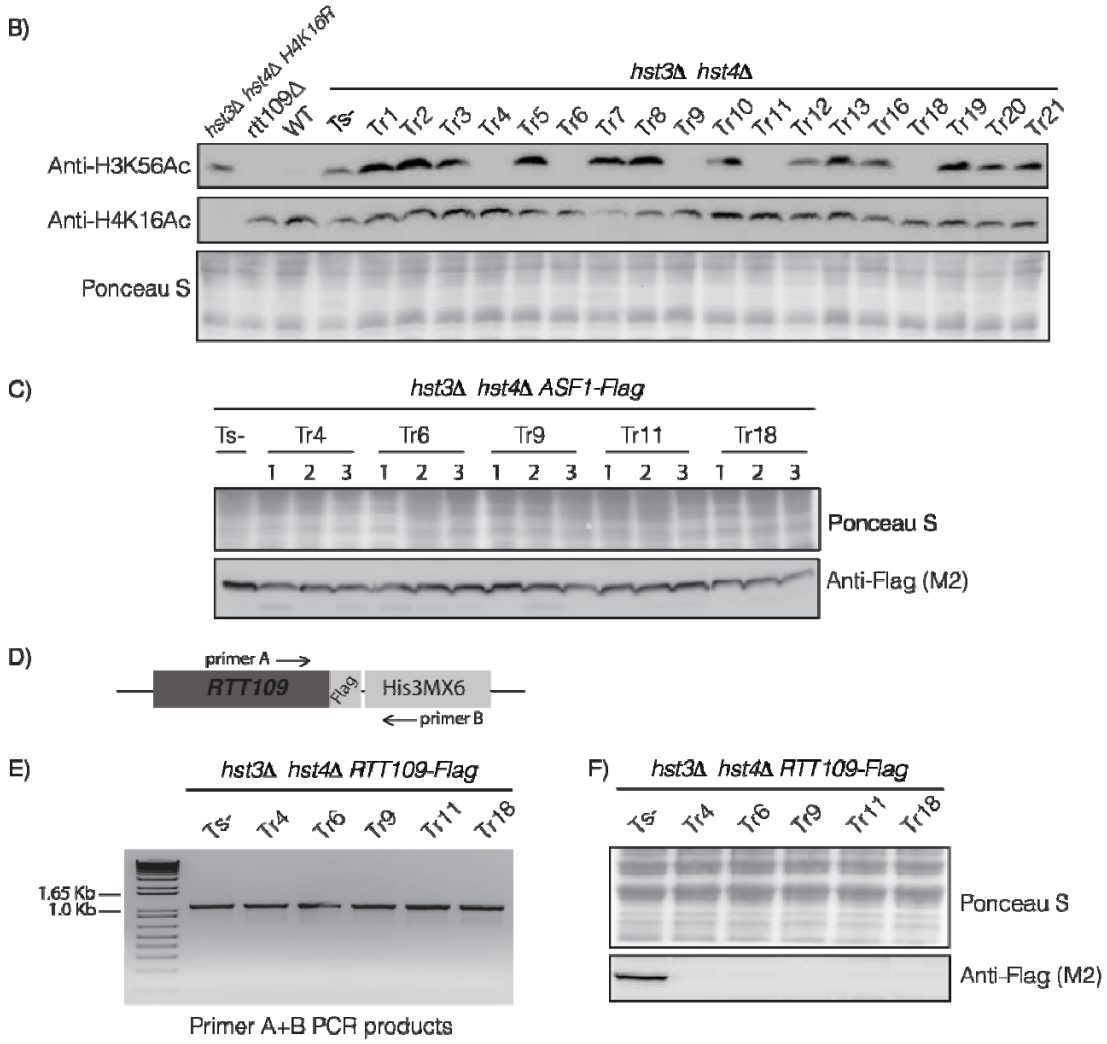


**Figure 6**

**Figure 3.6 Characterization of spontaneous suppressors of *hst3*Δ *hst4*Δ mutant phenotypes.** A) Five-fold serial dilutions were spotted on YPD plates containing the indicated concentration of genotoxic agents and incubated at either 25°C or 37°C. Ts- is the starting *hst3*Δ *hst4*Δ strain from which thermoresistant suppressors were isolated. B) Immunoblots of whole-cell lysates of exponentially growing cells were probed with antibodies against H3K56ac and H4K16ac. Ponceau S staining is shown as a loading control. Lysates from the *hst3*Δ *hst4*Δ *H4K16R* strain and the *rtt109*Δ strain serve as specificity controls for the antibodies against H4K16ac and H3K56ac, respectively. C) Asf1 was epitope-tagged in five thermoresistant spontaneous suppressors derived from *hst3*Δ *hst4*Δ cells. Three independent clones derived from tagging Asf1 in each Tr strain were selected. Immunoblots of whole-cell lysates were probed to detect Asf1-Flag. D) Location of PCR primers used to ensure that DNA integration correctly resulted in an *RTT109-FLAG* gene. E) PCR results showing that the *RTT109-FLAG* gene is present in each of the strains analyzed for Rtt109-FLAG protein expression in panel F.

F) The Rtt109-FLAG protein is not detectable in spontaneous suppressors that lack H3K56ac. Whole-cell lysates of exponentially growing cells were probed by immunoblotting with anti-Flag (M2) antibody.

## 3.5. Discussion

Genome-wide acetylation of H3K56 is a double-edged sword. H3K56ac is clearly important to promote resistance to genotoxic agents that damage DNA during replication (Alvaro, *et al.* 2007, Hyland, *et al.* 2005, Masumoto, *et al.* 2005, Munoz-Galvan, *et al.* 2013, Ozdemir, *et al.* 2005, Recht, *et al.* 2006, Reid, *et al.* 2011). However, failure to deacetylate H3K56 leads to more dramatic phenotypes than those of cells that cannot acetylate H3K56 (Celic, *et al.* 2006, Maas, *et al.* 2006, Masumoto, *et al.* 2005, Ozdemir, *et al.* 2005). These phenotypes include temperature sensitivity, a high incidence of spontaneous DNA damage, chromosome loss and rearrangements, and severe genotoxic agent sensitivity (Brachmann, *et al.* 1995, Celic, *et al.* 2006, Celic, *et al.* 2008, Hachinohe, *et al.* 2011, Maas, *et al.* 2006). The molecular basis of these phenotypes is poorly understood.

In this article, we showed that cells that cannot deacetylate H3K56ac are unable to complete DNA replication after transient exposure to MMS during S phase. This was accompanied by persistent activity of the DDR kinase Rad53 and histone H2A S128 phosphorylation (H2AP) (Figure 3.1). Although *hst3*Δ *hst4*Δ mutants consistently exhibit elevated levels of spontaneous and genotoxic agent-induced H2AP, our results suggest that the DNA lesions that are cytotoxic to these mutants may not be DSBs. First, although homologous recombination plays a major role in DSB repair in *S. cerevisiae*, the Rad51, Rad54, Rad55 and Rad57 proteins are not essential for viability of *hst3*Δ *hst4*Δ cells (Celic, *et al.* 2008). These results are consistent with the fact that the anti-recombinase Srs2, an enzyme that disassembles Rad51 nucleoprotein filaments (Veaute *et al.* 2003), is essential for viability of *hst3*Δ *hst4*Δ cells (Celic, *et al.* 2008). Second, several mutations that modulate chromatin structure suppress the Ts- and genotoxic agent sensitivity of *hst3*Δ *hst4*Δ mutants without significantly reducing the abundance of H2AP (Figure 3.4B).

Third, if a lack of DSB repair were responsible for the phenotypes of *hst3*Δ *hst4*Δ cells, it would be surprising that their genotoxic agent sensitivity could be suppressed in the absence of Rsc2 (Figure 3.4A). This is because the RSC complex is involved in the two major pathways of DSB repair: homologous recombination and non-homologous end joining (NHEJ) (Chai *et al.* 2005, Chambers*, et al.* 2012, Oum *et al.* 2011, Shim *et al.* 2005). There are two distinct RSC complexes with both overlapping and unique functions in the DDR (Chambers*, et al.* 2012). However, the Rsc2 complex is significantly more abundant than the Rsc1 complex (Cairns*, et al.* 1999, Ghaemmaghami *et al.* 2003) and cells lacking only Rsc2 are generally more defective in DSB repair than cells lacking only Rsc1 (Chambers*, et al.* 2012).

Caffeine, a known inhibitor of Mec1 and Tel1 (Saiardi*, et al.* 2005), increased survival and completion of DNA replication in *hst3*Δ *hst4*Δ cells after transient exposure to MMS during DNA replication (Figure 3.2). This result was surprising because we previously showed that Mec1 is essential for viability of *hst3*Δ *hst4*Δ cells (Celic*, et al.* 2008). However, our caffeine treatment was transient and may have inhibited the kinase activity of Mec1 only partially. Interestingly, we previously reported that, unlike Mec1, Rad53 is not essential in *hst3*Δ *hst4*Δ mutants (Celic*, et al.* 2008). Thus, at least some of the functions of DDR kinases are dispensable in *hst3*Δ *hst4*Δ cells. One of the functions of Mec1 and Rad53 is to inhibit the firing of late DNA replication origins (Santocanale *et al.* 1998). Based on this, it seems likely that persistent activity of DDR kinases in *hst3*Δ *hst4*Δ cells exposed to MMS (Figure 3.1C) would inhibit the firing of at least a subset of DNA replication origins. Our results with caffeine suggest that replication forks emanating from these origins are necessary to promote completion of genome duplication and survival of *hst3*Δ *hst4*Δ cells exposed to MMS. This would not be expected to occur if DSBs were impossible to repair in *hst3*Δ *hst4*Δ mutants.

We conclude that the presence of H3K56ac in front of DNA replication forks gives rise to the DNA damage sensitivity of *hst3*Δ *hst4*Δ cells because restoring the normal stoichiometry (roughly 50%) of H3K56ac behind replication forks does not improve the survival of the *hst3*Δ *hst4*Δ mutant after transient exposure to HU or MMS (Figure 3.3).

The reason why the presence of H3K56ac in front of forks is detrimental to *hst3*Δ *hst4*Δ cells transiently exposed to genotoxic agents is not known. In WT cells that sustain DNA damage, Hst3 is phosphorylated and degraded in a Mec1-dependent manner (Thaminy*, et al.* 2007). Hst3 degradation likely helps in protecting H3K56ac behind replication forks where DNA is damaged (Masumoto*, et al.* 2005). The existence of this regulation implies that, in addition to the role of H3K56ac in promoting chromatin assembly, K56-acetylated H3 molecules incorporated into chromatin contribute to the DDR. In WT cells, H3K56ac may create a chromatin environment that restricts the recruitment of DDR proteins specifically behind replication forks. In *hst3*Δ *hst4*Δ mutants, inappropriate presence of these proteins in front of DNA replication forks might impede the repair process. An alternative, but not mutually exclusive, possibility is that the lack of H3K56ac in front of forks in WT cells prevents recruitment of interfering proteins to sites located ahead of replication forks that encounter DNA lesions. These interfering proteins might prevent replication forks coming from the opposite direction from rescuing forks blocked by DNA lesions.

We found that a decrease in H4K16ac (*sas*2Δ mutation) and, to an even greater extent, a complete loss of H4K16ac (*H4K16R* mutation) suppress the Ts- phenotype, HU and MMS sensitivity of *hst3*Δ *hst4*Δ cells (Figure 3.4). Moreover, at least to some degree, an *H4K16R* mutation allows completion of chromosome duplication after transient exposure to MMS (Figure 3.5). Unlike *H4K16R*, single lysine-to-arginine mutations of the three other acetylateable lysine residues in the N-terminal tail of H4 (K5, K8 and K12) did not suppress the phenotypes of *hst3*Δ *hst4*Δ cells (Table 3.4). Interestingly, a previous study showed that K16-acetylated H4 molecules are very abundant in *S. cerevisiae*. Approximately 85% of H4 molecules are K16-acetylated in asynchronously proliferating WT cells (Smith *et al.* 2002). However, H4K16ac is absent from regions that are packaged into heterochromatin (Kimura*, et al.* 2002, Raisner*, et al.* 2008, Suka*, et al.* 2002). In fact, H4K16ac and the SAS-I enzyme (Sas2, Sas4 and Sas5) that acetylates H4K16 prevent the spreading of heterochromatin into euchromatic regions (Kimura*, et al.* 2002, Suka*, et al.* 2002). Thus, the boundaries between euchromatin and heterochromatin coincide with regions where there is a transition between nucleosomes that contain H4K16ac and

nucleosomes that lack H4K16ac. We found that, like the *H4K16R* and *sas2*Δ mutations, *rsc2*Δ and *yta7*Δ mutations suppress the Ts-, HU and MMS sensitivity of *hst3*Δ *hst4*Δ cells (Figure 3.4A). Interestingly, Rsc2 and Yta7 have been implicated in preventing heterochromatin spreading from the silent mating type locus and Yta7 can be detected near chromatin boundaries (Jambunathan*, et al.* 2005, Raisner*, et al.* 2008, Tackett*, et al.* 2005). Rsc2 and Yta7 also have roles in other processes such as DSB repair (Rsc2) and gene transcription (Yta7) (Kurat *et al.* 2011, Lombardi *et al.* 2011). Nonetheless, it is tempting to speculate that the *H4K16R*, *sas2*Δ, *rsc2*Δ and *yta7*Δ mutations suppress the phenotypes of *hst3*Δ *hst4*Δ mutants through a common mechanism.

One possibility for such a unifying mechanism is worth mentioning. In *hst3*Δ *hst4*Δ mutant cells, nucleosomes that contain both H3K56ac and H4K16ac are likely present throughout a major fraction of the genome because of the high stoichiometries of the two modifications (roughly 98% for H3K56ac and 85% for H4K16ac). DNA replication forks may not have evolved to progress through chromatin with a high density of nucleosomes that contain H3K56ac and H4K16ac. In WT cells, replication forks clearly do not progress through nucleosomes that contain H3K56ac because this modification is restricted to new H3 molecules that are mainly deposited behind replication forks (Kaplan*, et al.* 2008, Masumoto*, et al.* 2005). Intriguingly, the 17-polypeptide subunit Rsc1 and Rsc2 complexes each contain 5 bromodomains (Yang 2004). Rsc2 itself contains two bromodomains (Chambers*, et al.* 2012). In fact, the RSC complex contains most of the bromodomain polypeptides encoded in the *S. cerevisiae* genome. Furthermore, the Yta7 protein contains a bromodomain-like module (Jambunathan*, et al.* 2005). Bromodomains are generally involved in binding acetylated lysine residues within specific structural contexts (Filippakopoulos *et al.* 2012) but, with few exceptions, the physiologically relevant targets of most yeast bromodomain proteins are not known. It is therefore conceivable that inappropriate binding of RSC and/or Yta7 to nucleosomes that contain both H3K56ac and H4K16ac may interfere with DNA replication fork progression. Inappropriate binding of bromodomain proteins may be particularly problematic when DNA synthesis proceeds slowly because of the presence of MMS-induced DNA lesions or in HU-treated cells where dNTPs are limiting. We identified a group of suppressors of *hst3*Δ *hst4*Δ mutants that do

not exhibit a striking decrease in either H3K56ac or H4K16ac (Figure 3.6B). At first glance, this result seems inconsistent with the aforementioned model but this may not be the case. It is possible that the abundance of any one of several yeast bromodomain proteins is reduced in those suppressors. Alternatively, we previously reported that null mutations of the genes encoding the large subunits of three replication factor C-related complexes (*RAD24*, *ELG1* and *CTF18*) suppress *hst3*Δ *hst4*Δ mutant phenotypes without reducing H3K56ac (Celic*, et al.* 2008). Moreover, mutations of the genes encoding the three subunits of the PCNA-like 9-1-1 complex (*MEC3*, *DDC1* and *RAD17*) also suppress *hst3*Δ *hst4*Δ mutant phenotypes (Celic*, et al.* 2008). Reduced expression of any one of those proteins could explain why many spontaneous suppressors retain high levels of H3K56ac and H4K16ac. Further studies are clearly needed to understand how histone modifications affect replication fork progression through nucleosomes in the absence or presence of lesions in DNA template strands. Nonetheless, the genetic and molecular data presented here provide interesting avenues for future investigation.

**Table 3.3 Histone H3 gene mutations and phenotypes of *hst3*Δ *hst4*Δ mutant cells**

| Histone mutant | Sensitivity at 37°C | MMS sensitivity | HU sensitivity |
|---|---|---|---|
| *hst3*Δ *hst4*Δ *H3-WT* | Ts- | S | S |
| *H3 R2A* | Ts- | S | S |
| *H3 R2K* | Ts- | S | S |
| *H3 T6A* | Ts- | S | S |
| *H3 T6E* | Ts- | S | S |
| *H3 K9A* | Ts- | S | S |
| *H3 K9R* | Ts- | S | S |
| *H3 K9Q* | Ts- | S | S |
| *H3 S10A* | Ts- | S | S |
| *H3 S10E* | Ts- | S | S |
| *H3 T11A* | Ts- | S | S |
| *H3 T11E* | Ts- | S | S |
| *H3 K14A* | Ts- | S | S |
| *H3 K14R* | Ts- | S | S |
| *H3 K14Q* | Ts- | S | S |
| *H3 R17A* | Ts- | S | S |
| *H3 R17K* | Ts- | S | S |
| *H3 K18A* | Ts- | S | S |
| *H3 K18R* | Ts- | S | S |
| *H3 K18Q* | Ts- | S | S |
| *H3 K23A* | Ts- | S | S |
| *H3 K23R* | Ts- | S | S |
| *H3 K23Q* | Ts- | S | S |
| *H3 R26A* | Ts- | S | S |
| *H3 K26K* | Ts- | S | S |
| *H3 K27A* | Ts- | S | S |
| *H3 K27R* | Ts- | S | S |
| *H3 K27Q* | Ts- | S | S |

**Table 3.3 (continued)**

| Histone mutant | Sensitivity at 37°C | MMS sensitivity | HU sensitivity |
|---|---|---|---|
| *hst3*Δ *hst4*Δ *H3-WT* | Ts- | S | S |
| *H3 S28A* | Ts- | S | S |
| *H3 S28E* | Ts- | S | S |
| *H3 R52A* | Ts- | S | S |
| *H3 R52R* | sTr | sR | S |
| *H3 R52Q* | Ts- | S | S |
| *H3 R53A* | sTr | S | S |
| *H3 R53K* | Ts- | S | S |
| *H3 R53Q* | Ts- | S | S |
| *H3 K56A* | Tr | R | S |
| *H3 K56Q* | Tr | R | R |
| *H3K56R* | Tr | R | R |
| *H3 K59A* | Ts- | S | S |
| *H3 K59Q* | Ts- | S | S |
| *H3 K59R* | Ts- | S | S |
| *H3 K91A* | Ts- | S | S |
| *H3 K91R* | Ts- | S | S |
| *H3 K91Q* | Ts- | S | S |
| *H3 R92A* | Ts- | S | S |
| *H3 R92K* | Ts- | S | S |
| *H3 K115A* | Ts- | S | S |
| *H3 K115R* | Ts- | S | S |
| *H3 K115Q* | Ts- | S | S |
| *H3 T118A* | Ts- | S | S |
| *H3 T118E* | Ts- | S | S |
| *H3 K122A* | Ts- | S | S |
| *H3 K122R* | Ts- | S | S |
| *H3 K122Q* | Ts- | S | S |

**Table 3.4 Histone H4 gene mutations and phenotypes of *hst3*Δ *hst4*Δ mutant cells**

| Histone mutant | Sensitivity at 37°C | MMS sensitivity | HU sensitivity |
|---|---|---|---|
| *hst3*Δ *hst4*Δ *H4-WT* | Ts- | S | S |
| *H4 S1A* | Ts- | S | S |
| *H4 S1E* | Ts- | S | S |
| *H4 R3A* | Ts- | S | S |
| *H4 R3K* | Ts- | S | S |
| *H4 K5A* | Ts- | S | S |
| *H4 K5R* | Ts- | S | S |
| *H4 K5Q* | Ts- | S | S |
| *H4 K8A* | Ts- | S | S |
| *H4 K8R* | Ts- | S | S |
| *H4 K8Q* | Ts- | S | S |
| *H4 K12A* | Ts- | S | S |
| *H4 K12R* | Ts- | S | S |
| *H4 K12Q* | Ts- | S | S |
| *H4 K31A* | Ts- | S | S |
| *H4 K31R* | Ts- | S | S |
| *H4 K31Q* | Ts- | S | S |
| *H4 S47A* | Ts- | S | S |
| *H4 S47E* | Ts- | S | S |

Ts- : Thermo-sensitive (fails to grow at 37°C)
Tr: Thermo-resistant (grows at 37°C)
S: Growth compromised on plates containing either 0.01% MMS or 100mM HU
R: Histone gene mutations that rescue, at least partially, the MMS or HU sensitivity of *hst3*Δ *hst4*Δ cells.

## 3.6. References


Alvaro, D., Lisby, M. and Rothstein, R. (2007). Genome-wide analysis of Rad52 foci reveals diverse mechanisms impacting recombination. PLoS Genet 3, e228.

Barbour, L. and Xiao, W. (2006). Mating type regulation of cellular tolerance to DNA damage is specific to the DNA post-replication repair and mutagenesis pathway. Mol Microbiol 59, 637-50.

Benson, L. J., Gu, Y., Yakovleva, T., Tong, K., Barrows, C., Strack, C. L., Cook, R. G., Mizzen, C. A. and Annunziato, A. T. (2006). Modifications of H3 and H4 during chromatin replication, nucleosome assembly, and histone exchange. J Biol Chem 281, 9287-96.

Brachmann, C. B., Sherman, J. M., Devine, S. E., Cameron, E. E., Pillus, L. and Boeke, J. D. (1995). The SIR2 gene family, conserved from bacteria to humans, functions in silencing, cell cycle progression, and chromosome stability. Genes Dev 9, 2888-902.

Budzowska, M. and Kanaar, R. (2009). Mechanisms of dealing with DNA damage-induced replication problems. Cell Biochem Biophys 53, 17-31.

Burgess, R. J., Zhou, H., Han, J. and Zhang, Z. (2010). A role for Gcn5 in replication-coupled nucleosome assembly. Mol Cell 37, 469-80.

Cairns, B. R., Schlichter, A., Erdjument-Bromage, H., Tempst, P., Kornberg, R. D. and Winston, F. (1999). Two functionally distinct forms of the RSC nucleosome-remodeling complex, containing essential AT hook, BAH, and bromodomains. Mol Cell 4, 715-23.

Campos, E. I. and Reinberg, D. (2009). Histones: annotating chromatin. Annu Rev Genet 43, 559-99.

Celic, I., Masumoto, H., Griffith, W. P., Meluh, P., Cotter, R. J., Boeke, J. D. and Verreault, A. (2006). The sirtuins hst3 and Hst4p preserve genome integrity by controlling histone h3 lysine 56 deacetylation. Curr Biol 16, 1280-9.

Celic, I., Verreault, A. and Boeke, J. D. (2008). Histone H3 K56 hyperacetylation perturbs replisomes and causes DNA damage. Genetics 179, 1769-84.

Chai, B., Huang, J., Cairns, B. R. and Laurent, B. C. (2005). Distinct roles for the RSC and Swi/Snf ATP-dependent chromatin remodelers in DNA double-strand break repair. Genes Dev 19, 1656-61.

Chambers, A. L., Brownlee, P. M., Durley, S. C., Beacham, T., Kent, N. A. and Downs, J. A. (2012). The two different isoforms of the RSC chromatin remodeling complex play distinct roles in DNA damage responses. PLoS One 7, e32016.

Dang, W., Steffen, K. K., Perry, R., Dorsey, J. A., Johnson, F. B., Shilatifard, A., Kaeberlein, M., Kennedy, B. K. and Berger, S. L. (2009). Histone H4 lysine 16 acetylation regulates cellular lifespan. Nature 459, 802-7.

Downs, J. A., Lowndes, N. F. and Jackson, S. P. (2000). A role for Saccharomyces cerevisiae histone H2A in DNA repair. Nature 408, 1001-4.

Driscoll, R., Hudson, A. and Jackson, S. P. (2007). Yeast Rtt109 promotes genome stability by acetylating histone H3 on lysine 56. Science 315, 649-52.

Filippakopoulos, P., Picaud, S., Mangos, M., Keates, T., Lambert, J. P., Barsyte-Lovejoy, D., Felletar, I., Volkmer, R., Muller, S., Pawson, T., Gingras, A. C., Arrowsmith, C. H. and Knapp, S. (2012). Histone recognition and large-scale structural analysis of the human bromodomain family. Cell 149, 214-31.

Floer, M., Wang, X., Prabhu, V., Berrozpe, G., Narayan, S., Spagna, D., Alvarez, D., Kendall, J., Krasnitz, A., Stepansky, A., Hicks, J., Bryant, G. O. and Ptashne, M. (2010). A RSC/nucleosome complex determines chromatin architecture and facilitates activator binding. Cell 141, 407-18.

Ghaemmaghami, S., Huh, W. K., Bower, K., Howson, R. W., Belle, A., Dephoure, N., O'Shea, E. K. and Weissman, J. S. (2003). Global analysis of protein expression in yeast. Nature 425, 737-41.

Haase, S. B. and Reed, S. I. (2002). Improved flow cytometric analysis of the budding yeast cell cycle. Cell Cycle 1, 132-6.

Hachinohe, M., Hanaoka, F. and Masumoto, H. (2011). Hst3 and Hst4 histone deacetylases regulate replicative lifespan by preventing genome instability in Saccharomyces cerevisiae. Genes Cells 16, 467-77.

Haldar, D. and Kamakaka, R. T. (2008). Schizosaccharomyces pombe Hst4 functions in DNA damage response by regulating histone H3 K56 acetylation. Eukaryot Cell 7, 800-13.

Han, J., Zhou, H., Horazdovsky, B., Zhang, K., Xu, R. M. and Zhang, Z. (2007a). Rtt109 acetylates histone H3 lysine 56 and functions in DNA replication. Science 315, 653-5.

Han, J., Zhou, H., Li, Z., Xu, R. M. and Zhang, Z. (2007b). Acetylation of lysine 56 of histone H3 catalyzed by RTT109 and regulated by ASF1 is required for replisome integrity. J Biol Chem 282, 28587-96.

Hoppe, G. J., Tanny, J. C., Rudner, A. D., Gerber, S. A., Danaie, S., Gygi, S. P. and Moazed, D. (2002). Steps in assembly of silent chromatin in yeast: Sir3-independent binding of a Sir2/Sir4 complex to silencers and role for Sir2-dependent deacetylation. Mol Cell Biol 22, 4167-80.

Hyland, E. M., Cosgrove, M. S., Molina, H., Wang, D., Pandey, A., Cottee, R. J. and Boeke, J. D. (2005). Insights into the role of histone H3 and histone H4 core modifiable residues in Saccharomyces cerevisiae. Mol Cell Biol 25, 10060-70.

Imai, S., Armstrong, C. M., Kaeberlein, M. and Guarente, L. (2000). Transcriptional silencing and longevity protein Sir2 is an NAD-dependent histone deacetylase. Nature 403, 795-800.

Ito-Harashima, S. and McCusker, J. H. (2004). Positive and negative selection LYS5MX gene replacement cassettes for use in Saccharomyces cerevisiae. Yeast 21, 53-61.

Jackson, V., Granner, D. and Chalkley, R. (1976). Deposition of histone onto the replicating chromosome: newly synthesized histone is not found near the replication fork. Proc Natl Acad Sci U S A 73, 2266-9.

Jambunathan, N., Martinez, A. W., Robert, E. C., Agochukwu, N. B., Ibos, M. E., Dugas, S. L. and Donze, D. (2005). Multiple bromodomain genes are involved in restricting the spread of heterochromatic silencing at the Saccharomyces cerevisiae HMR-tRNA boundary. Genetics 171, 913-22.

Jasencakova, Z., Scharf, A. N., Ask, K., Corpet, A., Imhof, A., Almouzni, G. and Groth, A. (2010). Replication stress interferes with histone recycling and predeposition marking of new histones. Mol Cell 37, 736-43.

Kaplan, T., Liu, C. L., Erkmann, J. A., Holik, J., Grunstein, M., Kaufman, P. D., Friedman, N. and Rando, O. J. (2008). Cell cycle- and chaperone-mediated regulation of H3K56ac incorporation in yeast. PLoS Genet 4, e1000270.

Kimura, A., Umehara, T. and Horikoshi, M. (2002). Chromosomal gradient of histone acetylation established by Sas2p and Sir2p functions as a shield against gene silencing. Nat Genet 32, 370-7.

Kurat, C. F., Lambert, J. P., van Dyk, D., Tsui, K., van Bakel, H., Kaluarachchi, S., Friesen, H., Kainth, P., Nislow, C., Figeys, D., Fillingham, J. and Andrews, B. J. (2011). Restriction of histone gene transcription to S phase by phosphorylation of a chromatin boundary protein. Genes Dev 25, 2489-501.

Kushnirov, V. V. (2000). Rapid and reliable protein extraction from yeast. Yeast 16, 857-60.

Landry, J., Sutton, A., Tafrov, S. T., Heller, R. C., Stebbins, J., Pillus, L. and Sternglanz, R. (2000). The silencing protein SIR2 and its homologs are NAD-dependent protein deacetylases. Proc Natl Acad Sci U S A 97, 5807-11.

Li, Q., Zhou, H., Wurtele, H., Davies, B., Horazdovsky, B., Verreault, A. and Zhang, Z. (2008). Acetylation of histone H3 lysine 56 regulates replication-coupled nucleosome assembly. Cell 134, 244-55.

Livi, G. P. and Mackay, V. L. (1980). Mating-Type Regulation of Methyl Methanesulfonate Sensitivity in *Saccharomyces cerevisiae*. Genetics 95, 259-271.

Lombardi, L. M., Ellahi, A. and Rine, J. (2011). Direct regulation of nucleosome density by the conserved AAA-ATPase Yta7. Proc Natl Acad Sci U S A 108, E1302-11.

Maas, N. L., Miller, K. M., DeFazio, L. G. and Toczyski, D. P. (2006). Cell cycle and checkpoint regulation of histone H3 K56 acetylation by Hst3 and Hst4. Mol Cell 23, 109-19.

Maringele, L. and Lydall, D. (2006). Pulsed-field gel electrophoresis of budding yeast chromosomes. Methods Mol Biol 313, 65-73.

Masumoto, H., Hawke, D., Kobayashi, R. and Verreault, A. (2005). A role for cell-cycle-regulated histone H3 lysine 56 acetylation in the DNA damage response. Nature 436, 294-8.

Miller, K. M., Maas, N. L. and Toczyski, D. P. (2006). Taking it off: regulation of H3 K56 acetylation by Hst3 and Hst4. Cell Cycle 5, 2561-5.

Munoz-Galvan, S., Jimeno, S., Rothstein, R. and Aguilera, A. (2013). Histone H3K56 acetylation, Rad52, and non-DNA repair factors control double-strand break repair choice with the sister chromatid. PLoS Genet 9, e1003237.

Oum, J. H., Seong, C., Kwon, Y., Ji, J. H., Sid, A., Ramakrishnan, S., Ira, G., Malkova, A., Sung, P., Lee, S. E. and Shim, E. Y. (2011). RSC facilitates Rad59-dependent homologous recombination between sister chromatids by promoting cohesin loading at DNA double-strand breaks. Mol Cell Biol 31, 3924-37.

Ozdemir, A., Spicuglia, S., Lasonder, E., Vermeulen, M., Campsteijn, C., Stunnenberg, H. G. and Logie, C. (2005). Characterization of lysine 56 of histone H3 as an acetylation site in Saccharomyces cerevisiae. J Biol Chem 280, 25949-52.

Park, J. H., Cosgrove, M. S., Youngman, E., Wolberger, C. and Boeke, J. D. (2002). A core nucleosome surface crucial for transcriptional silencing. Nat Genet 32, 273-9.

Parthun, M. R., Widom, J. and Gottschling, D. E. (1996). The major cytoplasmic histone acetyltransferase in yeast: links to chromatin replication and histone metabolism. Cell 87, 85-94.

Pellicioli, A., Lucca, C., Liberi, G., Marini, F., Lopes, M., Plevani, P., Romano, A., Di Fiore, P. P. and Foiani, M. (1999). Activation of Rad53 kinase in response to DNA damage and its effect in modulating phosphorylation of the lagging strand DNA polymerase. EMBO J 18, 6561-72.

Raisner, R. M. and Madhani, H. D. (2008). Genomewide screen for negative regulators of sirtuin activity in Saccharomyces cerevisiae reveals 40 loci and links to metabolism. Genetics 179, 1933-44.

Ransom, M., Dennehey, B. K. and Tyler, J. K. (2010). Chaperoning histones during DNA replication and repair. Cell 140, 183-95.

Recht, J., Tsubota, T., Tanny, J. C., Diaz, R. L., Berger, J. M., Zhang, X., Garcia, B. A., Shabanowitz, J., Burlingame, A. L., Hunt, D. F., Kaufman, P. D. and Allis, C. D. (2006). Histone chaperone Asf1 is required for histone H3 lysine 56 acetylation, a modification associated with S phase in mitosis and meiosis. Proc Natl Acad Sci U S A 103, 6988-93.

Reid, R. J., Gonzalez-Barrera, S., Sunjevaric, I., Alvaro, D., Ciccone, S., Wagner, M. and Rothstein, R. (2011). Selective ploidy ablation, a high-throughput plasmid transfer protocol, identifies new genes affecting topoisomerase I-induced DNA damage. Genome Res 21, 477-86.

Ruiz-Carrillo, A., Wangh, L. J. and Allfrey, V. G. (1975). Processing of newly synthesized histone molecules. Science 190, 117-28.

Saiardi, A., Resnick, A. C., Snowman, A. M., Wendland, B. and Snyder, S. H. (2005). Inositol pyrophosphates regulate cell death and telomere length through phosphoinositide 3-kinase-related protein kinases. Proc Natl Acad Sci U S A 102, 1911-4.

Santocanale, C. and Diffley, J. F. (1998). A Mec1- and Rad53-dependent checkpoint controls late-firing origins of DNA replication. Nature 395, 615-8.

Segurado, M. and Diffley, J. F. (2008). Separate roles for the DNA damage checkpoint protein kinases in stabilizing DNA replication forks. Genes Dev 22, 1816-27.

Shim, E. Y., Ma, J. L., Oum, J. H., Yanez, Y. and Lee, S. E. (2005). The yeast chromatin remodeler RSC complex facilitates end joining repair of DNA double-strand breaks. Mol Cell Biol 25, 3934-44.

Smith, C. M., Haimberger, Z. W., Johnson, C. O., Wolf, A. J., Gafken, P. R., Zhang, Z., Parthun, M. R. and Gottschling, D. E. (2002). Heritable chromatin structure: mapping "memory" in histones H3 and H4. Proc Natl Acad Sci U S A 99 Suppl 4, 16454-61.

Smith, J. S., Brachmann, C. B., Celic, I., Kenna, M. A., Muhammad, S., Starai, V. J., Avalos, J. L., Escalante-Semerena, J. C., Grubmeyer, C., Wolberger, C. and Boeke, J. D. (2000). A phylogenetically conserved NAD+-dependent protein deacetylase activity in the Sir2 protein family. Proc Natl Acad Sci U S A 97, 6658-63.

Smith, J. S., Brachmann, C. B., Pillus, L. and Boeke, J. D. (1998). Distribution of a limited Sir2 protein pool regulates the strength of yeast rDNA silencing and is modulated by Sir4p. Genetics 149, 1205-19.

Su, D., Hu, Q., Li, Q., Thompson, J. R., Cui, G., Fazly, A., Davies, B. A., Botuyan, M. V., Zhang, Z. and Mer, G. (2012). Structural basis for recognition of H3K56-acetylated histone H3-H4 by the chaperone Rtt106. Nature 483, 104-7.

Suka, N., Luo, K. and Grunstein, M. (2002). Sir2p and Sas2p opposingly regulate acetylation of yeast histone H4 lysine16 and spreading of heterochromatin. Nat Genet 32, 378-83.

Sutton, A., Shia, W. J., Band, D., Kaufman, P. D., Osada, S., Workman, J. L. and Sternglanz, R. (2003). Sas4 and Sas5 are required for the histone acetyltransferase activity of Sas2 in the SAS complex. J Biol Chem 278, 16887-92.

Sweeney, F. D., Yang, F., Chi, A., Shabanowitz, J., Hunt, D. F. and Durocher, D. (2005). Saccharomyces cerevisiae Rad9 acts as a Mec1 adaptor to allow Rad53 activation. Curr Biol 15, 1364-75.

Tackett, A. J., Dilworth, D. J., Davey, M. J., O'Donnell, M., Aitchison, J. D., Rout, M. P. and Chait, B. T. (2005). Proteomic and genomic characterization of chromatin complexes at a boundary. J Cell Biol 169, 35-47.

Taddei, A., Roche, D., Sibarita, J. B., Turner, B. M. and Almouzni, G. (1999). Duplication and maintenance of heterochromatin domains. J Cell Biol 147, 1153-66.

Tang, Y., Holbert, M. A., Wurtele, H., Meeth, K., Rocha, W., Gharib, M., Jiang, E., Thibault, P., Verreault, A., Cole, P. A. and Marmorstein, R. (2008). Fungal Rtt109 histone acetyltransferase is an unexpected structural homolog of metazoan p300/CBP. Nat Struct Mol Biol 15, 738-45.

Tanny, J. C. and Moazed, D. (2001). Coupling of histone deacetylation to NAD breakdown by the yeast silencing protein Sir2: Evidence for acetyl transfer from substrate to an NAD breakdown product. Proc Natl Acad Sci U S A 98, 415-20.

Tercero, J. A. and Diffley, J. F. (2001). Regulation of DNA replication fork progression through damaged DNA by the Mec1/Rad53 checkpoint. Nature 412, 553-7.

Thaminy, S., Newcomb, B., Kim, J., Gatbonton, T., Foss, E., Simon, J. and Bedalov, A. (2007). Hst3 is regulated by Mec1-dependent proteolysis and controls the S phase checkpoint and sister chromatid cohesion by deacetylating histone H3 at lysine 56. J Biol Chem 282, 37805-14.

Tsubota, T., Berndsen, C. E., Erkmann, J. A., Smith, C. L., Yang, L., Freitas, M. A., Denu, J. M. and Kaufman, P. D. (2007). Histone H3-K56 acetylation is catalyzed by histone chaperone-dependent complexes. Mol Cell 25, 703-12.

Veaute, X., Jeusset, J., Soustelle, C., Kowalczykowski, S. C., Le Cam, E. and Fabre, F. (2003). The Srs2 helicase prevents recombination by disrupting Rad51 nucleoprotein filaments. Nature 423, 309-12.

Wurtele, H., Kaiser, G. S., Bacal, J., St-Hilaire, E., Lee, E. H., Tsao, S., Dorn, J., Maddox, P., Lisby, M., Pasero, P. and Verreault, A. (2012). Histone H3 lysine 56 acetylation and the response to DNA replication fork damage. Mol Cell Biol 32, 154-72.

Wurtele, H., Tsao, S., Lepine, G., Mullick, A., Tremblay, J., Drogaris, P., Lee, E. H., Thibault, P., Verreault, A. and Raymond, M. (2010). Modulation of histone H3 lysine 56 acetylation as an antifungal therapeutic strategy. Nat Med 16, 774-80.

Wurtele, H. and Verreault, A. (2006). Histone post-translational modifications and the response to DNA double-strand breaks. Curr Opin Cell Biol 18, 137-44.

Yang, X. J. (2004). Lysine acetylation and the bromodomain: a new partnership for signaling. Bioessays 26, 1076-87.

# 4. General conclusion and future perspectives

In *S. cerevisiae*, histone H3 lysine 56 acetylation (H3K56ac) peaks concomitantly with DNA synthesis and plays an essential role in resistance to DNA damage that occurs during S phase (Masumoto*, et al.* 2005). This modification is later removed from the genome during G2 or M phase (Masumoto*, et al.* 2005) by the two sirtuins Hst3 and Hst4 (Maas*, et al.* 2006, Thaminy*, et al.* 2007), although the former makes the major contribution to H3K56 deacetylation (Celic*, et al.* 2006). Given the importance of H3K56ac for the DNA damage response during S phase, H3K56 deacetylases should be degraded before the onset of DNA synthesis in the daughter cell such that H3K56ac can accumulate in the genome during the next round of replication. Indeed, it has been shown that both Hst3 and Hst4 are degraded prior to S phase (Maas*, et al.* 2006) by the ubiquitin-proteasome pathway (Tang*, et al.* 2005, Thaminy*, et al.* 2007). A previous study demonstrated that the degradation of Hst4 is triggered by the E3 ligase $SCF^{Cdc4}$(Tang*, et al.* 2005). However, the molecular machinery that controls destruction of Hst3 during the cell cycle remained unidentified. On the other hand, in spite of the critical function of H3K56ac in response to DNA damage, previous studies have established that hyperacetylation of H3K56 in cells lacking both Hst3 and Hst4 (*hst3*Δ *hst4*Δ mutants) gives rise to spontaneous DNA damage and genomic instability (Brachmann*, et al.* 1995, Celic*, et al.* 2008). Nonetheless, it was not clear how lack of H3K56 deacetylation results in such catastrophic consequences. Therefore, this thesis was mainly focused on studying the regulation of the H3K56 deacetylase Hst3 during the cell cycle and the mechanisms underlying the severe phenotypes of H3K56 deacetylase mutants in *S. cerevisiae*.

In chapter 2, we initiated a study on the regulation of the main H3K56 deacetylase, Hst3, during the cell cycle. First, we demonstrated that Hst3 degradation can be completed prior to entry into anaphase (Figure 2.1). Moreover, we found that Hst3 is phosphorylated at two Cdk1 sites, threonines 380 and 384, *in vivo* (Figure 2.2) and we established that these sites constitute a phosphodegron that triggers subsequent ubiquitylation and degradation of Hst3 (Figures 2.3 and 2.6). Surprisingly, these phosphorylation events were uncovered by a phosphoproteomics study in the absence of the proteasome inhibitor MG132, suggesting that phosphorylation of Hst3 at T380 and T384 does not target it immediately to the proteasome. Moreover, we showed that Hst3 was phosphorylated by the main mitotic

kinase Clb2-Cdk1 *in vitro* (Figure 2.6). As noted in the introduction, *HST3* and *CLB2* belong to a cluster of coregulated genes that are expressed simultaneously between late S phase and mitosis (Koranda*, et al.* 2000, Zhu*, et al.* 2000). This suggests that Hst3 may be phosphorylated by Clb2-Cdk1 as soon as it is synthesized. Hence, although paradoxical, the Hst3 destruction signal can be generated when this sirtuin is most needed for genome-wide removal of H3K56ac. A critical question that remains to be addressed is how phosphorylated Hst3 is protected from proteasomal degradation until it has completed H3K56 deacetylation. We speculated that the structure of the Hst3 phosphodegron may partially hinder its recognition by $SCF^{Cdc4}$ during mitosis. However, another attractive possibility is that the C-terminal phosphorylation sites of Hst3 are somehow masked from SCF until this sirtuin has completed H3K56ac removal. A potential mechanism for such protection could be association of Hst3 with other proteins or dimerization through its C-terminal domain. Thus, determining the structure of Hst3 and its protein interactions should greatly improve our understanding of its regulation by post-translational modifications *in vivo*.

Previous work from our laboratory demonstrated that repression of Hst3 by nicotinamide (NAM) is cytotoxic to several pathogenic fungi including *C. albicans* and *C. tropicalis* in which Hst3 is the only H3K56 deacetylase. *C. albicans* cells lacking Rtt109 are resistant to NAM suggesting that Hst3 repression is highly detrimental because it results in H3K56 hyperacetylation (Wurtele*, et al.* 2010). Given the clinical relevance of H3K56ac removal, it would be important to understand how Hst3 is regulated during the cell cycle in pathogenic fungi. Sequence alignments of Hst3 orthologs from several fungal species revealed that the Cdk1 sites of *S. cerevisiae* Hst3 and their spacing are conserved in *C. albicans* and *C. tropicalis* (Figure 2.2B). Therefore, our findings on the mechanism of Hst3 degradation in *S. cerevisiae* may provide insights into the post-translational control of H3K56 deacetylases in these fungal pathogens. The first step toward understanding the regulation of Hst3 in the aforementioned pathogenic fungi would be to verify whether the conserved Cdk1 sites of Hst3 get phosphorylated in these species.

In our study we originally hypothesized that, in the absence of Hst4, a non-degradable form of Hst3 would prematurely remove H3K56ac from the genome and render cells sensitive to genotoxic stress during S phase, because it would mimic the phenotype of *rtt109*Δ cells. However, our Cdk1 site mutants of Hst3 were still degraded prior to S phase (Figure 2.3), which might explain why these Hst3 mutants are at best mildly sensitive to genotoxic agents such as MMS (Figure 4.1). Nonetheless, complete stabilization of Hst3 during the cell cycle may not be sufficient to confer sensitivity to genotoxic agents. Because Hst3 is degraded by a Mec1 and Rad53-dependent pathway in response to DNA damage (Maas*, et al.* 2006, Thaminy*, et al.* 2007), Hst3 mutants that are not degradable during a normal cell cycle might still be phosphorylated by DNA damage response kinases and subsequently degraded. Hence, an important follow-up to our results would be to establish that the degradation of Hst3 is controlled by non-redundant pathways during the cell cycle and in response to DNA damage. Future studies should examine whether Hst3 is a direct target of Mec1 and/or Rad53 and identify sequence motifs that are required for its degradation in response to DNA damage. Moreover, it would be important to investigate whether E3 ligases other than $SCF^{Cdc4}$ are involved in the degradation of Hst3 in the face of genotoxic stress.

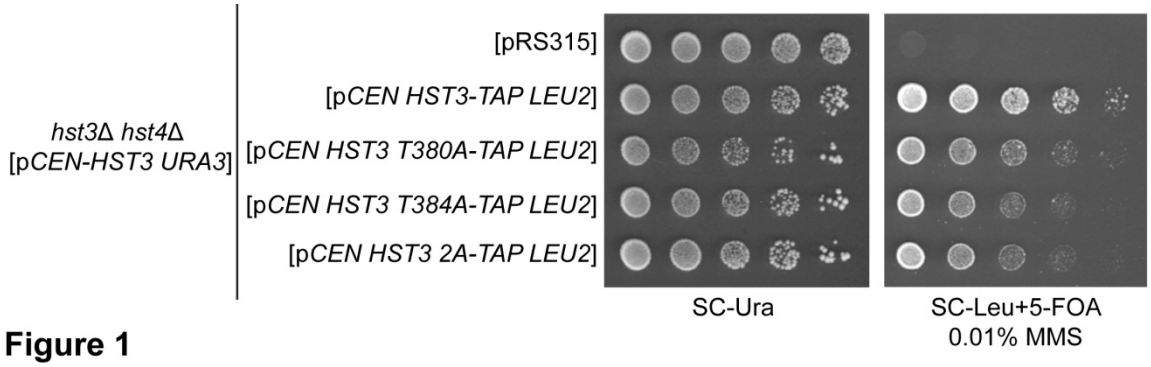


**Figure 4.1 Spot assay on strains expressing Cdk1 site mutants of Hst3.** 5-fold serial dilutions of each strain were spotted on Sc-Ura plate, or Sc-Leu medium containing 5-FOA and 0.0.1% MMS. Plates were incubated at 25°C.

Our results indicated that Hst3 carrying mutations of its two Cdk1 sites (T380 and T384) is not completely stabilized throughout the cell cycle (Figure 2.3). This observation might suggest that Hst3 contains unidentified degrons that direct its destruction by $SCF^{Cdc4}$ in the absence of T380 and T384. However, it is also possible that SCF is not the only E3 enzyme that controls degradation of Hst3 during the cell cycle. In spite of the fact that Hst3 can be degraded prior to anaphase in the absence of APC activity, two lines of evidence support an important role for this E3 ligase in timely degradation of Hst3. Based on a previous publication, Hst3 has a short half-life of 8.5 min during an unperturbed cell cycle (Thaminy*, et al.* 2007). However, in the absence of APC activity (nocodazole-treated cells or *cdc23-1* mutant cells at restrictive temperature), Hst3 levels persisted for much longer before it was eventually degraded by $SCF^{Cdc4}$ (Figure 2.1). Moreover, our unpublished results demonstrated that overexpressed Hst3 has a shorter half-life at mitotic exit and during G1 when APC is active than before entry into anaphase when APC is inactive (Figure 4.2). Taken together, these results suggest that APC may also contribute, either directly or indirectly, to degradation of Hst3 at the end of the cell cycle. Hst3 contains a consensus D-box motif, which is often found in APC substrates (Simpson-Lavy *et al.* 2010). Mutation of this putative D-box only slightly increased the stability of Hst3 *in vivo* (unpublished data). However, rather than direct ubiquitylation of Hst3, APC might have an indirect role in regulation of Hst3 levels during the cell cycle. For instance, it is possible that entry into anaphase, which requires the ubiquitin ligase activity of APC, somehow signals for rapid degradation of Hst3 by $SCF^{Cdc4}$. Future studies should determine the timing of degradation of Hst3 during an undisturbed cell cycle (*i.e.* in the absence of nocodazole) and investigate whether Hst3 is a direct target of the APC complex.

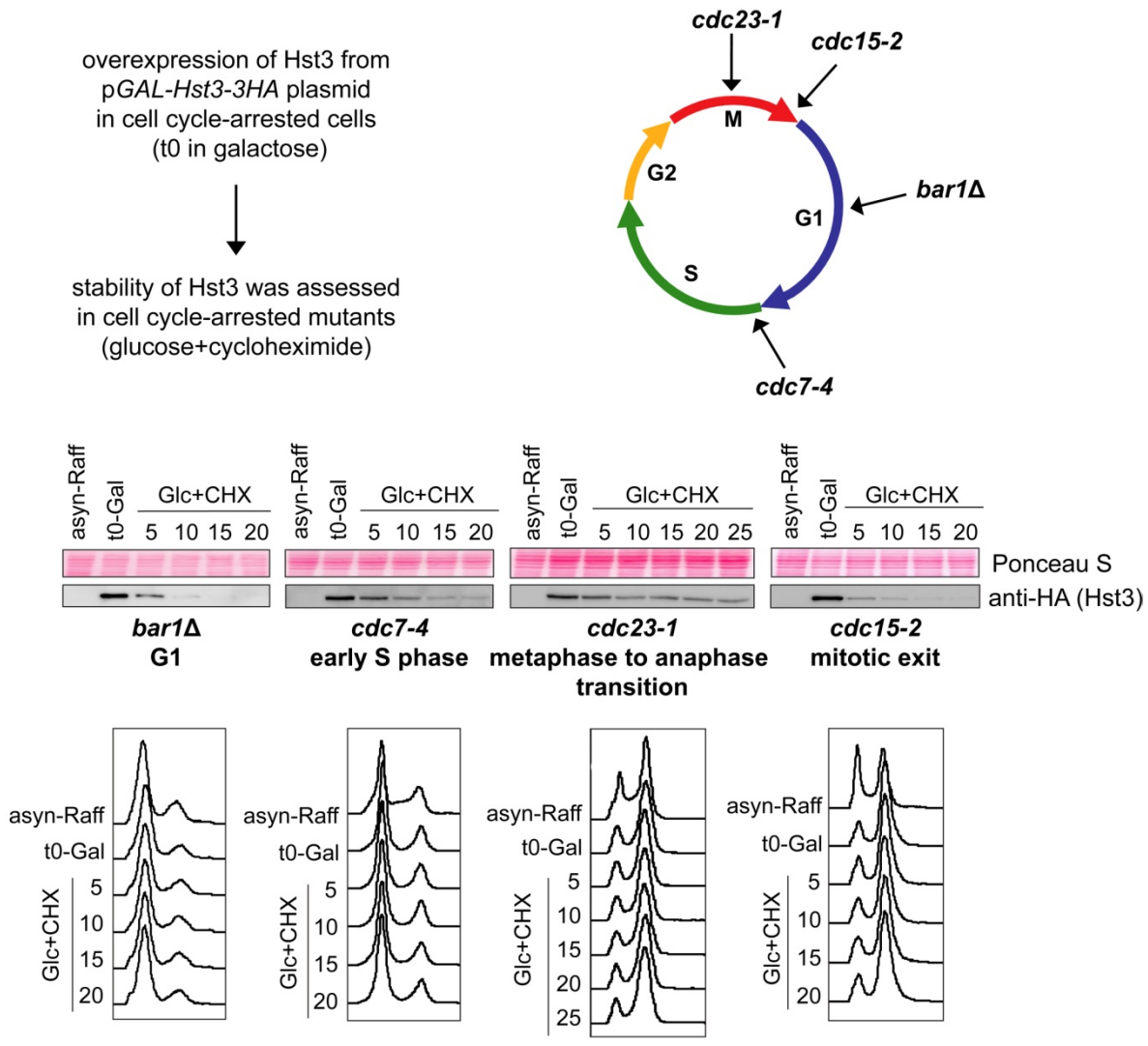


**Figure 2**

**Figure 4.2 Hst3 is most unstable at mitotic exit and during G1.** The experimental design is described on the figure. All mutant strains were grown to early log-phase in raffinose overnight (asyn-Raff). Cells that arrested the cell cycle at different stages were then grown in the presence of 2% galactose (Gal) to overexpress plasmid-borne Hst3 from a galactose-inducible promoter (t0-Gal). Overexpression of Hst3 was repressed by addition of 2% glucose (Glc) and protein translation was blocked by addition of cycloheximide (CHX), and samples were collected as a function of time. For each strain, whole cell extracts prepared from equal number of cells were resolved through SDS-PAGE and probed by immunoblotting with anti-HA antibody to assess the stability of Hst3. Cell cycle arrest was verified by FACS analysis.

A few studies have reported a complex network of genetic interactions between APC, SCF and components of the *de novo* chromatin assembly pathway. When grown at the restrictive temperature, the thermosensitive APC mutant *apc5*$^{CA}$ and mutants of the SCF ubiquitination pathway *cdc34-2* and *cdc53-1* show chromatin assembly defects *in vitro* (Arnason *et al.* 2005, Harkness *et al.* 2002). Moreover, mutations that cripple the chromatin assembly factor CAF-1 show genetic interactions with mutations in the APC complex: deletion of genes encoding CAF-1 subunits exacerbates the thermosensitivity (Ts) of the APC mutants *apc5*$^{CA}$, *apc10*Δ and *apc26*Δ. However, the connection between these E3 ligases and the chromatin assembly pathway remains utterly unclear. We propose that the role of SCF and APC in regulation of H3K56 deacetylases during the cell cycle might provide a functional link between these ubiquitin ligases and the chromatin assembly pathway. As mentioned in the introduction, H3K56ac promotes replication-coupled nucleosome assembly (Li*, et al.* 2008). On the other hand, SCF$^{Cdc4}$ targets both H3K56 deacetylases Hst3 and Hst4 to the proteasome. As mentioned above, APC activity probably also contributes, either directly or indirectly, to the degradation of Hst3 *in vivo*. Hence, mutations that impair SCF or APC activity should result in delayed or incomplete degradation of Hst3 and Hst4 during the cell cycle. Aberrant presence of H3K56 deacetylases during S phase might in turn cripple chromatin assembly by prematurely removing H3K56ac from new histone H3 molecules. Consistent with this model, overexpression of Rtt109, Asf1, CAF-1 or histones H3-H4 suppress *apc5*$^{CA}$ phenotypes (Harkness *et al.* 2005, Turner *et al.* 2010). H3K56ac is mediated by Rtt109 in collaboration with Asf1, and overexpression of Asf1 alone has been shown to increase H3K56ac levels in wild-type and *apc5*$^{CA}$ cells (Turner*, et al.* 2010). In addition to its direct contribution to H3K56ac, Asf1 probably also presents H3-H4 dimers to CAF-1 during *de novo* chromatin assembly (Zhang *et al.* 2013). Furthermore, increased levels of CAF-1 and histones H3-H4 might enhance nucleosome assembly behind replication forks and thus partially compensate for the lower affinity of CAF-1 and Rtt106 for histone H3 when H3K56ac is prematurely removed by Hst3/Hst4 during S phase. Indeed, previous studies showed that CAF-1 and Rtt106 bind more tightly to H3 molecules that are K56-acetylated than to non-modified H3 (Li*, et al.* 2008, Su*, et al.* 2012). Since SCF$^{Cdc4}$ has a central role in the degradation of H3K56 deacetylases, our proposed model predicts that mutations in the SCF

ubiquitination pathway should exacerbate the phenotypes of mutations in components of the *de novo* chromatin assembly machinery. It would be interesting to test this possibility in future studies. Based on our model, it would be also interesting to determine whether cell extracts containing abnormally high levels of Hst3 and/or Hst4 (*e.g.* extracts derived from cells expressing Cdk1 site mutants of *HST3*) are defective in chromatin assembly *in vitro*.

Before our study it was not known how degradation of H3K56 deacetylases always precedes S phase when H3K56ac needs to accumulate behind DNA replication forks. Previous findings and our data on regulation of both Hst3 and Hst4 (Tang, *et al.* 2005) by $SCF^{Cdc4}$ explains how timely destruction of H3K56 deacetylases is achieved during the cell cycle. As mentioned before, $SCF^{Cdc4}$ controls entry into S phase by triggering degradation of the Cdk1 inhibitor Sic1 (Verma, *et al.* 1997). Hence, expression of Hst3 and Hst4 after S phase (Maas, *et al.* 2006) and degradation of Hst3, Hst4 and Sic1 by $SCF^{Cdc4}$ allows entry into S phase in the absence of H3K56 deacetylases such that H3K56ac can accumulate in the genome and perform its important functions during S phase (Figure 4.3).

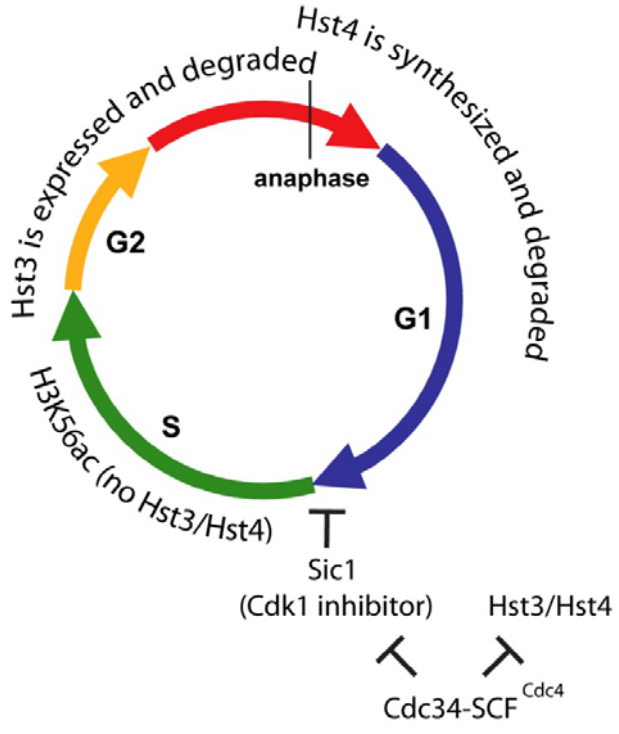


Figure 3

**Figure 4.3 A model for the expression and degradation of H3K56 deacetylases during the cell cycle in *S. cerevisiae*.**

In *S. cerevisiae*, cells that lack the sirtuins Hst3 and Hst4 (*hst3*Δ *hst4*Δ cells) show an elevated incidence of spontaneous DNA damage, hypersensitivity to genotoxic agents that damage DNA during replication and genomic instability (Brachmann*, et al.* 1995, Celic*, et al.* 2008, Hachinohe*, et al.* 2011, Thaminy*, et al.* 2007). Although the severe phenotypes of *hst3*Δ *hst4*Δ cells are known to stem from hyperacetylation of H3K56 (Celic*, et al.* 2006, Maas*, et al.* 2006), it is not clear why overabundance of this modification is so deleterious to genomic integrity. Therefore, in chapter 3 of this thesis we set out to decipher the molecular mechanisms that are responsible for the pronounced phenotypes of *hst3*Δ *hst4*Δ cells. In the first section of this study, we investigated the effect of transient treatment with genotoxic agents on the dynamics of DNA replication and the DNA damage response in H3K56 deacetylase mutants. In the second part of this chapter, we employed a genetic approach and discovered several novel classes of suppressors that partially alleviate the severe phenotypes of *hst3*Δ *hst4*Δ cells. Interestingly, we found that the majority of the identified suppressors do not have decreased levels of H3K56ac compared with *hst3*Δ *hst4*Δ cells. Thus, further characterization of these suppressors should yield valuable insights into how hyperacetylation of H3K56 interferes with normal DNA metabolism.

In chapter 3, we demonstrated for the first time that *hst3*Δ *hst4*Δ cells lose viability after treatment with MMS during a single round of S phase (Figure 3.1A). Importantly, we found that unlike wild-type cells, H3K56 deacetylase mutants failed to complete DNA replication long after removal of the exogenous source of DNA damage (Figure 3.1D). Moreover, our results indicated that the severe loss of viability of *hst3*Δ *hst4*Δ cells after transient genotoxic stress does not result from defects in activation of the DNA damage checkpoint. However, we found that *hst3*Δ *hst4*Δ cells showed persistent activation of the DNA damage checkpoint after transient exposure to MMS suggesting that these cells struggle to repair MMS-induced DNA adducts and, as a result, exhibit persistent checkpoint activation (Figure 3.1, B and C). Intriguingly, we observed that pharmacological inhibition of DNA damage checkpoint kinases Mec1 and Tel1 by caffeine improved the viability of MMS-treated H3K56 deacetylase mutants (Figure 3.2). In *hst3*Δ *hst4*Δ cells, almost 100% of H3 molecules are K56-acetylated (Celic*, et al.* 2006). Thus, during DNA synthesis nearly all the parental histone H3 molecules in front of replication

forks, as well as the parental and new histone H3 molecules deposited onto DNA behind replication forks, bear H3K56ac. In this study, we established that restoring the wild-type stoichiometry of H3K56ac (almost 50%) behind the replication fork does not improve the viability of *hst3*Δ *hst4*Δ cells after transient exposure to MMS (Figure 3.3). This result suggests that the severe genotoxic agent sensitivity of *hst3*Δ *hst4*Δ cells is caused by hyperacetylation of H3K56 in front of replication forks. Taken together, our findings demonstrate that hyperacetylation of H3K56 impedes completion of DNA replication after transient exposure to MMS.

In *S. cerevisiae*, histone H4 lysine 16 acetylation (H4K16ac) is a highly abundant modification that is present in almost 85% of H4 molecules (Smith *et al.* 2003). H4K16ac is mostly mediated by the histone acetyltransferase Sas2 and is removed from the genome by Sir2 (Kimura*, et al.* 2002, Suka*, et al.* 2002). Our data from a genetic screen demonstrated that point mutations of histone H4 lysine 16 strongly suppress the sensitivity phenotypes of *hst3*Δ *hst4*Δ mutants (Table 3.2). We found that mutations that abolish H4K16ac, namely the *H4K16R* mutation or *SAS2* deletion, alleviated the thermosensitivity and genotoxic agent sensitivity of *hst3*Δ *hst4*Δ cells (Figure 3.4A), without decreasing H3K56ac or H2AP levels (Figure 3.4B). Moreover, we observed stronger suppression of *hst3*Δ *hst4*Δ phenotypes by the *H4K16R* mutation than the *SAS2* deletion (Figure 3.4A). This probably reflects the fact that *sas2*Δ cells do not completely lack H4K16ac (Figure 3.4B). Interestingly, in spite of high levels of DNA damage as monitored by H2AP, *hst3*Δ *hst4*Δ *H4K16R* cells showed attenuated activation of the DNA damage checkpoint (Figure3.4B) and completed DNA replication after transient MMS exposure (Figure 3.5C). Collectively, these findings suggest that the genome-wide presence of H4K16ac is deleterious to cells that cannot deacetylate H3K56.

Our results suggest that the severe loss of viability of *hst3*Δ *hst4*Δ cells following genotoxic stress is mainly caused by failure to complete DNA synthesis rather than defects in repair of MMS-induced DNA lesions. As mentioned earlier, small perturbations to the replication machinery are toxic to *hst3*Δ *hst4*Δ cells, indicating that the H3K56 deacetylase mutants struggle with DNA synthesis even in the absence of exogenous DNA damage

(Celic*, et al.* 2008). In this study, we demonstrated that the *H4K16R* mutation or *SAS2* deletion strongly suppress the temperature and genotoxic agent sensitivity of *hst3*Δ *hst4*Δ cells without decreasing H3K56ac or H2AP levels. Moreover, mutations that reduce or abolish H4K16ac allow epitope tagging of replication proteins such as Cdc45 in the *hst3*Δ *hst4*Δ background, suggesting that they facilitate DNA replication in H3K56 deacetylase mutants. Consistent with this, pulsed field gel electrophoresis demonstrated that *hst3*Δ *hst4*Δ *H4K16R* mutants completed DNA synthesis after transient MMS treatment (Figure 3.5C). Hence, even in the presence of H3K56 hyperacetylation and high levels of H2AP, which is a surrogate marker of DNA DSBs, completion of DNA replication was associated with an improved viability of *hst3*Δ *hst4*Δ cells. In support of this idea, a previous study reported that overexpression of the large subunit of the RFC complex, Rfc1, partially suppresses the genotoxic agent sensitivity of *hst3*Δ *hst4*Δ cells (Celic*, et al.* 2008). Given that the RFC complex loads the DNA polymerase processivity factor PCNA onto DNA (Howell *et al.* 1994), overexpression of Rfc1 might also facilitate DNA replication in *hst3*Δ *hst4*Δ cells. To test this possibility, it would be important to verify whether overexpression of Rfc1 in *hst3*Δ *hst4*Δ cells allows completion of DNA replication after transient MMS exposure. Furthermore, it would be interesting to investigate whether overexpression of the PCNA subunits or replicative polymerases can also suppress the temperature and genotoxic agent sensitivity of cells lacking Hst3 and Hst4.

The contribution of the S phase checkpoint to resistance to genotoxic stress in *hst3*Δ *hst4*Δ cells remains enigmatic. Cells lacking Hst3 and Hst4 show synthetic lethality with deletion of several components of the S phase checkpoint including *MEC1*, *RAD9*, *DUN1* and subunits of the replication-pausing checkpoint complex *TOF1*, *MRC1* and *CSM3* (Brachmann*, et al.* 1995, Celic*, et al.* 2008, Thaminy*, et al.* 2007). On the other hand, deletion of *RAD24* or *ELG1*, which are the large subunits of alternative RFC-like complexes involved in the DNA damage response, strongly suppresses the thermosensitivity of *hst3*Δ *hst4*Δ cells (Celic*, et al.* 2008). Moreover, deletion of *DDC1*, *RAD17* or *MEC3* encoding the three subunits of the 9-1-1 clamp also suppresses the Ts phenotype of *hst3*Δ *hst4*Δ mutants. The 9-1-1 complex is a key mediator of the DNA

damage checkpoint that is loaded at sites of DNA damage by the Rad24-RFC clamp loader (Nyberg, *et al.* 2002). Hence, it is puzzling that *hst3*Δ *hst4*Δ cells, which suffer from endogenous DNA damage, benefit from a loss of these RFC-like complexes or the 9-1-1 clamp. Nonetheless, since the Rfc2-5 subunits are shared between the replicative clamp loader and RFC-like complexes, deletion of the large subunits of alternative clamp loaders might facilitate the action of the RFC complex that is essential for DNA replication (Celic, *et al.* 2008). Moreover, our results indicated that inhibition of Mec1 and Tel1 by caffeine partially improved the viability of *hst3*Δ *hst4*Δ cells after transient treatment with MMS (Figure 3.2). It is noteworthy that the DNA damage checkpoint inhibits the firing of late origins of replication (Nyberg, *et al.* 2002). Hence, inhibition of checkpoint kinases might improve cell viability by increasing the number of active origins and promoting completion of DNA replication in *hst3*Δ *hst4*Δ cells. In support of this idea, flow cytometry analysis demonstrated that the majority of *hst3*Δ *hst4*Δ cells treated with caffeine completed S phase after transient treatment with MMS (Figure 3.2B). In addition, we observed that completion of DNA replication in *hst3*Δ *hst4*Δ *H4K16R* cells correlated with diminished checkpoint signaling, as demonstrated by Rad53 autophosphorylation, in the presence of high levels of DNA damage measured by H2AP levels (Figure 3.4B). Altogether, these findings suggest that although the S phase checkpoint promotes cell survival in the face of genotoxic stress, its partial attenuation favors completion of DNA replication, which is highly beneficial for survival of *hst3*Δ *hst4*Δ cells treated with DNA damaging agents.

H4K16ac has been implicated in creating boundaries between heterochromatin and euchromatin. It has been shown that the opposing action of Sas2 and Sir2 establishes a gradient of H4K16ac at the transition zone between subtelomeric heterochromatin and euchromatin. The heterochromatic region is devoid of H4K16ac, whereas the euchromatic side of the boundary contains high levels of this modification. Moreover, mutations that abolish H4K16ac allow silencing factors such as Sir3 to spread from heterochromatin into adjacent euchromatic regions (Kimura, *et al.* 2002, Suka, *et al.* 2002). H4K16ac might also contribute to regulation of chromatin boundaries at silent mating type loci and ribosomal DNA (rDNA) because Sas2 and Sir2 are important for silencing at these genomic regions (Kimura *et al.* 2004). Therefore, suppression of the phenotypes of *hst3*Δ *hst4*Δ mutants in

the absence of H4K16ac might result from modulation of barriers between heterochromatin and neighboring euchromatic regions. Consistent with this mode of suppression, the *hst3*Δ *hst4*Δ phenotypes are also partially suppressed by deletion of *YTA7* or *RSC2*, which are important to prevent heterochromatin spreading away from the transcriptionally silent *HMR***a** mating type locus (Jambunathan*, et al.* 2005). As is the case for mutations that abolish H4K16ac, these suppressors did not show reduced levels of H3K56ac or H2AP (Figure 3.4B). Collectively, these results strongly suggest that modulation of chromatin boundaries improves the viability of H3K56 deacetylase mutants.

During DNA synthesis, replication forks pause when they encounter tightly-bound protein-DNA complexes at the rDNA locus, centromeres and telomeric regions of *S. cerevisiae* (Labib *et al.* 2007). Moreover, replication fork pausing has been reported at dormant replication origins close to the silent *HML*α mating type locus (Wang *et al.* 2001). The natural pause sites are associated with an increased frequency of DNA recombination, the underlying mechanism of which is poorly understood (Labib*, et al.* 2007). However, several studies have proposed that increased recombination at paused replication forks might be directly caused by an elevated incidence of replication fork collapse (Admire *et al.* 2006, Defossez *et al.* 1999, Kobayashi *et al.* 1998, Lambert *et al.* 2005). Hence, it is possible that replication fork pausing at chromatin regions that contain natural pause sites is problematic for the replication machinery of *hst3*Δ *hst4*Δ cells, which is sensitive to subtle perturbations such as epitope tagging of its protein components. This possibility is consistent with the elevated rates of spontaneous DNA damage and chronic activation of the DNA damage checkpoint in H3K56 deacetylase mutants (Celic*, et al.* 2008, Thaminy*, et al.* 2007). To test this possibility, future studies should assess the presence of DNA damage at natural pause sites in *hst3*Δ *hst4*Δ mutants, compared with wild-type cells.

As mentioned earlier, H4K16ac is likely important for creating boundaries at the aforementioned chromatin regions (Kimura*, et al.* 2004). An attractive hypothesis is that modulation of chromatin barriers facilitates replication of genomic regions that contain natural boundary elements in *hst3*Δ *hst4*Δ cells. In the absence of H4K16ac or proteins that contribute to boundary formation, such as Rsc2 or Yta7, the natural boundaries are

disrupted and heterochromatin spreads. However, limiting pools of Sir proteins will eventually restrict spreading of heterochromatin resulting in formation of new boundaries, the protein composition of which is most likely different from that of the natural boundaries. For instance, the boundaries of the silent *HMR***a** mating type locus contain tRNA genes whose promoters are tightly bound by RNA polymerase III transcription factors (Donze *et al.* 2001, Valenzuela *et al.* 2009). Therefore, it is possible that DNA replication forks can proceed more easily through these newly established chromatin barriers to complete genome duplication in *hst3*Δ *hst4*Δ cells. Programmed stalling of replication forks has been studied extensively at the replication fork barrier (RFB) present within the rDNA repeat unit. In support of our hypothesis, a previous study demonstrated that the stability of stalled replication forks at a plasmid-borne rDNA RFB site were compromised in *SIR2*-deleted cells (Benguria *et al.* 2003). This result supports the notion that modulation of H4K16ac levels might be important for stabilization of stalled replication forks at natural pause sites in *hst3*Δ *hst4*Δ mutants. Interestingly, *hst3*Δ *hst4*Δ cells exhibit an abnormally high rate of rDNA repeat number expansion, which naturally occurs within the *RDN1* locus through unequal sister chromatid recombination in response to changes in physiological conditions (Ide *et al.* 2013). This observation suggests that regulation of inter-repeat recombination at the *RDN1* locus is compromised in *hst3*Δ *hst4*Δ cells. Nevertheless, H4K16ac is a highly abundant genome-wide modification and its contribution to regulation of chromatin structure and function is probably not restricted to chromatin boundaries. Therefore, the presence of H4K16ac might have a more global effect on progression of DNA replication forks in H3K56 deacetylase mutants.

In chapter 3, we also described spontaneous suppressors that allow *hst3*Δ *hst4*Δ cells to grow at 37°C (Figure 3.6). We found that the vast majority of these spontaneous suppressors have acquired resistance to genotoxic agents, although a few of them showed various degrees of sensitivity to HU or MMS (Figure 3.6A). Simultaneous alleviation of the thermosensitivity and genotoxic agent sensitivity of *hst3*Δ *hst4*Δ cells in individual suppressors implies that these phenotypes are mechanistically linked. In other words, treatment with genotoxic agents might only exacerbate the intrinsic defects in DNA metabolism caused by hyperacetylation of H3K56 in *hst3*Δ *hst4*Δ cells. Moreover, we

identified a group of spontaneous suppressors that completely lacked H3K56ac, as judged by immunoblotting (Figure 3.6B). Further investigation revealed that this group of suppressors did not have detectable levels of Rtt109 (Figure 3.6F). The mechanism that leads to a loss of Rtt109 in these suppressors remains to be identified. However, all spontaneous suppressors lacking H3K56ac expressed normal levels of Asf1 (Figure 3.6C). This observation is surprising because, as is the case for Rtt109, lack of Asf1 also abolishes H3K56ac. The fact that, unlike Rtt109, Asf1 is never repressed in our spontaneous suppressors suggests the existence of selective pressure to retain Asf1. A possible explanation for this mode of suppression is that, in addition to its role in promoting H3K56ac, Asf1 also acts as a nucleosome assembly chaperone that binds to new H3-H4 dimers (Zhang*, et al.* 2013). In contrast, Rtt109 does not directly bind to new histones and, therefore, it may be less deleterious for *hst3*Δ *hst4*Δ cells to lose Rtt109, rather than Asf1. Interestingly, we found that the majority of spontaneous suppressors did not exhibit any striking decrease in either H3K56ac or H4K16ac levels (Figure 3.6B). Therefore, further characterization of these suppressors may identify additional pathways to circumvent the deleterious effects of H3K56 hyperacetylation. Moreover, although repression of Hst3 by NAM has been proposed as an anti-fungal therapy (Wurtele*, et al.* 2010), unpublished results from our laboratory demonstrated that *C. albicans* cells can develop resistance to NAM treatment. Hence, characterization of the spontaneous suppressors of *hst3*Δ *hst4*Δ phenotypes will probably unravel pathways that lead to the emergence of fungal pathogens (e.g. *C. albicans*) that are resistant to repression of Hst3 by NAM.

In summary, this thesis provides valuable insights into the regulation of H3K56 deacetylation and its physiological significance for cell survival following DNA damage in *S. cerevisiae*. Our work raises a number of important questions regarding the regulation of H3K56 deacetylases during the cell cycle and in response to DNA damage. Moreover, there is still much to understand about how hyperacetylation of H3K56 cripples different aspects of DNA metabolism even in the absence of exogenous DNA damage. H3K56ac is involved in critical cellular processes such as replication-coupled chromatin assembly and the DNA damage response, and its overabundance is associated with genomic instability and short replicative life span in *S. cerevisiae*. Therefore, deciphering the mechanisms that

control H3K56ac levels during the cell cycle and in response to DNA damage will improve our understanding of the intricate relationship between chromatin structure and genomic integrity.

## 4.1. References


Admire, A., Shanks, L., Danzl, N., Wang, M., Weier, U., Stevens, W., Hunt, E. and Weinert, T. (2006). Cycles of chromosome instability are associated with a fragile site and are increased by defects in DNA replication and checkpoint controls in yeast. Genes Dev 20, 159-73.

Alvaro, D., Lisby, M. and Rothstein, R. (2007). Genome-wide analysis of Rad52 foci reveals diverse mechanisms impacting recombination. PLoS Genet 3, e228.

Alvino, G. M., Collingwood, D., Murphy, J. M., Delrow, J., Brewer, B. J. and Raghuraman, M. K. (2007). Replication in hydroxyurea: it's a matter of time. Mol Cell Biol 27, 6396-406.

Annunziato, A. T. (2012). Assembling chromatin: The long and winding road. Biochim Biophys Acta 1819, 196-210.

Arnason, T. G., Pisclevich, M. G., Dash, M. D., Davies, G. F. and Harkness, T. A. (2005). Novel interaction between Apc5p and Rsp5p in an intracellular signaling pathway in Saccharomyces cerevisiae. Eukaryot Cell 4, 134-46.

Bannister, A. J. and Kouzarides, T. (2011). Regulation of chromatin by histone modifications. Cell Res 21, 381-95.

Bao, M. Z., Shock, T. R. and Madhani, H. D. (2010). Multisite phosphorylation of the Saccharomyces cerevisiae filamentous growth regulator Tec1 is required for its recognition by the E3 ubiquitin ligase adaptor Cdc4 and its subsequent destruction in vivo. Eukaryot Cell 9, 31-6.

Barbour, L. and Xiao, W. (2006). Mating type regulation of cellular tolerance to DNA damage is specific to the DNA post-replication repair and mutagenesis pathway. Mol Microbiol 59, 637-50.

Benguria, A., Hernandez, P., Krimer, D. B. and Schvartzman, J. B. (2003). Sir2p suppresses recombination of replication forks stalled at the replication fork barrier of ribosomal DNA in Saccharomyces cerevisiae. Nucleic Acids Res 31, 893-8.

Benson, L. J., Gu, Y., Yakovleva, T., Tong, K., Barrows, C., Strack, C. L., Cook, R. G., Mizzen, C. A. and Annunziato, A. T. (2006). Modifications of H3 and H4 during chromatin replication, nucleosome assembly, and histone exchange. J Biol Chem 281, 9287-96.

Brachmann, C. B., Sherman, J. M., Devine, S. E., Cameron, E. E., Pillus, L. and Boeke, J. D. (1995). The SIR2 gene family, conserved from bacteria to humans, functions in silencing, cell cycle progression, and chromosome stability. Genes Dev 9, 2888-902.

Branzei, D. and Foiani, M. (2006). The Rad53 signal transduction pathway: Replication fork stabilization, DNA repair, and adaptation. Exp Cell Res 312, 2654-9.

Brownell, J. E. and Allis, C. D. (1996). Special HATs for special occasions: linking histone acetylation to chromatin assembly and gene activation. Curr Opin Genet Dev 6, 176-84.

Burgess, R. J., Zhou, H., Han, J. and Zhang, Z. (2010). A role for Gcn5 in replication-coupled nucleosome assembly. Mol Cell 37, 469-80.

Celic, I., Masumoto, H., Griffith, W. P., Meluh, P., Cotter, R. J., Boeke, J. D. and Verreault, A. (2006). The sirtuins hst3 and Hst4p preserve genome integrity by controlling histone h3 lysine 56 deacetylation. Curr Biol 16, 1280-9.

Celic, I., Verreault, A. and Boeke, J. D. (2008). Histone H3 K56 hyperacetylation perturbs replisomes and causes DNA damage. Genetics 179, 1769-84.

Chen, C. C., Carson, J. J., Feser, J., Tamburini, B., Zabaronick, S., Linger, J. and Tyler, J. K. (2008). Acetylated lysine 56 on histone H3 drives chromatin assembly after repair and signals for the completion of repair. Cell 134, 231-43.

Cope, G. A., Suh, G. S., Aravind, L., Schwarz, S. E., Zipursky, S. L., Koonin, E. V. and Deshaies, R. J. (2002). Role of predicted metalloprotease motif of Jab1/Csn5 in cleavage of Nedd8 from Cul1. Science 298, 608-11.

D'Arcy, S. and Luger, K. (2011). Understanding histone acetyltransferase Rtt109 structure and function: how many chaperones does it take? Curr Opin Struct Biol 21, 728-34.

Das, C., Lucia, M. S., Hansen, K. C. and Tyler, J. K. (2009). CBP/p300-mediated acetylation of histone H3 on lysine 56. Nature 459, 113-7.

Defossez, P. A., Prusty, R., Kaeberlein, M., Lin, S. J., Ferrigno, P., Silver, P. A., Keil, R. L. and Guarente, L. (1999). Elimination of replication block protein Fob1 extends the life span of yeast mother cells. Mol Cell 3, 447-55.

Dhalluin, C., Carlson, J. E., Zeng, L., He, C., Aggarwal, A. K. and Zhou, M. M. (1999). Structure and ligand of a histone acetyltransferase bromodomain. Nature 399, 491-6.

Donze, D. and Kamakaka, R. T. (2001). RNA polymerase III and RNA polymerase II promoter complexes are heterochromatin barriers in Saccharomyces cerevisiae. EMBO J 20, 520-31.

Driscoll, R., Hudson, A. and Jackson, S. P. (2007). Yeast Rtt109 promotes genome stability by acetylating histone H3 on lysine 56. Science 315, 649-52.

Drogaris, P., Villeneuve, V., Pomies, C., Lee, E. H., Bourdeau, V., Bonneil, E., Ferbeyre, G., Verreault, A. and Thibault, P. (2012). Histone deacetylase inhibitors globally enhance h3/h4 tail acetylation without affecting h3 lysine 56 acetylation. Sci Rep 2, 220.

Fazly, A., Li, Q., Hu, Q., Mer, G., Horazdovsky, B. and Zhang, Z. (2012). Histone chaperone Rtt106 promotes nucleosome formation using (H3-H4)2 tetramers. J Biol Chem 287, 10753-60.

Fillingham, J., Kainth, P., Lambert, J. P., van Bakel, H., Tsui, K., Pena-Castillo, L., Nislow, C., Figeys, D., Hughes, T. R., Greenblatt, J. and Andrews, B. J. (2009). Two-color cell array screen reveals interdependent roles for histone chaperones and a chromatin boundary regulator in histone gene repression. Mol Cell 35, 340-51.

Finley, D. (2009). Recognition and processing of ubiquitin-protein conjugates by the proteasome. Annu Rev Biochem 78, 477-513.

Finley, D., Sadis, S., Monia, B. P., Boucher, P., Ecker, D. J., Crooke, S. T. and Chau, V. (1994). Inhibition of proteolysis and cell cycle progression in a multiubiquitination-deficient yeast mutant. Mol Cell Biol 14, 5501-9.

Finley, D., Ulrich, H. D., Sommer, T. and Kaiser, P. (2012). The ubiquitin-proteasome system of Saccharomyces cerevisiae. Genetics 192, 319-60.

Galan, J. M. and Peter, M. (1999). Ubiquitin-dependent degradation of multiple F-box proteins by an autocatalytic mechanism. Proc Natl Acad Sci U S A 96, 9124-9.

Glozak, M. A., Sengupta, N., Zhang, X. and Seto, E. (2005). Acetylation and deacetylation of non-histone proteins. Gene 363, 15-23.

Goh, P. Y. and Surana, U. (1999). Cdc4, a protein required for the onset of S phase, serves an essential function during G(2)/M transition in Saccharomyces cerevisiae. Mol Cell Biol 19, 5512-22.

Hachinohe, M., Hanaoka, F. and Masumoto, H. (2011). Hst3 and Hst4 histone deacetylases regulate replicative lifespan by preventing genome instability in Saccharomyces cerevisiae. Genes Cells 16, 467-77.

Haldar, D. and Kamakaka, R. T. (2008). Schizosaccharomyces pombe Hst4 functions in DNA damage response by regulating histone H3 K56 acetylation. Eukaryot Cell 7, 800-13.

Han, J., Zhou, H., Horazdovsky, B., Zhang, K., Xu, R. M. and Zhang, Z. (2007a). Rtt109 acetylates histone H3 lysine 56 and functions in DNA replication. Science 315, 653-5.

Han, J., Zhou, H., Li, Z., Xu, R. M. and Zhang, Z. (2007b). Acetylation of lysine 56 of histone H3 catalyzed by RTT109 and regulated by ASF1 is required for replisome integrity. J Biol Chem 282, 28587-96.

Harkness, T. A., Arnason, T. G., Legrand, C., Pisclevich, M. G., Davies, G. F. and Turner, E. L. (2005). Contribution of CAF-I to anaphase-promoting-complex-mediated mitotic chromatin assembly in Saccharomyces cerevisiae. Eukaryot Cell 4, 673-84.

Harkness, T. A., Davies, G. F., Ramaswamy, V. and Arnason, T. G. (2002). The ubiquitin-dependent targeting pathway in Saccharomyces cerevisiae plays a critical role in multiple chromatin assembly regulatory steps. Genetics 162, 615-32.

Hershko, A. and Ciechanover, A. (1998). The ubiquitin system. Annu Rev Biochem 67, 425-79.

Howell, E. A., McAlear, M. A., Rose, D. and Holm, C. (1994). CDC44: a putative nucleotide-binding protein required for cell cycle progression that has homology to subunits of replication factor C. Mol Cell Biol 14, 255-67.

Huang, S., Zhou, H., Katzmann, D., Hochstrasser, M., Atanasova, E. and Zhang, Z. (2005). Rtt106p is a histone chaperone involved in heterochromatin-mediated silencing. Proc Natl Acad Sci U S A 102, 13410-5.

Hyland, E. M., Cosgrove, M. S., Molina, H., Wang, D., Pandey, A., Cottee, R. J. and Boeke, J. D. (2005). Insights into the role of histone H3 and histone H4 core modifiable residues in Saccharomyces cerevisiae. Mol Cell Biol 25, 10060-70.

Ide, S., Saka, K. and Kobayashi, T. (2013). Rtt109 Prevents Hyper-Amplification of Ribosomal RNA Genes through Histone Modification in Budding Yeast. PLoS Genet 9, e1003410.

Jambunathan, N., Martinez, A. W., Robert, E. C., Agochukwu, N. B., Ibos, M. E., Dugas, S. L. and Donze, D. (2005). Multiple bromodomain genes are involved in restricting the spread of heterochromatic silencing at the Saccharomyces cerevisiae HMR-tRNA boundary. Genetics 171, 913-22.

Jenuwein, T. and Allis, C. D. (2001). Translating the histone code. Science 293, 1074-80.

Jin, L., Williamson, A., Banerjee, S., Philipp, I. and Rape, M. (2008). Mechanism of ubiquitin-chain formation by the human anaphase-promoting complex. Cell 133, 653-65.

Kaplan, T., Liu, C. L., Erkmann, J. A., Holik, J., Grunstein, M., Kaufman, P. D., Friedman, N. and Rando, O. J. (2008). Cell cycle- and chaperone-mediated regulation of H3K56ac incorporation in yeast. PLoS Genet 4, e1000270.

Khorasanizadeh, S. (2004). The nucleosome: from genomic organization to genomic regulation. Cell 116, 259-72.

Kimura, A. and Horikoshi, M. (2004). Partition of distinct chromosomal regions: negotiable border and fixed border. Genes Cells 9, 499-508.

Kimura, A., Umehara, T. and Horikoshi, M. (2002). Chromosomal gradient of histone acetylation established by Sas2p and Sir2p functions as a shield against gene silencing. Nat Genet 32, 370-7.

Kobayashi, T., Heck, D. J., Nomura, M. and Horiuchi, T. (1998). Expansion and contraction of ribosomal DNA repeats in Saccharomyces cerevisiae: requirement of replication fork blocking (Fob1) protein and the role of RNA polymerase I. Genes Dev 12, 3821-30.

Koranda, M., Schleiffer, A., Endler, L. and Ammerer, G. (2000). Forkhead-like transcription factors recruit Ndd1 to the chromatin of G2/M-specific promoters. Nature 406, 94-8.

Kurdistani, S. K. and Grunstein, M. (2003). Histone acetylation and deacetylation in yeast. Nat Rev Mol Cell Biol 4, 276-84.

Labib, K. and De Piccoli, G. (2011). Surviving chromosome replication: the many roles of the S-phase checkpoint pathway. Philos Trans R Soc Lond B Biol Sci 366, 3554-61.

Labib, K. and Hodgson, B. (2007). Replication fork barriers: pausing for a break or stalling for time? EMBO Rep 8, 346-53.

Lambert, S., Watson, A., Sheedy, D. M., Martin, B. and Carr, A. M. (2005). Gross chromosomal rearrangements and elevated recombination at an inducible site-specific replication fork barrier. Cell 121, 689-702.

Larson, K., Sahm, J., Shenkar, R. and Strauss, B. (1985). Methylation-induced blocks to in vitro DNA replication. Mutat Res 150, 77-84.

Lee, K. K. and Workman, J. L. (2007). Histone acetyltransferase complexes: one size doesn't fit all. Nat Rev Mol Cell Biol 8, 284-95.

Li, Q., Zhou, H., Wurtele, H., Davies, B., Horazdovsky, B., Verreault, A. and Zhang, Z. (2008). Acetylation of histone H3 lysine 56 regulates replication-coupled nucleosome assembly. Cell 134, 244-55.

Linghu, B., Callis, J. and Goebl, M. G. (2002). Rub1p processing by Yuh1p is required for wild-type levels of Rub1p conjugation to Cdc53p. Eukaryot Cell 1, 491-4.

Lisby, M. and Rothstein, R. (2009). Choreography of recombination proteins during the DNA damage response. DNA Repair (Amst) 8, 1068-76.

Lopes da Rosa, J., Boyartchuk, V. L., Zhu, L. J. and Kaufman, P. D. (2010). Histone acetyltransferase Rtt109 is required for Candida albicans pathogenesis. Proc Natl Acad Sci U S A 107, 1594-9.

Luger, K., Mader, A. W., Richmond, R. K., Sargent, D. F. and Richmond, T. J. (1997). Crystal structure of the nucleosome core particle at 2.8 A resolution. Nature 389, 251-60.

Lyons, N. A., Fonslow, B. R., Diedrich, J. K., Yates, J. R., 3rd and Morgan, D. O. (2013). Sequential primed kinases create a damage-responsive phosphodegron on Eco1. Nat Struct Mol Biol 20, 194-201.

Maas, N. L., Miller, K. M., DeFazio, L. G. and Toczyski, D. P. (2006). Cell cycle and checkpoint regulation of histone H3 K56 acetylation by Hst3 and Hst4. Mol Cell 23, 109-19.

Marmorstein, R. (2001a). Structure and function of histone acetyltransferases. Cell Mol Life Sci 58, 693-703.

Marmorstein, R. (2001b). Structure of histone deacetylases: insights into substrate recognition and catalysis. Structure 9, 1127-33.

Masumoto, H., Hawke, D., Kobayashi, R. and Verreault, A. (2005). A role for cell-cycle-regulated histone H3 lysine 56 acetylation in the DNA damage response. Nature 436, 294-8.

Merlet, J., Burger, J., Gomes, J. E. and Pintard, L. (2009). Regulation of cullin-RING E3 ubiquitin-ligases by neddylation and dimerization. Cell Mol Life Sci 66, 1924-38.

Miller, K. M., Maas, N. L. and Toczyski, D. P. (2006). Taking it off: regulation of H3 K56 acetylation by Hst3 and Hst4. Cell Cycle 5, 2561-5.

Miller, K. M., Tjeertes, J. V., Coates, J., Legube, G., Polo, S. E., Britton, S. and Jackson, S. P. (2010). Human HDAC1 and HDAC2 function in the DNA-damage response to promote DNA nonhomologous end-joining. Nat Struct Mol Biol 17, 1144-51.

Munoz-Galvan, S., Jimeno, S., Rothstein, R. and Aguilera, A. (2013). Histone H3K56 acetylation, Rad52, and non-DNA repair factors control double-strand break repair choice with the sister chromatid. PLoS Genet 9, e1003237.

Nash, P., Tang, X., Orlicky, S., Chen, Q., Gertler, F. B., Mendenhall, M. D., Sicheri, F., Pawson, T. and Tyers, M. (2001). Multisite phosphorylation of a CDK inhibitor sets a threshold for the onset of DNA replication. Nature 414, 514-21.

Neumann, H., Hancock, S. M., Buning, R., Routh, A., Chapman, L., Somers, J., Owen-Hughes, T., van Noort, J., Rhodes, D. and Chin, J. W. (2009). A method for genetically installing site-specific acetylation in recombinant histones defines the effects of H3 K56 acetylation. Mol Cell 36, 153-63.

Nyberg, K. A., Michelson, R. J., Putnam, C. W. and Weinert, T. A. (2002). Toward maintaining the genome: DNA damage and replication checkpoints. Annu Rev Genet 36, 617-56.

Ozdemir, A., Spicuglia, S., Lasonder, E., Vermeulen, M., Campsteijn, C., Stunnenberg, H. G. and Logie, C. (2005). Characterization of lysine 56 of histone H3 as an acetylation site in Saccharomyces cerevisiae. J Biol Chem 280, 25949-52.

Peng, J., Schwartz, D., Elias, J. E., Thoreen, C. C., Cheng, D., Marsischky, G., Roelofs, J., Finley, D. and Gygi, S. P. (2003). A proteomics approach to understanding protein ubiquitination. Nat Biotechnol 21, 921-6.

Petroski, M. D. and Deshaies, R. J. (2005). Mechanism of lysine 48-linked ubiquitin-chain synthesis by the cullin-RING ubiquitin-ligase complex SCF-Cdc34. Cell 123, 1107-20.

Pickart, C. M. (2001). Mechanisms underlying ubiquitination. Annu Rev Biochem 70, 503-33.

Pommier, Y., Redon, C., Rao, V. A., Seiler, J. A., Sordet, O., Takemura, H., Antony, S., Meng, L., Liao, Z., Kohlhagen, G., Zhang, H. and Kohn, K. W. (2003). Repair of and checkpoint response to topoisomerase I-mediated DNA damage. Mutat Res 532, 173-203.

Recht, J., Tsubota, T., Tanny, J. C., Diaz, R. L., Berger, J. M., Zhang, X., Garcia, B. A., Shabanowitz, J., Burlingame, A. L., Hunt, D. F., Kaufman, P. D. and Allis, C. D. (2006). Histone chaperone Asf1 is required for histone H3 lysine 56 acetylation, a modification associated with S phase in mitosis and meiosis. Proc Natl Acad Sci U S A 103, 6988-93.

Reichard, P. (1988). Interactions between deoxyribonucleotide and DNA synthesis. Annu Rev Biochem 57, 349-74.

Rufiange, A., Jacques, P. E., Bhat, W., Robert, F. and Nourani, A. (2007). Genome-wide replication-independent histone H3 exchange occurs predominantly at promoters and implicates H3 K56 acetylation and Asf1. Mol Cell 27, 393-405.

Saeki, Y., Kudo, T., Sone, T., Kikuchi, Y., Yokosawa, H., Toh-e, A. and Tanaka, K. (2009). Lysine 63-linked polyubiquitin chain may serve as a targeting signal for the 26S proteasome. EMBO J 28, 359-71.

Schneider, J., Bajwa, P., Johnson, F. C., Bhaumik, S. R. and Shilatifard, A. (2006). Rtt109 is required for proper H3K56 acetylation: a chromatin mark associated with the elongating RNA polymerase II. J Biol Chem 281, 37270-4.

Sedgwick, B. (2004). Repairing DNA-methylation damage. Nat Rev Mol Cell Biol 5, 148-57.

Simpson-Lavy, K. J., Oren, Y. S., Feine, O., Sajman, J., Listovsky, T. and Brandeis, M. (2010). Fifteen years of APC/cyclosome: a short and impressive biography. Biochem Soc Trans 38, 78-82.

Smith, C. M., Gafken, P. R., Zhang, Z., Gottschling, D. E., Smith, J. B. and Smith, D. L. (2003). Mass spectrometric quantification of acetylation at specific lysines within the amino-terminal tail of histone H4. Anal Biochem 316, 23-33.

Strahl, B. D. and Allis, C. D. (2000). The language of covalent histone modifications. Nature 403, 41-5.

Suka, N., Luo, K. and Grunstein, M. (2002). Sir2p and Sas2p opposingly regulate acetylation of yeast histone H4 lysine16 and spreading of heterochromatin. Nat Genet 32, 378-83.

Tang, X., Orlicky, S., Lin, Z., Willems, A., Neculai, D., Ceccarelli, D., Mercurio, F., Shilton, B. H., Sicheri, F. and Tyers, M. (2007). Suprafacial orientation of the SCFCdc4 dimer accommodates multiple geometries for substrate ubiquitination. Cell 129, 1165-76.

Tang, X., Orlicky, S., Liu, Q., Willems, A., Sicheri, F. and Tyers, M. (2005). Genome-wide surveys for phosphorylation-dependent substrates of SCF ubiquitin ligases. Methods Enzymol 399, 433-58.

Tercero, J. A., Longhese, M. P. and Diffley, J. F. (2003). A central role for DNA replication forks in checkpoint activation and response. Mol Cell 11, 1323-36.

Thaminy, S., Newcomb, B., Kim, J., Gatbonton, T., Foss, E., Simon, J. and Bedalov, A. (2007). Hst3 is regulated by Mec1-dependent proteolysis and controls the S phase checkpoint and sister chromatid cohesion by deacetylating histone H3 at lysine 56. J Biol Chem 282, 37805-14.

Tjeertes, J. V., Miller, K. M. and Jackson, S. P. (2009). Screen for DNA-damage-responsive histone modifications identifies H3K9Ac and H3K56Ac in human cells. EMBO J 28, 1878-89.

Tsubota, T., Berndsen, C. E., Erkmann, J. A., Smith, C. L., Yang, L., Freitas, M. A., Denu, J. M. and Kaufman, P. D. (2007). Histone H3-K56 acetylation is catalyzed by histone chaperone-dependent complexes. Mol Cell 25, 703-12.

Turner, E. L., Malo, M. E., Pisclevich, M. G., Dash, M. D., Davies, G. F., Arnason, T. G. and Harkness, T. A. (2010). The Saccharomyces cerevisiae anaphase-promoting complex interacts with multiple histone-modifying enzymes to regulate cell cycle progression. Eukaryot Cell 9, 1418-31.

Valenzuela, L., Dhillon, N. and Kamakaka, R. T. (2009). Transcription independent insulation at TFIIIC-dependent insulators. Genetics 183, 131-48.

van Leeuwen, F., Gafken, P. R. and Gottschling, D. E. (2002). Dot1p modulates silencing in yeast by methylation of the nucleosome core. Cell 109, 745-56.

Vempati, R. K., Jayani, R. S., Notani, D., Sengupta, A., Galande, S. and Haldar, D. (2010). p300-mediated acetylation of histone H3 lysine 56 functions in DNA damage response in mammals. J Biol Chem 285, 28553-64.

Verma, R., Annan, R. S., Huddleston, M. J., Carr, S. A., Reynard, G. and Deshaies, R. J. (1997). Phosphorylation of Sic1p by G1 Cdk required for its degradation and entry into S phase. Science 278, 455-60.

Verma, R., Chen, S., Feldman, R., Schieltz, D., Yates, J., Dohmen, J. and Deshaies, R. J. (2000). Proteasomal proteomics: identification of nucleotide-sensitive proteasome-interacting proteins by mass spectrometric analysis of affinity-purified proteasomes. Mol Biol Cell 11, 3425-39.

Verreault, A. (2000). De novo nucleosome assembly: new pieces in an old puzzle. Genes Dev 14, 1430-8.

Verzijlbergen, K. F., Menendez-Benito, V., van Welsem, T., van Deventer, S. J., Lindstrom, D. L., Ovaa, H., Neefjes, J., Gottschling, D. E. and van Leeuwen, F. (2010). Recombination-induced tag exchange to track old and new proteins. Proc Natl Acad Sci U S A 107, 64-8.

Wang, Y., Vujcic, M. and Kowalski, D. (2001). DNA replication forks pause at silent origins near the HML locus in budding yeast. Mol Cell Biol 21, 4938-48.

Willems, A. R., Schwab, M. and Tyers, M. (2004). A hitchhiker's guide to the cullin ubiquitin ligases: SCF and its kin. Biochim Biophys Acta 1695, 133-70.

Williams, S. K., Truong, D. and Tyler, J. K. (2008). Acetylation in the globular core of histone H3 on lysine-56 promotes chromatin disassembly during transcriptional activation. Proc Natl Acad Sci U S A 105, 9000-5.

Wurtele, H., Kaiser, G. S., Bacal, J., St-Hilaire, E., Lee, E. H., Tsao, S., Dorn, J., Maddox, P., Lisby, M., Pasero, P. and Verreault, A. (2012). Histone H3 lysine 56 acetylation and the response to DNA replication fork damage. Mol Cell Biol 32, 154-72.

Wurtele, H., Tsao, S., Lepine, G., Mullick, A., Tremblay, J., Drogaris, P., Lee, E. H., Thibault, P., Verreault, A. and Raymond, M. (2010). Modulation of histone H3 lysine 56 acetylation as an antifungal therapeutic strategy. Nat Med

Xie, Y. and Varshavsky, A. (2000). Physical association of ubiquitin ligases and the 26S proteasome. Proc Natl Acad Sci U S A 97, 2497-502.

Xu, F., Zhang, K. and Grunstein, M. (2005). Acetylation in histone H3 globular domain regulates gene expression in yeast. Cell 121, 375-85.

Xu, P., Duong, D. M., Seyfried, N. T., Cheng, D., Xie, Y., Robert, J., Rush, J., Hochstrasser, M., Finley, D. and Peng, J. (2009). Quantitative proteomics reveals the function of unconventional ubiquitin chains in proteasomal degradation. Cell 137, 133-45.

Yang, B., Miller, A. and Kirchmaier, A. L. (2008). HST3/HST4-dependent deacetylation of lysine 56 of histone H3 in silent chromatin. Mol Biol Cell 19, 4993-5005.

Ye, J., Ai, X., Eugeni, E. E., Zhang, L., Carpenter, L. R., Jelinek, M. A., Freitas, M. A. and Parthun, M. R. (2005). Histone H4 lysine 91 acetylation a core domain modification associated with chromatin assembly. Mol Cell 18, 123-30.

Yuan, J., Pu, M., Zhang, Z. and Lou, Z. (2009). Histone H3-K56 acetylation is important for genomic stability in mammals. Cell Cycle 8, 1747-53.

Yun, M., Wu, J., Workman, J. L. and Li, B. (2011). Readers of histone modifications. Cell Res 21, 564-78.

Zeng, L., Yap, K. L., Ivanov, A. V., Wang, X., Mujtaba, S., Plotnikova, O., Rauscher, F. J., 3rd and Zhou, M. M. (2008). Structural insights into human KAP1 PHD finger-bromodomain and its role in gene silencing. Nat Struct Mol Biol 15, 626-33.

Zhang, W., Tyl, M., Ward, R., Sobott, F., Maman, J., Murthy, A. S., Watson, A. A., Fedorov, O., Bowman, A., Owen-Hughes, T., El Mkami, H., Murzina, N. V., Norman, D. G. and Laue, E. D. (2013). Structural plasticity of histones H3-H4 facilitates their allosteric exchange between RbAp48 and ASF1. Nat Struct Mol Biol 20, 29-35.

Zhou, P. and Howley, P. M. (1998). Ubiquitination and degradation of the substrate recognition subunits of SCF ubiquitin-protein ligases. Mol Cell 2, 571-80.

Zhu, G., Spellman, P. T., Volpe, T., Brown, P. O., Botstein, D., Davis, T. N. and Futcher, B. (2000). Two yeast forkhead genes regulate the cell cycle and pseudohyphal growth. Nature 406, 90-4

# APPENDIX A:

# Structure of the Rtt109-AcCoA/Vps75 complex and implications for chaperone-mediated histone acetylation

Yong Tang, Marc A. Holbert*, Neda Delgoshaie*, Hugo Wurtele*, Benoît Guillemette*, Katrina Meeth, Hua Yuan, Paul Drogaris, Eun-Hye Lee, Chantal Durette, Pierre Thibault, Alain Verreault, Philip A. Cole, Ronen Marmorstein

* These authors contributed equally to this work

*Structure* (2011) **19**(2):221-31

## Abstract

Yeast Rtt109 promotes nucleosome assembly and genome stability by acetylating K9, K27 and K56 of histone H3 through interaction with either of two distinct histone chaperones, Vps75 or Asf1. We report the crystal structure of an Rtt109-AcCoA/Vps75 complex revealing an elongated Vps75 homodimer bound to two globular Rtt109 molecules to form a symmetrical holoenzyme with a ~12 Å diameter central hole. Vps75 and Rtt109 residues that mediate complex formation in the crystals are also important for Rtt109-Vps75 interaction and H3K9/K27 acetylation both *in vitro* and in yeast cells. The same Rtt109 residues do not participate in Asf1-mediated Rtt109 acetylation *in vitro* or H3K56 acetylation in yeast cells, demonstrating that Asf1 and Vps75 dictate Rtt109 substrate specificity through distinct mechanisms. These studies also suggest that Vps75 binding stimulates Rtt109 catalytic activity by appropriately presenting the H3–H4 substrate within the central cavity of the holoenzyme to promote H3K9/K27 acetylation of new histones before deposition.

## Introduction

Histone acetyltransferase (HAT) enzymes modify histone lysine residues to modulate various DNA-templated processes including replication, transcription, and DNA repair. Rtt109 is a fungal-specific HAT that acetylates lysine 56 on newly synthesized histone H3 (H3K56) during S-phase to mediate nucleosome assembly during DNA replication and DNA repair. Rtt109 is also important for cell survival after treatment with a number of genotoxic agents (Collins et al., 2007; Driscoll et al., 2007; Han et al., 2007a; Tsubota et al., 2007). Together with Gcn5, Rtt109 was more recently shown to contribute to the acetylation of histone H3K9 (Fillingham et al., 2008) and H3K27 (Burgess et al., 2010). Rtt109 harbors very low acetyltransferase activity on its own (Driscoll et al., 2007; Tsubota et al., 2007), but its activity is stimulated by association with either of the histone chaperone proteins Asf1 or Vps75 (Albaugh et al., 2010; Berndsen et al., 2008; Han et al., 2007b, c; Tsubota et al., 2007). *In vivo*, Rtt109-mediated acetylation of H3K56 requires

Asf1, an evolutionarily conserved histone chaperone that binds to H3–H4 dimers (English et al., 2006), although Asf1 does not appear to form a stable complex with Rtt109 *in vitro* (Driscoll et al., 2007; Han et al., 2007b; Tsubota et al., 2007). In addition, both the Asf1 and Vps75 histone chaperones contribute to H3K9 acetylation *in vivo* (Adkins et al., 2007; Berndsen et al., 2008; Fillingham et al., 2008). Vps75 is a member of the NAP1 histone chaperone family that binds to both $(H3–H4)_2$ tetramers and H2A–H2B dimers (Park et al., 2008; Selth and Svejstrup, 2007). The Rtt109/Vps75 complex can also acetylate H3K56 *in vitro* (Berndsen et al., 2008; Lin and Yuan, 2008; Tsubota et al., 2007), but a *vps75* null mutant shows no decrease in H3K56 acetylation *in vivo* (Tsubota et al., 2007; Han et al., 2007c). Recently, H3K56 acetylation has been observed to overlap strongly with the binding of key pluripotency regulators at active and inactive promoters in human embryonic stem cells (Xie et al., 2009), but there have been conflicting reports about whether this modification is mediated by the GCN5 (Tjeertes et al., 2009) or p300/CBP HAT in association with ASF1 (Das et al., 2009).

Our group and others have reported on the X-ray crystal structure of Rtt109 (Lin and Yuan, 2008; Stavropoulos et al., 2008; Tang et al., 2008a), leading to the unexpected observation that Rtt109 is structurally related to p300/CBP, despite the lack of significant sequence conservation. We and others have also reported that Vps75 adopts a dimeric head-phone-like structure (Berndsen et al., 2008; Park et al., 2008; Tang et al., 2008b) that is distinct from the monomeric β-sandwich fold of Asf1 (Daganzo, 2003; English et al., 2006). To obtain direct molecular insights into how Rtt109 activity is modulated by the binding of histone chaperones, we now report on the X-ray crystal structure of an Rtt109-AcCoA/Vps75 complex. We also present structure-based mutagenesis, combined with biochemical and, enzymological data, and studies in yeast cells to derive molecular insights into the mechanism by which histone chaperones enhance and mediate lysine-specific histone acetylation by Rtt109.

## Results

### Rtt109/Vps75 forms a symmetrical ring with a 2:2 stoichiometry

We prepared the Rtt109/Vps75 complex by coexpressing the full-length Rtt109 protein with the core domain of Vps75 (residues 1–232) in bacteria and purifying the tightly associated complex to homogeneity using a combination of affinity, ion exchange and size exclusion chromatography. The protein complex was mixed with acetyl coenzyme A (AcCoA) and crystals were obtained in spacegroup $P2_12_12$ (native crystal) that diffracted to 3.2 Å resolution. Soaking of these crystals with a 14-amino acid peptide centered around H3K9 (peptide soaked crystal) produced crystals that diffracted to a higher resolution of 2.8 Å, but with the peptide bound in a non-physiologically relevant manner, but otherwise essentially identical to the native Rtt109/Vps75 complex (see Figure S1 and Supplemental Experimental Procedures for more details). Because of its higher resolution, the peptide-soaked Rtt109/Vps75 complex is used for further analysis as described below. Within the crystal lattice, each asymmetric unit contains one molecule each of Rtt109 bound to AcCoA and Vps75, related by a crystallographic 2-fold symmetry axis to form the functional heterotetramer with two bound AcCoA molecules. The structure was refined to 2.8 Å resolution with refinement statistics of $R_{work}$=0.191 ($R_{free}$=0.253) and geometrical parameters of root-mean-square deviation $(RMSD)_{bond\ length}$=0.009 Å and $RMSD_{bond\ angle}$=1.154° (Table 1).

**Table 1. Data collection and refinement statistics**

| | Rtt109–AcCoA-Vps75(1-232) Complex | |
|---|---|---|
| | Peptide-Soaked Crystal PDB ID 3Q33 | Native Crystal PDB ID 3Q35 |
| Data collection | | |
| Space group | $P2_12_12$ | $P2_12_12$ |
| Cell dimensions | | |
| *a*, *b*, *c* (Å) | 97.543, 119.570, 80.566 | 98.085, 119.001, 80.292 |
| $\alpha$, $\beta$, $\gamma$ (°) | 90.0, 90.0, 90.0 | 90.0, 90.0, 90.0 |
| Wavelength (Å) | 0.984 | 0.984 |
| Resolution (Å)[a] | 50–2.75 (2.85–2.75) | 50–3.3 (3.42–3.30) |
| $R_{sym}$ | 0.047 (0.363) | 0.083 (0.427) |
| $I/\sigma I$ | 26.1(2.4) | 16.5 (3.6) |
| Completeness (%) | 94.9 (78.1) | 99.7 (97.2) |
| Redundancy | 4.8 (3.8) | 7.1 (6.2) |
| Refinement | | |
| Resolution (Å) | 50–2.8 | 50–3.3 |
| No. reflections | 22,879 | 14,631 |
| $R_{work}/R_{free}$ | 0.191/0.253 | 0.207/0.248 |
| No. atoms | | |
| Protein | 5000/611 aa | 4975/607 aa |
| H3 peptide | 25/4 aa | NONE |
| AcCoA | 51/1 molecule | 51/1 molecule |
| Ethylene glycol | 4/1 molecule | 4/1 molecule |
| Water | 23 | 11 |
| *B*-factors | | |
| Protein (R/V/H3) | 81.9, 86.2, 85.3 | 89.3, 92.6 |
| AcCoA/ethylene G | 83.4/76.1 | 82.2/65.7 |
| Water | 64.1 | 46.8 |
| Root-mean-square deviations | | |
| Bond lengths (Å) | 0.009 | 0.011 |
| Bond angles (°) | 1.154 | 1.309 |

[a] Values in parentheses are for the highest-resolution shell.

The Rtt109-AcCoA/Vps75 complex reveals that the obligate Vps75 homodimeric headphone-like structure, which contains an elongated helical dimerization domain and globular earmuff domains at each end of the dimerization domain, is bound on opposite ends by two globular Rtt109 molecules to form a symmetrical ring with a hole of ~12 Å diameter (Figure 1). The two Rtt109 subunits make extensive sequence-specific contacts with the Vps75 dimer burying a solvent-accessible surface (SAS) of 3725 $Å^2$ for each Rtt109-Vps75 pair, whereas the two Rtt109 subunits make more modest and non-specific interactions with each other burying 1736 $Å^2$ of SAS. Each Rtt109 subunit contacts the Vps75 dimer in two distinct regions. The Rtt109-α8-α9 helices pack against the α2-α5 helices of the Vps75 earmuff domain (burying 1982 $Å^2$ of SAS) and the Rtt109 130–179 segment reaches around the Vps75 earmuff domain to engage the Vps75 dimerization helices (burying 1743 $Å^2$ of SAS). The less extensive Rtt109-Rtt109 interface primarily involves non-specific contacts between the α7-β7 loops of both molecules.

## The tightly associated Rtt109-AcCoA/Vps75 complex does not involve significant structural changes in Rtt109 or Vps75

The Rtt109-α8-α9 helices make predominantly hydrogen-bond contacts to the α2-α5 helices of the Vps75 earmuff domain (Figure 2A). Specifically, lysines 356 and 363 of Rtt109-α8 hydrogen bond to Gln64 of Vps75-α2 and Asn70 of Vps75-α3, respectively; and Tyr364 of Rtt109-α8 makes van der Waals contact to Ala74 of Vps75-α4. Glu374, Glu378, and Arg390 of Rtt109-α9 make salt-bridges to Arg173 and Lys177 of Vps75-α5, and Arg73 and Asp81 of Vps75-α4, respectively. Asn382 of Rtt109-α9 also makes a hydrogen bond to the backbone NH of Ala74, and Leu389 of Rtt109-α9 makes van der Waals contacts to Phe77 and the aliphatic region of Lys78 of Vps75-α4.

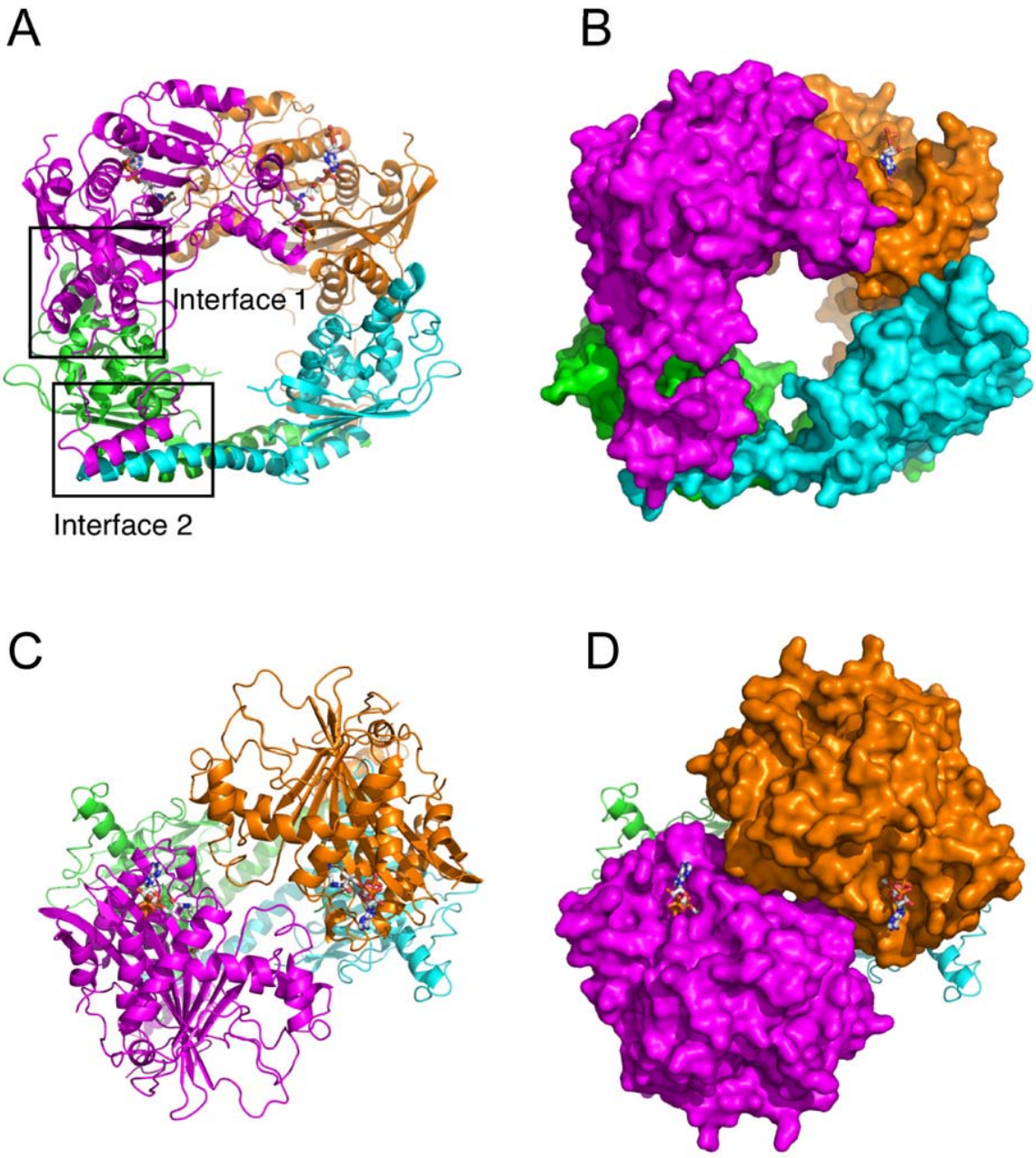


**Figure 1. Overall structure of the Rtt109/Vps75 complex.** (A and C) Two orthogonal views of the Rtt109/Vps75 complex. The obligate Vps75 homodimer is shown with subunits in blue and green and the two Rtt109 subunits are shown in purple and orange. The proteins are shown in cartoon representation. The two interfaces that are boxed are shown in molecular detail in figures 2A and 2B. (B) and (D) are the same views as (A) and (C), respectively, but shown in surface representation.

The 130–179 segment of Rtt109 is not conserved in all species of yeast (Figure S2) and is either absent (deleted from the crystallized protein) or disordered in previously reported Rtt109 structures (Lin and Yuan, 2008; Tang et al., 2008a). However, in the Rtt109-AcCoA/Vps75 complex, this segment contains a well-ordered central helix from residues 144–155 (called $\alpha3^i$ as it forms in between the previously defined α3 and α4 helices) and surrounding loop regions that are partially ordered (Figure 2B). The Rtt109-$\alpha3^i$ helix contacts both Vps75 subunits through a combination of hydrogen bonding and van der Waals interactions. Arg154 of Rtt109-$\alpha3^i$ forms a salt bridge with Asp222 of Vps75-α8, a residue at the base of the Vps75 earmuff domain that also forms two main-chain H-bonds with Ile138 of Rtt109. In addition, Arg149 of Rtt109-$\alpha3^i$ forms a salt-bridge with Glu23 of Vps75-α1′ from the opposite subunit. Other residues of Rtt109-$\alpha3^i$ also contact the α8 and α1′ helices of the Vps75 earmuff and dimerization domains, respectively, through mostly van der Waals interactions (Figure 2B). Specifically, Ala145, Leu148, Ile150, Leu151, and Ala152 of Rtt109-$\alpha3^i$ and Ile138 within the preceding loop form a hydrophobic network with a cluster of Vps75-α8 (Val213 and Tyr216) and α1′ (Phe15, Leu16, and Ala19) residues.

Except for the 130–179 segment of the Rtt109-CoA/Vps75 complex, the uncomplexed Rtt109 and Vps75 proteins superimpose well with no significant structural changes and RMS deviations for all ordered Cα atoms of 0.75 Å and 1.14 Å, respectively. Strikingly, even the Rtt109 active site residues Tyr199 and Trp222, the bound AcCoA and the acetylated Lys290 superimpose well (Figure 2C). This observation suggests that Vps75-mediated stimulation of Rtt109 HAT activity does not involve an alteration of Rtt109 conformation or its active site on Vps75 binding. Vps75 binding to Rtt109 strongly stimulates the $k_{cat}$ (~100-fold) and has little effect on the $K_m$ for H3 substrates (Berndsen et al., 2008). Based on this and the structures of the holoenzyme and free Rtt109, we propose that Vps75 stimulates Rtt109 HAT activity by productively positioning specific lysine residues of histone H3 within the Rtt109 active site.

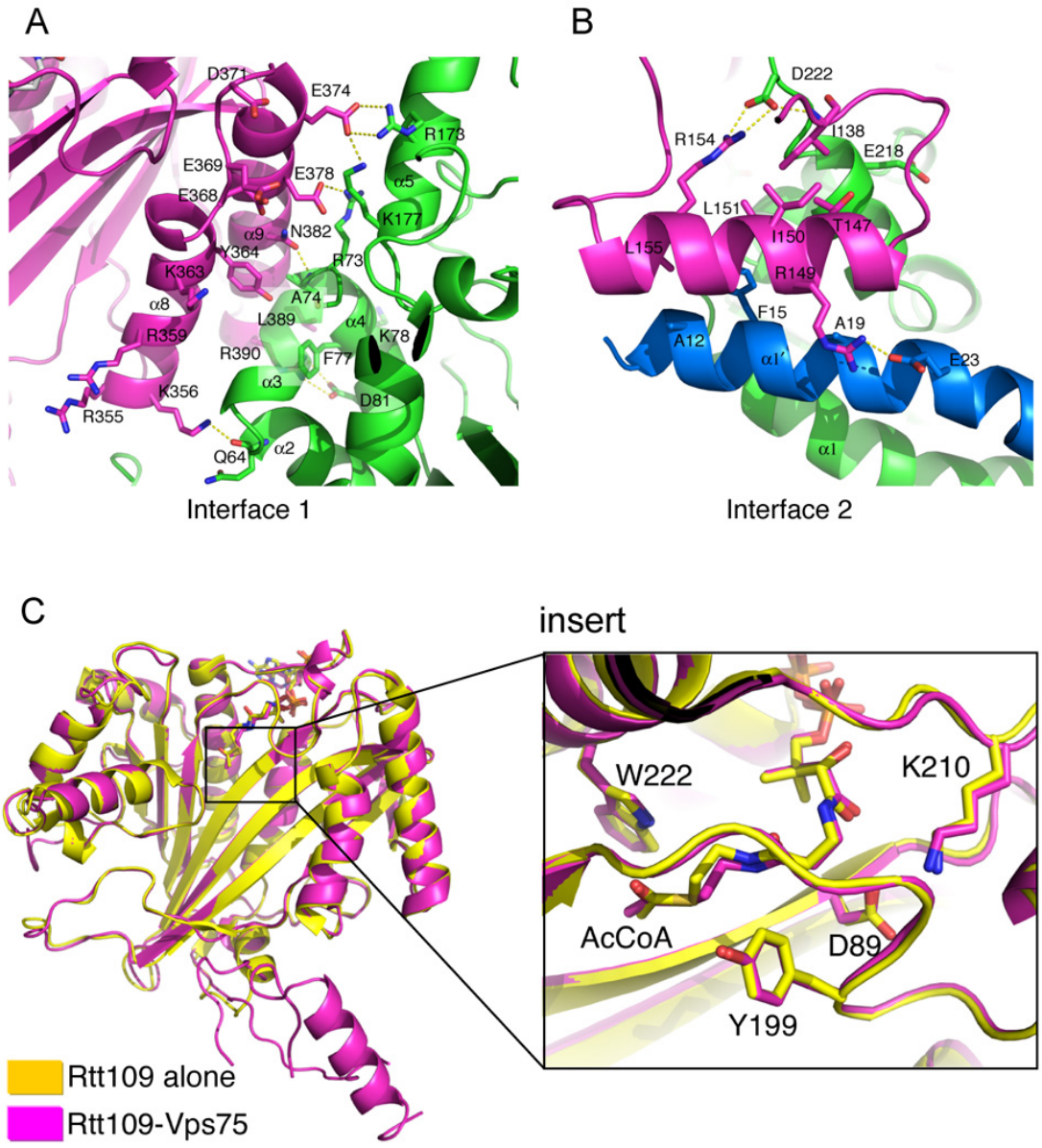


**Figure 2. Details of the two Rtt109-Vps75 interaction surfaces**. (A) The Rtt109 interface with the Vps75 earmuff domain is shown in cartoon representation. Residues that mediate protein-protein interaction or near the protein-protein interface and targeted for mutagenesis are shown as stick models in CPK coloring. Hydrogen bonds are indicated as yellow dashed lines. The orientation is similar to figure 1A (boxed interface 1). (B) The Rtt109 interface with the Vps75 dimerization domain rendered as described above. (C) A superposition of the Rtt109 active site in the apo- and Vps75-bound forms is shown in cartoon representation. Active site residues in the insert are shown as stick models in CPK coloring (Lys290 is too far away to be included in the insert).

## Stable Rtt109-Vps75 interaction is required for optimal HAT activation

To determine the functional significance of the Rtt109-Vps75 contacts that are observed in the crystal structure of the complex, we carried out structure-based mutagenesis of Rtt109 followed by Rtt109-Vps75 interaction and enzymatic assays using recombinant $(H3–H4)_2$ tetramer as a substrate.

Given that in the Rtt109-AcCoA/Vps75 complex, one Rtt109 molecule contacts both Vps75 subunits, we first asked whether Vps75 dimerization is required for its ability to stimulate Rtt109 HAT activity. For this purpose, we prepared the Vps75-(C21E,V25S,I28E,V32E) mutant previously shown to produce monomeric Vps75 (Berndsen et al., 2008) and found that it is strongly defective in binding to Rtt109 (Figure 3A) as well as in stimulating Rtt109 HAT activity (Figure 3B). This result confirms that Vps75 dimer formation is required for Rtt109 interaction and optimal stimulation of Rtt109 HAT activity.

As Rtt109 interacts with Vps75 through two distinct surfaces (Figures 2 and S2A), we also asked whether both surfaces are required for Rtt109 function *in vitro*. We have previously reported mutagenesis data implicating two distinct Vps75 surfaces for Rtt109 interaction (Tang et al., 2008b). Specifically, we showed that the Vps75-(E218K,D222K) mutant abolishes Rtt109 interaction, whereas the distal Vps75-(R173E,K177E) mutant and Vps75-Δ(167–178) deletion greatly compromise Rtt109 interaction. This data is consistent with the Rtt109-AcCoa/Vps75 structure reported here. Vps75-Asp222 and –Glu218 interact with the 130–179 segment of Rtt109 (Figure 2B), whereas Vps75-Arg173 and -Lys177 interact with the α8-α9 region of Rtt109. As shown in Figure 3A, another mutation, Vps75-(R73D,A74D), that disrupts the interface with Rtt109-α8-α9, completely abolishes interaction with Rtt109. Vps75 mutations that reduce its interaction with Rtt109 in pull-down assays also show a diminished ability to stimulate Rtt109 HAT activity (Figure 3B). In particular, the Rtt109 binding defective mutants, Vps75-(R73D, A74D),

-(R173E,K177E), and -(E218K,D222K) each show a reduced ability to stimulate Rtt109 HAT activity relative to the wild-type Vps75 protein.

Mutation of Rtt109 residues that contact Vps75 also show a defect in pull-down assays and Vps75-mediated stimulation of Rtt109 HAT activity. As shown in Figure 3C, removal of the 130–179 segment of Rtt109 that contacts the Vps75 dimerization domain, or substitution mutations of Vps75-interacting residues in this segment, Rtt109-(L148D) or Rtt109-(I150D,L151D), abolish Vps75 binding. Similarly, combined substitution mutations in the Rtt109 α8-α9 residues that mediate contacts with the Vps75 earmuff domain, Rtt109-(E378R,N382R) and Rtt109-(R355E,K356E), also diminish Vps75 binding. Correlating with the reduced Rtt109-Vps75 interaction, each of these Rtt109 mutants show reduced Vps75-stimulated HAT activity relative to wild-type Rtt109 (Figure 3D). Taken together, these studies indicate that the 130–179 segment and α8-α9 region of Rtt109 (Figure S2B) are both required for optimal Vps75 interaction and HAT activity stimulation.

Comparison of free and Vps75-bound Rtt109 structures suggests that the Rtt109 130–179 segment is only ordered in the presence of Vps75 (Lin and Yuan, 2008; Tang et al., 2008a). To confirm that this is also true in solution, we probed the proteolytic sensitivity of Rtt109 as a function of Vps75 binding. To carry out these studies, we prepared three recombinant Rtt109 proteins: wild-type Rtt109, Rtt109-Δ(130–179) in which residues 130–179 are removed and Rtt109-(L148D), a mutant defective in Vps75 binding. As shown in Figure 3E, in the absence of Vps75, Rtt109-wt and Rtt109-(L148D) are readily cleaved by trypsin, whereas the Rtt109-Δ(130–179) mutant is significantly more protease resistant. In the presence of Vps75, however, Rtt109-wt is protected from proteolysis. In contrast, the Rtt109-(L148D) mutant that cannot bind to Vps75 but retains the 130–179 segment, remains sensitive to trypsin even in the presence of Vps75. Taken together, these studies reveal that, in the absence of Vps75, Rtt109 is highly susceptible to trypsin cleavage, and this appears to be nucleated by the 130–179 segment of Rtt109. Interestingly, a recent report has shown that the *in vivo* stability of Rtt109 is compromised in cells lacking Vps75 (Fillingham et al., 2008). Based on the structural and biochemical results reported here, we hypothesize that the reduced stability of Rtt109 in the absence of Vps75 *in vivo* correlates

with the exposure of the 130–179 segment, which renders Rtt109 susceptible to degradation. Interestingly, Rtt109 orthologs from several yeast species do not contain the 130–179 region (Figure S2B), suggesting that these species may compensate for the absence of the 130–179 segment by employing other surfaces of Rtt109 to stabilize its interaction with Vps75. Alternatively, these species may not use Vps75 stimulate the HAT activity of Rtt109.

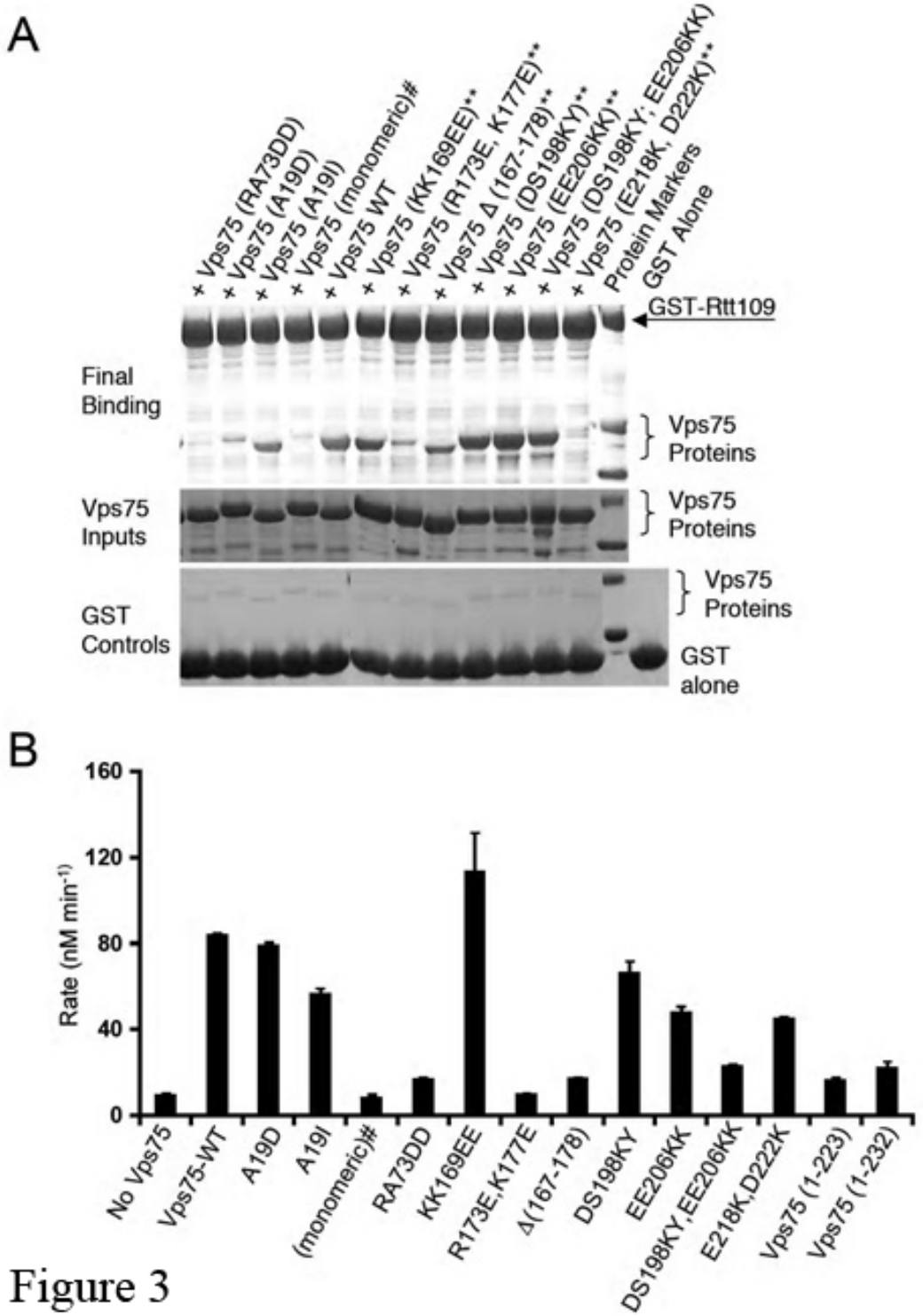
A
+ Vps75 (RA73DD)
+ Vps75 (A19D)
+ Vps75 (A19I)
+ Vps75 (monomeric)#
+ Vps75 WT
+ Vps75 (KK169EE)**
+ Vps75 (R173E, K177E)**
+ Vps75 Δ (167-178)**
+ Vps75 (DS198KY)**
+ Vps75 (EE206KK)**
+ Vps75 (DS198KY; EE206KK)**
Protein Markers
GST Alone
GST-Rtt109
Final Binding
Vps75 Proteins
Vps75 Inputs
Vps75 Proteins
GST Controls
Vps75 Proteins
GST alone
B
Rate (nM min-1)
160
120
80
40
0
No Vps75
Vps75-WT
A19D
A19I
(monomeric)#
RA73DD
KK169EE
R173E,K177E
Δ(167-178)
DS198KY
EE206KK
DS198KY,EE206KK
E218K,D222K
Vps75 (1-223)
Vps75 (1-232)

Figure 3

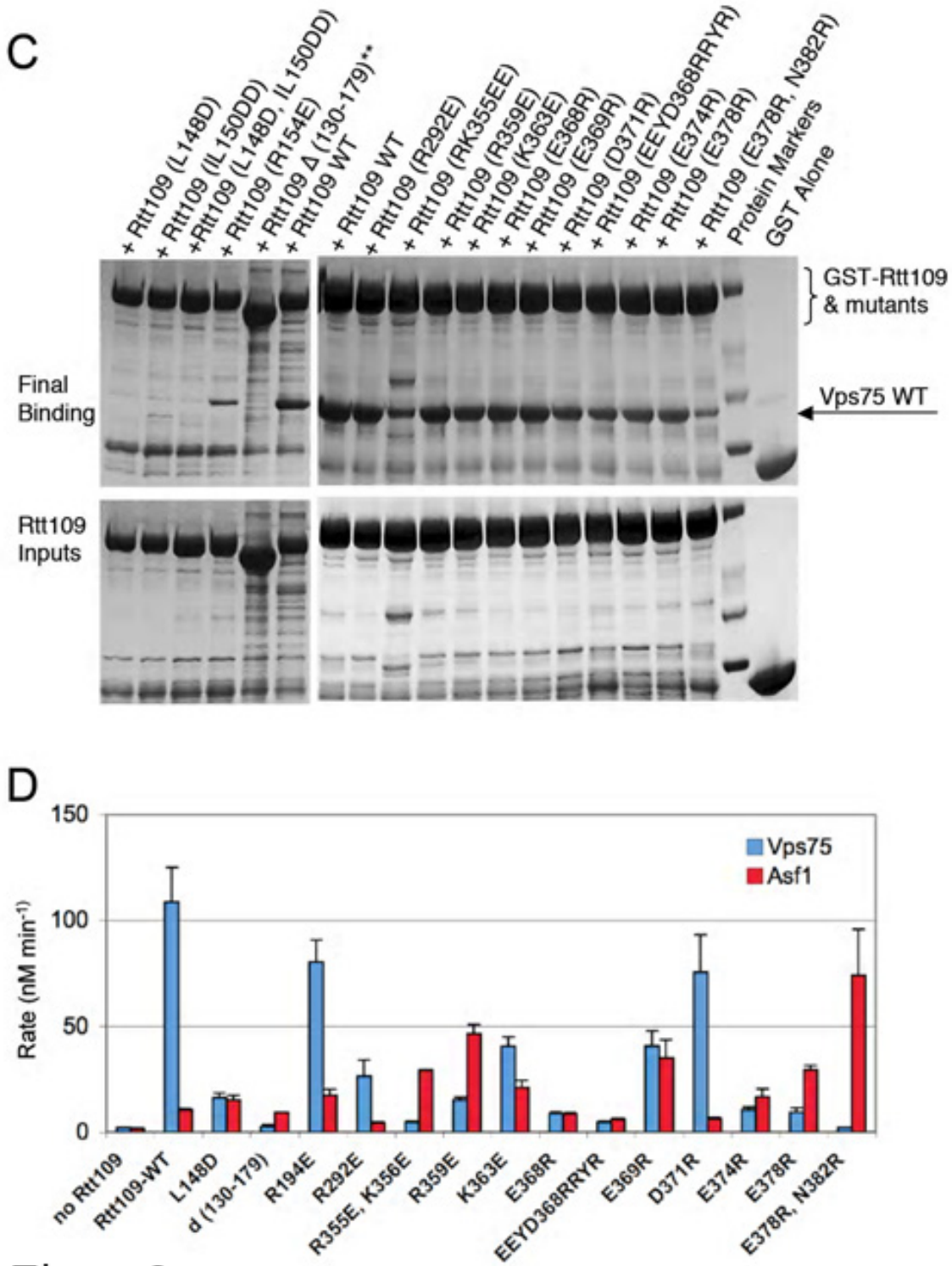
C
+ Rtt109 (L148D)
+ Rtt109 (IL150DD)
+Rtt109 (L148D, IL150DD)
+ Rtt109 (R154E)
+ Rtt109 Δ (130-179)**
+ Rtt109 WT
+ Rtt109 WT
+ Rtt109 (R292E)
+ Rtt109 (RK355EE)
+ Rtt109 (R359E)
+ Rtt109 (K363E)
+ Rtt109 (E368R)
+ Rtt109 (E369R)
+ Rtt109 (D371R)
+ Rtt109 (EEYD368RRYR)
+ Rtt109 (E374R)
+ Rtt109 (E378R)
+ Rtt109 (E378R, N382R)
Protein Markers
GST Alone
GST-Rtt109 & mutants
Vps75 WT
Final Binding
Rtt109 Inputs
D
Rate (nM min-1)
150
100
50
0
Vps75
Asf1
no Rtt109
Rtt109-WT
L148D
d (130-179)
R194E
R292E
R355E, K356E
R359E
K363E
E368R
EEYD368RRYR
E369R
D371R
E374R
E378R
E378R, N382R

Figure 3

E

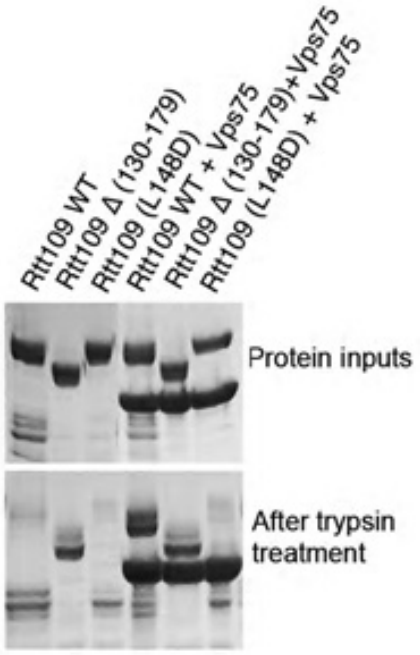


F

| Substrate | kcat ($min^{-1}$) | | | |
|---|---|---|---|---|
| | Rtt109-WT + Vps75 | Rtt109-R292E + Vps75 | Rtt109-WT + Asf1 | Rtt109-R292E + Asf1 |
| H3-WT | 4.06 ± 0.26 (Km=2.12±0.63 μM) | 2.88 ± 0.21 (Km=2.72±0.79 μM) | 0.91 ± 0.12 (Km=1.84±0.81 μM) | 0.076 ± 0.005 (Km=7.02±1.05 μM) |
| H3-K9R/K27R | 0.50 ± 0.02 | 0.20 ± 0.01 | N.D. | N.D. |
| H3-K9R/K56R | 0.50 ± 0.05 | 0.26 ± 0.01 | N.D. | N.D. |
| H3-K27R/K56R | 4.61 ± 0.35 | 1.60 ± 0.17 | N.D. | N.D. |
| H3-K9R/K27R/K56R | 0.55 ± 0.03 | 0.15 ± 0.02 | N.D. | N.D. |

**Figure 3. Identification and characterization of key residues that mediate Rtt109-Vps75 complex formation, Rtt109 HAT stimulation by Vps75 or Asf1, and H3 substrate specificity by mutagenesis, pull-down, and enzymatic assays.** (A) Pull-down studies of Vps75-wt and mutants by GST-Rtt109-wt. Published mutants (**) were included for comparison (Tang et al., 2008b). Vps75-(monomeric) number is Vps5-(C21E,V25S,I28E,V32E) (Berndsen et al., 2008). (B) HAT assays were performed with $(H3–H4)_2$ tetramer and [$^{14}$C]AcCoA substrates and complexes of GST-Rtt109-wt with Vps75-wt and mutants. (C) Pull-down studies of Vps75-wt by GST-Rtt109-wt and mutants. A published mutant (**) was included for comparison (Tang et al., 2008b). (D) Enzymatic studies of GST-Rtt109-wt and mutants in the presence of Vps75-wt or yAsf1N (1–154). HAT assays were performed with $(H3–H4)_2$ tetramer and [$^{14}$C]AcCoA substrates. (E) Limited proteolysis of Rtt109/Vps75 complexes containing wild-type, mutant or truncated forms of Rtt109. Reaction products after 10 min of trypsin digestion are shown. A 30 min reaction showed a nearly identical pattern of digestion. (F) Catalytic rates ($k_{cat}$) were measured for Rtt109-WT and Rtt109-(R292E) using the following substrates in the

context of the $(H3–H4)_2$ tetramer: H3-WT, H3-(K9R/K56R), H3-(K27/K56R), H3-(K9/K27R) and H3-(K9R, K27/K56R) (Figure S3). All parameters were determined by a non-linear regression fit to the Michaelis-Menten equation (see Experimental Procedures).

## Asf1 and Vps75 stimulate Rtt109 HAT activity through distinct mechanisms

Given that Rtt109 HAT activity can be stimulated by both the Vps75 and Asf1 histone chaperones, we asked whether the regions of Rtt109 that mediate Vps75 interaction and stimulation of HAT activity are also employed for Asf1-mediated Rtt109 stimulation. To determine whether the stimulation of HAT activity by Asf1 requires the 130–179 segment of Rtt109, we assayed the acetyltransferase activity of Rtt109-wt and two Rtt109 mutants, Rtt109-Δ(130–179) and Rtt109-(L148D), in the presence or absence of Asf1. As shown in Figure 3D, Asf1 enhances the HAT activity of the Rtt109-Δ(130–179) and Rtt109-(L148D) mutants as effectively if not better than the wild-type protein, demonstrating that Asf1 does not employ the 130–179 segment of Rtt109 to stimulate its HAT activity. This is in striking contrast to Vps75, which poorly increases the HAT activity of Rtt109-Δ(130–179) and Rtt109-(L148D) (Figure 3D). In addition, Rtt109 α8-α9 mutations that significantly cripple stimulation of Rtt109 HAT activity by Vps75 do not show a defect in Asf1-stimulated HAT activity (Figure 3D). These include Rtt109-(R355E,K356E), Rtt109-(E374R), Rtt109-(E378R) and Rtt109-(E378R,N382R). Taken together, these results suggest that Vps75 and Asf1 stimulate Rtt109 HAT activity through distinct mechanisms.

To further probe the lysine substrate specificity of the Rtt109/Vps75 complex, we prepared histone H3 mutants that contain either K9R/K27R (K56 is available for acetylation), K27R/K56R (K9 is available for acetylation) or K9R/K56R (K27 is available for acetylation) substitutions in the context of the $(H3–H4)_2$ tetramer and used them as substrates for Rtt109/Vps75. Kinetic analysis revealed that the wild-type Rtt109/Vps75 complex exhibits comparable catalytic efficiency towards the wild-type and H3-K27R/K56R mutant histone substrates but significant defects towards any of the histone substrates harboring a K9R mutation, showing a decrease in $k_{cat}$ of ~10-fold and elevated

$K_m$ values (Figure 3F; Figure S3A). This data is consistent with quantitative MS and Edman sequencing analyses of the reaction products obtained with wild-type $(H3–H4)_2$, which showed that the Rtt109/Vps75 complex preferentially acetylates H3K9 over H3K56 and other acetylation sites in the N-terminal tail of H3 (Figure S3D).

In our survey of Rtt109 mutants that exhibit reduced HAT activity in the presence of histone chaperones, we were intrigued by an Rtt109-(R292E) mutant that did not affect Rtt109/Vps75 complex formation (Figure 3C) and only had a modest effect on Vps75-stimulated H3 acetylation, but showed more dramatic defects in Asf1-stimulated acetylation (Figure 3D). To further probe this mutation, we carried out more detailed kinetics on the Rtt109/Asf1 and Rtt109-(R292E)/Asf1 complexes using the wild-type $(H3–H4)_2$ substrate. We found that, in contrast to wild-type Rtt109/Vps75 and Rtt109-(R292E)/Vps75 that acetylate the $(H3–H4)_2$ substrate with comparable activity (< 2-fold decrease in $k_{cat}/K_m$) and similar activity profiles for each of the substrates bearing H3 mutants (Figures 3F; Figure S3B), the Rtt109-(R292E)/Asf1 mutant shows about a 45-fold decrease in $k_{cat}/K_m$ for the $(H3–H4)_2$ substrate relative to wild-type Rtt109/Asf1 (Figures 3F and S3C). This observation demonstrates that residue Rtt109-R292 plays a more important role in Asf1- over Vps75-mediated Rtt109 acetylation of histone H3.

## Histone substrates bind within the interior of the Rtt109-AcCoA/Vps75 ring

The observation that the acetyl group of AcCoA and the active site residues of Rtt109 are facing towards the interior of the ring structure implies that the histone substrate is bound in the interior of the ring-shaped Rtt109-AcCoA/Vps75 complex. This hypothesis is supported by a mapping of sequence conservation onto the surfaces of both Rtt109 and Vps75, which reveals that the most highly conserved surfaces of Rtt109 and Vps75 are brought together in the interior of the ring (Figures 4A and 4B). In contrast, the exterior surface of the complex shows relatively poor sequence conservation (Figure 4C).

We also identified several conserved and solvent exposed Vps75 and Rtt109 residues within the ring that result in reduced HAT activity when mutated (Figures 3B, 3D and 4D). These mutants included Rtt109-(R194E), Rtt109-(E368R) and Rtt109-(EEYD368RRYR), as well as Vps75-(E206K,E207K). To determine the histone acetylation defects of these mutants more accurately, we determined their steady-state kinetic parameters in the presence of a large excess (presumed saturating) of Ac-CoA (Figure 4E; Figure S4). This analysis revealed that the Vps75-(E206K,E207K) mutant predominantly has a histone tetramer $K_m$ defect (> 10-fold), whereas the other mutants have defects in $k_{cat}$ of between 4- and 70-fold. Although the $K_m$ defect of the Vps75-(E206K,E207K) mutant likely reflects a defect in histone binding, the $k_{cat}$ defect of the other mutants could reflect a destabilization of the transition state of the acetylation reaction. Given that the mutated residues are not near the active site of the enzyme and are not involved in Rtt109/Vps75 interaction, we propose that they mediate correct positioning of the histone H3 substrate in the active site for optimal acetylation. This proposal is consistent with our structural observation that Vps75 binding to Rtt109 does not significantly alter the Rtt109 active site (Figure 2C), as well as a previous report showing that Vps75 binding stimulates Rtt109 activity by elevating the $k_{cat}$, rather than by reducing the $K_m$ for the H3 substrate (Berndsen et al., 2008). Taken together, these data further support the role of the interior of the ring-shaped complex in binding the histone substrate in a manner that is productive for H3 acetylation.

It has been reported that a truncation of the C-terminal acidic tail of Vps75 (residues 224–264) impairs its ability to activate Rtt109 without affecting Vps75 binding to Rtt109 (Park et al., 2008). Because we found Vps75 residues as C-terminal as Asp225 are involved in Rtt109 interaction, we asked how the longer fragment (residues 1–232) used in our structure determination may impact Rtt109 HAT activity. To this end, we compared the Rtt109 activation capabilities of Vps75-wt, Vps75-(1–232) and Vps75-(1–223). We found that Vps75-(1–232) and Vps75-(1–223) activate Rtt109 to similar levels, and with an ~4-fold reduced rate relative to full-length Vps75 (Figure 3B). These results suggest that Vps75 residues C-terminal to Leu232 are required for optimal activation of Rtt109. Because the last ordered residue of Vps75 in the structure of the complex, Glu226, points

toward the interior of the ring, we propose that the Vps75 C-terminal acidic tail may also be in position to associate with histones bound within the ring-shaped enzyme complex.

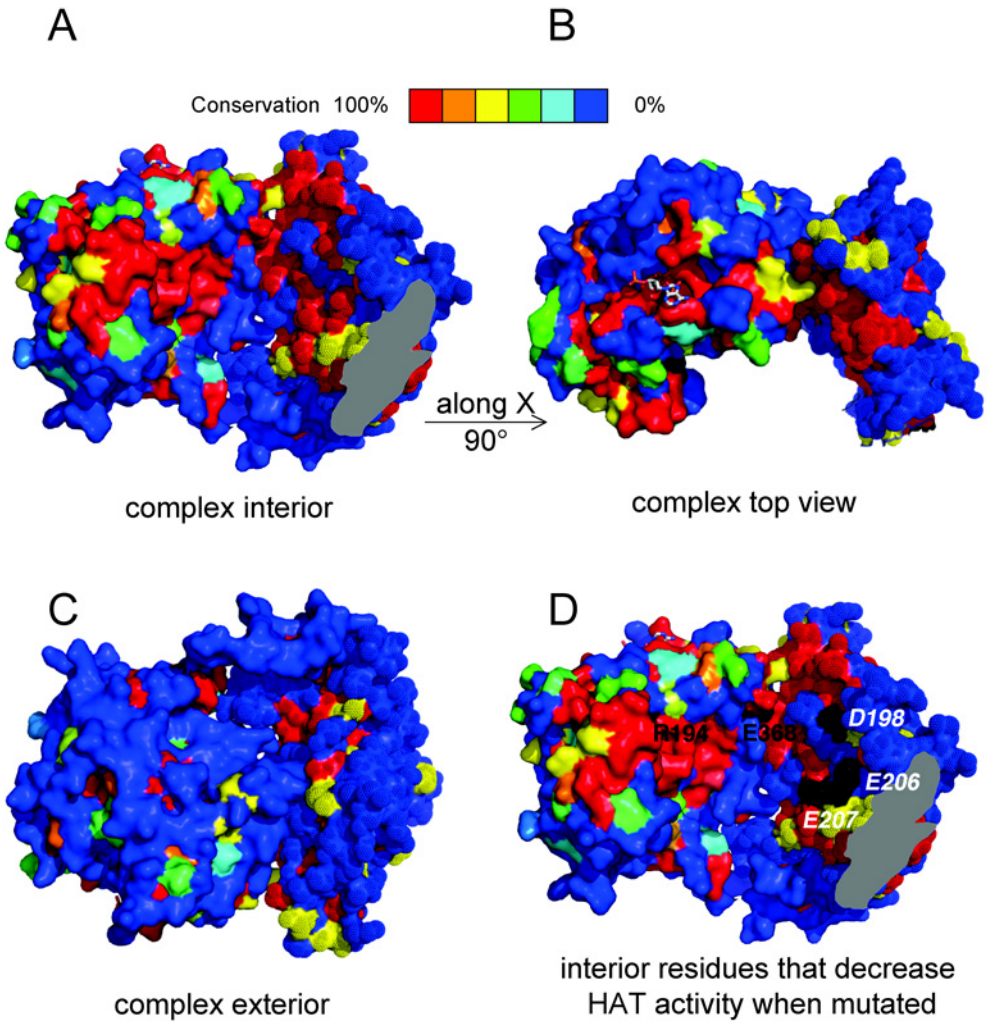


E

| Sample | Km (μM) | kcat ($min^{-1}$) | *kcat/Km* ($min^{-1}$ $\mu M^{-1}$) |
|---|---|---|---|
| Rtt109-WT/Vps75-WT | 1.84 ± 0.60 | 6.95 ± 0.60 | 3.77 ± 1.23 |
| Rtt109-R194 E | 4.98 ± 1.90 | 0.46 ± 0.07 | 0.092 ± 0.035 |
| Rtt109-E368R | 0.21 ± 0.13 | 0.24 ± 0.01 | 1.14 ± 0.71 |
| Rtt109-EEYD368RRYR | 2.09 ± 0.60 | 0.077 ± 0.006 | 0.037 ± 0.011 |
| Vps75-D198K/S199Y | 2.24 ± 0.75 | 1.49 ± 0.10 | 0.66 ± 0.22 |
| Vps75-E206K/E207K | > 22 | N.D. | 0.25 ± 0.05 |

**Figure 4. Histone binding by the Rtt109-AcCoA/Vps75 complex.** (A and B) Orthogonal surface representations of the Rtt109-AcCoA/Vps75 complex reveal a high degree of sequence conservation within the interior of the ring-shaped complex. The color-coding indicates the degree of conservation as shown in the bar key, with sequence conservation

information derived from previously published alignments (Tang et al., 2008a; Tang et al., 2008b). For clarity, only one Rtt109 molecule and half of the Vps75 homodimer are shown (gray patch represents the cross section at point of omission). The orientation of (A) is the same as in Figure S2A. (C) The exterior surface of the ring-shaped Rtt109/Vps75 complex shows a low degree of sequence conservation. (D) Location of Rtt109 (Arg194 and Glu368) and Vps75 (Asp198, Glu206, and Glu207) residues whose mutation decreases HAT activity (E). These residues are not involved in mediating Rtt109-Vps75 interaction and do not appear to be part of the active site and, therefore, are suggested to participate in histone binding. The view is as in (A). (E) Summary of kinetic parameters of selected Rtt109 and Vps75 mutants within the ring interior of the Rtt109-AcCoA/Vps75 complex (Figure S4). All parameters were determined by a non-linear regression fit to the classical Michaelis- Menten equation (see Experimental Procedures). N.D.: not determined due to experimental considerations.

## Mutations that decrease Rtt109/Vps75 HAT activity *in vitro* reduce H3K9 and H3K27, but not H3K56 acetylation *in vivo*

*In vitro*, the Rtt109/Vps75 holoenzyme cannot acetylate nucleosomes (Han et al., 2007c; Tsubota et al., 2007a), suggesting that it may exclusively act on newly synthesized histones prior to their deposition onto DNA. Among the five acetylatable lysine residues in the N-terminal tail of H3, lysines K9 and K27 were found to be the most extensively acetylated after a short pulse of [$^3$H]-lysine in *Saccharomyces cerevisiae* (Kuo et al., 1996). Furthermore, in contrast to H3K56 acetylation, which is entirely dependent upon Rtt109 and Asf1 (Driscoll et al., 2007; Drogaris et al., 2008; Han et al., 2007a; Tsubota et al., 2007a), both Gcn5 and Rtt109-Vps75 contribute to H3K9 and H3K27 acetylation *in vivo* (Berndsen et al., 2008; Burgess et al., 2010; Fillingham et al., 2008).

To characterize the effects of the structure-based Rtt109 mutations *in vivo*, we first validated our assays by monitoring H3K9/K27 and H3K56 acetylation in strains where selected HAT genes were deleted. Based on mass spectrometry (MS), H3K9 and H3K27 acetylation is abundant *in vivo*, with ~20% of H3 molecules acetylated at K9 and K27 in wild-type cells (Figure 5B–C). As judged by MS, the levels of H3K9 and H3K27 acetylation were considerably reduced, but not completely abolished in *gcn5* single mutants, whereas H3K56 acetylation was as abundant as in wild-type cells (Figure 5A–C). In contrast, essentially no H3K9 or H3K27 acetylation remained in *gcn5*Δ *vps75*Δ or

*gcn5*Δ *rtt109*Δ double mutants and, consistent with previous reports, the *rtt109*Δ mutation essentially abolished H3K56 acetylation (Figure 5A–C) (Driscoll et al., 2007; Han et al., 2007b). As judged by MS, a*vps75* null mutation did not significantly cripple acetylation of H3K14, H3K18 or H3K23, whereas H3K18 was essentially abolished in *gcn5* single mutants **(**data not shown**).** These results demonstrate that, *in vivo*, the Rtt109/Vps75 enzyme functionally overlaps with Gcn5 to acetylate H3K9 and H3K27, whereas Rtt109 and Asf1 cooperate to promote H3K56 acetylation.

Importantly, when introduced into either *gcn5*Δ *rtt109*Δ or *gcn5*Δ *vps75*Δ double mutants, low copy plasmids expressing wild-type Rtt109-Flag or Vps75-Flag, respectively, from their natural promoters, restored H3K9, K27 and K56 acetylation (Figures 5A–H). This provided assays to monitor the effects of structure-based Rtt109 mutations on histone acetylation. The structure-based Rtt109 mutants that we tested *in vivo* showed defects in H3K9 and K27 acetylation, with the Rtt109-(L148D) and Rtt109-(E378R,N382R) mutants being the most defective (Figures 5E–G and data not shown). Therefore, we focused our *in vivo* studies on these two Rtt109 mutants. Based on MS and immunoblotting, the Rtt109-(L148D) and Rtt109-(E378R,N382R) were defective in H3K9/K27 acetylation, but not H3K56 acetylation *in vivo* (Figures 5D–G). As judged by MS and immunoblotting, the Rtt109-(L148D) mutation abolished its interaction with Vps75 whereas the Rtt109-(E378R,N382R) mutant showed residual binding to Vps75 *in vivo* (Figures 6A and 6B). Consistent with the greater sensitivity of Rtt109-L148D and Rtt109-E378R,N382R to mutations, these residues are located within the Rtt109 (130–179) segment and α8-α9 helix region of Rtt109, respectively, which mediate contacts to the two distinct binding surfaces on Vps75 (Figure 2). In the absence of Vps75, Rtt109 has been reported to be less stable than in wild-type cells (Fillingham et al., 2008). In agreement with its strong defect in interaction with Vps75, the Rtt109-(L148D) mutation (and to a lesser extent the Rtt109-(E378R,N382R) mutation) destabilized the protein to an extent similar to that observed in a *vps75* null mutant even though each of the mutant proteins are expressed at similar steady-state levels (Figure 6D).

We also determined the effects of Vps75 mutations on histone acetylation and complex formation *in vivo*. In keeping with the structure of the holoenzyme (Figure 2), the Vps75-(R173E,K177E) and Vps75-(E218K,D222K) mutations reduced the interaction of Vps75 mutants with Rtt109 both *in vitro* (Figure 3A) and *in vivo* (Figure 6C). In contrast, mutation of residues E206 and E207, which line the central cavity of the Rtt109/Vps75 holoenzyme and are not involved in interaction with Rtt109 (Figures 3A and 4D), only has a mild effect on the interaction of Rtt109 and Vps75 *in vivo* (Figure 6C). However, compared with WT Vps75, all three Vps75 mutations reduced H3K9/K27 acetylation without perturbing H3K56 acetylation *in vivo* (Figure 5H). These results taken together, demonstrate that mutations that decrease Rtt109/Vps75 interaction and H3K9 but not H3K56 acetyltransferase activity *in vitro* correlates with similar activities *in vivo*.

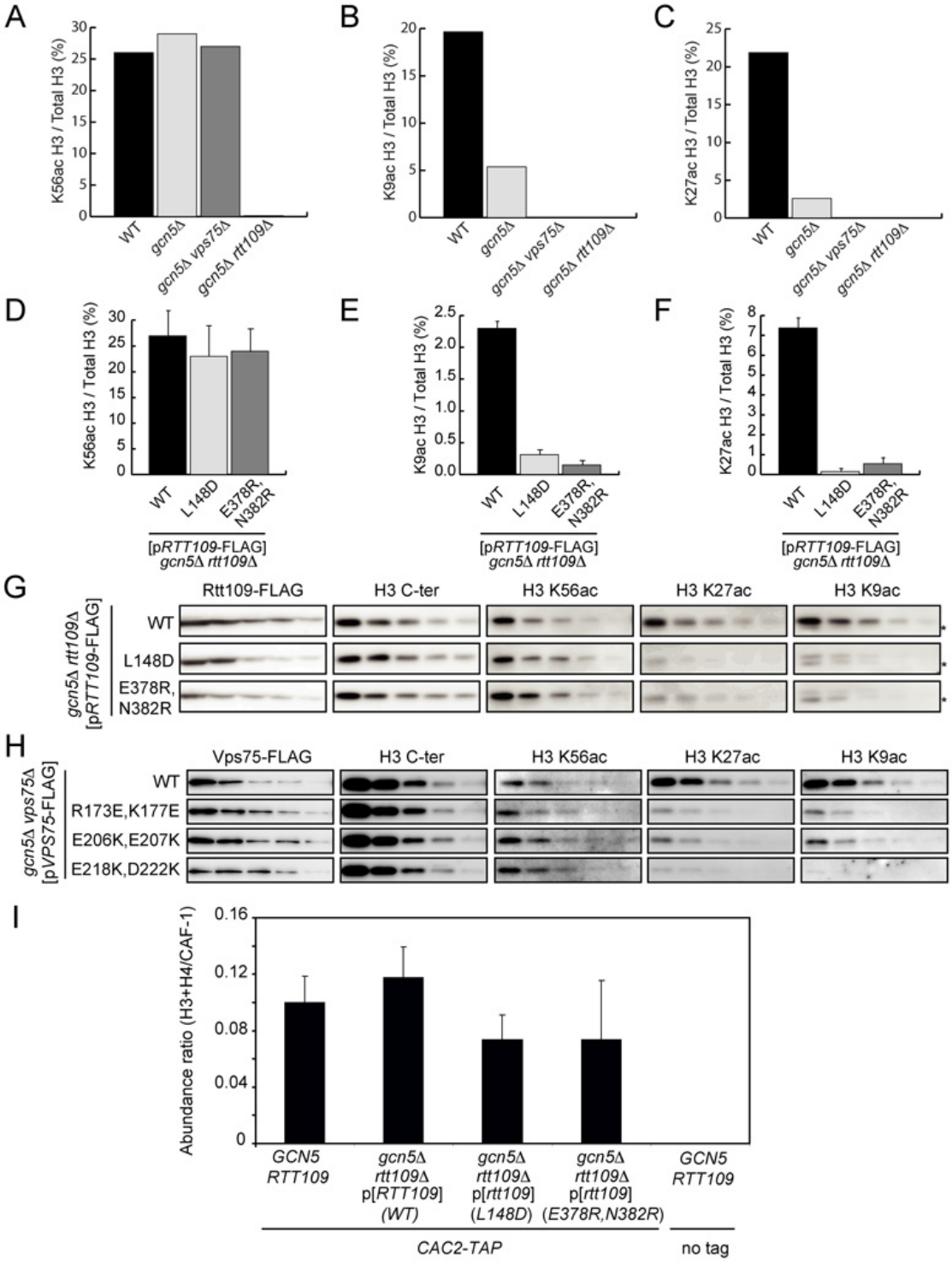


**Figure 5.** ***In vivo*** **analysis of wild-type and mutant forms of the Rtt109/Vps75 holoenzyme**. (A–F) Histone lysine specificity of *gcn5*, *rtt109* and *vps75* null mutants and selected mutants that specifically target the integrity of the Rtt109/Vps75 holoenzyme as

determined by mass spectrometry. Total histones were purified from asynchronously growing cells and analyzed by mass spectrometry (Supplemental Experimental Procedures) to determine the fraction of H3 molecules acetylated at K9, K27 and K56. (G and H) Histone lysine specificity of selected Rtt109 and Vps75 mutants as determined by immunoblotting. 1.5-fold serial dilutions of whole-cell lysates (from left to right) were probed by immunoblotting to determine the levels of H3K9, K27 and K56 acetylation in cells expressing Rtt109 or Vps75 mutants. The asterisk points to a non-specific band that is weakly detected by our anti-H3K9ac in *H3K9R*mutant cells (not shown). (I) Effect of selected Rtt109 mutants on histone assembly. Complexes of CAF-1 and histones H3/H4 were affinity-purified from yeast cells to determine the amounts of histones bound to CAF-1 in strains expressing Rtt109 mutants.

## Mutations that decrease the H3K9 HAT activity of the Rtt109/Vps75 complex *in vitro* and *in vivo* are not sufficient to confer phenotypes associated with defects in nucleosome assembly

*In vivo*, mutations that cripple the acetylation of new histones or interfere with replication-coupled nucleosome assembly confer sensitivity to genotoxic agents and defects in cell proliferation and heterochromatin-mediated gene silencing (Burgess et al., 2010; Driscoll et al., 2007; Han et al., 2007a; Han et al., 2007b; Li et al., 2008; Tsubota et al., 2007). This is indeed what we observed in *rtt109* single and *rtt109 gcn5* double mutants (Figures S5 and S6). In *rtt109*Δ *gcn5*Δ double mutants, H3K9/K27 in the N-terminal tail and H3K56 acetylation are essentially abolished (Figure 5A–5C). However, none of our structure-based mutations that selectively disrupt the structure and/or activity of the Rtt109/Vps75 holoenzyme resulted in proliferation, genotoxic agent sensitivity or heterochromatin-mediated silencing (Figures S5A, S5B and S6C). This was true even when structure-based Rtt109/Vps75 mutations were combined with other mutations that should reduce the efficiency of the replication-coupled nucleosome assembly pathway, such as null mutations in *gcn5* (that reduces N-terminal acetylation of new H3 molecules (Burgess et al., 2010), *hat1* (an enzyme that acetylates new H4 molecules at lysines 5 and 12) (Kelly et al., 2000; Qin and Parthun, 2002) or *rtt106* (a chaperone that binds to new H3/H4 molecules) (Huang et al., 2007) (Figures S5B and S6A–C). These results suggested that the absence of the Rtt109/Vps75 enzyme is not sufficient to confer a physiologically significant defect in replication-coupled nucleosome assembly. To further confirm this

hypothesis, we affinity-purified Chromatin Assembly Factor 1 (CAF-1) and determined by MS the amounts of histones bound to CAF-1. CAF-1 is the prototypical replication-coupled nucleosome assembly factor (Kaufman et al., 1997) and cells where H3K56 acetylation is impaired contain low amounts of H3/H4 bound to CAF-1 (Kaufman et al., 1997; Li et al., 2008). Consistent with the fact that they do not confer any striking phenotype, the Rtt109-(L148D) and Rtt109-(E378R,N382R) mutants did not show any striking decrease in the amounts of H3/H4 bound to CAF-1, even in cells lacking Gcn5 (Figure 5I). Taken together, these studies show that the H3K9/K27 acetylation activity of the Rtt109/Vps75 complex is not sufficient to confer phenotypes associated with defects in nucleosome assembly.

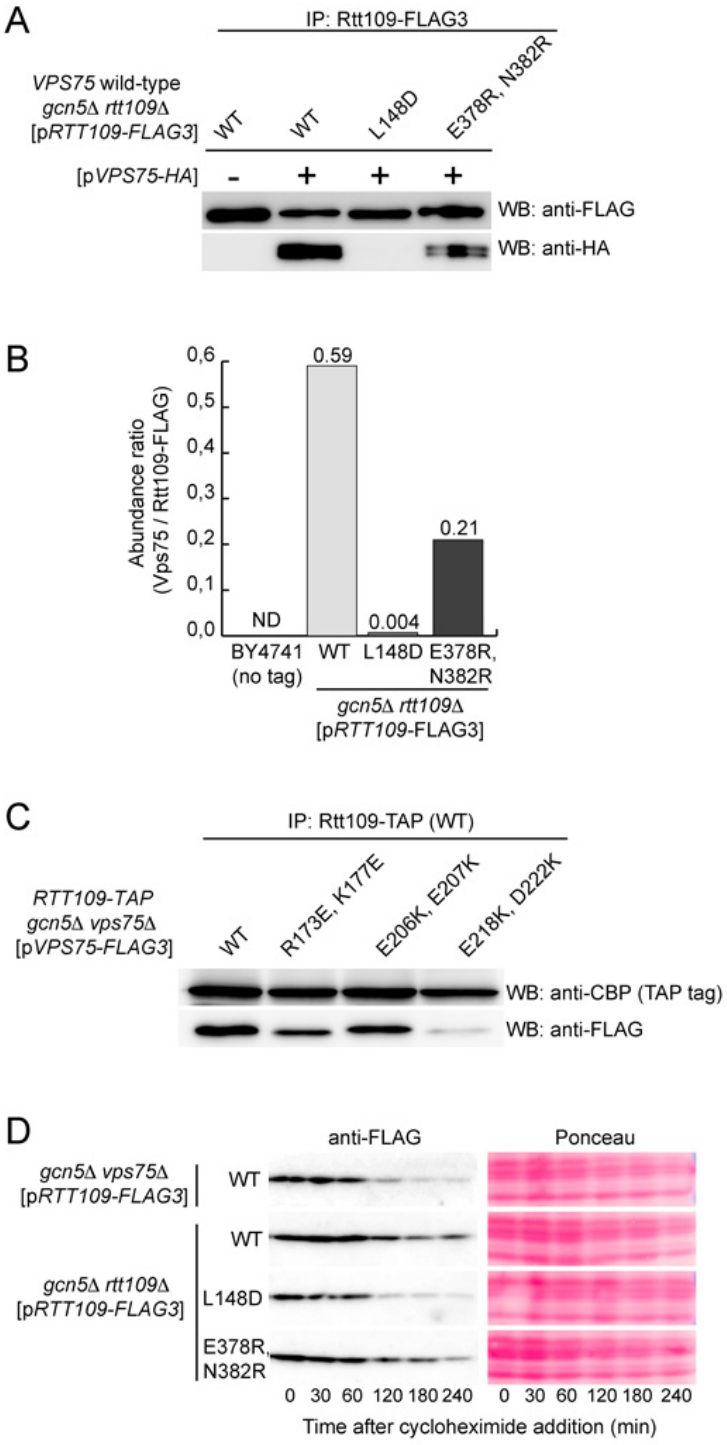


**Figure 6. *In vivo* analysis of the integrity of the Rtt109/Vps75 holoenzyme as a function of structure-based mutations**. (A and B) Effect of selected Rtt109 mutations on the Rtt109-Vps75 interaction. Copurification of Rtt109 and Vps75 from strains expressing Rtt109 mutants was monitored by immunoblotting (A) or mass spectrometry (B), see Supplemental Experimental Procedures). All the strains used in (A) contain a wild-type

chromosomal *VPS75* gene and an additional plasmid encoding a wild-type *VPS75-HA* gene. (C) Effect of selected Vps75 mutations on the Rtt109-Vps75 interaction. Co-purification of Rtt109 and Vps75 from strains expressing Vps75 mutants was monitored by immunoblotting. (D) Stability of Rtt109 mutants. The stability of Rtt109 mutants was determined by immunoblotting as a function of time after the addition of cycloheximide. The top panel is a control showing the reduced stability of wild-type Rtt109 in cells that lack Vps75.

## Discussion

The Rtt109 histone acetyltransferase promotes nucleosome assembly and genome stability by acetylating K9, K27 and K56 on new non-nucleosomal histone H3 molecules through its interactions with either of two distinct histone chaperones, Vps75 or Asf1. H3K9 acetylation, in particular, is evolutionarily conserved from yeast to human cells and is the most prominent site of acetylation in the N-terminal tail of new H3 molecules in *S. cerevisiae* (Adkins et al., 2007; Kuo et al., 1996). Despite the importance of the acetylation of new histones, the mechanism and the molecular basis of chaperone-mediated histone lysine acetylation specificity have gone largely unexplored.

To explore the mechanism by which histone chaperones promote Rtt109 HAT activity and lysine specificity, we determined the X-ray crystal structure of an Rtt109-AcCoA/Vps75 complex that revealed a 2-fold symmetrical heterotetrameric ring containing an interior cavity of ~12 Å diameter. Biochemical, enzymatic and *in vivo* studies further demonstrated that Rtt109-Vps75 contacts observed in the crystals are important for optimal H3K9/K27 but not H3K56 acetylation both *in vitro* and in yeast cells. A comparison of the Rtt109-AcCoA/Vps75 complex with the free Rtt109 and Vps75 proteins also showed that Vps75 binding to Rtt109 does not alter the Rtt109 active site, suggesting that Vps75 binding stimulates Rtt109 catalytic activity by appropriately presenting histone H3 for acetylation.

We also used information derived from the structure of the Rtt109-AcCoA/Vps75 complex to demonstrate that Asf1 and Vps75 stimulate the HAT activity of Rtt109 via different mechanisms. Along with other groups, we previously reported the identification of residues generally important for Rtt109-mediated H3 acetylation, including Rtt109 residues Asp89,

Tyr199, Trp222 and Asp287 (Han et al., 2007b; Tang et al., 2008a; Tsubota et al., 2007). In this study, we extended these findings to residues that play more dedicated roles in Vps75-mediated activation of Rtt109 for H3K9 acetylation. We showed that the 130–179 segment of Rtt109 and other residues that contribute to interaction surfaces between Rtt109 and Vps75 play a particularly important role in Vps75-dependent histone H3K9 acetylation both *in vitro* and in yeast cells. We also showed that Rtt109-R292 plays a more important role in Asf1-mediated histone acetylation.

The structure of the Rtt109-AcCoA/Vps75 complex, together with results from *in vitro* enzymological assays and analysis of acetylation in yeast cells, also indicate that histone substrate binding occurs within the interior surface of the ring-shaped Rtt109/Vps75 complex. Three lines of evidence support this model. First, the acetyl groups of the two Rtt109-bound AcCoA cofactors in the complex point into the interior of the ring. Second, the internal surface of the ring shows a much higher degree of sequence conservation than the exterior. Third, we have identified several Rtt109 and Vps75 substitution mutations within the interior of the ring that reduce histone H3 acetylation *in vitro* and H3K9/K27 but not H3K56 acetylation *in vivo*. The 2:2 stoichiometry and 2-fold symmetry of the complex are also consistent with the observation that Vps75 preferentially binds $(H3–H4)_2$ heterotetramers (Selth and Svejstrup, 2007) and strongly suggests that both H3 molecules of the heterotetramer are acetylated for histone deposition. In this way, the Vps75 histone chaperone serves as a cofactor for Rtt109-mediated acetylation by both appropriately positioning histone H3K9 for acetylation in the Rtt109 active site and ensuring homogenous histone H3 acetylation before H3–H4 deposition into nascent chromatin.

The structure of the Rtt109-AcCoA/Vps75 complex also enabled us to design Rtt109 and Vps75 separation-of-function mutants. These mutations leave H3K56 acetylation unaffected, but completely abolish the H3K9/K27 acetylation that remains in *gcn5*Δ cells (Figures 5 and 6). Significantly, mutations that selectively perturb the Rtt109/Vps75 enzyme do not exacerbate the phenotypes of *gcn5*Δ cells nor do they exhibit phenotypes that are commonly observed in mutants where replication-coupled nucleosome assembly is

defective. This is likely because of the overlapping substrate specificity of Gcn5 and Rtt109/Vps75 for H3K9/K27 and suggests that the Rtt109/Vps75 complex contributes to, but is not essential for replication-coupled nucleosome assembly.

It is currently unclear why several distinct HATs (Hat1, Gcn5, Rtt109/Vps75, Rtt109/Asf1, and possibly others) contribute to the acetylation of new H3/H4 molecules. By analogy with isoenzymes, some of these HATs may not be functionally redundant under certain growth or cellular stress conditions. However, new tools will be necessary to determine whether this is the case. Thus far, studies aimed at assigning functions to the acetylation of newly synthesized histones have been mainly performed by creating yeast strains where H3 and H4 carry several lysine-to-arginine mutations in the N-terminal tails. This experimental strategy has been helpful, but suffers from two limitations. First, these mutations cripple the acetylation of both newly synthesized and pre-existing histones and global disruption of histone acetylation interferes with transcription. Second, phenotypes that result from histone lysine-to-arginine substitutions might be due to mutations of the lysines, rather than the absence of acetylation. Rtt109/Vps75 is an enzyme that exclusively acetylates non-nucleosomal histones at two specific residues in the N-terminal tails of new H3 molecules. Therefore, the structure-based Rtt109 mutants described here, which are specifically defective in H3K9/H3K27, but not H3K56 acetylation, may provide invaluable tools to investigate the elusive function of the acetylation of the N-terminal tails of newly synthesized histones.

## Experimental procedures

Individual Rtt109 and Vps75 proteins were engineered as GST fusions as previously described (Tang et al., 2008a; Tang et al., 2008b), with the GST moiety removed by TEV protease as necessary. Quick-change site-directed mutagenesis (Stratagene) was used to introduce selected protein mutations. Recombinant human 6His-ASF1a protein (Tang et al., 2006) and yeast $(H3–H4)_2$ heterotetramer (Luger et al., 1999) were prepared as previously described. Yeast 6His-Asf1N(1–154) was cloned and prepared similarly to human ASF1a.

To produce complexes by coexpression, we subcloned DNAs encoding full-length Vps75 (or a 1–232 fragment as used in crystallization) and full-length Rtt109 proteins into the MCS1 and MCS2 sites, respectively, of a modified 6His-TEV-pCDF-Duet1 vector. Protein complexes were expressed in bacteria and purified to homogeneity through a combination of Ni-affinity, TEV protease cleavage, MonoQ anion exchange and Superdex S200 gel filtration chromatography.

Rtt109-Vps75 pull-down assays were carried out with wild-type or mutant GST-Rtt109 proteins bound to glutathione resin and untagged wild-type or mutant forms of Vps75. After binding reactions, proteins retained on the resin were resolved by SDS-PAGE. For enzymatic assays, we adapted the radioactive HAT assay as previously described (Lau et al., 2000; Thompson et al., 2001) using yeast $(H3–H4)_2$ tetramer as a substrate. Proteolysis studies of Rtt109 protein constructs were carried out with trypsin protease in the absence or presence of stoichiometric amounts of full length Vps75 and terminated by boiling the samples for resolution on SDS-PAGE.

Native crystals of the Rtt109-AcCoA/Vps75-(1–232) complex were obtained using hanging-drop vapor-diffusion from a reservoir solution containing 10.0% (v/v) PEG8000, 8% (v/v) ethylene glycol, and 100 mM HEPES pH 7.5 buffer. Peptide-soaked Rtt109-AcCoA/Vps75-(1–232) crystals were prepared by soaking native crystals with 1 mM CoA and 1 mM of a H3K9 14-amino acid peptide. The structure of the peptide soaked Rtt109-AcCoA/Vps75-(1–232) complex was determined to 2.8 Å resolution using molecular replacement with Rtt109-Δ (130–179) (PDB ID 3D35) (Tang et al., 2008a) and a Vps75-(1–232) monomer (PDB ID 3DM7) (Tang et al., 2008b) as search models. The models were adjusted and refined to include the 130–179 segment of Rtt109, AcCoA, and residues 11–14 of the H3K9 peptide [(NH2)A-R-T-K-Q-T-A-R-K-S-T-G-G-K (CONH2)] (Figure S1; Table 1). Given that the peptide does not make extensive protein contact and is located far from the active site, we infer that this peptide-binding mode is not biologically relevant. The final model, with the addition of 23 water molecules, was checked for errors using composite simulated annealing omit maps (Table 1). The structure of the native Rtt109-AcCoA/Vps75-(1–232) crystals was determined using the refined peptide-soaked

Rtt109-AcCoA/Vps75-(1–232) model and refined to 3.3 Å resolution (Table 1). Comparison of the two crystal forms reveals that the presence of the H3K9 peptide does not alter the overall Rtt109-AcCoa/Vps75 complex structure.

Yeast strains and plasmids to express Rtt109, as well as protocols to monitor H3K9 and K56 acetylation by immunoblotting and mass spectrometry, are described in detail in the Table S1 and Supplemental Experimental Procedures.

## Accession numbers

Atomic coordinates and structure factors of the Rtt109-AcCoA/Vps75 complexes have been deposited in the Protein Data Bank with accession codes 3Q35 (native crystal) and 3Q33 (peptide-soaked crystal), respectively.

## Acknowledgements

We thank X. Liu for initial contributions to this project and Dr. Zhiguo Zhang for the gift of an antibody specific for histone H3K27 acetylation. This work was supported by NIH grants to R.M. (R01 GM060293, P01 AG031862) and P.A.C (R01 GM062437), and by funds from CIHR and NSERC to A.V. and P.T. IRIC's infrastructure is supported by the Canadian Center of Excellence in Commercialization and Research, the Canadian Foundation for Innovation, and the Fonds de la Recherche en Santé du Québec. Part of this research was conducted at GM/CA-CAT beamline 23ID-B at the Advanced Photon Source, Argonne National Laboratory. Use of the APS was supported by the U.S. Department of Energy, Office of Science, Office of Basic Energy Sciences, under Contract No. W-31-109-ENG-38.

## References


Adkins MW, Carson JJ, English CM, Ramey CJ, Tyler JK. The histone chaperone anti-silencing function 1 stimulates the acetylation of newly synthesized histone H3 in S-phase. J Biol Chem.2007;282:1334–1340.

Albaugh BN, Kolonko EM, Denu JM. Kinetic mechanism of the Rtt109-Vps75 histone acetyltransferase-chaperone complex. Biochemistry. 2010;49:6375–6385.

Berndsen CE, Tsubota T, Lindner SE, Lee S, Holton JM, Kaufman PD, Keck JL, Denu JM. Molecular functions of the histone acetyltransferase chaperone complex Rtt109-Vps75. Nat Struct Mol Biol. 2008;15:948–956.

Burgess RJ, Zhou H, Han J, Zhang Z. A role for Gcn5 in replication-coupled nucleosome assembly. Mol Cell. 2010;37:469–480.

Collins SR, Miller KM, Maas NL, Roguev A, Fillingham J, Chu CS, Schuldiner M, Gebbia M, Recht J, Shales M, et al. Functional dissection of protein complexes involved in yeast chromosome biology using a genetic interaction map. Nature. 2007;446:806–810.

Daganzo SM. Structure and function of the conserved core of histone deposition protein Asf1.Curr Biol. 2003;13:2148–2158.

Das C, Lucia MS, Hansen KC, Tyler JK. CBP/p300-mediated acetylation of histone H3 on lysine 56. Nature. 2009;459:113–117.

Driscoll R, Hudson A, Jackson SP. Yeast Rtt109 promotes genome stability by acetylating histone H3 on lysine 56. Science. 2007;315:649–652.

English CM, Adkins MW, Carson JJ, Churchill ME, Tyler JK. Structural basis for the histone chaperone activity of Asf1. Cell. 2006;127:495–508.

Fillingham J, Recht J, Silva AC, Suter B, Emili A, Stagljar I, Krogan NJ, Allis CD, Keogh MC, Greenblatt JF. Chaperone control of the activity and specificity of the histone H3 acetyltransferase Rtt109. Mol Cell Biol. 2008;28:4342–4353.

Han J, Zhou H, Horazdovsky B, Zhang K, Xu RM, Zhang Z. Rtt109 acetylates histone H3 lysine 56 and functions in DNA replication. Science. 2007a;315:653–655.

Han J, Zhou H, Li Z, Xu RM, Zhang Z. Acetylation of lysine 56 of histone H3 catalyzed by RTT109 and regulated by ASF1 is required for replisome integrity. J Biol Chem.2007b;282:28587–28596.

Han J, Zhou H, Li Z, Xu RM, Zhang Z. The Rtt109-Vps75 histone acetyltransferase complex acetylates non-nucleosomal histone H3. J Biol Chem. 2007c;282:14158–14164.

Huang S, Zhou H, Tarara J, Zhang Z. A novel role for histone chaperones CAF-1 and Rtt106p in heterochromatin silencing. EMBO J. 2007;26:2274–2283.

Kaufman PD, Kobayashi R, Stillman B. Ultraviolet radiation sensitivity and reduction of telomeric silencing in Saccharomyces cerevisiae cells lacking chromatin assembly factor-I.Genes Dev. 1997;11:345–357.

Kelly TJ, Qin S, Gottschling DE, Parthun MR. Type B histone acetyltransferase Hat1p participates in telomeric silencing. Mol Cell Biol. 2000;20:7051–7058.

Kuo MH, Brownell JE, Sobel RE, Ranalli TA, Cook RG, Edmondson DG, Roth SY, Allis CD. Transcription-linked acetylation by Gcn5p of histones H3 and H4 at specific lysines. Nature.1996;383:269–272.

Lau OD, Courtney AD, Vassilev A, Marzilli LA, Cotter RJ, Nakatani Y, Cole PA. p300/CBP-associated factor histone acetyltransferase processing of a peptide substrate. Kinetic analysis of the catalytic mechanism. J Biol Chem. 2000;275:21953–21959.

Li Q, Zhou H, Wurtele H, Davies B, Horazdovsky B, Verreault A, Zhang Z. Acetylation of histone H3 lysine 56 regulates replication-coupled nucleosome assembly. Cell. 2008;134:244–255.

Lin C, Yuan YA. Structural insights into histone H3 lysine 56 acetylation by Rtt109. Structure.2008;16:1503–1510.

Luger K, Rechsteiner TJ, Richmond TJ. Preparation of nucleosome core particle from recombinant histones. Methods Enzymol. 1999;304:3–19.

Park YJ, Sudhoff KB, Andrews AJ, Stargell LA, Luger K. Histone chaperone specificity in Rtt109 activation. Nat Struct Mol Biol. 2008;15:957–964.

Qin S, Parthun MR. Histone H3 and the histone acetyltransferase Hat1p contribute to DNA double-strand break repair. Mol Cell Biol. 2002;22:8353–8365.

Selth L, Svejstrup JQ. Vps75, a new yeast member of the NAP histone chaperone family. J Biol Chem. 2007;282:12358–12362.

Stavropoulos P, Nagy V, Blobel G, Hoelz A. Molecular basis for the autoregulation of the protein acetyl transferase Rtt109. Proc Natl Acad Sci U S A. 2008;105:12236–12241.

Tang Y, Holbert MA, Wurtele H, Meeth K, Rocha W, Gharib M, Jiang E, Thibault P, Verreault A, Cole PA, et al. Fungal Rtt109 histone acetyltransferase is an unexpected structural homolog of metazoan p300/CBP. Nat Struct Mol Biol. 2008a;15:738–745.

Tang Y, Meeth K, Jiang E, Luo C, Marmorstein R. Structure of Vps75 and implications for histone chaperone function. Proc Natl Acad Sci U S A. 2008b;105:12206–12211.

Tang Y, Poustovoitov MV, Zhao K, Garfinkel M, Canutescu A, Dunbrack R, Adams PD, Marmorstein R. Structure of a human ASF1a-HIRA complex and insights into specificity of histone chaperone complex assembly. Nat Struct Mol Biol. 2006;13:921–929.

Thompson PR, Kurooka H, Nakatani Y, Cole PA. Transcriptional coactivator protein p300. Kinetic characterization of its histone acetyltransferase activity. J Biol Chem. 2001;276:33721–33729.

Tjeertes JV, Miller KM, Jackson SP. Screen for DNA-damage-responsive histone modifications identifies H3K9Ac and H3K56Ac in human cells. EMBO J. 2009;28:1878–1889.

Tsubota T, Berndsen CE, Erkmann JA, Smith CL, Yang L, Freitas MA, Denu JM, Kaufman PD. Histone H3-K56 acetylation is catalyzed by histone chaperone-dependent complexes. Mol Cell.2007;25:703–712.

Xie W, Song C, Young NL, Sperling AS, Xu F, Sridharan R, Conway AE, Garcia BA, Plath K, Clark AT, et al. Histone h3 lysine 56 acetylation is linked to the core transcriptional network in human embryonic stem cells. Mol Cell. 2009;33:417–427.

## Supplementary material

### TABLE OF CONTENTS

## Supplemental figures

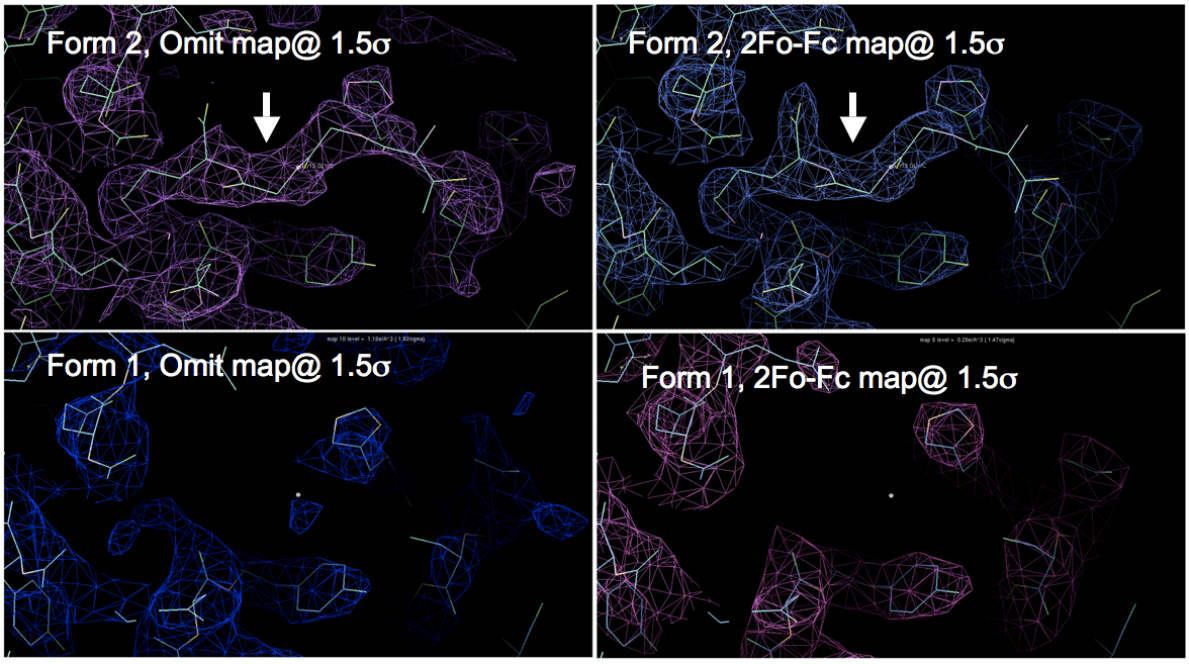


**Figure S1, related to Figure1. Electron density maps of Rtt109/Vps75 complexes.** Composite omit and 2Fo-Fc maps of the native Rtt109/Vps75 complex crystal (lower panels) and the peptide-soaked Rtt109/Vps75 complex crystal (upper panels) structures. The two crystal structures superimpose with an RMSD of 0.54 Å for all Cα atoms. This data shows that the binding of the H3K9 peptide (arrow) at the Rtt109-Vps75 interface does not cause local conformation changes.

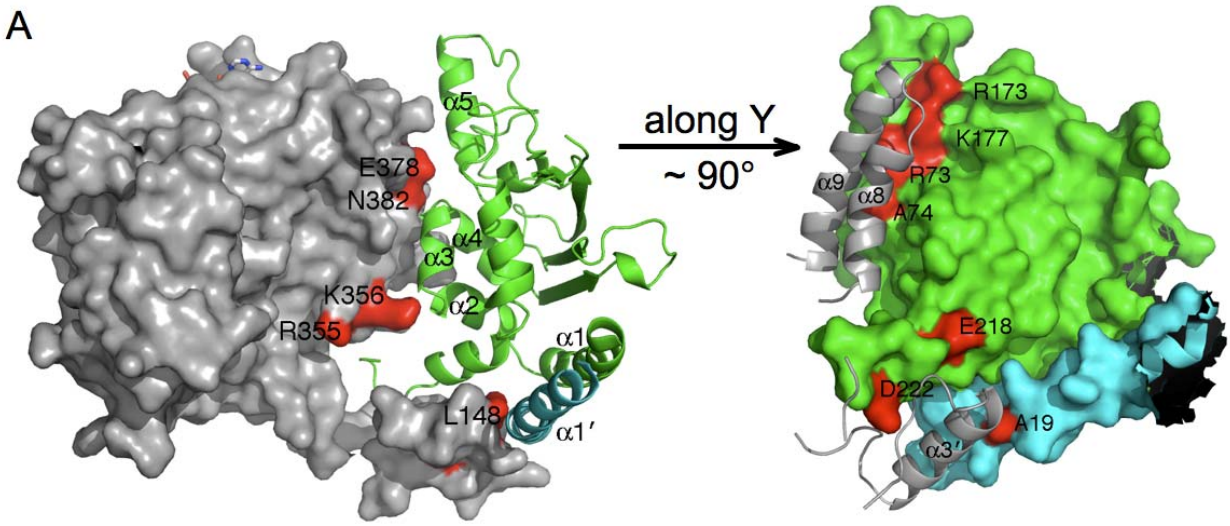


B

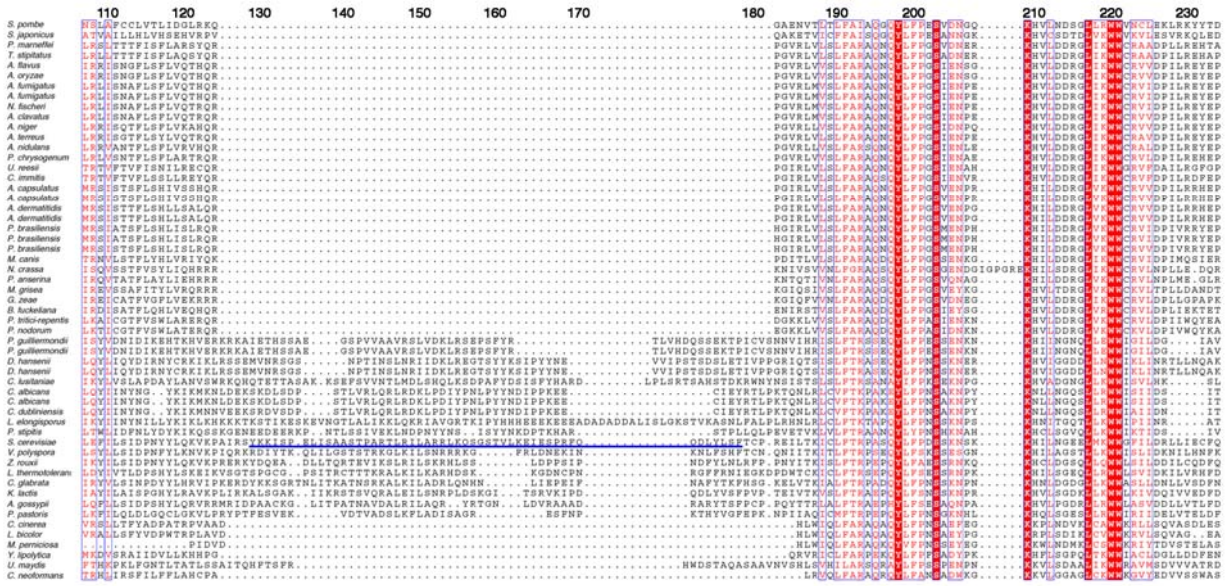

**Figure S2, related to Figure 2**. (A) Interaction-defective mutations mapped onto Rtt109 and Vps75: Right panel: Vps75 mutations that decrease both Rtt109 pull-down and Vps75-stimulated Rtt109 HAT activity are highlighted in red on the surface representation of the Vps75 dimer. For clarity only one subunit of Vps75 and the a1′ helix of the opposing subunit are shown. The interacting segments of the Rtt109 subunit (grey, helices α8, α9 and $\alpha3^{i}$) are shown in grey cartoon; Left panel: Rtt109 mutations that decrease both Vps75 pull-down and Vps75-stimulated Rtt109 HAT activity (by at least 2-fold) are indicated in red on the surface representation of one Rtt109 subunit (grey). Only one subunit of Vps75 and the a1′ helix of the opposing subunit are shown in cartoon representation. This figure

shows that mutations that affect the activity of the Rtt109/Vps75 holoenzyme correlate with positions that are associated with protein complex formation. The relative orientation of the right and left panels is indicated. (B): Sequence alignment of Rtt109 and homologs around the 130-179 segment. The residue numbers of *S. cerevisiae* Rtt109 is indicated at the top, with the 130-179 segment underlined in blue. This figure shows that Rtt109's 130-179 segment is evolutionarily conserved only in a subset of species.

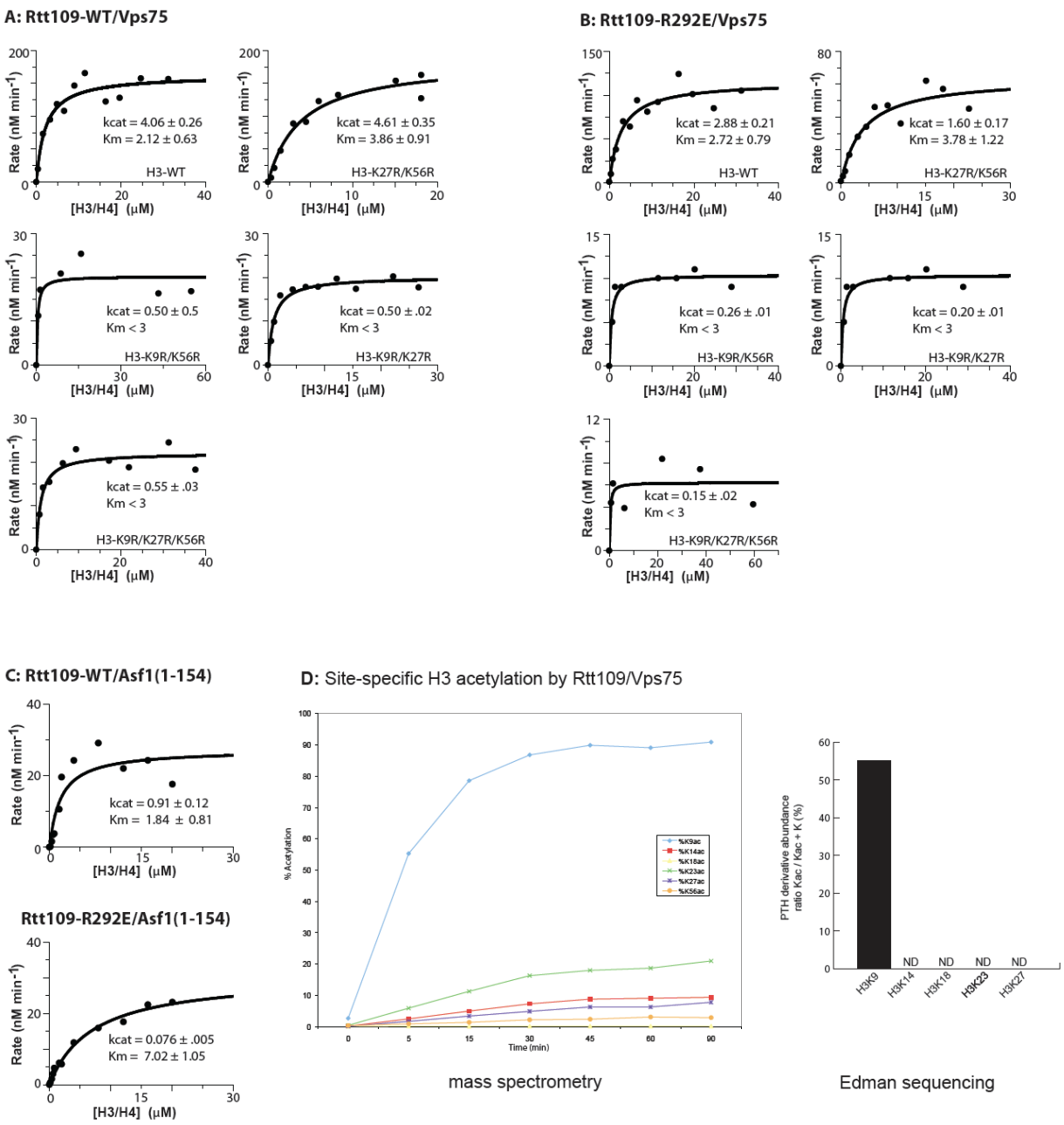


**Figure S3, related to Figure 3. Kinetics of histone H3 acetylation by (A) Rtt109-WT/Vps75, (B) Rtt109-(R292E)/Vps75 and (C) Rtt109-WT/Asf1 and Rtt109-(R292E)/Asf1 complexes.** The studies were carried out using 30 nM of the respective enzyme complex, saturating levels of acetyl coenzyme A and H3-WT and mutants (K9R/K27R, K9R/K56R, or K27R/K56R) in the context of the $(H3\text{-}H4)_2$ substrate at specified concentrations. The averages of two duplicate experiments are shown for each data point. The kinetic parameters were determined by a non-linear regression fit to the Michaelis-Menten equation. This data shows that the Rtt109-WT/Vps75 complex preferentially acetylates H3K9 *in vitro*. (D) Lysine substrate selectivity of the

Rtt109/Vps75 complex isolated from yeast. The kinetics of histone H3 acetylation by the Rtt109-TAP/Vps75 complex (400 nM) purified from yeast cells with 20 μM acetyl-coenzyme A and H3 substrate in the context of 8.2 μM recombinant yeast $(H3\text{-}H4)_2$ substrate. At each time point, proteins were precipitated with acetone. (Left panel) Proteins were resuspended in 0.1 M ammonium bicarbonate, propionylated, and subjected to trypsin digestion to determine the degree of site-specific histone H3 acetylation by mass spectrometry. (Right panel) Proteins from the 5-min time point were precipitated with acetone, resuspended in SDS-PAGE sample buffer and resolved through an SDS-15% polyacrylamide gel. After protein transfer to a PVDF membrane, Edman sequencing of H3 was performed for 30 cycles. For each acetylatable lysine, the approximate abundance of the phenylthiohydantoin (PTH) derivatives of acetyl-lysine and lysine was determined. ND: Not detected. These studies demonstrate that the Rtt109/Vps75 enzyme preferentially acetylates H3K9 over K14, K18, K23, K27, or K56.

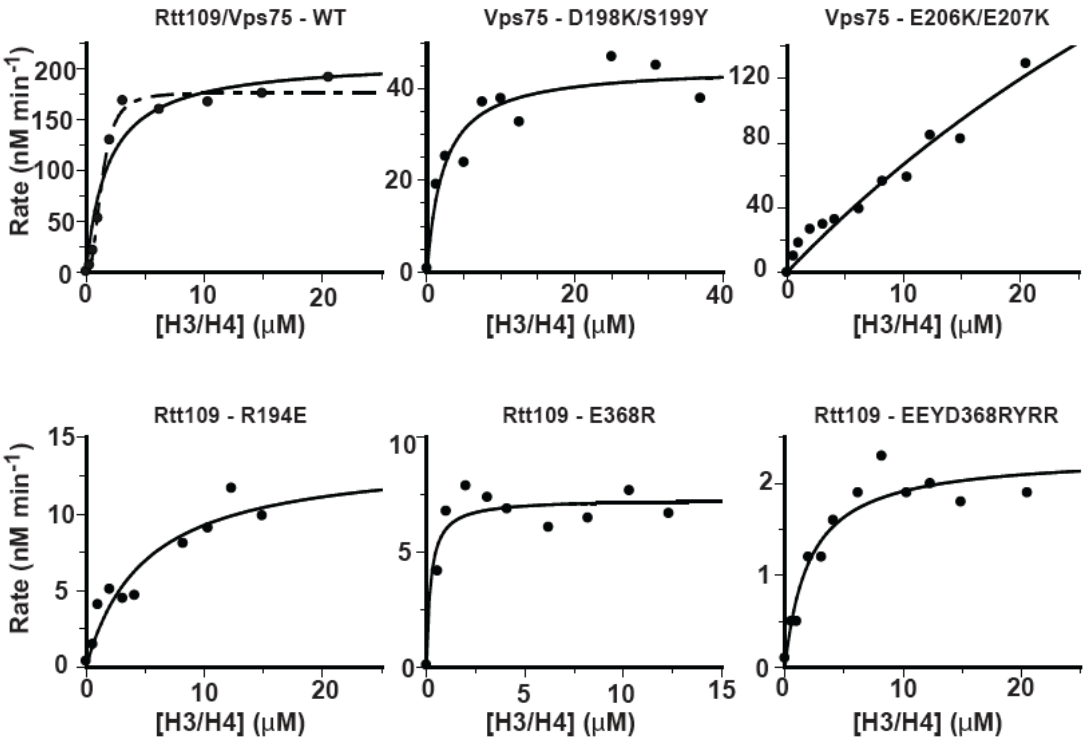


**Figure S4, related to Figure 4. Kinetics of histone H3 acetylation by Rtt109 and Vps75 mutants.** Reactions were carried out with 30 nM of Rtt109 (WT, unless otherwise indicated), 150 nM of Vps75 (WT, unless otherwise indicated), 20 μM acetyl coenzyme A (saturating concentration for Rtt109 WT and Vps75 WT), and $(H3\text{-}H4)_2$ substrate at specified concentrations. The average of two duplicate experiments are shown for each data point. The kinetic parameters were determined by a non-linear regression fit to the Michaelis-Menten equation. This data identifies several Rtt109 and Vps75 mutations that decrease the activity of the holoenzyme.

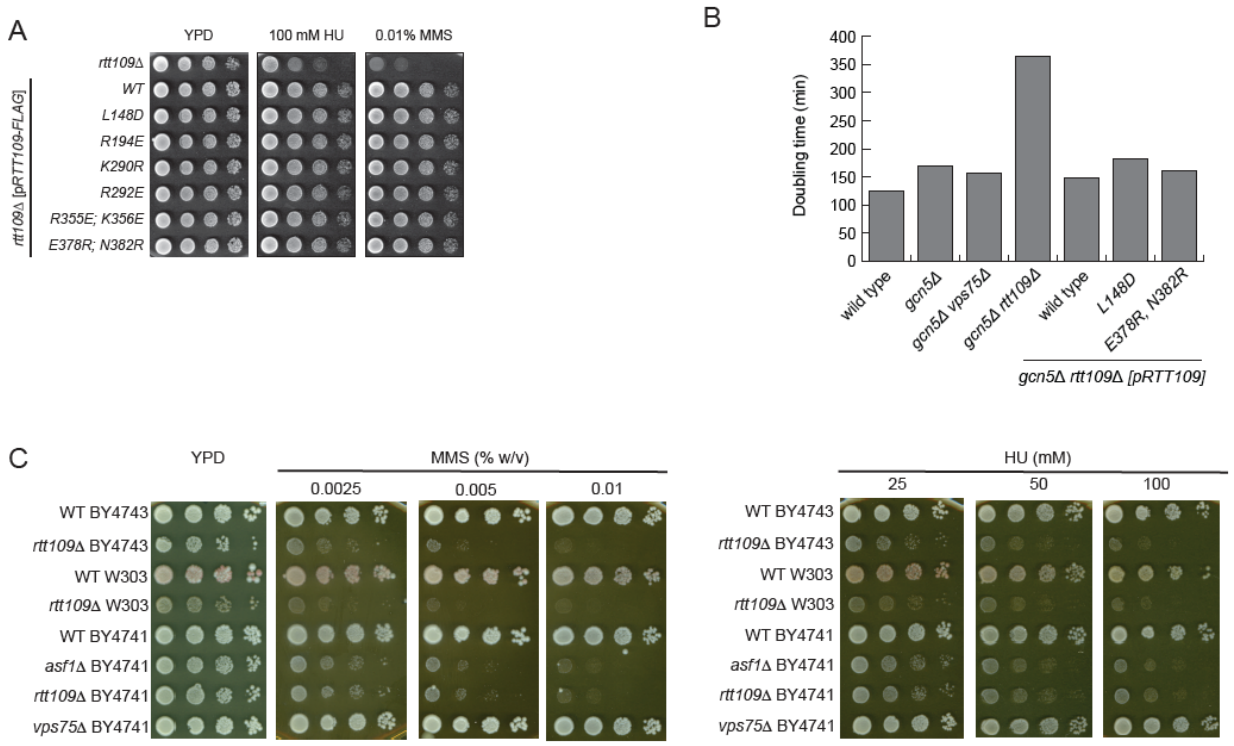


**Figure S5, related to Figure 5. Genotoxic agent sensitivity of mutants that disrupt the Rtt109/Vps75 complex.** (A) 5-fold serial dilutions of each strain were analysed for colony formation on rich medium (YPD) or plates containing the genotoxic agents methyl methane sulfonate (MMS) and hydroxyurea (HU). (B) Proliferation of *gcn5*, *rtt109* and *vps75* single and double mutants was monitored by measuring absorbance at 660 nm. (C) Same as in A. The plates show 5-fold serial dilutions of each strain from left to right. These data show that mutations that selectively disrupt the Rtt109/Vps75 enzyme, without reducing H3K56 acetylation, do not result in genotoxic agent sensitivity or slow proliferation.

**A**

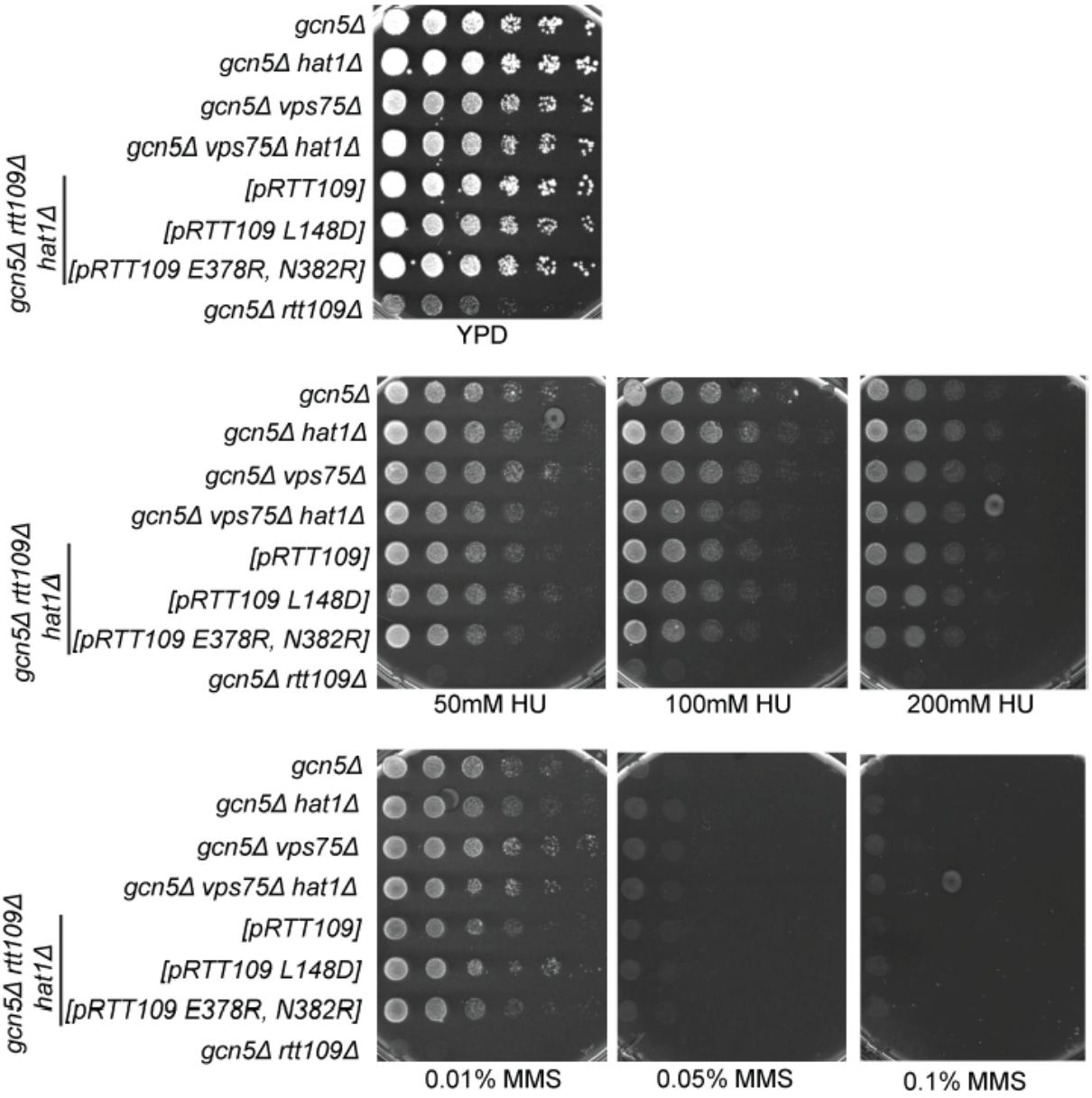
gcn5Δ
gcn5Δ hat1Δ
gcn5Δ vps75Δ
gcn5Δ vps75Δ hat1Δ
gcn5Δ rtt109Δ hat1Δ
[pRTT109]
[pRTT109 L148D]
[pRTT109 E378R, N382R]
gcn5Δ rtt109Δ
YPD
50mM HU
100mM HU
200mM HU
0.01% MMS
0.05% MMS
0.1% MMS

**B**

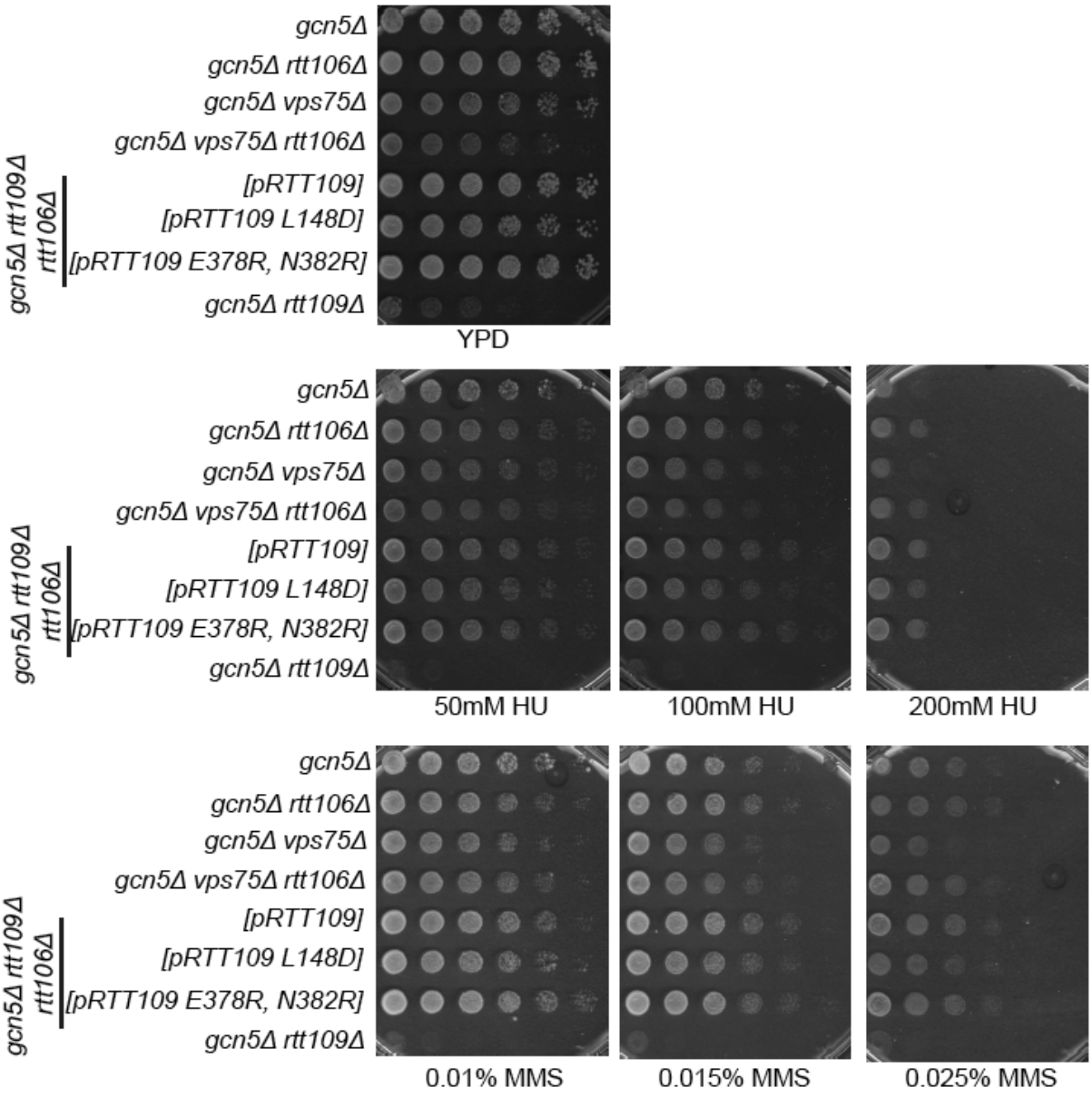
gcn5Δ
gcn5Δ rtt106Δ
gcn5Δ vps75Δ
gcn5Δ vps75Δ rtt106Δ
gcn5Δ rtt109Δ rtt106Δ
[pRTT109]
[pRTT109 L148D]
[pRTT109 E378R, N382R]
gcn5Δ rtt109Δ
YPD
50mM HU
100mM HU
200mM HU
0.01% MMS
0.015% MMS
0.025% MMS

C

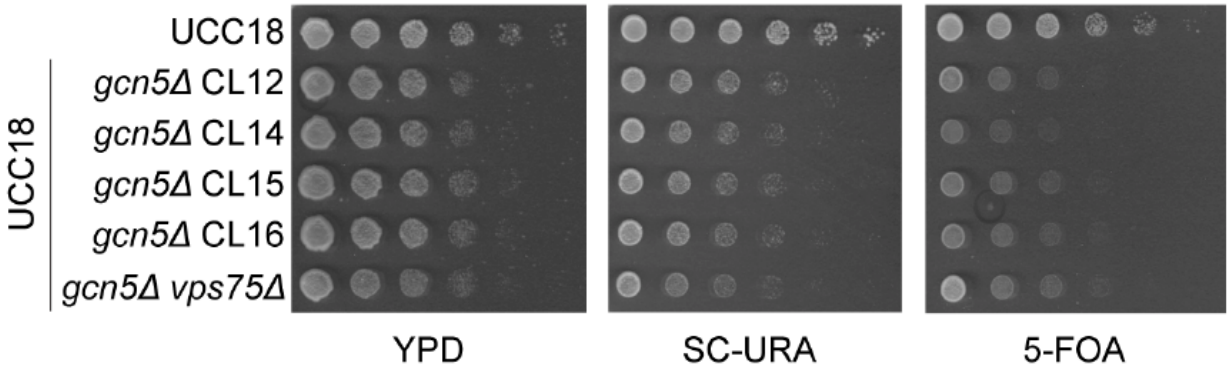


**Figure S6, related to Figure 5. Phenotypic effect of mutations that impair Gcn5, Hat1 or Rtt106 when combined with mutations that abolish the function of the Rtt109/Vps75 enzyme.** (A-B) Each strain was tested for growth on rich medium (YPD) or plates containing the genotoxic agents methyl methanesulfonate (MMS) and hydroxyurea (HU). The plates show 5-fold serial dilutions of each strain. (C) Expression of a sub-telomeric *URA3* reporter gene located on the left arm of chromosome VII was monitored by colony formation assays on minimal medium lacking uracil (SC-URA) or medium containing 5-Fluoroorotic acid (a drug that is cytotoxic to cells expressing the *URA3* reporter gene). The figure shows 5-fold serial dilutions of wild-type cells (UCC18), four independent *gcn5*Δ isolates and one *gcn5*Δ *vps75*Δ clone derived from UCC18 *gcn5*Δ cells. This experiment shows that the silencing defect of a sub-telomeric heterochromatin reporter gene in a *gcn5* null mutant strain is not enhanced by a *vps75*Δ mutation that disrupts the function of the Rtt109/Vps75 holoenzyme.

## Supplemental experimental procedures

### Protein preparation

For biochemical studies, N-terminal GST-fusion proteins of full-length Rtt109 and Vps75 were prepared as recombinant proteins from bacteria as previously described (Tang et al., 2008a; Tang et al., 2008b), and Quick-change site-directed mutagenesis (Stratagene) was employed to introduce selected protein mutations. An N-terminal 6xHis-fusion protein of full-length human ASF1a was prepared as previously described (Tang et al., 2006) and an analogous fusion protein to the *S. cerevisiae* Asf1 core domain (residues 1-154) was also prepared similarly. Both 6xHis-fusion proteins were purified through nickel affinity and size exclusion chromatography in Assay Buffer (25 mM HEPES pH 7.5, 300 mM NaCl, and 0.1 mM TCEP) and stored at 4°C before use. Overexpression plasmids encoding full-length *S. cerevisiae* H3 and H4 proteins were a gift from Dr. Bradley Cairns (University of Utah) and were used to prepare recombinant $(H3\text{-}H4)_2$ tetramers using co-refolding of H3 and H4 followed by gel filtration to isolate homogeneous complexes as previously reported (Luger et al., 1999), which were stored in Assay Buffer at 4°C.

To prepare wild-type and mutant Rtt109-Vps75 complexes for enzymatic assays, we subcloned DNAs encoding full-length wild-type or mutant forms of Vps75 and Rtt109 into the BamHI/SalI and NdeI/XhoI sites, respectively, of a modified 6His-TEV-pCDF-Duet1 vector. To facilitate protein cocrystallization, we used gene fragments encoding Vps75-(1-232) and full-length Rtt109. We transformed these plasmids into *E. coli* BL21 (DE3) Gold cells followed by cell growth at 37°C in LB medium and induction at $OD_{600}$=0.8 with 0.8 mM IPTG at 18°C overnight. Cells were harvested by centrifugation and lysed by sonication in 20 mM HEPES pH 7.5, 500 mM NaCl, 10 mM Imidazole (pH 7.0), and 5 mM 2-Mercaptoethanol (2-ME), supplemented with protease inhibitor cocktail. The tightly associated complex was purified to homogeneity using a combination of Ni-affinity, overnight cleavage with TEV protease, and further purification by MonoQ anion exchange (in 20 mM HEPES pH 7.5 buffer with a NaCl gradient from 50 mM to 1000 mM and 5 mM

2-ME) and Superdex 200 gel filtration chromatography in Gel Filtration Buffer (20 mM HEPES pH 7.5, 150 mM NaCl and 5 mM 2-ME). The purified protein complex was concentrated using an Amicon concentrator to 10 mg/ml in the Gel Filtration Buffer for crystallization or dialyzed against Assay Buffer for enzymatic assays before flash freezing the protein complex in liquid nitrogen until use.

### *In vitro* Rtt109-Vps75 binding (pull-down) assays

Wild-type and mutant GST-Vps75 fusion proteins were subjected to on-resin cleavage with TEV protease over-night, incubated with nickel resin to remove TEV protease, and the supernatant was dialyzed against PBS-βME for storage at 4 °C before use. Wild-type and mutant GST-Rtt109 proteins were retained on glutathione-Sepharose resin, aliquoted into 1.5 ml Eppendorf tubes, washed 3 times with PBS-βME buffer and stored at 4°C before use. Samples were quantitated by SDS-PAGE analysis with BSA controls before addition of stoichiometric amounts of Vps75 protein to GST-Rtt109-bound glutathione-Sepharose resin. Binding reactions were incubated at 4°C for 1 h with gentle rotation followed by washing the resin 3 times with PBS-βME buffer. Protein retained on the resin was resolved by SDS-PAGE and visualized by Coomassie blue staining. As a negative control, Vps75 proteins were also incubated with GST alone showing no detectable Vps75 binding to the resin.

### Histone Acetyltransferase (HAT) enzyme assay

Wild-type or mutant GST-Rtt109 protein, eluted off glutathione resin with reduced glutathione, was dialyzed against Assay Buffer, quantified, and stored at 4°C before use. For enzymatic assays, we adapted the radioactive HAT assay as previously described (Lau et al., 2000; Thompson et al., 2001). Briefly, GST-Rtt109 proteins (36 nM) were mixed with excess chaperone (200 nM): either wild-type yAsf1N(1-154) or wild-type or mutant Vps75 proteins for 10 min before $(H3\text{-}H4)_2$ tetramers were added to a final concentration of 8.2 μM and equilibrated at 30ºC for 10 min. [$^{14}$C]-AcCoA was added to a final

concentration of 20.8 μM and allowed to react for 5 min. We determined the reaction rates for the respective Rtt109/histone chaperone complex and mutants using the previously described gel-based assay that measures the incorporation of a $^{14}$C-labeled acetyl group into the yeast $(H3\text{-}H4)_2$ substrate.

For the determination of the apparent $K_m$ values for the $(H3\text{-}H4)_2$ substrates (either wild type or bearing the H3 mutations K9R/K56R, K9R/K27R or K27R/K56R) in the presence of wild-type or mutant enzyme and Vps75 chaperone, GST-Rtt109 proteins (36 nM) were mixed with excess Vps75 (170 nM) for 10 min before the H3-H4 substrate was added over a range of concentrations and equilibrated at 30ºC for 10 min. The reaction was initiated with [$^{14}$C]-AcCoA at a final concentration of 20.4 μM. The data that was generated is shown in Supplemental Figures 3 and 4**.** All assays were performed in duplicate at least two times and the data generally agreed within 20%. It should be noted that the approximate 40% difference between the $k_{cat}$ values for WT Rtt109 in Figures 3F and 4E are likely due to the use of two different enzyme and substrate preparations that were employed on separate occasions for these measurements.

**Limited proteolysis studies**

We employed three Rtt109 proteins for limited proteolysis studies: full-length Rtt109, Rtt109-Δ(130-179) and Rtt109-(L148D). These proteins were prepared by treating the corresponding GST-fusion proteins with TEV protease and isolating the cleaved Rtt109 proteins by Superdex 200 gel filtration chromatography in Gel Filtration Buffer. Incubation of the proteins, diluted to a concentration of 0.3 mg/ml (~6 μM), with trypsin protease (0.3 μg/ml) in the absence or presence of stoichiometric amounts of full length Vps75 was carried out for 10 min and 30 min and terminated by boiling the samples in SDS-PAGE sample buffer. The reaction products were analyzed by SDS-PAGE.

**Crystallization and structure determination of the Rtt109-Ac-CoA /Vps75 complex**

We obtained small crystals of the Rtt109/Vps75 (1-232) complex mixed with Ac-CoA (native crystal, PDB entry XXXX) using hanging-drop vapor-diffusion at room temperature from a reservoir solution containing 10.0% (v/v) PEG8000, 8% (v/v) ethylene glycol and 100 mM HEPES pH 7.5 buffer. We cryoprotected these crystals in a solution containing reservoir supplemented with increasing amounts of glycerol solution (0%, 10% and 20% (v/v)), soaking the crystals for about 5 min in each solution prior to flash freezing the crystals in liquid nitrogen. Peptide-soaked crystal (PDB entry YYYY) was prepared by soaking the native crystal above with 1 mM CoA and 1 mM of an H3K9 14-residue peptide, with sequence (NH2)A-R-T-K-Q-T-A-R-K-S-T-G-G-K (CONH2).

Crystallographic data was collected using beamline GM-CA/CAT 23ID-B at the Advanced Photon Source at a wavelength of 0.997 Å at 100 K. The data was processed and scaled using the HKL2000 suite (Dauter et al., 2000). The native and peptide-soaked crystals diffracted to useful resolution limits of 3.2 and 2.8 Å, respectively. The structure of the peptide-soaked crystal (PDB entry YYYY) was determined by molecular replacement using one Rtt109-Δ(130-179) (PDB ID 3D35) (Tang et al., 2008a) and one subunit of the Vps75-(1-232) homodimer (PDB ID 3DM7) (Tang et al., 2008b) as search models using the program PHASER (Potterton et al., 2003). The protein model was adjusted with reference to 2Fo-Fc and Fo-Fc difference fourier maps using the program COOT (Emsley and Cowtan, 2004) and the REFMAC library (Vagin et al., 2004) and refined with CNS (Brunger et al., 1998) using iterative model building, simulated annealing, and positional and B-factor refinement strategies. At the latter stages of the refinement, the Ac-CoA cofactor and segments of residues 130-179 of Rtt109 were modeled into difference Fourier maps and refined. Before the addition of water molecules, residues 11-14 of the H3K9 peptide could be modeled into a continuous stretch of density near the Rtt109-Vps75 interface. The presence of these peptide residues in the crystal lattice was confirmed with simulated annealing omit maps and the inclusion of this peptide fragment improved the refinement statistics. However, given that the peptide does not make extensive protein contact and is located far from the active site, we infer that this peptide-binding mode is not

biologically relevant. The 2.8 Å resolution refined model with the inclusion of 54 water molecules was checked for errors using composite simulated annealing omit maps (Table 1). We evaluated the final model with PROCHECK (Laskowski et al., 1993) revealing good stereochemical parameters and Ramachandran plot statistics for most residues. Protein residues not modeled in the final structure due to poor electron density include residues 130-133, 166-171 and 405-436 of Rtt109 and residues 1-8, 131-135 and 227-232 of Vps75. The structure of the native crystal (PDB entry XXXX) was determined using the refined native crystal structure as a model and refined to a resolution of 3.2 Å (Table 1). Comparison of the two crystal structures reveals that the presence of the H3K9 peptide in the crystal lattice of the peptide-soaked crystal does not alter the overall Rtt109-CoA/Vps75 complex structure, in particular at the Rtt109-Vps75 interface that it contacts (Figure S1).

**Yeast expression plasmids**

The backbone vector for construction of yeast Rtt109 and Vps75 expression plasmids from their natural promoters was the modified YCplac111 3Flag *His3MX1 LEU2* plasmid, which we previously described (Tang et al., 2008a). *RTT109* wild-type and mutant genes were obtained by excising a *BamH*I-*Sma*I fragment from the modified 6His-TEV-pCDF-Duet1 vector for bacterial expression of each Rtt109 construct. Restriction fragments were purified from agarose gels using QIAquick Gel Extraction Kit (QIAGEN). Insertion of *RTT109* fragments into a yeast expression vector was achieved by homologous recombination *in vivo*. For this purpose, we co-transformed the *BamH*I-*Sma*I restriction fragments encoding the wild-type or mutant *RTT109* genes along with the *Not*I linearized YCplac111 3Flag *His3MX1 LEU2* plasmid into the ZGY954 yeast cells. Yeast Rtt109 expression plasmids were recovered from $Leu^+$ colonies and their sequence was verified by DNA sequencing. A DNA fragment containing the *VPS75* promoter (408bp) and the *VPS75* ORF (792bp) was inserted in-frame with the 3Flag epitope between the *Kpn*I and *Pac*I sites of the YCplac111 3Flag *His3MX1 LEU2* plasmid. These plasmids were then used to transform the various yeast strains described in this study (Table S1). After plasmid transformation into *gcn5 rtt109* double mutants, two clones of cells were analyzed further

for each Rtt109 expression vector. To rule out the possibility of reversion of Rtt109/Vps75 point mutations, plasmids were isolated and sequenced from the strains used to monitor genotoxic agent sensitivity and *in vivo* acetylation.

**Yeast strains**

The BY4741 wild-type and deletion strains used in Figure S5C were purchased from Open Biosystems. The genotypes of all the other yeast strains used in this study are described in Table S1.

**Table S1. List of yeast strains**

| Strain | Genotype | Source |
|---|---|---|
| RMY212 | *MAT***a** *ade2–101$^{(och)}$ his3$^{200}$ lys2–801$^{(amp)}$ trp1$^{901}$ ura3–52 hht1-hhf1::LEU2 hht2-hhf2::HIS3* pRM212 [*CEN4 ARS1 TRP1 hht2-K9R HHF2*] | (Zhang et al., 1998) |
| WT | BY4741 *MAT***a** *ura3Δ0 leu2Δ0 his3Δ1 met15Δ0* | Fillingham et al., 2008 |
| JF81 | BY4741 *gcn5Δ::KanMX6* | Fillingham et al., 2008 |
| JF103 | BY4741 *MAT***a** *gcn5Δ::KanMX6 rtt109Δ::NatMX* | Fillingham et al., 2008 |
| DWY01 | BY4741 *rtt109Δ::KanMX* | (Pan et al., 2004) |
| DWY02 | BY4741 *gcn5Δ::KanMX6 vps75Δ::HphMX* | This work |
| DWY03 | JF103 p[*ARS CEN LEU2 HIS3MX1 RTT109-(WT)-FLAG3*] | This work |
| DWY04 | JF103 p[*ARS CEN LEU2 HIS3MX1 rtt109-(L148D)-FLAG3*] | This work |
| DWY05 | JF103 p[*ARS CEN LEU2 HIS3MX1 rtt109-(R194E) –FLAG3*] | This work |
| DWY06 | JF103 p[*ARS CEN LEU2 HIS3MX1 rtt109-(K290R)-FLAG3*] | This work |

| | | |
|---|---|---|
| DWY07 | JF103 p[*ARS CEN LEU2 HIS3MX1 rtt109-(R292E)-FLAG3*] | This work |
| DWY08 | JF103 p[*ARS CEN LEU2 HIS3MX1 rtt109 (R355E, K356E)-FLAG3*] | This work |
| DWY09 | JF103 p[*ARS CEN LEU2 HIS3MX1 rtt109 (E378R, N382R*) –*FLAG3*] | This work |
| DWY10 | DWY01 p[*ARS CEN LEU2 HIS3MX1 RTT109-(WT)-FLAG3*] | This work |
| DWY11 | DWY01 p[*ARS CEN LEU2 HIS3MX1 rtt109-(L148D)-FLAG3*] | This work |
| DWY12 | DWY01 p[*ARS CEN LEU2 HIS3MX1 rtt109-(R194E)-FLAG3*] | This work |
| DWY13 | DWY01 p[*ARS CEN LEU2 HIS3MX1 rtt109-(K290R-FLAG3*] | This work |
| DWY14 | DWY01 p[*ARS CEN LEU2 HIS3MX1 rtt109-(R292E)-FLAG3*] | This work |
| DWY15 | DWY01 p[*ARS CEN LEU2 HIS3MX1 rtt109-(R355E, K356E) –FLAG3*] | This work |
| DWY16 | DWY01 p[*ARS CEN LEU2 HIS3MX1 rtt109-(E378R, N382R*) *–FLAG3*] | This work |
| D10 | W303 *MAT***a** *leu2-3,112 ura3-1 his3-11,15 trp1-1 ade2-1 bar1::HIS3* | Tang et al., 2008a |
| ZGY954 | W303 *MAT***a** *leu2-3,112 ura3-1 his3-11,15 trp1-1 ade2-1 bar1*Δ*::HIS3 rtt109*Δ*::KanMX6* | Han et al., 2007 |
| WT BY4743 | *MAT***a** *ura3*Δ*0 leu2*Δ*0 his3*Δ*1* | This work |
| *rtt109*Δ BY4743 | *MAT***a** *ura3*Δ*0 leu2*Δ*0 his3*Δ *rtt109*Δ*::KanMX* | This work |
| DWY17 | DWY03 p[*ARS CEN LEU2 URA3 VPS75-(WT)-HA*] | This work |
| DWY18 | DWY04 p[*ARS CEN LEU2 URA3 VPS75-(WT)-HA*] | This work |
| DWY19 | DWY09 p[*ARS CEN LEU2 URA3 VPS75-(WT)-HA*] | This work |
| DWY20 | BY4741 *gcn5*Δ*::KanMX6 vps75*Δ*::HphMX RTT109-TAP::HIS3MX6* p[*ARS CEN LEU2 HIS3MX1 VPS75-(WT)-* | This work |

| | | |
|---|---|---|
| | *FLAG3*] | |
| DWY21 | BY4741 *gcn5*Δ*::KanMX6 vps75*Δ*::HphMX RTT109-TAP::HIS3MX6* p[*ARS CEN LEU2 HIS3MX1 vps75-(R173E, K177E)-FLAG3*] | This work |
| DWY22 | BY4741 *gcn5*Δ*::KanMX6 vps75*Δ*::HphMX RTT109-TAP::HIS3MX6* p[*ARS CEN LEU2 HIS3MX1 vps75-(E206K, E207K)-FLAG3*] | This work |
| DWY23 | BY4741 *gcn5*Δ*::KanMX6 vps75*Δ*::HphMX RTT109-TAP::HIS3MX6* p[*ARS CEN LEU2 HIS3MX1 vps75-(E218K, D222K)-FLAG3*] | This work |
| DWY24 | BY4741 *gcn5*Δ*::KanMX6 hat1*Δ*::URA3* | This work |
| DWY25 | BY4741 *gcn5*Δ*::KanMX6 vps75*Δ*::HphMX hat1*Δ*::URA3* | This work |
| DWY26 | BY4741 *gcn5*Δ*::KanMX6 rtt109*Δ*::NatMX hat1*Δ*::URA3* p[*ARS CEN LEU2 HIS3MX1 RTT109-(WT)-FLAG3*] | This work |
| DWY27 | BY4741 *gcn5*Δ*::KanMX6 rtt109*Δ*::NatMX hat1*Δ*::URA3* p[*ARS CEN LEU2 HIS3MX1 rtt109-(L148D)-FLAG3*] | This work |
| DWY28 | BY4741 *gcn5*Δ*::KanMX6 rtt109*Δ*::NatMX hat1*Δ*::URA3* p[*ARS CEN LEU2 HIS3MX1 rtt109-(E378R, N382R*)-*FLAG3*] | This work |
| DWY29 | BY4741*gcn5*Δ*::KanMX6 rtt106*Δ*::URA3* | This work |
| DWY30 | BY4741 *gcn5*Δ*::KanMX6 vps75*Δ*::HphMX rtt106*Δ*::URA3* | This work |
| DWY31 | BY4741 *gcn5*Δ*::KanMX6 rtt109*Δ*::NatMX rtt106*Δ*::URA3* p[*ARS CEN LEU2 HIS3MX1 RTT109-(WT)-FLAG3*] | This work |
| DWY32 | BY4741 *gcn5*Δ*::KanMX6 rtt109*Δ*::NatMX rtt106*Δ*::URA3* p[*ARS CEN LEU2 HIS3MX1 rtt109-(L148D)-FLAG3*] | This work |
| DWY33 | BY4741 *gcn5*Δ*::KanMX6 rtt109*Δ*::NatMX rtt106*Δ*::URA3* p[A*RS CEN LEU2 HIS3MX1 rtt109-(E378R, N382R*)-*FLAG3*] | This work |
| UCC18 | W303 *MAT***a** TEL VII-L *adh4::URA3* | (Aparicio et al., 1991) |

| | | |
|---|---|---|
| YAV178 | UCC18 *gcn5*Δ*::HphMX* | This work |
| YAV179 | UCC18 *gcn5*Δ*::HphMX rtt109*Δ*::KanMX* | This work |
| YAV183 | YAV179 p[*ARS CEN LEU2 HIS3MX1 RTT109-(WT)-FLAG3*] | This work |
| YAV184 | DWY35 p[*ARS CEN LEU2 HIS3MX1 rtt109-(E378R, N382R)-FLAG3*] | This work |
| YAV180 | UCC18 *gcn5*Δ*::HphMX vps75*Δ*::KanMX* | This work |
| YAV181 | YAV180 p[*ARS CEN LEU2 HIS3MX1 VPS75-(WT)-FLAG3*] | This work |
| YAV182 | DWY40 p[*ARS CEN LEU2 HIS3MX1 vps75-(E206K, E207K)-FLAG3*] | This work |
| YAV174 | BY4741 *CAC2-TAP::HIS3MX6* | Open Biosystems |
| YAV175 | JF103 *CAC2-TAP::URA3* p[*ARS CEN LEU2 HIS3MX1 RTT109-(WT)-FLAG3*] | This work |
| YAV176 | JF103 *CAC2-TAP::URA3* p[*ARS CEN LEU2 HIS3MX1 RTT109-(L148D)-FLAG3*] | This work |
| YAV177 | JF103 *CAC2-TAP::URA3* p[*ARS CEN LEU2 HIS3MX1 RTT109-(E378R,N382R)-FLAG3*] | This work |

**Genotoxic agent susceptibility assays**

These assays were performed as previously described (Tang et al., 2008a).

**Immunoblotting**

Strains RMY212, WT, JF81, JF103, DWY01 and DWY02, which all lack $LEU^+$ plasmids, were grown to exponential phase in minimal medium containing leucine at 30°C. Strains DWY03-DWY16, which contain $LEU^+$ plasmids for expression of Rtt109-Flag, were grown to exponential phase in minimal medium lacking leucine at 30°C. Whole-cell lysates were prepared from 1-2×$10^7$ cells using an alkaline extraction method (Kushnirov, 2000).

Proteins from whole-cell lysates were separated in SDS-15% polyacrylamide gels. To verify expression of Rtt109-Flag proteins in strains DWY03-DWY09), proteins were transferred to PVDF membranes by semi-dry transfer for 1:15 h at 15 V using 1X Towbin buffer (25 mM Tris, 192 mM Glycine, pH 8.3), containing 5% Methanol and 0.02% SDS. Immunoblotting was performed using an antibody against the Flag epitope (anti-Flag M2, Sigma). For histone immunoblots, proteins were transferred to nitrocellulose membranes by semi-dry transfer for 1 h at 10 V using 1X Towbin buffer containing 20% Methanol and 0.02% SDS. To probe for histone H3K56Ac, we used the H3K56Ac antibody (AV105) that we described previously (Masumoto et al., 2005). For histone H3K9Ac blots, we used a commercial antibody (Upstate, catalogue number: 07-352, Lot: DMA 1394804). For histone H3K27Ac blots, we used an antibody specific for histone H3K27 acetylation that was a gift from Dr. Zhiguo Zhang. Probing for histone H3 as a loading control was performed using a previously described rabbit polyclonal antibody (YAV77/78) raised against a C-terminal peptide of H3 that is not subject to post-translational modification (Tang et al., 2008a).

**Mass Spectrometry (MS) to quantify the stoichiometry of histone acetylation**

Histones were isolated from asynchronously growing *S. cerevisiae* cells using two different procedures that gave rise to similar results. In the first approach, we purified histones from yeast cells as previously described (Poveda et al., 2004). The second procedure was performed as follows: 250 µl of protein A-Sepharose beads (GE healthcare) were incubated with 300 µg of affinity-purified antibody against the N-terminal domain of yeast H3 (AV71/72) for 1 h at 4ºC in 10 mM Tris-HCl pH 8.0 (Xhemalce et al., 2007). The antibody beads were then washed three times with the same buffer. *S. cerevisiae* cells (1 ml cell pellet) were resuspended in 1 ml of lysis buffer (100 mM Tris-HCl pH 8.0, 200 mM NaCl, 1X EDTA-free complete protease inhibitor cocktail (Roche), 100 mM sodium butyrate, 10 µM trichostatin A, 100 mM nicotinamide, 1 mM dithiothreitol) and lysed using a 6850 Freezer Mill (SPEX certiprep). The cell lysates were then incubated in the presence of 200 µg/ml of ethidium bromide for 30 min on ice to force histone dissociation from DNA. After two brief (5-10 seconds) pulses of sonication, the cell lysates were centrifuged at

3000 rpm and 4ºC for 15 min in a tabletop centrifuge (Heraeus Multifuge 3S-R). The supernatant was mixed with 50 µl of H3 antibody beads and incubated overnight at 4ºC. The beads were washed five times in wash buffer (100 mM Tris-HCl pH 8, 100 mM NaCl), resuspended in 1X SDS-PAGE sample buffer and boiled for 5 min to elute bound proteins.

Two alternative procedures were used to obtain histone H3 tryptic peptides for mass spectrometry (MS). In the first approach, acid extracts containing core histones were fractionated by reverse phase HPLC and the H3 fractions were pooled and processed for propionylation of unmodified lysine residues and trypsin digestion (Drogaris et al., 2008). Alternatively, acid extracts containing core histones were resolved in an SDS-15% polyacrylamide gel (29:1 acrylamide:N,N`-methylene bisacrylamide molar ratio), which was stained with Bio-Safe Coomassie G-250 stain (Bio-Rad) and destained in water. The bands corresponding to histone H3 were then cut from the gel for mass spectrometry. The gel bands were cut into small slices, transferred to Eppendorf tubes and incubated twice for at least 3 h with 1.5 ml of 5% acetic acid, 10% methanol. This solution was removed and gel bands were destained using deionized (DI) water, 50:50 DI water: acetonitrile (ACN), and pure ACN. The bands were washed and resuspended in a 0.1 M ammonium bicarbonate (Ambic) solution (pH 8.0). A propionic anhydride reagent (2:1 PA:water) was added to the bands in a 1:1 volume ratio and incubated for 1 h at room temperature with shaking. The buffer and derivatization mixture was replaced with fresh reagents to perform a second propionylation reaction for 1 h. After removing excess reagent, the bands were washed with a 0.1 M Ambic solution, and evaporated to dryness in a Speed-Vac. Rehydration with 0.1 M Ambic was followed by the addition of 1 µg of trypsin and overnight protein digestion. The digest supernatant was placed in a separate Eppendorf tube. Peptides were extracted twice with a 50:50 DI water:ACN solution containing 5% TFA (v:v:v). The bands were incubated for 15 min at room temperature with shaking. The two solutions containing extracted peptides were recovered, combined with the original tryptic digest supernatant, and evaporated to dryness in a Speed-Vac. Peptides were dissolved in the initial mobile phase (95:5 DI water:ACN, 0.2% formic acid (v:v:v) prior to injection onto the LC-MS instrument, an AB/Sciex API 4000 Q-Trap mass spectrometer (Thornhill, ON, Canada) equipped with a Nanospray II interface.

The different acetylated forms of H3 were detected by multiple reaction monitoring (MRM) (Lange et al., 2008). For each acetylated peptide, two to four precursor – product ion pairs corresponding to the following MRM transitions were monitored (ac, acetylation; pr, propionylation of ε-amino group):

A) Doubly charged H3 peptide 54-FQK(ac)STELLIR-63:
*m/z* 638.9 → 1001.6 and *m/z* 638.9 → 831.5
B) Doubly charged H3 peptide 54-FQK(pr)STELLIR-63:
*m/z* 645.9 → 1015.6 and *m/z* 638.9 → 831.5
C) Doubly charged H3 peptide 9-K(ac)STGGK(pr)APR-17:
*m/z* 500.3→ 742.4 and *m/z* 500.3→ 829.5
D) Doubly charged H3 peptide 9-K(pr)STGGK(ac)APR-17:
*m/z* 500.3 → 728.4 and *m/z* 500.3 → 815.4
E) Doubly charged H3 peptide 9-K(ac)STGGK(ac)APR-17:
*m/z* 493.3 → 728.4 and *m/z* 493.3 → 815.4
F) Doubly charged H3 peptide 9-K(pr)STGGK(pr)APR-17:
*m/z* 507.3 → 742.4 and *m/z* 507.3 → 742.4
G) Doubly charged H3 peptide 18-K(ac)QLASK(pr)AAR-26:
*m/z* 535.8 → 772.5 and *m/z* 535.8 → 659.4
H) Doubly charged H3 peptide 18-K(pr)QLASK(ac)AAR-26:
*m/z* 535.8 → 758.5 and *m/z* 535.8 → 645.4
I) Doubly charged H3 peptide 18-K(pr)QLASK(pr)AAR-26:
*m/z* 542.8 → 772.5 and *m/z* 542.8 → 659.4
J) Triply charged H3 peptide 27-K(ac)SAPSTGGVK(pr)K(pr)PHR-40:
*m/z* 535.3 → 990.6, *m/z* 535.3 → 777.5, *m/z* 535.3 → 329.2, and *m/z* 535.3 → 1275.7
K) Triply charged H3 peptide 27-K(pr)SAPSTGGVK(pr)K(pr)PHR-40:
*m/z* 540.0 → 990.6, *m/z* 540.0 → 777.5, *m/z* 540.0 → 343.2, and *m/z* 540.0 → 1275.7
L) H3 peptide YK(pr)PGTVALR, a non-modified peptide used for normalization of H3 quantities in each gel band and for fluctuations in the MS response: *m/z* 530.8 → 713.4

First, the abundance for each peptide MRM transitions (A to L) was normalized to the abundance of the non-modified peptide transition (L). These normalized values (An to Ln) were then used to calculate the stoichiometry of acetylation at each lysine residue as follows.

%H3K56ac = 100 x An / (An + Bn)
%H3K9ac = 100 x (Cn + En) / (Cn + Dn + En + Fn)
%H3K14ac = 100 x (Dn + En) / (Cn + Dn + En + Fn)

**Purification of Rtt109-TAP/Vps75 complexes from yeast cells**

Cells expressing Rtt109-TAP or Rtt109-FLAG fusion proteins were grown to $2x10^7$cells/ml in two liters of Synthetic Complete (SC) medium lacking leucine (to select for plasmids expressing Rtt109 or Vps75) and harvested. The volume of packed cells was estimated, and an equal volume of 2x lysis buffer (50 mM Tris-HCl pH 7.5, 100 mM NaCl, 20% glycerol, 10 mM $MgCl_2$, 10 mM 2-mercaptoethanol, 1 μM MG132) was added. The yeast cell suspension was frozen as droplets in liquid nitrogen and the cells were disrupted using a freezer mill as described below for the purification of CAF-1/histone complexes. The cell lysate was thawed out on ice, and incubated for 30 min with 100 μg/ml ethidium bromide and 1 U/ml of benzonase (Novagen). This was followed by two successive rounds of centrifugation for 20 min at 20,000 x g and 4ºC. To isolate Rtt109/Vps75 complexes, the supernatant cleared of debris was incubated for 60 min with IgG-agarose (Sigma) or anti-FLAG M2-agarose beads (Sigma). After washing five times with 1.4 ml lysis buffer, proteins were eluted from the beads with SDS-PAGE sample buffer and resolved through SDS-12% or 15% polyacrylamide gels. The immunoprecipitated complexes were detected by immunoblotting with antibodies against CBP to detect Rtt109-TAP (Open Biosystems), HA (12CA5, Sigma) or FLAG (M2, Sigma). For mass spectrometry, the complexes affinity-purified with anti-FLAG M2-agarose beads were eluted with 0.1 M formic acid. The acid eluate was dried in a Speed-Vac, resuspended in 0.1 M ammonium bicarbonate (without pH adjustment) and subjected to trypsin digestion and MS analysis as described below.

**Affinity purification of Cac2-TAP/H3/H4 complexes**

Yeast strains expressing Cac2-TAP and either WT or mutant forms of Rtt109 were cultured up to $2x10^7$ cells/ml in SC minus leucine (to select for the Rtt109 expression plasmids) and harvested. The volume of packed cells was estimated, and an equal volume of 2x lysis buffer (50 mM Tris-HCl, pH 7.5, 200 mM NaCl, 2 mM DTT, 20% glycerol) was added. The cell suspension was frozen into droplets using liquid nitrogen. Yeast cells were broken by grinding in a Spex Certiprep 6850 freezer mill (4 cycles of cell breakage at 10 impacts per second with 2 min cooling intervals between each cycles of cell breakage). After thawing the cell lysate at 4ºC, 1X EDTA-free Protease Inhibitor Cocktail (Roche) and 100 µg/ml ethidium bromide were added and, 15 min later, two rounds of centrifugation (20 min, 16,000 rpm, 4ºC, SS-34 rotor) were performed to remove insoluble debris. The cleared supernatant was incubated with IgG-agarose beads (Sigma) for 2 h at 4ºC. The beads were recovered by low speed centrifugation (600 rpm, 1 min, 4ºC) and the supernatant was discarded. The beads were transferred into an Eppendorf tube and washed four times with 1.4 ml TEV cleavage buffer (10 mM Tris-HCl pH 7.5, 100 mM NaCl). The beads were resuspended in 200 µl TEV cleavage buffer. The CAF-1/histone complexes were eluted from the beads by cleavage with 7.5 µl 10 U/µl AcTEV protease (Invitrogen) and incubation for 1 h at 16ºC and 1000 rpm in a Thermomixer. The supernatant was recovered and the beads were washed three more times with 200 µl TEV cleavage buffer in order to recover as much as possible of the protein complexes released by the TEV protease. The four eluates were combined. Because a large excess of AcTEV protease was used, the His-tagged AcTEV protease was removed from the eluted protein complexes by incubation with 5µl nickel-NTA-agarose beads (Qiagen) for 2 h at 4ºC and 1000 rpm in a Thermomixer. The supernatant was concentrated in a Speed-Vac prior to mass spectrometry.

Affinity-purified complexes were dialyzed against 0.1 M ammonium bicarbonate (the pH was not adjusted) and digested overnight at 37˚C with 1 µg of trypsin. Tryptic digests were evaporated to dryness in a Speed-Vac and subsequently dissolved in a 95:5 water:

acetonitrile mixture containing 0.2% formic acid (v:v:v) prior to nanoLC-MS/MS analyses using an Eksigent nano-2D LC system coupled to an LTQ-Orbitrap Velos mass spectrometer (Thermo Fisher Scientific, Bremen, Germany). Peptides were separated on a 150-µm x 10-cm $C_{18}$ (3 µm Jupiter particles, Supelco) analytical column using a gradient of 5-40% acetonitrile (in 0.2% formic acid) over 65 min. The mass spectrometer was operated in a data-dependent acquisition mode with a 1 sec survey scan at 60,000 resolution, followed by six ion trap product ion spectra (MS/MS) of the most abundant precursor ions. The centroided data were merged into single peak-list files and searched with the Mascot search engine v2.10 (Matrix Science) against a custom database comprising *S. cerevisiae* Rtt109 (WT, L148D or E378R,N382R), Vps75, Cac1, Cac2, Cac3, H3 and H4. All MS/MS spectra with Mascot scores above 25 were selected and validated manually to confirm assignment. To determine the abundance of H3 and H4, the three most abundant tryptic peptides identified were selected, whereas the five most abundant peptides were analyzed for Rtt109, Vps75, Cac1, Cac2 and Cac3. The abundance of the same group of peptides was determined in complexes purified from each strain. The relative proportion of Rtt109 and Vps75 was obtained from the ratio of the summed abundance of tryptic peptides derived from each protein (five peptides each for Rtt109 and Vps75). Similarly, the relative proportion of histones and CAF-1 was determined from the ratio of the summed abundance of tryptic peptides derived from [H3+H4] and [Cac1+Cac2+Cac3] (three peptides each for H3 and H4, and five peptides each for Cac1, Cac2 and Cac3).

## Supplemental references


Aparicio, O.M., Billington, B.L., and Gottschling, D.E. (1991). Modifiers of position effect are shared between telomeric and silent mating-type loci in S. cerevisiae. Cell *66*, 1279-1287.

Brunger, A.T., Adams, P.D., Clore, G.M., DeLano, W.L., Gros, P., Grosse-Kunstleve, R.W., Jiang, J.S., Kuszewski, J., Nilges, M., Pannu, N.S.*, et al.* (1998). Crystallography & NMR system: A new software suite for macromolecular structure determination. Acta Crystallogr *D54*, 905-921.

Dauter, Z., Dauter, M., and Rajashankar, K.R. (2000). Novel approach to phasing proteins: derivatization by short cryo-soaking with halides. Acta Crystallogr D*56*, 232-237.

Drogaris, P., Wurtele, H., Masumoto, H., Verreault, A., and Thibault, P. (2008). Comprehensive profiling of histone modifications using a label-free approach and its applications in determining structure-function relationships. Anal Chem *80*, 6698-6707.

Emsley, P., and Cowtan, K. (2004). Coot: model-building tools for molecular graphics. Acta Crystallogr D*60*, 2126-2132.

Kushnirov, V.V. (2000). Rapid and reliable protein extraction from yeast. Yeast *16*, 857-860.

Lange, V., Malmstrom, J.A., Didion, J., King, N.L., Johansson, B.P., Schafer, J., Rameseder, J., Wong, C.H., Deutsch, E.W., Brusniak, M.Y.*, et al.* (2008). Targeted quantitative analysis of Streptococcus pyogenes virulence factors by multiple reaction monitoring. Mol Cell Proteomics *7*, 1489-1500.

Laskowski, R.A., MacArthur, M.A., Moss, D.S., and Thornton, J.M. (1993). PROCHECK: a program to check the stereochemical quality of protein structures. J Appl Cryst *26*, 283-291.

Lau, O.D., Courtney, A.D., Vassilev, A., Marzilli, L.A., Cotter, R.J., Nakatani, Y., and Cole, P.A. (2000). p300/CBP-associated factor histone acetyltransferase processing of a peptide substrate. Kinetic analysis of the catalytic mechanism. J Biol Chem *275*, 21953-21959.

Luger, K., Rechsteiner, T.J., and Richmond, T.J. (1999). Preparation of nucleosome core particle from recombinant histones. Methods Enzymol *304*, 3-19.

Masumoto, H., Hawke, D., Kobayashi, R., and Verreault, A. (2005). A role for cell-cycle-regulated histone H3 lysine 56 acetylation in the DNA damage response. Nature *436*, 294-298.

Pan, X., Yuan, D.S., Xiang, D., Wang, X., Sookhai-Mahadeo, S., Bader, J.S., Hieter, P., Spencer, F., and Boeke, J.D. (2004). A robust toolkit for functional profiling of the yeast genome. Mol Cell *16*, 487-496.

Potterton, E., Briggs, P., Turkenburg, M., and Dodson, E. (2003). A graphical user interface to the CCP4 program suite. Acta Crystallogr D*59*, 1131-1137.

Poveda, A., Pamblanco, M., Tafrov, S., Tordera, V., Sternglanz, R., and Sendra, R. (2004). Hif1 is a component of yeast histone acetyltransferase B, a complex mainly localized in the nucleus. J Biol Chem *279*, 16033-16043.

Tang, Y., Holbert, M.A., Wurtele, H., Meeth, K., Rocha, W., Gharib, M., Jiang, E., Thibault, P., Verreault, A., Cole, P.A.*, et al.* (2008a). Fungal Rtt109 histone acetyltransferase is an unexpected structural homolog of metazoan p300/CBP. Nat Struct Mol Biol *15*, 738-745.

Tang, Y., Meeth, K., Jiang, E., Luo, C., and Marmorstein, R. (2008b). Structure of Vps75 and implications for histone chaperone function. Proc Natl Acad Sci U S A *105*, 12206-12211.

Tang, Y., Poustovoitov, M.V., Zhao, K., Garfinkel, M., Canutescu, A., Dunbrack, R., Adams, P.D., and Marmorstein, R. (2006). Structure of a human ASF1a-HIRA complex and insights into specificity of histone chaperone complex assembly. Nat Struct Mol Biol *13*, 921-929.

Thompson, P.R., Kurooka, H., Nakatani, Y., and Cole, P.A. (2001). Transcriptional coactivator protein p300. Kinetic characterization of its histone acetyltransferase activity. J Biol Chem *276*, 33721-33729.

Vagin, A.A., Steiner, R.A., Lebedev, A.A., Potterton, L., McNicholas, S., Long, F., and Murshudov, G.N. (2004). REFMAC5 dictionary: organization of prior chemical knowledge and guidelines for its use. Acta Crystallogr D*60*, 2184-2195.

Xhemalce, B., Miller, K.M., Driscoll, R., Masumoto, H., Jackson, S.P., Kouzarides, T., Verreault, A., and Arcangioli, B. (2007). Regulation of histone H3 lysine 56 acetylation in Schizosaccharomyces pombe. J Biol Chem *282*, 15040-15047.

Zhang, W., Bone, J.R., Edmondson, D.G., Turner, B.M., and Roth, S.Y. (1998). Essential and redundant functions of histone acetylation revealed by mutation of target lysines and loss of the Gcn5p acetyltransferase. EMBO J *17*, 3155-3167.